

FINAL SAFETY ANALYSIS REPORT

for the

HOLTEC INTERNATIONAL STORAGE, TRANSPORT
AND REPOSITORY CASK SYSTEM
(HI-STAR 100 CASK SYSTEM)

NRC DOCKET NO. 72-1008

HOLTEC REPORT HI-2012610, VOLUME II of II

Prepared by



FINAL SAFETY ANALYSIS REPORT

for the

HOLTEC INTERNATIONAL

STORAGE, TRANSPORT,

AND REPOSITORY CASK SYSTEM

(HI-STAR 100 CASK SYSTEM)

DOCKET 72-1008

VOLUME II OF II

CHAPTER 4 THERMAL EVALUATION

4.0 INTRODUCTION

The HI-STAR 100 System is designed for the long-term storage of spent nuclear fuel (SNF) in a vertical position. An array of HI-STAR 100 Systems regularly spaced on a square pitch will be stored on a concrete ISFSI pad in an open environment. In this section, compliance of the HI-STAR 100 thermal performance to 10CFR72 requirements for storage under normal conditions is established. The analysis considers passive rejection of decay heat from the stored SNF assemblies to the environment under the most severe design basis ambient conditions. Effects due to incident solar radiation as well as partial radiation blockage due to the presence of neighboring casks at an ISFSI site are included in the analyses.

The guidelines presented in NUREG-1536 [4.1.3] include eight specific acceptance criteria that should be fulfilled by the cask thermal design. These eight criteria are summarized here as follows:

1. The fuel cladding temperature at the beginning of dry cask storage should generally be below the anticipated damage-threshold temperatures for normal conditions and a minimum of 20 years of cask storage.
2. The fuel cladding temperature should generally be maintained below 570°C (1058°F) for short-term accident, short-term off-normal, and fuel transfer conditions.
3. The maximum internal pressure of the cask should remain within its design pressures for normal (1% rod rupture), off-normal (10% rod rupture), and accident (100% rod rupture) conditions.
4. The cask and fuel materials should be maintained within their minimum and maximum temperature criteria for normal, off-normal, and accident conditions.
5. For fuel assemblies proposed for storage, the cask system should ensure a very low probability of cladding breach during long-term storage.
6. Fuel cladding damage resulting from creep cavitation should be limited to 15% of the original cladding cross sectional area.
7. The cask system should be passively cooled.

8. The thermal performance of the cask should be within the allowable design criteria specified in FSAR Chapters 2 and 3 for normal, off-normal, and accident conditions.

As demonstrated in this chapter (see Section 4.5), the HI-STAR 100 System is designed to comply with *all* eight criteria listed above. All thermal analyses to evaluate the normal condition performance of a HI-STAR 100 System are described in Section 4.4. All analyses for off-normal conditions are described in Section 11.1. All analyses for accident conditions are described in Section 11.2. Section 4.2 lists the material properties data required to perform the thermal analyses and Section 4.3 provides the applicable temperature limits criteria required to demonstrate the adequacy of the HI-STAR 100 System design under all conditions. This FSAR chapter is in full compliance with NUREG-1536 requirements, subject to the exceptions and clarifications discussed in Chapter 1, Table 1.0.3.

4.1 DISCUSSION

A sectional view of the HI-STAR 100 dry storage system has been presented earlier (see Figure 1.2.1). The system consists of an MPC loaded into an overpack with a bolted closure plate. The fuel assemblies reside inside the MPC which is sealed with a welded lid to form the confinement boundary. The MPC contains a stainless steel honeycomb basket structure which provides square-shaped fuel compartments (called boxes) of appropriate dimensions to facilitate insertion of fuel assemblies prior to welding of the lid. Each box panel (except the periphery panels of the MPC-68) is provided with Boral thermal neutron absorber sandwiched between a sheathing plate and the box panel along the entire length of the active fuel region. Prior to sealing the lid, the MPC is backfilled with helium up to the design basis initial loading (Table 1.2.2). This provides a stable and inert environment for long-term storage of the SNF. Additionally, the annular gap formed between the MPC and the overpack is backfilled with helium of the same quality before the overpack vent and drain port plugs are installed. Heat is transferred from the SNF in a HI-STAR 100 System to the environment by passive heat transport mechanisms only.

The helium backfill gas is an integral part of the MPC and overpack thermal designs. The helium fills all the spaces between solid components and provides an improved conduction medium (compared to air) for dissipating decay heat in the MPC. Additionally, helium in the spaces between the fuel basket and the MPC shell is heated differentially and, therefore, subject to the "Rayleigh" effect which is discussed in detail later. To ensure that the helium gas is retained and is not diluted by lower conductivity air, the MPC confinement boundary is designed to comply with the provisions of the ASME B&PV Code Section III, Subsection NB, as an all-seal-welded pressure vessel with redundant closures. Similarly, the overpack helium retention boundary is designed as an ASME B&PV Code Section III, Subsection NB pressure vessel. Both the MPC confinement boundary and the overpack helium retention boundary are required to meet maximum leakage rate Technical Specifications included in Chapter 12 of this FSAR. These leakage rate criteria are selected to ensure the presence of helium during the entire storage life. It is additionally demonstrated in Section 11.1.3 that the failure of one confinement boundary seal, a severe off-normal event, will not result in a breach of the confinement boundary. The helium gas is therefore retained and undiluted, and may be credited in the thermal analyses.

An important thermal design criterion imposed on the HI-STAR 100 System is to limit the maximum fuel cladding temperature to within design basis limits (Table 2.2.3) for long-term storage of design basis fuel assemblies. An equally important design criterion is to reduce temperature gradients within the MPC to minimize thermal stresses. In order to meet these design objectives, the HI-STAR 100 MPC basket is designed to possess certain distinctive characteristics, which are summarized in the following.

The MPC design minimizes resistance to heat transfer within the basket and basket periphery regions. This is ensured by an uninterrupted panel-to-panel connectivity realized in the all-welded honeycomb basket structure. Furthermore, the MPC design incorporates top and bottom plena with interconnected downcomer paths. The top plenum is formed by the gap between the bottom

of the MPC lid and the top of the honeycomb fuel basket, and by elongated semicircular holes in each basket cell wall. The bottom plenum is formed by large elongated semicircular holes at the base of all cell walls. The MPC basket is designed to eliminate structural discontinuities (i.e., gaps) which introduce large thermal resistances to heat flow. Consequently, temperature gradients are minimized in the design, which results in lower thermal stresses within the basket. Low thermal stresses are also ensured by an MPC design which permits unrestrained axial and radial growth of the basket to eliminate the possibility of thermally induced stresses due to restraint of free-end expansion.

Finally, it is heuristically apparent from the geometry of the MPC that the basket metal, the fuel assemblies, and the contained helium mass will be at their peak temperatures at or near the longitudinal axis of the MPC. The temperatures will attenuate with increasing radial distance from this axis, reaching their lowest values at the outer surface of the MPC shell. Conduction along the metal walls and radiant heat exchange from the fuel assemblies to the MPC metal mass would therefore result in substantial differences in the bulk temperatures of helium columns in different fuel storage cells. Since two fluid columns at different temperatures in communicative contact cannot remain in static equilibrium, the non-isotropic temperature field in the MPC internal space due to conduction and radiation heat transfer mechanisms guarantee the incipience of the third mode of heat transfer: natural convection.

The helium columns traverse the vertical storage cavity spaces, redistributing heat within the MPC. Elongated holes in the bottom of the cell walls, liberal flow space and elongated holes at the top, and wide open downcomers along the outer periphery of the basket ensure a smooth helium flow regime. The most conspicuous beneficial effect of the helium thermosiphon circulation, as discussed above, is the mitigation of internal thermal stresses in the MPC. Another beneficial effect is reduction of the peak fuel cladding temperatures of the fuel assemblies located in the interior of the basket. However, in the interest of conservatism, *no credit* for the thermosiphon action is taken in the thermal analysis reported in this chapter. To partially compensate for the reduction in the *computed* heat rejection capability due to the complete neglect of the global thermosiphon action within the MPC, flexible heat conduction elements made of aluminum are interposed in the large peripheral spaces between the MPC shell and the fuel basket. These heat conduction elements, shown in the MPC Drawings 1392, 1395, and 1401 in Section 1.5, are engineered to possess lateral flexibility such that they can be installed in the peripheral spaces to create a nonstructural thermal connection between the basket and the MPC shell. In their installed condition, the heat conduction elements will conform to and contact the MPC shell and the basket walls. MPC manufacturing procedures have been established to ensure that the thermal design objectives for the conduction elements set forth in this document are realized in the actual hardware.

Two distinct MPC basket geometries are included in the HI-STAR 100 System for storage of PWR and BWR SNF assemblies. For intact PWR fuel storage, a 24-assembly design is depicted in Figure 1.2.4. A 68-assembly design for storage of intact or damaged BWR fuel is shown in Figure 1.2.2. Damaged BWR fuel and fuel debris must comply with design basis characteristics

listed in Table 2.1.7 to allow storage in the MPC-68 and MPC-68F, respectively. Each basket design must comply with the applicable temperature limits for normal, off-normal and accident conditions under the imposed heat generation loads from stored fuel assemblies.

The design basis intact PWR and BWR decay heat per assembly and the MPC total decay heat load for the two basket configurations (i.e., MPC-24, and MPC-68) are stated in Tables 2.1.6 and 1.2.2, respectively. Table 2.1.7 lists the design basis thermal requirements for damaged fuel assemblies. Table 2.1.11 lists the design basis thermal requirements for stainless steel clad fuel assemblies for storage in the MPC-24 or MPC-68. The HI-STAR 100 System consisting of the overpack and MPCs under normal storage conditions at an ISFSI pad is conservatively analyzed for the limiting design basis heat loads.

Thermal analysis of the HI-STAR 100 System is based on including all three fundamental modes of heat transfer: conduction, natural convection and radiation. Different combinations of these modes are active in different regions of the system. These modes are properly identified and conservatively analyzed within each region of the MPC and overpack to enable bounding calculations of the temperature distribution within the HI-STAR 100 System.

On the outside surface of the overpack, heat is dissipated to the environment by buoyancy induced convective air flow (natural convection) and thermal radiation. In the overpack internal metal structure, only conductive heat transport is possible. Between metal surfaces (e.g., between neighboring fuel rod surfaces) heat transport is due to a combination of conduction through a gaseous medium (helium) and thermal radiation. The heat transfer between the fuel basket external surface and the MPC shell's inner surface is further influenced by the so-called "Rayleigh" effect. However, in the interest of conservatism, the most potent heat transport mechanism, the buoyancy induced thermosiphon which occurs within the MPC basket (aided by the MPC design which provides low pressure drop helium flow recirculation loops formed by the fuel cells, top plenum, downcomers and bottom plenum) is neglected.

The total heat generation in each assembly is non-uniformly distributed over the active fuel length to account for the design basis fuel burnup distribution listed in Chapter 2 (Table 2.1.8). As discussed later in this chapter (Subsection 4.4.6), an array of conservative assumptions bias the results of the thermal analysis towards much reduced computed margins than would be obtained by a rigorous analysis of the problem.

The complete thermal analysis is performed using the industry standard ANSYS finite element modeling package [4.1.1] and the finite volume Computational Fluid Dynamics (CFD) code FLUENT [4.1.2]. ANSYS has been previously used and accepted by the NRC on numerous dockets [4.1.3, 4.V.5.a]. The FLUENT CFD program is independently benchmarked and validated with a wide class of theoretical and experimental studies reported in the technical journals. Additionally, Holtec has confirmed the code's capability to reliably predict temperature

fields in dry storage applications using independent full-scale test data from a loaded cask [4.1.4]. This study concluded that FLUENT can be used to model all modes of heat transfer, namely, conduction, convection, and radiation in dry cask systems.

4.2 SUMMARY OF THERMAL PROPERTIES OF MATERIALS

Materials used in the HI-STAR 100 System include stainless steels (Alloy X), carbon steels, Holtite-A neutron shield, Boral neutron absorber, aluminum alloy 1100 heat conduction elements, and helium. In Table 4.2.1, a summary of references used to obtain cask material properties for performing all thermal analyses is presented.

Thermal conductivities of the constituent Alloy X steels and the bounding Alloy X thermal conductivity are reported in Appendix 1.A of this report. Tables 4.2.2, 4.2.3 and 4.2.9 provide numerical thermal conductivity data of materials at several representative temperatures. Table 4.2.8 lists the thermal properties of Boral components (i.e., B₄C core and aluminum cladding materials). Surface emissivity data for key materials of construction is provided in Table 4.2.4.

The emissivity properties of painted external cask surfaces are generally excellent. Kern [4.2.5] reports an emissivity range of 0.8 to 0.98 for a wide variety of paints. In the HI-STAR 100 thermal analysis, an emissivity of 0.85[†] is applied to external painted surfaces. A conservative solar absorptivity coefficient of 1.0 is applied to all exposed cask surfaces.

In Table 4.2.5, the heat capacity and density of different cask materials are presented. These properties are used in performing transient (i.e., hypothetical fire accident condition) analyses. Table 4.2.6 provides viscosity data on the helium gas.

The overpack outside surface heat transfer coefficient is calculated by accounting for both natural convection heat transfer and radiation. The natural convection coefficient depends upon the product of Grashof (Gr) and Prandtl (Pr) numbers. Following the approach developed by Jakob and Hawkins [4.2.9], the product Gr×Pr is expressed as $L^3 \Delta T Z$, where L is the height of the cask, ΔT is the overpack surface-to-ambient temperature differential and Z is a parameter which depends upon air properties (which are known functions of temperature) evaluated at the average film temperature. The temperature dependence of Z for air is provided in Table 4.2.7.

[†] This is conservative with respect to prior cask industry practice, which has historically accepted higher emissivities. For example, a higher emissivity for painted surfaces ($\epsilon = 0.95$) is used in the TN-32 cask TSAR (Docket 72-1021).

Table 4.2.1

SUMMARY OF HI-STAR 100 SYSTEM MATERIALS
THERMAL PROPERTY REFERENCES

Material	Emissivity	Conductivity	Density	Heat Capacity
Helium	N/A	Handbook [4.2.2]	Ideal Gas Law	Handbook [4.2.2]
Air	N/A	Handbook [4.2.2]	Ideal Gas Law	Handbook [4.2.2]
Zircaloy	EPRI [4.2.3]	NUREG [4.2.6], [4.2.7]	Rust [4.2.4]	Rust [4.2.4]
UO ₂	Not Used	NUREG [4.2.6], [4.2.7]	Rust [4.2.4]	Rust [4.2.4]
Stainless steel	Kern [4.2.5]	ASME [4.2.8]	Marks [4.2.1]	Marks [4.2.1]
Carbon steel	Kern [4.2.5]	ASME [4.2.8]	Marks [4.2.1]	Marks [4.2.1]
Aluminum Alloy 1100 (Heat Conduction Elements)	Handbook [4.2.2]	ASME [4.2.8]	ASME [4.2.8]	ASME [4.2.8]
Boral†	Not Used	Test Data	Test Data	Test Data
Holtite-A‡	Not Used	Test Data	Test Data	Test Data

† AAR Structures Boral thermophysical test data.

‡ From neutron shield manufacturer's data (Appendix 1.B).

Table 4.2.2

SUMMARY OF HI-STAR 100 SYSTEM MATERIALS THERMAL
CONDUCTIVITY DATA

Material	@ 200°F (Btu/ft-hr-°F)	@ 450°F (Btu/ft-hr-°F)	@ 700°F (Btu/ft-hr-°F)
Helium	0.0976	0.1289	0.1575
Air	0.0173	0.0225	0.0272
Alloy X	8.4	9.8	11.0
Carbon Steel Radial Connectors	29.2	27.1	24.6
Carbon Steel Gamma Shield Layers	24.4	23.9	22.4
Holtite-A [†]	0.373	0.373	0.373
Cryogenic Steel	23.8	23.7	22.3

[†] No credit taken for conduction through Holtite-A for the steady-state analysis. Before and after fire conditions for fire accident analysis (i.e., the conductivity is conservatively set equal to zero). A conductivity of 1.0 Btu/ft-hr-°F is conservatively applied during fire condition.

Table 4.2.3

SUMMARY OF FUEL ELEMENT COMPONENTS THERMAL
CONDUCTIVITY DATA

Zircaloy Cladding		Fuel (UO ₂)	
Temperature (°F)	Conductivity (Btu/ft-hr-°F)	Temperature (°F)	Conductivity (Btu/ft-hr-°F)
392	8.28 [§]	100	3.48
572	8.76	448	3.48
752	9.60	570	3.24
932	10.44	793	2.28 ^{**}

§ Lowest value of conductivity is used in the thermal analysis for conservatism.

Table 4.2.4

SUMMARY OF MATERIALS SURFACE EMISSIVITY DATA

Material	Emissivity
Zircaloy cladding	0.80
Painted surfaces	0.85
Rolled carbon steel	0.66
Stainless steel	0.36
Sandblasted aluminum	0.40

Table 4.2.5

MATERIALS DENSITY AND HEAT CAPACITY PROPERTIES SUMMARY

Material	Density (lbm/ft³)	Heat Capacity (Btu/lbm-°F)
Helium	(Ideal Gas Law)	1.24
Zircaloy cladding	409	0.0728
Fuel (UO ₂)	684	0.056
Carbon steel	489	0.1
Stainless steel	501	0.12
Boral	154.7	0.13
Aluminum Alloy 1100	169.9	0.23
Holtite-A	105.0	0.39

Table 4.2.6

HELIUM GAS VISCOSITY^{††} VARIATION WITH TEMPERATURE

Temperature (°F)	Viscosity (Micropoise)
167.4	220.5
200.3	228.2
297.4	250.6
346.9	261.8
463.0	288.7
537.8	299.8
737.6	338.8

†† Obtained from Rohsenow and Hartnett [4.2.2].

Table 4.2.7

VARIATION OF NATURAL CONVECTION PROPERTIES
PARAMETER "Z" FOR AIR WITH TEMPERATURE††

Temperature, (°F)	Z (ft ⁻³ °F ⁻¹)
40	2.1x10 ⁶
140	9.0x10 ⁵
240	4.6x10 ⁵
340	2.6x10 ⁵
440	1.5x10 ⁵

†† Obtained from Jakob and Hawkins [4.2.9]

Table 4.2.8

BORAL COMPONENT MATERIALS[†]
THERMAL CONDUCTIVITY DATA

Temperature (°F)	B ₄ C Core Conductivity (Btu/ft-hr-°F)	Aluminum Cladding Conductivity (Btu/ft-hr-°F)
212	48.09	100.00
392	48.03	104.51
572	47.28	108.04
752	46.35	109.43

[†] Both B₄C and aluminum cladding thermal conductivity values are obtained from AAR Structures Boral thermophysical test data.

Table 4.2.9

HEAT CONDUCTION ELEMENTS (ALUMINUM ALLOY 1100)
THERMAL CONDUCTIVITY DATA

Temperature (°F)	Conductivity (Btu/ft-hr-°F)
100	131.8
200	128.5
300	126.2
400	124.5

4.3 SPECIFICATIONS FOR COMPONENTS

HI-STAR 100 System materials and components designated as "Important to Safety" (i.e., required to be maintained within their safe operating temperature ranges to ensure their intended function) which warrant special attention are summarized in Table 4.3.1. Long-term stability and continued neutron shielding ability of Holtite-A neutron shield material under normal storage conditions are ensured when material exposure temperatures are maintained below the maximum allowable limit. The integrity of the overpack helium retention boundary is assured by maintaining the temperature of the mechanical seals within the manufacturer's recommended operating temperature limits. Long-term integrity of SNF is ensured by the HI-STAR 100 System thermal performance, which demonstrates that fuel cladding temperatures are maintained below design basis limits. Boral used in MPC baskets for criticality control (a composite material composed of B₄C and aluminum) is stable up to 1000°F for short-term and 850°F for long-term dry storage[†]. However, for conservatism, a significantly lower maximum temperature limit is imposed.

Compliance to 10CFR72 requires, in part, identification and evaluation of short-term off-normal and severe hypothetical accident conditions. The inherent mechanical stability characteristics of cask materials and components ensure that no significant functional degradation is possible due to exposure to short-term temperature excursions outside the normal long-term temperature limits. For evaluation of HI-STAR 100 System thermal performance under off-normal or hypothetical accident conditions, material temperature limits for short-duration events are provided in Table 4.3.1.

Demonstration of fuel cladding integrity against the potential for degradation and gross rupture throughout the entire dry cask storage period is mandated by the Code of Federal Regulations (Part 72, Section 72.72(h)). The specific criteria required to demonstrate fuel cladding integrity is set forth in the NUREG-1536 document as listed below.

- A. The dry cask storage system shall ensure a less than 0.5 percent probability of cladding failure during long-term storage.
- B. Fuel cladding damage shall be limited to 15% of the original cladding cross section.

Several potential damage mechanisms for zircaloy clad fuel have been discussed by Schwartz and Witte [4.3.6] and Levy et al. [4.3.1]. These mechanisms are listed below:

- i. stress corrosion cracking
- ii. hydriding
- iii. creep induced stress rupture
- iv. Diffusion Controlled Cavity Growth (DCCG)

[†] AAR Structures Boral thermophysical test data.

Out of the four potential damage mechanisms listed above, two mechanisms, namely creep-induced stress rupture [4.3.1] and DCCG [4.3.6], are the controlling mechanisms established for zircaloy cladding life prediction during dry storage of spent nuclear fuel. Pacific Northwest Laboratory (PNL) has established a Commercial Spent Fuel Management (CSFM) model based on creep rupture data for zircaloy [4.3.1]. The CSFM model enables a cask designer to determine fuel-specific maximum initial peak cladding temperature limits. The zircaloy cladding temperature limit established using the generic CSFM Inerted Dry Storage (IDS) temperature limit curves [4.3.1] meets the NUREG-1536 Criterion (A) discussed earlier in this section. This requires a less than 0.5% probability of rods rupture during the entire storage life (assumed to equal 40 years) against creep rupture mode of local cladding damage, which may result in pinhole or through-cladding cracks during dry storage.

The DCCG mode of cladding damage is concluded in the above-mentioned Schwarz et al., report to be the only mechanism which may result in gross cladding damage [4.3.6]. This mode of cladding damage manifests itself as a sudden non-ductile type of fracture. NUREG-1536 (Criterion (B), discussed earlier in this section), requires that the total damage from the DCCG mode of degradation be limited to 15% of the original cladding cross sectional area during the entire dry storage period.

In accordance with the NUREG-1536 criteria, the HI-STAR 100 storage system is designed to preclude *both* local and gross fuel cladding failures during the entire duration of storage. Initial maximum peak cladding temperature limits are determined using the CSFM IDS temperature limit curves to preclude local cladding failure [4.3.1] and the LLNL methodology to preclude gross cladding failure [4.3.6]. A discussion on the application of the PNL and LLNL methodologies in establishing the HI-STAR system specific fuel types cladding temperature limits criteria is provided in the balance of this section.

The generic CSFM IDS temperature limit curves [4.3.1] define the maximum allowable initial storage temperature at initial cladding stresses as a function of fuel age. Therefore, for SNF of a given age (decay time), the permissible peak cladding temperature is a direct function of the cladding hoop stress, which in turn depends on the radius-to-thickness ratio of the fuel rod and its internal pressure. The rod internal pressure P_i is calculated based upon the maximum initial fill pressures (Tables 4.3.2 and 4.3.5) with fission gas release at a conservatively bounding maximum burnup under HI-STAR 100 System storage conditions (40,000 MWD/MTU for BWR fuel and 42,500 MWD/MTU for PWR fuel). The free rod volumes in the third column of Tables 4.3.2 and 4.3.5 are defined as free rod volumes, in each fuel rod, available for pressurization with fill gas. The free rod volume is the cumulative sum of the open top plenum space, the pellet-to-cladding annular space and the inter-pellet junction space. As a lower bound value of the free rod volume will lead to a conservative estimate of the cladding stress at operating temperatures, the nominal gas plenum space is included in the free rod volume. The plenum length for miscellaneous BWR fuel assemblies is set to 12 inches. The fission gas release fraction data is based on Regulatory Guide 1.25 (Table 4.3.4). The radius-to-thickness ratio r^* is determined based on rod nominal dimension values (Tables 4.3.3 and 4.3.6) including the maximum cladding thickness loss due to

in-reactor oxidation, as reported in the PNL study [4.3.4].

By utilizing P_i and r^* , the cladding stress for various PWR fuel types is calculated from Lamé's formula and summarized in Table 4.3.3. It can be seen from Figure 4.4.21 that the average temperature of the gas in the fuel rods, a great bulk of which is located in the top region of the SNF, is well below 300°C for the PWR fuel array types. Therefore, to compute the cladding hoop stress in a conservative manner, the ideal gas law is used to obtain the value of the in-rod gas pressure at 300°C. An inspection of cladding stress data summarized in Table 4.3.3 indicates 96.7 MPa is the bounding value of cladding stress (σ_{\max}) for the PWR SNF. Corresponding fill gas data and calculations of cladding stress for the various BWR SNF types are summarized in Tables 4.3.5 and 4.3.6, respectively. It can be seen from Figure 4.4.22 that the average temperature of gas in the fuel rods, a great bulk of which is located in the top region of the SNF, is well below 300°C for *all* BWR fuel array types considered in this topical report. Therefore, to compute the cladding hoop stress in a conservative manner, the ideal gas law is used to obtain the value of the in-rod gas pressure at 300°C. An inspection of the cladding stress data in Table 4.3.6 indicates that the bounding value of the cladding hoop stress for all SNF types is 54.7 MPa (except for 8x8 GE Dresden-1 and 6x6 GE Humboldt Bay fuel types).

The bounding values of σ_{\max} for the array of PWR and BWR SNF types are thus 96.7 MPa and 54.7 MPa, respectively (except for 8x8 GE Dresden-1 and 6x6 GE Humboldt Bay fuel assembly types for which the bounding value of σ_{\max} is 59.1 MPa).

Several implicit assumptions in the calculation of σ_{\max} , such as neglect of the rod cavity growth due to thermal expansion, internal fill pressure, and in-core irradiation, ensure that the hoop stress value (which is the sole determinant in the establishment of permissible cladding temperature for a given cooling time) is indeed a bounding number.

The generic CSFM IDS temperature limit curves developed in the PNL study [4.3.1] are used to determine zircaloy cladding temperature limits at the conservative 300°C average rod temperature. The fuel cladding temperature limits obtained from these PNL curves ensure a low failure probability for rods (less than 0.5% over the 40-year dry storage life).

The value of σ_{\max} is also required to establish the peak cladding temperature limit using the DCCG method, which we discuss in the following. The DCCG model-based zircaloy cladding temperature limit computation, in accordance with the LLNL procedure [4.3.6], requires a solution to the following equation expressed in terms of the area fraction of de-cohesion (A):

$$\int_{A_i}^{A_f} \frac{dA}{f(A)} = \int_{t_0}^{t_0 + t_s} G(t) dt$$

where:

- A_i = initial area fraction of de-cohesion
 A_f = end of storage life area fraction of de-cohesion (limited to 0.15)
 t_o = age of fuel prior to dry cask storage
 t_s = dry cask storage period (40 years)
 $f(A)$ = area fraction of de-cohesion function

$$f(A) = \frac{[1 - (\frac{A_i}{A})^{1/2}] (1 - A)}{A^{1/2} [\frac{1}{2} \ell n \frac{1}{A} - \frac{3}{4} + A (1 - \frac{A}{4})]}$$

$$G(t) = \frac{32}{3\pi^{1/2}} \frac{F_b^{3/2}(\alpha)}{F_v(\alpha)} \frac{\Omega \delta \sigma_\infty(t)}{K \lambda^3} \frac{D_{GB} [T(t)]}{T(t)}$$

$$F_B(\nabla) = \pi \sin^2(\alpha)$$

$$F_v(\nabla) = \frac{2\pi}{3} (2 - 3 \cos \alpha + \cos^3 \alpha)$$

T = time-dependent peak cladding temperature

K = Boltzmann constant (1.38053×10^{-23} J/K)

A discussion on the balance of parameters in the $G(t)$ damage function is provided below.

Cladding Hoop Stress ($\sigma_\infty(t)$)

The cladding hoop stress is principally dependent upon the specific fuel rod dimensions, initial fill rod pressure, time-dependent storage temperature, and fuel burnup dependent fission gas release from the fuel pellets into the rod plenum space. The peak fuel rod pressure for various PWR and BWR fuel types at the start of the dry storage period are summarized in Tables 4.3.3 and 4.3.6. The highest peak rod stress among the various PWR fuel types and a bounding peak rod stress for BWR fuel are applied as constant (time-independent) cladding hoop stresses in the DCCG model-based damage function.

Grain Boundary Cavity Dihedral Angle (α)

The LLNL report [4.3.6] has determined the dihedral angle (α) for pure metals to be 75° . To account for possible non-ideal conditions, a conservatively lower α equal to 60° is applied to the DCCG model.

Zirconium Atomic Volume (Ω)

The zirconium atomic volume estimated from several literature sources as documented in the LLNL report [4.3.6] is in the range of $2.31 \times 10^{-29} \text{ m}^3$ to $3.37 \times 10^{-29} \text{ m}^3$. In the interest of conservatism, the *maximum* estimated atomic volume equal to $3.37 \times 10^{-29} \text{ m}^3$ is used for the analysis.

Grain Boundary Thickness (δ)

The LLNL report [4.3.6] has recommended a grain boundary thickness of three Burgers vectors to be adequate for the analysis. Thus, $\delta = 3 (3.23 \times 10^{-10}) = 9.69 \times 10^{-10} \text{ m}$ is used in the analysis.

Average Cavity Spacing (λ)

Cavity spacing is controlled by the type of nucleation mechanism and the density of nucleation sites. The LLNL report [4.3.6] references an experimental study which found that the cavity spacing is in the range of 10×10^{-6} to $20 \times 10^{-6} \text{ m}$. In the interest of conservatism, the *minimum* reported cavity spacing equal to $10 \times 10^{-6} \text{ m}$ is used in the analysis.

Grain Boundary Diffusion Rate (D_{GB})

Two grain boundary diffusion rate correlations for zirconium are reported in the LLNL report [4.3.6]. The two correlations provide diffusion rate estimates which are approximately two orders of magnitude apart from each other. Consequently, the more conservative correlation (i.e., $D_{gb} = 5.9 \times 10^{-6} \exp [-131,000/RT] \text{ m}^2/\text{s}$) which provides a higher estimate of the grain boundary diffusion rate is used in the analysis.

Time-Dependent Peak Cladding Temperature (T)

The steady state peak cladding temperature during long-term storage is principally dependent upon the thermal heat load from the stored fuel assemblies which is imposed on the cask. It is well established that the rate of radioactive decay in a fuel assembly exponentially attenuates with the age of fuel. Consequently, the peak cladding temperature during long-term storage will also attenuate rapidly as a direct consequence of the heat load reduction with time. In recognition of this anticipated decaying cask temperature response, the PNL report [4.3.1] recommends a uni-modal power law type decaying temperature model of the form $T = T_0 t^\gamma$. In the DCCG analysis, an improved multi-modal exponentially attenuating decay heat model based on the *Branch*

Technical Position Paper ASB 9-2 is used. Thus, the form of the decaying temperature model is expressed as:

$$T = \frac{\sum_{K=0}^{10} A_K \exp(-a_k t)}{\sum_{K=0}^{10} A_K \exp(-a_k t_0)} [(T_0 - T_a)] + T_a$$

where:

$A_0 = 0.5980$	$a_0 = 1.772$
$A_1 = 1.65$	$a_1 = 5.774 \times 10^{-1}$
$A_2 = 3.1$	$a_2 = 6.743 \times 10^{-2}$
$A_3 = 3.87$	$a_3 = 6.214 \times 10^{-3}$
$A_4 = 2.33$	$a_4 = 4.739 \times 10^{-4}$
$A_5 = 1.29$	$a_5 = 4.810 \times 10^{-5}$
$A_6 = 0.462$	$a_6 = 5.344 \times 10^{-6}$
$A_7 = 0.328$	$a_7 = 5.716 \times 10^{-7}$
$A_8 = 0.17$	$a_8 = 1.036 \times 10^{-7}$
$A_9 = 0.0865$	$a_9 = 2.959 \times 10^{-8}$
$A_{10} = 0.1140$	$a_{10} = 7.585 \times 10^{-10}$

$t =$ time after reactor discharge (s)

$t_0 =$ initial age of fuel at start of storage (s)

$T_0 =$ initial peak cladding temperature limit ($^{\circ}\text{K}$)

$T_a =$ ambient temperature ($^{\circ}\text{K}$)

It should be noted that the area fraction of de-cohesion function $f(A)$ approaches zero in the

limit as $A \rightarrow A_i$. Consequently, the mathematical singularity in the integral $\int_{A_i}^A \frac{dA}{f(A)}$ is

numerically accommodated by using an alternate form given below:

$$\int_{A_i}^A \frac{dA}{f(A)} = \text{Limit } \varepsilon \rightarrow 0 \int_{A_i+\varepsilon}^{A_f} \frac{A^{1/2} \left[\frac{1}{2} \ln \frac{1}{A} - \frac{3}{4} + A \left(1 - \frac{A}{4} \right) \right] dA}{\left[1 - \left(\frac{A_i}{A} \right) \right]^{1/2} (1-A)}$$

The allowable area fraction of de-cohesion using $A_i = 0.05$, $\varepsilon = 0.0001$, and $A_f = 0.15$ is determined to be equal to 0.15211. This is consistent with an alternate form of the DCCG model reported in the PNL study [4.3.1, Appendix D] as reproduced below:

$$A_f = \int_0^{t_f} G(t) dt \leq 0.15$$

All parameters in the G(t) function (except for the initial peak cladding temperature limit T_o), have been defined as discussed previously in this section. The cumulative cladding damage experienced during the proposed 40-year dry cask storage period is determined by integrating the G(t) function. The initial peak cladding temperature limit parameter T_o is iteratively adjusted to limit the cumulative damage to 15% as required by the NUREG-1536 Criterion (B) discussed earlier in this section. The initial peak cladding temperature limit for 5-year old fuel is determined to be 388.5°C (731°F) and 405.4°C (762°F) for the bounding PWR and BWR fuel assemblies (except for 8x8 GE Dresden-1, 6x6 Dresden 1, 6x6 Humboldt Bay, and Quad⁺ fuel types), respectively. The temperature limits are slightly higher than the respective temperature limits determined from the generic CSFM IDS temperature limit curves [4.3.1]. Consequently, the more conservative peak cladding temperature limits obtained from the generic CSFM IDS temperature limit curves are applied to the HI-STAR 100 System thermal analysis for long-term storage.

4.3.1 Evaluation of Stainless Steel Clad Fuel

Approximately 2,200 PWR and BWR fuel assemblies stored in the United States employ stainless steel cladding. All stainless steel cladding materials are of the austenitic genre with the ASTM alloy compositions being principally type 304 and 348H. The long-term storage condition peak allowable temperature applicable to stainless steel fuel is significantly higher than that applicable to zircaloy clad fuel. A recent EPRI/PNL study [4.3.5] recommends a 430°C (806°F) peak stainless steel cladding temperature limit versus a typical 380°C (716°F) [4.3.1] peak zircaloy cladding temperature limit. Since the peak cladding temperature limits applied to the thermal analysis herein for both zircaloy clad and stainless steel clad fuel are based on the zircaloy clad limit, it is readily apparent that the PNL criteria [4.3.1] is overly restrictive for stainless steel clad fuel. The peak cladding temperature limits applied to both zircaloy and stainless steel clad fuel assemblies are provided in Table 4.3.1.

It is recognized that the peak cladding temperature of stainless fuel will differ from zircaloy clad fuel principally due to the following differences:

- i. Differences in decay heat levels
- ii. Differences in cladding emissivity
- iii. Differences in cladding conductivity
- iv. Differences in fuel rod array dimensions

The net planar thermal resistance of the equivalent homogenized axisymmetric MPC basket containing stainless steel clad fuel is greater than that with zircaloy clad fuel. The higher resistance arises principally from the significantly lower emissivity of the stainless steel cladding. This factor is, however, offset by significantly lower design basis heat loads prescribed for a HI-STAR 100 System containing stainless steel clad fuel. A 20% reduction in the design basis heat duty for

stainless steel fuel (20% lower than zircaloy clad fuel) bounds the nominal percentage decrease in MPC basket effective thermal conductivity[†] (stainless steel fueled baskets are between 9% (MPC-68) to 13% (MPC-24) less conducting, as shown in Table 4.4.7). As can be seen by comparing the design basis maximum allowable decay heat loads for zircaloy clad (Tables 4.4.18 and 4.4.19) and stainless steel clad (Table 2.1.11) fuel assemblies, the allowable assembly decay heat load for stainless steel clad fuel is approximately 73% of the PWR zircaloy clad fuel heat load and 35% of the BWR zircaloy clad fuel heat load. Therefore, it is concluded that the peak cladding temperature for stainless steel clad fuel will be bounded by zircaloy clad fuel results. Consequently, in view of significantly higher peak stainless steel cladding temperature limits recommended by the EPRI study [4.3.5] and the conservative heat loads prescribed for stainless steel clad fuel, a separate thermal analysis to demonstrate the adequacy of stainless steel clad integrity for storage in the HI-STAR 100 System is not necessary.

4.3.2 Short-Term Cladding Temperature Limit

For short-term durations, relatively high fuel cladding temperature limits have been historically accepted by the USNRC. For example, the Safety Analysis Report of the STC transport cask (Docket No. 71-9235), recently certified by the USNRC, permits 1200°F (approximately 649°C) as the maximum value of the peak cladding temperature (T_{max}) for transport of SNF with up to 45,000 MWD/MTU burnup. NUREG-1536 and PNL test data [4.3.4], limiting themselves to medium burnup levels (28,800 MWD/MTU), endorse a somewhat lower T_{max} value ($T_{max} = 570^{\circ}\text{C}$ or 1058°F). Based on the published industry test data, guidance in the literature, and analytical reasoning, we herein prescribe 570°C as the admissible value of T_{max} for the SNF for the relatively lower burnup levels in the HI-STAR 100 System for storage[†].

A Brookhaven report written for EPRI [4.3.7] asserts that fuel cladding rupture becomes "virtually absent at stresses below about 200 MPa". It can be readily deduced that the peak cladding stress for the limiting condition of 570°C cladding temperature will be below 200 MPa for the SNF burnup levels considered in this FSAR. Recalling σ_{max} at 96.7 MPa (Table 4.3.3) at 300°C gas temperature, the cladding circumferential stress (σ_{peak}) at 570°C is obtained by direct proportionality in absolute gas temperature:

$$\sigma_{peak} = \sigma_{max} (570 + 273)/(300 + 273) = 142.3 \text{ MPa (approximately 20,600 psi)}$$

[†] The term "effective conductivity" of the fuel basket is defined in Section 4.4.1.

[†] 40,000 MWD/MTU for BWR fuel and 42,500 MWD/MTU for PWR fuel bounds permissible maximum burnups.

Therefore, short-term temperature values (T_{\max}) of 570°C are considered safe to preclude fuel cladding failure.

The EPRI report cites experiments on fourteen irradiated Turkey Point Unit 3 rods carried out by Einziger et al.^{††} in 1982 which showed no breach in cladding even after as much as 7% strain was accumulated in elevated temperatures lasting for 740-1,000 hours. Einziger's test data corroborates our selection of $T_{\max} = 570^{\circ}\text{C}$ as the short duration limiting temperature.

^{††} "High Temperature Post Irradiation Materials Performance of Spent Pressurized Water Reactor Fuel Rods under Dry Storage Conditions," by R.E. Einziger, S.D. Atkin, D.E. Stallrecht, and V.S. Pasupathi, Nuclear Technology, 57:65-80 (1982).

Table 4.3.1

HI-STAR 100 SYSTEM MATERIAL TEMPERATURE [°F] LIMITS

Material	Normal Long-Term Temperature Limits	Short-Term Temperature Limits
Fuel cladding (zircaloy and stainless steel)	See Table 4.3.7	1058
Boral [†]	800	950
Overpack closure plate mechanical seal, vent and drain port plug seals	See Table 2.2.3	See Table 2.2.3
Holtite-A ^{††}	300	300

† Based on AAR Structures Boral thermophysical test data.

†† Neutron shield manufacturer's test data (Appendix 1.B).

Table 4.3.2

SUMMARY OF PWR ASSEMBLY RODS INITIAL GAS FILL DATA

Assembly Type	Rods Per Assembly	Free Rod Volume (in. ³)	Fill Pressure (psig) at 70°F	Fill Gas Volume at STP†	
				(Liters) Per Rod	(Liters) Per Assembly
W-14x14 Std.	179	1.72	0-460	0.845	151.2
W-15x15 Std.	204	1.25	0-475	0.633	129.1
W-17x17 Std.	264	1.05-1.25	275-500	0.666	175.8
B&W-15x15 Mark B	208	1.308	415	0.582	121.1
B&W-17x17 Mark C	264	0.819	435	0.381	100.6
CE-14x14 Std.	164	1.693	300-450	0.814	133.5
CE-16x16 Std.	220	1.411	300-450	0.678	149.2
B&W-15x15 Mark B-11	208	1.260	415	0.560	116.5
CE-14x14 (MP2)	176	1.728	300-450	0.831	146.2

† STP stands for standard temperature (°C) and pressure (1 atmosphere).

Table 4.3.3
 BOUNDING VALUES OF FUEL CLADDING STRESS FOR PWR SNF

	W-14X14 Std	W-15x15 Std	W-17x17 Std	B&W-15x15 Mark B	B&W-17x17 Mark C	CE-14x14 Std	CE-16x16 Sys 80	B&W-15x15 Mark B-11	CE-14x14 (MP2)
Fresh Fuel Rods O.D. (inch)	0.4220	0.422	0.374	0.430	0.379	0.440	0.382	0.414	0.440
End of Life Oxidation Thickness (inch) [†]	0.0027	0.0027	0.0027	0.0027	0.0027	0.0027	0.0027	0.0027	0.0027
End of Life Rods O.D. (inch)	0.4166	0.4166	0.3686	0.4246	0.3736	0.4346	0.3766	0.4086	0.4346
Rods I.D. (inch)	0.3734	0.373	0.329	0.377	0.331	0.384	0.332	0.370	0.388
Average tube Diameter (inch)	0.3950	0.3948	0.3488	0.4008	0.3523	0.4093	0.3493	0.3893	0.4113
Wall Thickness (inch)	0.0216	0.0218	0.0198	0.0238	0.0213	0.0253	0.0223	0.0193	0.0233
Hot Volume Pressure at 300°C (MPa) ^{††}	9.77	10.67	10.08	9.62	10.87	10.01	9.61	9.76	9.67
Cladding Stress (MPa)	89.3	96.7	88.8	81.0	90.0	81.0	75.2	98.4	85.3

† PNL-4835 [4.3.4] reported maximum cladding thickness loss due to in-reactor oxidation.

†† This average rod gas temperature conservatively bounds the plenum gas temperature, which, as can be seen from Figure 4.4.21, is approximately 225°C. The cladding stresses reported in the bottom row of this table will be accordingly reduced by the factor $(225+273)/(300+273) = 0.87$. However, 96.7 MPa cladding stress for PWR SNF is used as the upper bound value in this FSAR.

Table 4.3.4

SUMMARY OF FISSION GASES RELEASE PER ASSEMBLY[†]

Component	Release ^{††} Fraction	Release Amount (g-moles/ PWR assembly)	Release Amount (g-moles/ BWR assembly)
Tritium	0.3	0.004	0.003
⁸⁵ Kr	0.3	0.805	0.297
¹²⁹ I	0.12	0.137	0.050
¹³¹ Xe	0.10	2.664	0.985

[†] Bounding for 42,500 MWD/MTU burnup PWR assemblies and 40,000 MWD/MTU burnup BWR assemblies.

^{††} From Regulatory Guide 1.25.

Table 4.3.5
SUMMARY OF BWR ASSEMBLY RODS INITIAL GAS FILL DATA

Assembly Type	Rods/ Assembly	Free Rod Volume (in ³)	Fill Pressure (psig) at 70°F	Fill Gas Volume at STP	
				(liters) Per Rod	(liters) Per Assembly
GE-7x7 (1966)	49	2.073	0-44.1 [†]	0.126	6.17
GE-7x7 (1968)	49	2.073	0-44.1	0.126	6.17
GE-7x7R	49	1.991	0-44.1	0.121	5.93
GE-8x8	60	1.504	0-44.1	0.0915	5.49
GE-8x8R	60	1.433	0-147 ^{††}	0.240	14.4
EXXON-9x9	79	1.323	58.8-88.2 ^{†††}	0.141	11.1
6x6 GE Dresden-1	36	2.304	58.8-88.2	0.245	8.82
6x6 Dresden-1 MOX	36	2.286	58.8-88.2	0.243	8.75
6x6 GE Humboldt Bay	36	2.346	58.8-88.2	0.250	9.0
7x7 GE Humboldt Bay	49	1.666	58.8-88.2	0.177	8.67
8x8 GE Dresden-1	64	1.235	58.8-88.2	0.131	8.38
8x8 SPC	63	1.615	58.8-88.2	0.172	10.8
9x9 SPC-2 wtr. Rods	79	1.248	58.8-88.2	0.133	10.5
9x9 SPC-1 wtr. Rod	80	1.248	58.8-88.2	0.133	10.6
9x9 GE11/GE13	74	1.389	58.8-88.2	0.150	11.1
9x9 Atrium 9B SPC	72	1.366	58.8-88.2	0.145	10.4
10x10 SVEA-96	96	1.022	58.8-88.2	0.109	10.5
10x10 GE12	92	1.167	58.8-88.2	0.124	11.4
6x6 Dresden Thin Clad	36	2.455	58.8-88.2	0.261	9.4
7x7 Oyster Creek	49	2.346	58.8-88.2	0.250	12.2
8x8 Oyster Creek	64	1.739	58.8-88.2	0.185	11.8
8x8 Quad [†] Westinghouse	64	1.201	58.8-88.2	0.128	8.2
8x8 TVA Browns Ferry	61	1.686	58.8-88.2	0.179	10.9
9x9 SPC-5	76	1.249	58.8-88.2	0.133	10.1

[†] Conservatively bounding for GE-7x7 (1966), GE-7x7 (1968), GE-7x7R and GE-8x8 (ORNL/TM-9591/V1-R1).

^{††} Conservatively bounding initial fill pressure. ORNL/TM-9591/V1-R1 reports GE-8x8R prepressurized to 3 atm.

^{†††} BWR fuel rods internal pressurization between 4 to 6 atm (PNL-4835).

Table 4.3.6

BOUNDING VALUES OF FUEL CLADDING STRESS FOR BWR SNF

Fuel Type	Fresh Fuel Rod O.D. (inch)	End of Life Oxidation Thickness (inch)	End of Life Rods O.D. (inch)	Rods I.D. (inch)	Average Tube Diameter (inch)	Wall Thickness (inch)	Hot Volume Pressure at 300°C (MPa)	Cladding Stress (MPa)
GE-7x7 (1966)	0.563	0.0047	0.5536	0.499	0.5263	0.0273	4.61	44.4
GE-7x7 (1968)	0.570	0.0047	0.5606	0.499	0.5298	0.0308	4.61	39.6
GE-7x7R	0.563	0.0047	0.5536	0.489	0.5213	0.0323	4.76	38.4
GE-8x8	0.493	0.0047	0.4836	0.425	0.4543	0.0293	5.08	39.4
GE-8x8R	0.483	0.0047	0.4736	0.419	0.4463	0.0273	6.68	54.7
EXXON-9x9	0.42	0.0047	0.4106	0.36	0.3853	0.0253	5.08	38.7
6x6 GE Dresden-1	0.5645	0.0047	0.5551	0.4945	0.5248	0.0303	6.1	52.8
6x6 Dresden-1 MOX	0.5625	0.0047	0.5531	0.4925	0.5228	0.0303	6.1	52.8
6x6 GE Humboldt Bay	0.563	0.0047	0.5536	0.499	0.5263	0.0273	5.98	57.6 [†]
7x7 GE Humboldt Bay	0.486	0.0047	0.4766	0.4204	0.4485	0.0281	6.13	48.9
8x8 GE Dresden-1	0.412	0.0047	0.4026	0.362	0.3813	0.0203	6.29	59.1 [†]
8x8 SPC	0.484	0.0047	0.4746	0.414	0.4443	0.0303	5.19	38.0
9x9 SPC-2 wtr. Rods	0.424	0.0047	0.4146	0.364	0.3893	0.0253	5.32	40.9
9x9 SPC-1 wtr. Rod	0.423	0.0047	0.4136	0.364	0.3888	0.0248	5.25	41.1
9x9 GE11/GE13	0.44	0.0047	0.4306	0.384	0.4073	0.0233	5.17	45.2
9x9 Atrium 9B SPC	0.433	0.0047	0.4236	0.3808	0.4022	0.0214	5.32	50.0

[†] These two fuel types are separately analyzed for peak fuel cladding temperature limits.

Table 4.3.6 (continued)

BOUNDING VALUES OF FUEL CLADDING STRESS FOR BWR SNF

Fuel Type	Fresh Fuel Rod O.D. (inch)	End of Life Oxidation Thickness (inch)	End of Life Rods O.D. (inch)	Rods I.D. (inch)	Average Tube Diameter (inch)	Wall Thickness (inch)	Hot Volume Pressure at 300°C (MPa)	Cladding Stress (MPa)
10x10 SVEA-96	0.379	0.0047	0.3696	0.3294	0.3495	0.0201	4.38	38.1
10x10 GE12	0.404	0.0047	0.3946	0.352	0.3733	0.0213	4.99	43.7
6x6 Dresden Thin Clad	0.5625	0.0047	0.5531	0.5105	0.5318	0.0213	5.77	72.5†
7x7 Oyster Creek	0.5700	0.0047	0.5606	0.499	0.5298	0.0308	4.74	40.7
8x8 Oyster Creek	0.5015	0.0047	0.4921	0.4295	0.4608	0.0313	4.87	35.9
8x8 Quad ⁺ Westinghouse	0.4576	0.0047	0.4482	0.3996	0.4239	0.0243	6.42	56.0†
8x8 TVA Browns Ferry	0.483	0.0047	0.4736	0.423	0.4483	0.0253	5.14	45.5
9x9 SPC-5	0.417	0.0047	0.4076	0.364	0.3858	0.0218	5.46	48.3

† These fuel types are separately analyzed for peak fuel cladding temperature limits.

Table 4.3.7

INITIAL PEAK ZIRCALOY* CLADDING TEMPERATURE LIMITS FOR STORAGE

Fuel Age (years)	Temperature Limits for PWR SNF (°C) [°F]	Temperature Limits for Design Basis BWR SNF (except 8x8 GE Dresden-1, 6x6 Dresden 1, 6x6 GE Humboldt Bay, and Quad ⁺) (°C) [°F]	Temperature Limits for 8x8 GE Dresden- 1, 6x6 Dresden-1, 6x6 GE Humboldt Bay, and 8x8 Quad ⁺ SNF ^{††} (°C) [°F]
5	382.3 [720]	398.2 [749]	391.2 [736]
6	370.2 [698]	382.3 [720]	376.2 [709]
7	347.0 [657]	357.9 [676]	352.2 [666]
10	341.6 [647]	351.4 [665]	346.6 [656]
15	334.1 [633]	344.9 [653]	339.5 [643]

* The listed limits are conservatively applied to stainless steel clad fuel assemblies, which actually have substantially higher limits.

†† The 8x8 GE Dresden-1, 6x6 Dresden-1, Quad⁺ and 6x6 Humboldt Bay fuel types are low heat emitting assemblies. The Technical Specifications limit the heat load for these assemblies to 115 watts per assembly (approximately 58% lower than the design basis maximum heat load for BWR fuel (Table 4.4.19) (183.5 watts/assembly for Quad⁺). Consequently, these assembly types are not deemed to be limiting.

4.4 THERMAL EVALUATION FOR NORMAL CONDITIONS OF STORAGE

4.4.1 Thermal Model

The HI-STAR 100 MPC basket designs consist of two distinct geometries to hold 24 PWR or 68 BWR fuel assemblies. The basket is a matrix of square compartments (called boxes) to hold the fuel assemblies in a vertical position. The basket is a honeycomb structure of Alloy X plates with full-length edge-welded intersections to form an integral basket configuration. Individual cell walls (except outer periphery MPC-68 cell walls) are provided with Boral neutron absorber sandwiched between the box wall and a sheathing plate over the full length of the active fuel region.

The design basis decay heat generation (per PWR or BWR assembly) for long-term normal storage is specified in Table 2.1.6. The decay heat is conservatively considered to be non-uniformly distributed over the active fuel length based on the design basis axial burnup distribution provided in Chapter 2 (Table 2.1.8).

Transport of heat from the interior of the MPC basket to its outer periphery is accomplished by a combination of conduction through the MPC basket metal grid structure, conduction and radiation heat transfer in the relatively small helium gaps between the fuel assemblies and basket cell walls, and radiation and conduction from the fuel basket periphery to the MPC shell. Heat dissipation across the gap between the MPC basket periphery and the MPC shell is by a combination of helium conduction, natural convection (by means of the "Rayleigh" effect), radiation across the gap, and conduction in the aluminum alloy 1100 heat conduction elements. Between the MPC exterior and the overpack interior is a small clearance region which is evacuated and backfilled with helium. Helium, besides being inert, is a better heat conduction medium than air. Thus, heat conduction through the MPC/overpack helium gap will minimize temperature differentials across this region.

The overpack, under normal storage conditions, passively rejects heat to the outside environment. Cooling of the outside overpack vertical and horizontal (top) surfaces is by natural convection and thermal radiation. The bottom surface conducts heat through the ISFSI concrete pad to the ground. Analytical modeling details of the various thermal transport mechanisms are provided in the following.

4.4.1.1 Analytical Model - General Remarks

Transport of heat from the heat generation region (fuel assemblies) to the outside environment (ambient air or ground) is analyzed broadly in terms of three interdependent thermal models. The first model considers transport of heat from the fuel assembly to the basket cell walls. This model recognizes the combined effects of conduction (through helium) and radiation, and is essentially a finite element technology based update of the classical Wootton & Epstein [4.4.1] (which considered radiative heat exchange between fuel rod surfaces) formulation. The second model

considers heat transport within an MPC cross section by conduction and radiation. The effective cross sectional thermal conductivity of the basket and basket periphery regions, obtained from a combined fuel assembly/basket heat conduction-radiation model developed on ANSYS, are applied to an axisymmetric thermal model of the HI-STAR 100 System on the FLUENT [4.1.2] code. The third model deals with the transmission of heat from the MPC exterior surface to the external environment (heat sink). From the MPC shell to the overpack exterior surface, heat is conducted through an array of concentric shells representing the MPC-to-overpack helium gap, overpack inner shell, intermediate shells, Holtite-A and overpack outer shell. Heat rejection from the outside cask surfaces to ambient air is considered by accounting for natural convection and thermal radiation heat transfer mechanisms from the vertical (cylindrical shell) and top cover (flat) surfaces. The bottom overpack face, in contact with the ISFSI pad, rejects a small quantity of heat by conduction through the pad to the ground. The reduction in radiative heat exchange between cask outside vertical surfaces and ambient air because of blockage from the neighboring casks arranged for normal storage in a regular square array on the ISFSI pad is recognized in the analysis. The overpack closure plate is modeled as a heated surface in convective and radiative heat exchange with air and as a recipient of heat input through insolation. Insolation on the cask surfaces is based on 12-hour levels prescribed in 10CFR71, averaged over a 24-hour period, after accounting for partial blockage conditions.

Subsections 4.4.1.1.1 through 4.4.1.1.11 contain a systematic description of the mathematical models devised to articulate the temperature field in the HI-STAR 100 System. Table 4.4.2 shows the relationship between the mathematical models and the corresponding regions (i.e., fuel, MPC, overpack, etc.) of the HI-STAR 100 System. The description begins with the method to characterize the heat transfer behavior of the prismatic (square) opening referred to as the "fuel space" with a heat emitting fuel assembly situated in it. The methodology utilizes a finite element procedure to replace the heterogeneous SNF/fuel space region with an equivalent solid body having a well-defined temperature-dependent conductivity. In the following subsection, the method to replace the "composite" walls of the fuel basket cells with an equivalent "solid" wall is presented. Having created the mathematical equivalents for the SNF/fuel spaces and the fuel basket walls, the method to represent the MPC cylinder containing the fuel basket by an equivalent cylinder whose thermal conductivity is a function of the spatial location and coincident temperature is presented.

Following the approach of presenting descriptions starting from the inside and moving to the outer region of a cask, the next subsections present the mathematical model to simulate the overpack. Subsection 4.4.1.1.11 concludes the presentation with a description of how the different models for the specific regions within the HI-STAR 100 System are assembled into the final FLUENT model. Finally, a subsection to describe the solution for the special case of vacuum in the MPC space (no helium) is presented.

4.4.1.1.1 Overview of the Thermal Model

Thermal analysis of the HI-STAR 100 System is performed by assuming that the system is subject to its maximum heat duty with each storage location occupied and with the heat generation rate in each stored fuel assembly equal to design basis maximum value. While the assumption of equal heat generation imputes a certain symmetry to the cask thermal problem, the thermal model must incorporate three attributes of the physical problem to perform a rigorous analysis of a fully loaded cask:

- i. While the rate of heat conduction through metals is a relatively weak function of temperature, radiation heat exchange is a nonlinear function of surface temperatures.
- ii. Heat generation in the MPC is axially non-uniform due to non-uniform axial burnup profile in the fuel assemblies.
- iii. Inasmuch as the transfer of heat occurs from inside the basket region to the outside, the temperature field in the MPC is spatially distributed with the maximum values reached in the central core region.

It is clearly impractical to model every fuel rod in every stored fuel assembly explicitly. Instead, the cross section bounded by the inside of the storage cell, which surrounds the assemblage of fuel rods and the interstitial helium gas, is replaced with an "equivalent" square (solid) section characterized by an effective thermal conductivity. Figure 4.4.1 pictorially illustrates the homogenization concept. Further details of this procedure for determining the effective conductivity are presented in Subsection 4.4.1.1.2; it suffices to state here that the effective conductivity of the cell space will be a function of temperature because the radiation heat transfer (a major component of the heat transport between the fuel rods and the surrounding basket cell metal) is a strong function of the temperatures of the participating bodies. Therefore, in effect, every storage cell location will have a different value of effective conductivity (depending on the coincident temperature) in the homogenized model. The temperature-dependent fuel assembly region effective conductivity is determined by a finite volume procedure, as described in Subsection 4.4.1.1.2.

In the next step of homogenization, a planar section of MPC is considered. With each storage cell inside space replaced with an equivalent solid square, the MPC cross section consists of a metallic gridwork (basket cell walls with each square cell space containing a solid fuel cell square of effective thermal conductivity, which is a function of temperature) circumscribed by a circular ring (MPC shell). There are five distinct materials in this section, namely the homogenized fuel cell squares, the Alloy X structural materials in the MPC (including Boral sheathing), Boral, alloy 1100 aluminum heat conduction elements, and helium gas. Each of the five constituent materials in this section has a different conductivity. It is emphasized that the conductivity of the homogenized fuel cells is a strong function of temperature.

In order to replace this thermally heterogeneous MPC section with an equivalent conduction-only region, resort to the finite element procedure is necessary. Because the rate of transport of heat within the MPC is influenced by radiation, which is a temperature-dependent effect, the equivalent conductivity of the MPC region must also be computed as a function of temperature. Finally, it is recognized that the MPC section consists of two discrete regions, namely, the basket region and the peripheral region. The peripheral region is the space between the peripheral storage cells and the MPC shell. This space is essentially full of helium surrounded by Alloy X plates and alloy 1100 aluminum heat conduction elements. Accordingly, as illustrated in Figure 4.4.2 for MPC-68, the MPC cross section is replaced with two homogenized regions with temperature-dependent conductivities. In particular, the effective conductivity of the fuel cells is subsumed into the equivalent conductivity of the basket cross section. The finite element procedure used to accomplish this is described in Subsection 4.4.1.1.4. The ANSYS finite element code is the vehicle for all modeling efforts described in the foregoing.

In summary, appropriate finite element models are used to replace the MPC cross section with an equivalent two region homogeneous conduction lamina whose local conductivity is a known function of coincident absolute temperature. Thus, the MPC cylinder containing discrete fuel assemblies, helium, Boral and Alloy X, is replaced with a right circular cylinder whose material conductivity will vary with the radial and axial position as a function of the coincident temperature.

The MPC-to-overpack gap is simply an annular space which is readily modeled with an equivalent conductivity which reflects conduction and radiation modes of heat transfer. The overpack is a radially symmetric structure except for the neutron absorber region which is built from radial connectors and Holtite-A (see Figure 4.4.7). Using the classical equivalence procedure described in Subsection 4.4.1.1.9, this region is replaced with an equivalent radially symmetric annular cylinder.

The thermal analysis procedure described above makes frequent use of equivalent thermal properties to ease the geometric modeling of the cask components. These equivalent properties are rigorously calculated values based on detailed evaluations of actual cask system geometries. All these calculations are performed conservatively to ensure a bounding representation of the cask system. This process, commonly referred to as submodeling, yields accurate (not approximate) results. Given the detailed nature of the submodeling process, experimental validation of the individual submodels is not necessary.

In this manner, a HI-STAR 100 System overpack containing a loaded MPC standing upright on the ISFSI pad is replaced with a right circular cylinder with spatially varying temperature-dependent conductivity. Heat is generated within the basket space in this cylinder in the manner of the prescribed axial burnup distribution. In addition, heat is deposited from insolation on the external surface of the overpack. Under steady state conditions the total heat due to internal generation and insolation is dissipated from the outer cask surfaces by natural convection and

thermal radiation to the ambient environment. Details of the elements of mathematical modeling are provided in the following.

4.4.1.1.2 Fuel Region Effective Thermal Conductivity Calculation

Thermal properties of a large number of PWR and BWR fuel assembly configurations manufactured by the major fuel suppliers (i.e., Westinghouse, CE, B&W, and GE) have been evaluated for inclusion in the HI-STAR 100 System thermal analysis. It is noted that PWR fuel assemblies are equipped with removable non-fuel hardware, in particular, control rods which are inserted in guide tube locations for in-core usage. In dry cask storage, PWR fuel is optionally stored with the control rods. The control rods, when inserted in the fuel assemblies, displace gas in the guide tubes replacing it with solid materials (neutron absorbers and metals) which conduct heat much more readily. As a result, dissipation of heat in the fuel assemblies is enhanced by the presence of these control rods. For conservatism, credit for presence of control rods in fuel assemblies is neglected. Bounding PWR and BWR fuel assembly configurations are determined using the simplified procedure described below. This is followed by the determination of temperature-dependent properties of the bounding PWR and BWR fuel assembly configurations to be used for cask thermal analysis using a finite volume (FLUENT) approach.

To determine which of the numerous PWR assembly types listed in Table 4.4.5 should be used in the thermal model for the MPC-24 fuel basket, we must establish which assembly has the maximum thermal resistance. The same determination must be made for the MPC-68, out of the menu of SNF types listed in Table 4.4.6. For this purpose, we utilize a simplified procedure which we describe below.

Each fuel assembly consists of a large array of fuel rods typically arranged on a square layout. Every fuel rod in this array is generating heat due to radioactive decay in the enclosed fuel pellets. There is a finite temperature difference required to transport heat from the innermost fuel rods to the storage cell walls. Heat transport within the fuel assembly is based on principles of conduction heat transfer combined with the highly conservative analytical model proposed by Wooton and Epstein [4.4.1]. The Wooton-Epstein model considers radiative heat exchange between individual fuel rod surfaces as a means to bound the hottest fuel rod cladding temperature.

Transport of heat energy within any cross section of a fuel assembly is due to a combination of radiative energy exchange and conduction through the helium gas which fills the interstices between the fuel rods in the array. With the assumption of uniform heat generation within any given horizontal cross section of a fuel assembly, the combined radiation and conductive heat transport effects result in the following heat flow equation:

$$Q = \sigma C_o F_s A [T_C^4 - T_B^4] + 13.5740 L K_{cs} [T_C - T_B]$$

where:

$$F_{\varepsilon} = \text{Emissivity Factor}$$
$$= \frac{1}{\left(\frac{1}{\varepsilon_C} + \frac{1}{\varepsilon_B} - 1\right)}$$

$\varepsilon_C, \varepsilon_B$ = emissivities of fuel cladding, fuel basket (see Table 4.2.4)

$$C_o = \text{Assembly Geometry Factor}$$
$$= \frac{4N}{(N + 1)^2} \text{ (when } N \text{ is odd)}$$
$$= \frac{4}{N + 2} \text{ (when } N \text{ is even)}$$

N = Number of rows or columns of rods arranged in a square array

A = fuel assembly "box" heat transfer area
= $4 \times \text{width} \times \text{length}$

L = fuel assembly length

K_{cs} = fuel assembly constituent materials volume fraction weighted mixture conductivity

T_C = hottest fuel cladding temperature ($^{\circ}\text{R}$)

T_B = box temperature ($^{\circ}\text{R}$)

Q = net radial heat transport from the assembly interior

σ = Stefan-Boltzmann Constant ($0.1714 \times 10^{-8} \text{ Btu/ft}^2\text{-hr-}^{\circ}\text{R}^4$)

In the above heat flow equation, the first term is the Wooten-Epstein radiative heat flow contribution while the second term is the conduction heat transport contribution based on the classical solution to the temperature distribution problem inside a square shaped block with uniform heat generation [4.4.5]. The 13.574 factor in the conduction term of the equation is the shape factor for two-dimensional heat transfer in a square section. Planar fuel assembly heat transport by conduction occurs through a series of resistances formed by the interstitial helium fill gas, fuel cladding and enclosed fuel. An effective planar mixture conductivity is determined by a volume fraction weighted sum of the individual constituent material resistances. For BWR assemblies, this formulation is applied to the region inside the fuel channel. A second conduction

and radiation model is applied between the channel and the fuel basket gap. These two models are combined, in series, to yield a total effective conductivity.

The effective conductivity of the fuel for several representative PWR and commonly used BWR assemblies is presented in Tables 4.4.5 and 4.4.6. At higher temperatures (approximately 450°F and above), the zircaloy clad fuel assemblies with the lowest effective thermal conductivities are the W-17×17 OFA (PWR) and the GE11-9×9 (BWR). A discussion of fuel assembly conductivities for some of the newer 10×10 array and plant specific BWR fuel designs is presented near the end of this subsection. As noted in Table 4.4.6, the Dresden 1 (intact and damaged) fuel assemblies are excluded from consideration. The design basis decay heat load for Dresden-1 intact and damaged fuel (Table 2.1.7) is approximately 58% lower than the MPC-68 design basis maximum heat load (Table 4.4.19). Examining Table 4.4.6, the effective conductivity of the damaged Dresden-1 fuel assembly in a damaged fuel container is approximately 40% lower than the bounding (GE-11 9×9) fuel assembly. Consequently, the fuel cladding temperatures in the HI-STAR 100 System with Dresden-1 intact or damaged fuel assemblies will be bounded by design basis fuel cladding temperatures. This is demonstrated in Subsection 4.4.1.1.16. Based on this simplified analysis, the W-17×17 OFA PWR and GE11-9×9 BWR fuel assemblies are determined to be the bounding configurations for analysis of zircaloy clad fuel at design basis maximum heat loads. As discussed in Section 4.3.1, stainless clad fuel assemblies with significantly lower decay heat emission characteristics are not deemed to be bounding.

Having established the governing (most resistive) PWR and BWR SNF types, we use a finite volume code to determine the effective conductivities in a conservative manner. Detailed conduction-radiation finite volume models of the bounding PWR and BWR fuel assemblies are developed in the FLUENT code as shown in Figures 4.4.8 and 4.4.9, respectively. The PWR model was originally developed on the ANSYS code which enables individual rod-to-rod and rod-to-basket wall view factor calculations to be performed by the AUX12 procedure for the special case of black body radiation (surfaces emissivity = 1). Limitations of radiation modeling techniques implemented in ANSYS do not permit taking advantage of quarter symmetry of the fuel assembly geometry. Unacceptably long CPU time and large workspace requirements necessary for performing gray body radiation calculations for a complete fuel assembly geometry on ANSYS prompted the development of an alternate simplified model on the FLUENT code. The FLUENT model is benchmarked with the ANSYS model results for a Westinghouse 17×17 fuel assembly geometry for the case of black body radiation (emissivities = 1). The FLUENT model is found to yield conservative results in comparison to the ANSYS model for the "black" surface case. The FLUENT model benchmarked in this manner is used to solve the gray body radiation problem to provide the necessary results for determining the effective thermal conductivity of the governing PWR fuel assembly. The same modeling approach using FLUENT is then applied to the governing BWR fuel assembly, and the effective conductivity of GE11-9×9 fuel determined.

The combined fuel rods-helium matrix is replaced by an equivalent homogeneous material which fills the basket opening by the following two-step procedure. In the first step, the FLUENT-based

fuel assembly model is solved by applying equal heat generation per unit length to the individual fuel rods and a uniform boundary temperature along the basket cell opening inside periphery. The temperature difference between the peak cladding and boundary temperatures is used to determine an effective conductivity as described in the next step. For this purpose, we consider a two-dimensional cross section of a square shaped block of size equal to $2L$ and a uniform volumetric heat source (q_g) cooled at the periphery with a uniform boundary temperature. Under the assumption of constant material thermal conductivity (K), the temperature difference (ΔT) from the center of the cross section to the periphery is analytically given by [4.4.5]:

$$\Delta T = 0.29468 \frac{q_g L^2}{K}$$

This analytical formula is applied to determine the effective material conductivity from a known quantity of heat generation applied in the FLUENT model (smeared as a uniform heat source, q_g) basket opening size and ΔT calculated in the first step.

As discussed earlier, the effective fuel space conductivity is a function of the temperature coordinate. The above two step analysis is carried out for a number of reference temperatures. In this manner, the effective conductivity as a function of temperature is established.

In Table 4.4.23, 10×10 array type BWR fuel assembly conductivity results from a simplified analysis are presented to determine the most resistive fuel assembly in this class. From the data in Table 4.4.23, the Atrium-10 fuel type is determined to be the most resistive in this class of fuel assemblies. A detailed finite element model of this assembly type was developed to rigorously quantify the heat dissipation characteristics. The results of this study are presented in Table 4.4.24 and compared to the BWR bounding fuel assembly conductivity depicted in Figure 4.4.14. The results of this study demonstrate that the bounding fuel assembly conductivity is conservative with respect to the 10×10 class of BWR fuel assemblies.

Table 4.4.25 summarizes plant specific fuel types effective conductivities. From these analytical results, the SPC-5 is determined to be the most resistive fuel assembly in this group of fuel types. A rigorous finite element model of SPC-5 fuel assembly was developed to confirm that its in-plane heat dissipation characteristics are bounded from below by the Design Basis BWR fuel conductivities used in the HI-STAR thermal analysis.

Temperature-dependent effective conductivities of PWR and BWR design basis fuel assemblies (most resistive SNF types) are shown in Figure 4.4.14. The finite volume computational results are also compared to results reported from independent technical sources. From this comparison, it is readily apparent that FLUENT-based fuel assembly conductivities are conservative. The

FLUENT computed values (not the published literature data) are used in the MPC thermal analysis presented in this document.

4.4.1.1.3 Effective Thermal Conductivity of Boral/Sheathing/Box Wall Sandwich

Each MPC basket cell wall (except the MPC-68 outer periphery cell walls) is manufactured with a Boral neutron absorbing plate for criticality control. Each Boral plate is sandwiched in a sheathing-to-basket wall pocket. A schematic of the "Box Wall-Boral-Sheathing" sandwich geometry of an MPC basket is illustrated in Figure 4.4.3. During fabrication, a uniformly normal pressure is applied to each "Box Wall-Boral-Sheathing" sandwich in the assembly fixture during stitch-welding of the sheathing periphery on the box wall. This ensures adequate surface-to-surface contact for elimination of any macroscopic air gaps. The mean coefficient of linear expansion of the Boral is higher than the thermal expansion coefficients of the basket and sheathing materials. Consequently, basket heat-up from the stored SNF will further ensure a tight fit of the Boral plate in the sheathing-to-box pocket. The presence of small microscopic gaps due to less than perfect surface finish characteristics requires consideration of an interfacial contact resistance between the Boral and box-sheathing surfaces. A conservative contact resistance resulting from a 2 mil Boral to pocket air gap is applied in the analysis. Note that this gap would actually be filled with helium, so this is very conservative. In other words, no credit is taken for the interfacial pressure between Boral and stainless plate/sheet stock produced by the fixturing and welding process. Furthermore, no credit is taken for the presence of helium and radiative heat exchange across the Boral-to-sheathing or Boral-to-box wall gaps.

Heat conduction properties of a composite "Box Wall-Boral-Sheathing" sandwich in the two principal basket cross sectional directions as illustrated in Figure 4.4.3 (i.e., lateral "out-of-plane" and longitudinal "in-plane") are unequal. In the lateral direction, heat is transported across layers of sheathing, air-gap, Boral (B_4C and cladding layers) and box wall resistances which are essentially in series (except for the small helium filled end regions shown in Figure 4.4.4). Heat conduction in the longitudinal direction, in contrast, is through an array of essentially parallel resistances comprised of these several layers listed above. Resistance network models applicable to the two directions are illustrated in Figure 4.4.4. It is noted that, in addition to the essentially series and parallel resistances of the composite wall layers for the "out-of-plane" and "in-plane" directions respectively, the effect of small helium filled end regions is also included in the resistance network analogy. For the ANSYS based MPC basket thermal model, corresponding non-isotropic effective thermal conductivities in the two orthogonal sandwich directions are determined and applied in the analysis.

4.4.1.1.4 Finite Element Modeling of Basket In-Plane Conductive Heat Transport

The heat rejection capability of each MPC basket design (i.e., MPC-24, and MPC-68) is evaluated by developing a thermal model of the combined fuel assemblies and composite basket walls geometry on the ANSYS finite element code. The ANSYS model includes a geometric layout of the basket structure in which the basket "Box Wall-Boral-Sheathing" sandwich is replaced by a

"homogeneous wall" with an equivalent thermal conductivity. Since the thermal conductivity of the Alloy X material is a weakly varying function of temperature, the equivalent "homogeneous wall" must have a temperature-dependent effective conductivity. Similarly, as illustrated in Figure 4.4.4, the conductivities in the "in-plane" and "out-of-plane" directions of the equivalent "homogeneous wall" are different. Finally, as discussed earlier, the fuel assemblies and the surrounding basket cell openings are modeled as homogeneous heat generating regions with effective temperature dependent in-plane conductivity. The methodology used to reduce the heterogeneous MPC basket - fuel assemblage to an equivalent homogeneous region with effective thermal properties is discussed in the following.

Consider a cylinder of height, L , and radius, r_o , with a uniform volumetric heat source term, q_g , insulated top and bottom faces, and its cylindrical boundary maintained at a uniform temperature, T_c . The maximum centerline temperature (T_h) to boundary temperature difference is readily obtained from classical one-dimensional conduction relationships (for the case of a conducting region with uniform heat generation and a constant thermal conductivity K_s):

$$(T_h - T_c) = q_g r_o^2 / (4 K_s)$$

Noting that the total heat generated in the cylinder (Q_t) is $B r_o^2 L q_g$, the above temperature rise formula can be reduced to the following simplified form in terms of total heat generation per unit length (Q_t/L):

$$(T_h - T_c) = (Q_t / L) / (4 B K_s)$$

This simple analytical approach is employed to determine an effective basket cross-sectional conductivity by applying an equivalence between the ANSYS finite element model of the basket and the analytical case. The equivalence principle employed in the HI-STAR 100 System thermal analysis is depicted in Figure 4.4.2. The 2-dimensional ANSYS finite element model of each MPC basket is solved by applying a uniform heat generation per unit length in each basket cell region and a constant basket periphery boundary temperature, T_c' . Noting that the basket region with uniformly distributed heat sources and a constant boundary temperature is equivalent to the analytical case of a cylinder with uniform volumetric heat source discussed earlier, an effective MPC basket conductivity (K_{eff}) is readily derived from the analytical formula and ANSYS solution leading to the following relationship:

$$K_{eff} = N (Q_f'/L) / (4 B [T_h' - T_c'])$$

where:

N = number of fuel assemblies

(Q_f'/L) = per fuel assembly heat generation per unit length applied in ANSYS model

T_h' = peak basket cross-section temperature from ANSYS model

Cross sectional views of MPC basket ANSYS models are depicted in Figures 4.4.11 and 4.4.12. Notice that many of the basket supports and all shims have been conservatively neglected in the models. This conservative geometry simplification, coupled with the conservative neglect of thermal expansion which would minimize the gaps, yields conservative gap thermal resistances. Temperature-dependent equivalent thermal conductivities of fuel region and composite basket walls, as determined from analysis procedures described earlier, are applied to the ANSYS model. The planar ANSYS conduction model is solved by applying a constant basket periphery temperature with uniform heat generation in the fuel region. Table 4.4.7 summarizes effective thermal conductivity results of each basket design obtained from the ANSYS models. The effective calculated basket cross sectional conductivity and the effective *axial* direction effective conductivity is *conservatively* assumed to be equal in the comprehensive HI-STAR 100 System thermal model (see Section 4.4.1.1.11). It is recalled that the equivalent thermal conductivity values presented in Table 4.4.7 are lower bound values because, among other elements of conservatism, the effective conductivity of most resistive SNF types (Tables 4.4.5 and 4.4.6) are used in the MPC finite element simulations.

4.4.1.1.5 Heat Transfer in MPC Basket Peripheral Region

Each of the two MPC designs for storing PWR or BWR fuel are provided with relatively large regions, formed between the relatively cooler MPC shell and hot basket peripheral panels, filled with helium gas. Heat transfer in these helium-filled regions corresponds to the classical case of heat transfer in a differentially heated closed cavity. Experimental studies of this arrangement have been performed by many investigators, including Eckert and Carlson (Int. J. Heat Mass Transfer, vol. 2, p. 106, 1961) and Elder (J. Fluid Mech., vol. 23, p. 77, 1965). The peripheral region between the basket and MPC inner surface is simulated as a tall fluid-filled cavity of height H formed between two differentially heated surfaces (T) separated by a small distance L. In a closed cavity, an exchange of hot and cold fluids occurs near the top and bottom ends of the cavity, resulting in a net transport of heat across the gap. The rate of heat transfer across the cavity is characterized by a Rayleigh number, Ra_L , defined as:

$$Ra_L = \frac{C_p \rho^2 g \beta \Delta T L^3}{\mu K}$$

where:

- C_p = fluid heat capacity
- ρ = fluid density
- g = acceleration due to gravity

β	=	coefficient of thermal expansion (equal to reciprocal of absolute temperature for gases)
ΔT	=	temperature difference between the hot and cold surfaces
L	=	spacing between the hot and cold surfaces
μ	=	fluid viscosity
K	=	fluid conductivity

Hewitt et al. [4.4.6] recommends the following Nusselt number correlation for heat transport in tall cavities:

$$Nu_L = 0.42 Ra_L^{1/4} Pr^{0.012} \left(\frac{H}{L}\right)^{-0.3}$$

where Pr is the Prandtl number of the cavity fill gas.

A Nusselt number of unity implies heat transfer by fluid conduction only, while a higher than unity Nusselt number is due to the so-called "Rayleigh" effect which monotonically increases with increasing Rayleigh number. Nusselt numbers applicable to helium-filled PWR and BWR fueled HI-STAR 100 MPCs in the peripheral voids are provided in Table 4.4.1.

4.4.1.1.6 Effective Conductivity of Multilayered Intermediate Shell Region

Fabrication of the multi-layered overpack shell is discussed in Section 1.2 which explains how an interfacial contact between successive layers from the fabrication process is ensured. In the thermal analysis, each intermediate shell metal-to-metal interface presents an additional resistance to heat transport. The contact resistance arises from microscopic pockets of air entrapped between surface irregularities of the contacting surfaces. Since air is a relatively poor conductor of heat, this results in a reduction in the ability to transport heat across the interface compared to that of the base metal. Interfacial contact conductance depends upon three principal factors, namely: (i) base material conductivity, (ii) interfacial contact pressure, and (iii) surface finish. Rohsenow and Hartnett [4.2.2] have reported results from experimental studies of contact conductance across air entrapped stainless steel surfaces with a typical 100 μ -inch surface finish. A minimum contact conductance of 350 Btu/ft²-hr-°F is determined from extrapolation of Rohsenow, et al. data to zero contact pressure.

Thermal conductivity of carbon steel is about three times that of stainless steel. Thus, the choice of carbon steel as base material in a multi-layered construction significantly improves heat transport across interfaces. The fabrication process, as discussed in Section 1.2, guarantees significant interfacial contact. Contact conductance values extrapolated to zero contact pressure are therefore conservative. The surface finish of the hot-rolled carbon steel plate stock is generally

in the range of 250-1000 μ -inch [4.2.1]. The process of forming hot-rolled flat plate stock to cylindrical shapes to form the intermediate shells will result in additional smoothening of the surfaces (from the large surface pressures exerted by the hardened roller faces which flatten out any surface irregularities).

In the HI-STAR 100 thermal analysis, a conservatively bounding interfacial contact conductance value is determined using the following assumptions:

1. No credit is taken for higher base metal conductivity (carbon versus stainless steel).
2. No credit is taken for interfacial contact pressure.
3. No credit is taken for a smooth surface finish resulting from rolling of hot-rolled plate stock to cylindrical shapes.
4. Contact conductance is based on a uniform 2000 μ -inch (1000 μ -inch for each surface condition) interfacial air gap at all interfaces.
5. No credit for radiation heat exchange across this hypothetical inter-surface air gap.
6. Bounding low thermal conductivity at 200°F.

These assumptions guarantee a conservative assessment of heat dissipation characteristics of the multi-layered intermediate shell region. The resistance of the five carbon steel layers along with the associated interfacial resistances are combined as resistances in series to determine an effective conductivity of this region leading to the following relationship:

$$K_i = r_o \ln \left(\frac{r_5}{r_o} \right) \left[\sum_{i=1}^5 \frac{\delta}{K_{air}} \frac{r_o}{r_i} + \frac{r_o \ln \frac{r_5}{r_o}}{K_{cst}} \right]^{-1}$$

where (in conventional U.S. units):

K_i	=	effective intermediate shell region thermal conductivity
r_o	=	inside radius of inner intermediate shell
r_i	=	outer radius of i^{th} intermediate shell
δ	=	interfacial air gap (2000 μ -inch)
K_{air}	=	air thermal conductivity
K_{cst}	=	carbon steel thermal conductivity

4.4.1.1.7 Heat Rejection from Overpack Exterior Surfaces

Jacob and Hawkins [4.2.9] recommend the following correlations for natural convection heat

transfer to air from heated vertical or horizontal surfaces:

Turbulent range:

$$h = 0.19 (\Delta T)^{1/3} \text{ (Vertical, } GrPr > 10^9)$$
$$h = 0.22 (\Delta T)^{1/3} \text{ (Horizontal, } GrPr > 10^7)$$

(in conventional U.S. units)

Laminar Range:

$$h = 0.29 \left(\frac{\Delta T}{L}\right)^{1/4} \text{ (Vertical } GrPr < 10^9)$$
$$h = 0.27 \left(\frac{\Delta T}{L}\right)^{1/4} \text{ (Horizontal } GrPr < 2 \times 10^7)$$

(in conventional U.S. units)

where ΔT is the temperature differential between the overpack surface and ambient air. The length scale L is the overpack height for vertical surfaces or the overpack diameter for the top horizontal surface. Noting that $GrPr$ is expressed as $L^3 \Delta T Z$, where Z (from Table 4.2.7) is at least 2.6×10^5 at a conservatively high upper bound overpack exterior air film temperature of 340°F , it is apparent that the turbulent condition is always satisfied for ΔT in excess of a small fraction of 1°F . Under turbulent conditions, the more conservative heat transfer correlation for vertical surfaces (i.e., $h = 0.19 \Delta T^{1/3}$) is applied for thermal analysis to all exposed overpack surfaces.

Including both natural convection and thermal radiation heat loss from the overpack outer surfaces, the following relationship for surface heat flux is developed:

$$q_s = 0.19 (T_s - T_A)^{4/3} + \sigma \varepsilon F_{1,A} [(T_s + 460)^4 - (T_A + 460)^4]$$

where:

- T_s, T_A = surface, ambient temperatures ($^\circ\text{F}$)
- q_s = surface heat flux ($\text{Btu}/\text{ft}^2\text{-hr}$)
- ε = surface emissivity
- $F_{1,A}$ = view factor between surface and air
- σ = Stefan Boltzman constant ($0.1714 \times 10^{-8} \text{ Btu}/\text{ft}^2\text{-hr-}^\circ\text{R}^4$)

In order to determine the view factor for vertical overpack outside surfaces, an ANSYS [4.1.1] finite-element based radiation heat transfer model is developed. The model geometry is based on

a HI-STAR 100 System array layout depicted schematically in Figure 1.4.1. The design basis HI-STAR 100 System ISFSI storage square layout pitch is provided in Section 1.4. The ANSYS model developed is shown in Figure 4.4.5. In this figure, a center HI-STAR 100 System cask is shown surrounded by two rows of casks on all sides. The ANSYS solution determines view factors between this most adversely located system in the middle with all other neighboring casks. A sum of all these individual blockages gives the total blockage factor. Thus, the view factor $F_{1,A}$ between this most adversely affected HI-STAR 100 System and outside air is determined by the following relationship:

$$F_{1,A} = 1 - \sum_K F_{1,K}$$

where $F_{1,K}$ is the view factor between HI-STAR 100 System 1 and a neighboring system K. This factor is determined by a series of ANSYS solutions as a function of ISFSI cask array pitch, and the results are shown in Figure 4.4.6.

4.4.1.1.8 Determination of Solar Heat Input

The intensity of solar radiation incident on an exposed surface depends on a number of time varying terms. The solar heat flux strongly depends upon the time of the day as well as on latitude and day of the year. Also, the presence of clouds and other atmospheric conditions (dust, haze, etc.) can significantly attenuate solar intensity levels. Rapp [4.4.2] has discussed the influence of such factors in considerable detail.

Consistent with the guidelines in NUREG-1536 [4.1.3], solar input to the exposed surfaces of the overpack is determined based on 12-hour insolation levels recommended in 10CFR71 (averaged over a 24-hour period) and applied to the most adversely located cask after accounting for partial blockage of incident solar radiation on the lateral surfaces of the cask by surrounding casks. The blocking factor is identical to the radiative blocking considered for cooling of outside surfaces to the ambient environment. This is conservative compared to the case of an isolated cask with significantly improved radiative cooling and higher insolation levels because the cask is emitting much more heat than the insolation heat input. The imposed steady insolation level for the exposed top lid is based on a view factor equal to unity. The solar absorptivity of all exposed cask surfaces is assumed to be a conservatively bounding value of *unity*.

4.4.1.1.9 Effective Thermal Conductivity of Holtite Neutron Shielding Region

In order to minimize heat transfer resistance limitations due to the poor thermal conductivity of the Holtite-A neutron shield material, a large number of thick radial channels of high strength and conductivity carbon steel material are embedded in the neutron shield region. The legs of the radial channels form highly conducting heat transfer paths for efficient heat removal. Each channel leg is welded to the outside surface of the outermost intermediate shell. Enclosure shell panels are welded to the radial channels to form the external wall of the overpack, and thus provide a continuous path for heat removal to the ambient environment.

The effective thermal conductivity of the composite neutron shield and the network of radial channel legs is determined by combining the heat transfer resistance of individual components in a parallel network. In determining the heat transfer capability of this region to the outside ambient environment for normal long-term storage conditions, *no credit is taken for conduction through the neutron shielding material*. Thus, heat transport from the outer intermediate shell surface to the overpack outer shell is conservatively based on heat transfer through the carbon steel radial connectors alone. Thermal conductivity of the parallel neutron shield and radial channel leg region is given by the following formula:

$$K_{ne} = \frac{K_r N_r t_r \ln\left(\frac{r_B}{r_A}\right)}{2\pi \ell_R} + \frac{K_{ns} N_r t_{ns} \ln\left(\frac{r_B}{r_A}\right)}{2\pi \ell_R}$$

where (in consistent U.S. units):

- K_{ne} = effective thermal conductivity of Holtite region
- r_A = inner radius of neutron shielding
- r_B = outer radius of neutron shielding
- K_r = effective thermal conductivity of carbon steel radial channel leg
- N_r = total number of radial channel legs (also equal to number of neutron shield sections)
- t_r = minimum (nominal) thickness of each radial channel leg
- P_R = effective radial heat transport length through radial channel leg
- K_{ns} = neutron shield thermal conductivity
- t_{ns} = neutron shield thickness (between two radial channel legs)

The radial channel-to-outer intermediate shell surface weld thickness is equal to half the plate thickness. The additional weld resistance is accounted for by reducing the plate thickness in the weld region for a short radial span equal to the weld size. As a result, the conductivity of the radial carbon steel connectors based on full thickness for the entire radial span is reduced. Figure 4.4.7 depicts a resistance network developed to combine the neutron shield and radial connectors resistances to determine an effective conductivity of the neutron shield region. Note that in the resistance network analogy, only the annulus region between overpack outer enclosure inner surface and intermediate shells outer surface is considered in this analysis. The effective thermal conductivity of the neutron shield/radial channel leg region is provided in Table 4.4.8.

4.4.1.1.10 Effective Thermal Conductivity of Flexible MPC Basket-to-Shell Aluminum Heat Conduction Elements

As shown in HI-STAR 100 System MPC Drawings 1395, and 1401 in Section 1.5, flexible full-length heat conduction elements fabricated from thin aluminum alloy 1100 sheet metal are inserted in the large MPC basket-to-shell gaps to provide uninterrupted metal pathways to transport heat from the basket to the MPC shell. Due to the high thermal conductivity of aluminum alloy 1100 (about 15 times that of Alloy X), a significant rate of heat transfer is possible along thin flexible plates. Flexibility of the heat conduction elements is an important asset to enable a snug fit in the confined spaces and for ease of installation. Figure 4.4.13 shows the mathematical idealization of a typical conduction element inserted in a basket periphery panel-to-MPC shell space. The aluminum heat conduction element is shown to cover the MPC basket Alloy X peripheral panel and MPC shells (Regions I and III depicted in Figure 4.4.13) surfaces along the full-length of the basket. Heat transport to and from the aluminum heat conduction element is conservatively postulated to occur across a thin helium gap as shown in the figure (i.e., no credit is taken for aluminum heat conduction element to Alloy X metal-to-metal contact). Aluminum surfaces inside the hollow region are sandblasted prior to fabrication to result in a rough surface finish which has a significantly higher emissivity compared to smooth surfaces of rolled aluminum. The untreated aluminum surfaces directly facing Alloy X panels have a smooth finish to minimize contact resistance.

Net heat transfer resistance from the hot basket periphery panel to the relatively cooler MPC shell along the aluminum heat conduction element pathway is a sum of three individual resistances in regions labeled I, II, and III as shown in Figure 4.4.13. In Region I, heat is transported from the basket to the aluminum heat conduction element surface directly facing the basket panel across a thin helium resistance gap. Longitudinal transport of heat (in the z direction) in the aluminum plate (in Region I) will result in an axially non-uniform temperature distribution. Longitudinal one-dimensional heat transfer in the Region I aluminum plate was analytically formulated to result in the following ordinary differential equation for the non-uniform temperature distribution:

$$t K_{Al} \frac{\partial^2 T}{\partial z^2} = - \frac{K_{He}}{h} (T_h - T) \quad \text{(Equation a)}$$

Boundary Conditions

$$\begin{aligned}\frac{\partial T}{\partial z} &= 0 \text{ at } z = 0 \\ T &= T_h' \text{ at } z = P\end{aligned}\tag{Equation b}$$

where (see Figure 4.4.13):

$T(z)$ = non-uniform aluminum metal temperature distribution

t = heat conduction element thickness

K_{Al} = heat conduction element conductivity

K_{He} = helium conductivity

h = helium gap thickness

T_h = hot basket temperature

T_h' = heat conduction element Region I boundary temperature at $z = P$

P = heat conduction element Region I length

W = conduction element Region II length

Solution of this ordinary differential equation subject to the imposed boundary condition is:

$$(T_h - T) = (T_h - T_h') \left[\frac{e^{\frac{z}{\sqrt{\alpha}}} + e^{-\frac{z}{\sqrt{\alpha}}}}{e^{\frac{P}{\sqrt{\alpha}}} + e^{-\frac{P}{\sqrt{\alpha}}}} \right]\tag{Equation c}$$

where α is a dimensional parameter equal to $(h \times t \times K_{Al} / K_{He})$. The net heat transfer (Q_1) across the Region I helium gap can be determined by the following integrated heat flux to a heat conduction element of length L as:

$$Q_1 = \int_0^P \frac{K_{He}}{h} (T_h - T) (L) dz\tag{Equation d}$$

Substituting the analytical temperature distribution result obtained in Equation c, the following expression for net heat transfer is obtained:

$$Q_1 = \frac{K_{He} L \sqrt{\alpha}}{h} \left(1 - \frac{1}{e^{\frac{P}{\sqrt{\alpha}}} + e^{-\frac{P}{\sqrt{\alpha}}}} \right) (T_h - T_h')\tag{Equation e}$$

Based on this result, an expression for Region I resistance is obtained as shown below:

$$R_I = \frac{T_h - T_h'}{Q_I} = \frac{h}{K_{He} L \sqrt{\alpha}} \left(1 - \frac{1}{e^{\frac{P}{\sqrt{\alpha}}} + e^{-\frac{P}{\sqrt{\alpha}}}} \right)^{-1} \quad (\text{Equation f})$$

The Region II resistance expression can be developed from the following net heat transfer equation in the vertical leg of the conduction element as shown below:

$$Q_{II} = \frac{K_{Al} L t}{W} (T_h' - T_c') \quad (\text{Equation g})$$

$$R_{II} = \frac{T_h' - T_c'}{Q_{II}} = \frac{W}{K_{Al} L t} \quad (\text{Equation h})$$

Similarly, a Region III resistance expression can be analytically determined as shown below:

$$R_{III} = \frac{(T_c' - T_c)}{Q_{III}} = \frac{h}{K_{He} L \sqrt{\alpha}} \left(1 - \frac{1}{e^{\frac{P}{\sqrt{\alpha}}} + e^{-\frac{P}{\sqrt{\alpha}}}} \right)^{-1} \quad (\text{Equation i})$$

This completes the analysis for the total thermal resistance attributable to the heat conduction elements, equal to the sum of the three individual resistances. The total heat conduction element resistance is smeared across the basket-to-MPC shell region as an effective uniform annular gap conductivity (see Figure 4.4.2). We note that heat transport along the conduction elements is an independent conduction path in parallel with conduction and radiation mechanisms in the large helium gaps. Helium conduction and radiation in the MPC basket-to-MPC shell peripheral gaps is accounted for separately in the ANSYS models for the MPCs, described earlier. Therefore, the total MPC basket-to-MPC shell peripheral gaps conductivity will be the sum of the heat conduction elements effective conductivity and the helium gap conduction-radiation effective conductivity.

4.4.1.1.11 FLUENT Model for HI-STAR 100 Temperature Field Computation

In the preceding subsection, a series of analytical and numerical models to define the thermal characteristics of the various elements of the HI-STAR 100 System are presented. The thermal modeling begins with the replacement of the SNF cross section and surrounding fuel cell space with a solid region with an equivalent conductivity. Since radiation is an important constituent of the heat transfer process in the SNF/storage cell space, and the rate of radiation heat transfer is a strong function of the surface temperatures, it is necessary to treat the equivalent region conductivity as a function of temperature. Because of the relatively large range of temperatures in a loaded HI-STAR 100 System under the design basis heat loads, the effects of variation in the thermal conductivity of materials with temperature throughout the system model are included. The presence of significant radiation effects in the storage cell spaces adds to the imperative to

treat the equivalent storage cell lamina conductivity as temperature-dependent.

FLUENT finite volume simulations have been performed to establish the equivalent thermal conductivity as a function of temperature for the limiting (thermally most resistive) BWR and PWR spent fuel types. Utilizing the limiting SNF (established through a simplified analytical process for comparing conductivities) ensures that the numerical idealization for the fuel space effective conductivity is conservative for all non-limiting fuel types.

Having replaced the fuel spaces by solid square blocks with temperature-dependent conductivity essentially renders the basket into a non-homogeneous three-dimensional solid where the non-homogeneity is introduced by the honeycomb basket structure. The basket panels themselves are a composite of Alloy X cell wall, Boral neutron absorber, and Alloy X sheathing metal. A conservative approach to replace this composite section with an equivalent "solid wall" was described earlier.

In the next step, a planar section of the MPC is considered. The MPC contains a non-symmetric basket lamina wherein the equivalent fuel spaces are separated by the "equivalent" solid metal walls. The space between the basket and the MPC, called the peripheral gap, is filled with helium gas and aluminum heat conduction elements (shown in MPC drawings 1395 and 1401 in Section 1.5). The equivalent thermal conductivity of the MPC section is computed using a finite element procedure on ANSYS. To the "helium conduction-radiation" based peripheral gap conductivity, the effective conductivity of the aluminum conduction elements is added to obtain a combined peripheral gap effective conductivity. At this stage in the thermal analysis, the SNF/basket/MPC assemblage has been replaced with a two-zone (Figure 4.4.2) cylindrical solid whose thermal conductivity is a strong function of temperature.

The idealization for the overpack is considerably more straightforward. The overpack is radially symmetric except for the neutron absorber (Holtite-A) region (Figure 4.4.7). The procedure to replace the multiple shell layers, Holtite-A and radial connectors with an equivalent solid utilizes classical heat conduction analogies, as discussed in Sections 4.4.1.1.6 and 4.4.1.1.9.

In the final step of the analysis, the equivalent two-zone MPC cylinder, equivalent overpack shell, top and bottom plates, and ISFSI pad are assembled into a comprehensive finite volume model. A cross section of this axisymmetric model implemented on FLUENT is shown in Figure 4.4.15. A summary of the essential features of this model is presented in the following:

- The overpack shell is represented by 840 axisymmetric elements.

- The overpack bottom plate and bolted closure plate are modeled by 312 axisymmetric elements.
- The two-zone MPC "solid" (including the baseplate, lid and shell) is represented by 1188 axisymmetric elements.
- The ISFSI pad is conservatively modeled as a thermal resistance from a 36" thick concrete cylinder whose bottom surface is at 60°F. The portion of the concrete outside the footprint of the cask is conservatively omitted from the model.
- The space between the MPC and the overpack interior inner surface contains helium.
- Heat input due to insolation is applied to the top surface and the cylindrical surface of the overpack.
- The heat generation in the MPC is assumed to be uniform in each horizontal plane, but to vary in the axial direction to correspond to the axial power distribution listed in Table 2.1.8.
- The most disadvantageously placed cask in a HI-STAR cask array (i.e., the one subjected to maximum radiative blockage (see Subsection 4.4.1.1.7), is modeled.

The emissivity applied to the external surfaces of the HI-STAR model accounts for radiation-blockage of the outer enclosure surface and no blockage for the overpack closure plate top surface.

The finite element model constructed in this manner will produce an axisymmetric temperature distribution. The peak temperature will occur at the centerline and is expected to occur at the axial location of peak heat generation. As we will see later, the results from the finite volume solution bear out these observations.

4.4.1.1.12 MPC Temperature Distribution Under Vacuum Conditions

The initial loading of SNF in the MPC requires that the water within the MPC be drained and replaced with helium. This operation on the HI-STAR MPCs will be carried out using a conventional vacuum drying approach. In this method, removal of the last traces of residual moisture from the MPC cavity is accomplished by evacuating the MPC for a short time after draining the MPC.

Prior to the start of the MPC draining operation, both the overpack annulus and the MPC are full of water. The presence of water in the MPC ensures that the fuel cladding temperatures are lower than design basis limits by large margins. As the heat generating active fuel length is

uncovered during the draining operation, the fuel and basket mass will undergo a gradual heat up from the initially cold conditions when the heated surfaces were submerged under water.

Thermal analysis of the MPC basket for bounding design basis decay heat loads is performed on the ANSYS finite element code. The ANSYS model is constructed to evaluate the heat rejection ability of the basket under evacuated conditions. The vacuum condition effective fuel assembly conductivity is determined by procedures discussed earlier (Subsection 4.4.1.1.2) after setting the thermal conductivity of the gaseous medium to a small fraction (one part in one thousand) of helium conductivity in the fuel assembly finite element model. Basket periphery-to-MPC shell heat transfer occurs through conduction and radiation. During draining and vacuum drying operations, the overpack annulus is required to be kept filled with water. Thus, the MPC thermal analysis problem is formulated with cooling of the MPC shell with water, which under worst case conditions would be slightly higher than its normal boiling temperature at the bottom of the overpack annulus. Results of vacuum condition analyses are provided in Subsection 4.4.2.2.

4.4.1.1.13 Effect of Fuel Cladding Crud Resistance

In this subsection, a conservatively bounding estimate of temperature drop across a crud film adhering to a fuel rod during dry storage conditions is determined. The evaluation is performed for a BWR fuel assembly based on an upper bound crud thickness obtained from the PNL-4835 report ([4.3.4], Table 3). The crud present on the fuel assemblies is predominately iron oxide mixed with small quantities of other metals such as cobalt, nickel, chromium, etc. Consequently, the effective conductivity of the crud mixture is expected to be in the range of typical metal alloys. However, in the interest of extreme conservatism, the crud layer thickness is replaced by a film of helium. The calculation is performed in two steps. In the first step, a crud film resistance is determined based on bounding maximum film on the fuel rod surfaces. This is followed by a peak local cladding heat flux calculation for the GE 7x7 array fuel assembly postulated to emit a conservatively bounding decay heat equal to 0.5kW. The temperature drop across the crud film obtained as a product of the heat flux and crud resistance terms is determined to be less than 0.1°F. The calculations are presented below.

Bounding Crud Thickness(s) (PNL-4835)	=	130μm (4.26×10 ⁻⁴ ft)
Crud Conductivity (K) (Conservative Assumption)	=	0.1 Btu/ft-hr-°F

GE 7x7 Fuel Assembly:

Rod O.D.	=	0.563"
Active Fuel Length	=	150"
Heat Transfer Area	=	(7x7) (π×0.563) × 150/144
	=	90.3 ft ²

Axial Peaking Factor = 1.195 (Burnup distribution Table 2.1.8)

Decay Heat = 500W
(Conservative Assumption)

$$\text{Crud Resistance} = \frac{\delta}{K} = \frac{4.26 \times 10^{-4}}{0.1} = 4.26 \times 10^{-3} \frac{\text{ft}^2 \cdot \text{hr} \cdot ^\circ\text{F}}{\text{Btu}}$$
$$\text{Peak Heat Flux} = \frac{(500 \times 3.417) \text{ Btu/hr}}{90.3 \text{ ft}^2} \times 1.195 = 22.6 \frac{\text{Btu}}{\text{ft}^2 \cdot \text{hr}}$$

$$\begin{aligned} \therefore \text{Temperature drop } (\Delta T_c) \text{ across crud film} \\ = 4.26 \times 10^{-3} \frac{\text{ft}^2 \cdot \text{hr} \cdot ^\circ\text{F}}{\text{Btu}} \times 22.6 \frac{\text{Btu}}{\text{ft}^2 \cdot \text{hr}} = 0.096^\circ\text{F} \\ \text{(i.e., less than } 0.1^\circ\text{F)} \end{aligned}$$

Therefore, it is concluded that deposition of crud does not materially change the SNF cladding temperature.

4.4.1.1.14 Maximum Time Limit During Wet Transfer

In accordance with NUREG-1536, water inside the MPC cavity during wet transfer operations is not permitted to boil in the HI-STAR 100 System. Consequently, uncontrolled pressures in the de-watering, purging, and recharging system which may result from two-phase condition, are completely avoided. This requirement is accomplished by imposing a limit on the maximum allowable time duration for fuel to be submerged in water after a loaded HI-STAR cask is removed from the pool and prior to the start of vacuum drying operations.

When the HI-STAR overpack and the loaded MPC under water-flooded conditions are removed from the pool, the combined mass of the water, the fuel, the MPC, and the HI-STAR will absorb the decay heat emitted by the fuel assemblies. This results in a slow temperature rise of the entire system with time, starting from an initial temperature of the contents. The rate of temperature rise is limited by the thermal inertia of the HI-STAR system. To enable a bounding heat-up rate determination for the HI-STAR system, the following conservative assumptions are imposed:

- i. Heat loss by natural convection and radiation from the exposed HI-STAR surfaces to the pool building ambient air is neglected (i.e., an adiabatic temperature rise calculation is performed).

- ii. Design Basis maximum decay heat input from the loaded fuel assemblies is imposed on the HI-STAR system.
- iii. The smallest of the *minimum* MPC cavity-free volumes among the two MPC types is considered for flooded water mass determination.
- iv. Fifty percent of the water mass in the MPC cavity is credited towards water thermal inertia evaluation.

Table 4.4.20 summarizes the weights and thermal inertias of several components in the loaded HI-STAR system. The rate of temperature rise of the HI-STAR and its contents during an adiabatic heat-up is governed by the following equation:

$$\frac{dT}{dt} = \frac{Q}{C_h}$$

where:

Q = decay heat load (Btu/hr)
 [equal to Design Basis maximum (among the two MPC types) 19.0 kW (i.e., 64,847 Btu/hr)]

C_h = combined thermal inertia of the loaded HI-STAR system (Btu/°F)

T = temperature of the contents (°F)

t = time after HI-STAR system is removed from the pool (hr)

A bounding heat-up rate for the HI-STAR system contents is determined to be equal to 2.08°F/hr. From this adiabatic rate of temperature rise estimate, the maximum allowable time duration (t_{max}) for fuel to be submerged in water is determined as follows:

$$t_{\max} = \frac{T_{\text{boil}} - T_{\text{initial}}}{(dT/dt)}$$

where:

T_{boil} = boiling temperature of water
 (equal to 212°F at the water surface in the MPC cavity)

T_{initial} = initial temperature of the HI-STAR contents when removed from the pool

Table 4.4.21 provides a summary of t_{max} at several initial HI-STAR contents temperatures.

As set forth in the HI-STAR 100 operating procedures, in the unlikely event where the maximum allowable time provided in Table 4.4.21 is found to be insufficient to complete all wet transfer operations, a forced water circulation shall be initiated and maintained to remove the decay heat from the MPC cavity. In this case, relatively cooler water will enter via the MPC lid drain port connection and heated water will exit from the vent port. The minimum water flow rate required to maintain the MPC cavity water temperature below boiling with an adequate subcooling margin is determined as follows:

$$M_w = \frac{Q}{C_{pw} (T_{max} - T_{in})}$$

where:

M_w = minimum water flow rate (lb/hr)

C_{pw} = water heat capacity (Btu/lb-°F)

T_{max} = maximum MPC cavity water mass temperature

T_{in} = temperature of water supply to MPC

With the MPC cavity water temperature limited to 150°F, MPC inlet water maximum temperature equal to 125°F and at the design basis maximum heat load, the water flow rate is determined to be 2,594 lb/hr (5.3 gpm).

4.4.1.1.15 Cask Cooldown and Reflood Analysis During Fuel Unloading Operation

NUREG-1536 requires an evaluation of cask cooldown and reflood procedures to support fuel unloading from a dry condition. Past industry experience generally supports cooldown of cask internals and fuel from hot storage conditions by direct water quenching. However, the extremely rapid cooldown rates that are typical during water injection, to which the hot cask internals and fuel cladding are subjected to, may result in uncontrolled thermal stresses and failure in the structural members. Moreover, water injection results in large amounts of steam generation and unpredictable transient two-phase flow conditions inside the MPC cavity, which may result in over-pressurization of the confinement boundary and a potentially unacceptable reduction in the safety margins to prevent criticality. To avoid potential safety concerns related to rapid cask cooldown by direct water quenching, the HI-STAR MPCs are designed to be cooled in a gradual manner, thereby eliminating thermal shock loads on the cask internals and fuel cladding.

In the unlikely event that a HI-STAR system is required to be unloaded, it will be transported back to the fuel handling building. Prior to reflooding the MPC cavity with water, a forced flow helium recirculation system with adequate flow capacity shall be operated to remove the decay heat and initiate a slow cask cooldown lasting for several days. The operating procedures in Chapter 8 (Section 8.3) provide a detailed description of the steps involved in the cask unloading. In this section, an analytical evaluation is presented to provide the basis for helium flow rates and time of forced cooling to meet the objective of eliminating thermal shock when the MPC cavity is eventually flooded with water.

Under a closed loop forced helium circulation condition, the helium gas is cooled via an external chiller, down to 100°F, and then introduced inside the MPC cavity from the drain line near the bottom baseplate. The helium gas enters the MPC basket from the bottom oversized flow holes and moves upwards through the hot fuel assemblies, removing heat and cooling the MPC internals. The heated helium gas exits from the basket top and collects in the top plenum, from where it is expelled through the MPC lid vent connection to the helium recirculation and cooling system. The MPC contents bulk average temperature reduction as a function of time is principally dependent upon the rate of helium circulation. The temperature transient is governed by the following heat balance equation

$$C_h \frac{dT}{dt} = Q_D - m C_p (T - T_i) - Q_c$$

Initial Condition: $T = T_o$ at $t = 0$

where:

$T =$ MPC bulk average temperature (°F)

$T_o =$ initial MPC bulk average temperature in the HI-STAR system
(equal to 439°F)

$t =$ time after start of forced circulation (hrs)

$Q_D =$ decay heat load (Btu/hr)
(equal to Design Basis maximum 19.0 kW (i.e., 64,847 Btu/hr))

$m =$ helium circulation rate (lb/hr)

$C_p =$ helium heat capacity (Btu/lb-°F)
(equal to 1.24 Btu/lb-°F)

$Q_c =$ heat rejection from cask exposed surfaces to ambient (Btu/hr) (conservatively neglected)

C_h = thermal capacity of the loaded MPC (Btu/°F)

(For a bounding upper bound 100,000 lb loaded MPC weight, and heat capacity of Alloy X equal to 0.12 Btu/lb-°F, the heat capacity is equal to 12,000 Btu/°F.)

T_i = MPC helium inlet temperature (°F)

The differential equation is analytically solved, yielding the following expression for time-dependent MPC bulk temperature.

$$T(t) = (T_i + \frac{Q_D}{m C_p}) (1 - e^{-\frac{m C_p}{C_h} t}) + T_o e^{-\frac{m C_p}{C_h} t}$$

This equation is used to determine the minimum helium mass flow rate which would cool the MPC cavity down from initially hot conditions to less than 200°F in 72 hours. The required helium mass flow rate is 546 lb/hr (i.e., 817 SCFM).

Once the helium gas circulation has cooled the MPC internals to less than 200°F, water can be injected to the MPC without risk of boiling and the associated thermal stress concerns. Because of the relatively long cooldown period, the thermal stress contribution to the total cladding stress would be negligible, and the total stress would therefore be bounded by the normal (dry) condition. The elimination of boiling eliminates any concern of over-pressurization due to steam production.

4.4.1.1.16 HI-STAR Temperature Field With Low Emitting Fuel

The HI-STAR 100 thermal evaluations for BWR fuel are divided in two groups of fuel assemblies proposed for storage in MPC-68. These groups are classified as Low Heat Emitting (LHE) fuel assemblies and Design Basis (DB) fuel assemblies. The LHE group of fuel assemblies are characterized by low burnup, long cooling time, and short active fuel lengths. Consequently, their heat loads are dwarfed by the DB group of fuel assemblies. The Dresden-1 (6x6 and 8x8), Quad⁺, and Humboldt Bay (7x7 and 6x6) fuel characteristics warrant their classification as LHE fuel. These characteristics, including burnup and cooling time limits imposed on this class of fuel, are presented in Table 2.1.6. This fuel (except Quad⁺) is permitted to be loaded when encased in Damaged Fuel Containers (DFCs). As a result of interruption of radiation heat exchange between the fuel assembly and the fuel basket by the DFC boundary, this loading configuration is bounding for thermal evaluation. In Subsection 4.4.1.1.2, two canister designs for encasing LHE fuel are evaluated – a previously approved Holtec Design (Holtec Drawing-1783) and an existing canister in which some of the Dresden-1 fuel is currently stored (Transnuclear D-1 Canister). The most resistive fuel assembly determined by analytical evaluation is considered for thermal evaluation (see Table 4.4.6). The MPC-68 basket effective conductivity, loaded with the most resistive fuel assembly from the LHE group of fuel (encased in a canister) is provided in Table 4.4.7. To this basket, LHE decay heat load is applied and a HI-STAR 100 System temperature field obtained. The low heat load burden limits the initial peak cladding temperature to 595°F which is

substantially below the temperature limit for long-cooled fuel (~643°F).

A thoria rod canister designed to hold a maximum of 20 fuel rods arrayed in a 5x4 configuration is currently stored at the Dresden-1 spent fuel pool. The fuel rods contain a mixture of enriched UO_2 and Thorium Oxide in the fuel pellets. The fuel rods were originally constituted as part of an 8x8 fuel assembly and used in the second and third cycle of Dresden-1 operation. The maximum fuel burnup of these rods is quite low (~14,400 MWD/MTU). The thoria rod canister internal design is a honeycomb structure formed from 12 gage stainless steel plates. The rods are loaded in individual square cells and are isolated from each other by the cell walls. The few number of rods (18 per assembly) and very low burnup of fuel stored in these Dresden-1 canisters render them as miniscule sources of decay heat. The canister all-metal internal honeycomb construction serves as an additional means of heat dissipation in the fuel cell space. In accordance with preferential fuel loading requirements imposed in the Technical Specifications, low burnup fuel shall be loaded toward the basket periphery (i.e., away from the hot central core of the fuel basket). All these considerations provide ample assurance that these fuel rods will be stored in a benign thermal environment and therefore remain protected during long-term storage.

4.4.1.2 Test Model

A detailed analytical model for thermal design of the HI-STAR 100 System was developed using the FLUENT CFD code and the industry standard ANSYS modeling package, as discussed in Subsection 4.4.1.1. As discussed throughout this chapter and specifically in Section 4.4.6, the analysis incorporates significant conservatism so as to predict the fuel cladding temperature with considerable margins. Furthermore, compliance with specified limits of operation is demonstrated with adequate margins. In view of these considerations, the HI-STAR 100 System thermal design complies with the thermal criteria set forth in the design basis (Sections 2.1 and 2.2) for long-term storage under normal conditions. Additional experimental verification of the thermal design is therefore not required.

4.4.2 Maximum Temperatures

4.4.2.1 Maximum Temperatures Under Normal Storage Conditions

The two MPC basket designs developed for the HI-STAR 100 System have been analyzed to determine the temperature distribution under long-term normal storage conditions. The MPC baskets are considered to be loaded at design basis maximum heat loads with PWR or BWR fuel assemblies, as appropriate. The systems are considered to be arranged in an ISFSI array and subjected to design basis normal ambient conditions with insolation.

Applying the radiative blocking factor applicable for the worst case cask location, converged temperature contours are shown in Figures 4.4.17 and 4.4.18 for the MPC-24, and MPC-68 basket designs. The temperatures in these two figures are in degrees Kelvin. The calculated

temperatures presented in this chapter are based on an array of analyses that incorporate many conservatisms. As such, the calculated temperatures are upper bound values which would exceed actual temperatures.

The maximum fuel clad temperatures for zircaloy clad fuel assemblies are listed in Tables 4.4.10 and 4.4.11, which also summarize maximum calculated temperatures in different parts of the HI-STAR 100 System. Figures 4.4.21 and 4.4.22 show the axial temperature variation of the hottest fuel rod in the MPC-24 and MPC-68 basket designs, respectively. Figures 4.4.24 and 4.4.25 show the radial temperature profile in the MPC-24 and MPC-68 basket designs, respectively, in the horizontal plane where maximum fuel cladding temperature is indicated.

As discussed in Subsection 4.4.1.1.1, the thermal analysis is performed using a submodeling process where the results of an analysis on an individual component are incorporated into the analysis of a larger set of components. Specifically, the submodeling process yields directly computed fuel temperatures from which fuel basket temperatures are indirectly calculated. This modeling process differs from previous analytical approaches wherein the basket temperatures were evaluated first and then a basket-to-cladding temperature difference calculation by Wooten-Epstein or other means provided a basis for cladding temperatures. Subsection 4.4.1.1.2 describes the calculation of an effective fuel assembly thermal conductivity for an equivalent homogenous region. It is important to note that the result of this analysis is a function for thermal conductivity versus temperature. This function for fuel thermal conductivity is then input to the fuel basket effective thermal conductivity calculation described in Subsection 4.4.1.1.4. This calculation uses a finite-element methodology, wherein each fuel cell region containing multiple finite-elements has temperature varying thermal conductivity properties. The resultant temperature varying fuel basket thermal conductivity computed by this basket-fuel composite model is then input to the fuel basket region of the FLUENT cask model.

Because the FLUENT cask model incorporates the results of the fuel basket submodel, which in turn incorporates the fuel assembly submodel, the peak temperature reported from the FLUENT model is the peak temperature in any component. In a dry storage cask, the hottest components are the fuel assemblies. It should be noted that, because the fuel assembly models described in Subsection 4.4.1.1.2 include the fuel pellets, the FLUENT calculated peak temperatures reported in Tables 4.4.10 and 4.4.11 are actually peak pellet centerline temperatures which bound the peak cladding temperatures. We conservatively assume that the peak clad temperature is equal to the peak pellet centerline temperature.

The following additional observations can be derived by inspecting the temperature field obtained from the finite volume analysis:

- The maximum fuel cladding temperature is well within the PNL [4.3.1] and the LLNL [4.3.6] recommended temperature limits.
- The maximum temperature of the basket structural material is within the stipulated Design Temperature.
- The maximum temperature of the Boral neutron absorber is below the material supplier's recommended limit.
- The maximum temperatures of the MPC pressure boundary materials are well below their respective ASME Code limits.
- The maximum temperatures of the overpack pressure boundary material are well below their respective ASME Code limits.
- The neutron shielding material (Holtite-A) will not experience temperatures in excess of its qualified limit.
- The local temperatures of the mechanical seals are well below their respective long-term limits (Table 4.3.1).

Noting that the allowable maximum initial peak cladding temperature is significantly lower for older fuel, parametric peak fuel cladding temperature versus total decay heat load tables for each of the two basket designs were developed. This lower than design basis heat load performance data is presented in Tables 4.4.18 and 4.4.19. The decay heat limit curve in Figure 2.1.8 is developed based on these tables and the allowable fuel cladding temperature limits listed in Table 2.2.3.

The above observations lead us to conclude that the temperature field in the HI-STAR 100 System with a fully loaded MPC containing design-basis heat emitting SNF complies with all regulatory and industry temperature limits. In other words, the thermal environment in the HI-STAR 100 System will be conducive to long-term safe storage of spent nuclear fuel.

4.4.2.2 Maximum MPC Basket Temperature Under Vacuum Conditions

A plot of typical steady-state temperature contours under vacuum conditions is shown in Figure 4.4.19. The peak fuel clad temperature during short-term vacuum drying operations is limited to less than 950°F for both baskets at design basis maximum heat loads by a significant margin. This limit is lower than the recommended fuel cladding temperature (see Table 4.3.1) limits for short-term conditions by a large margin.

4.4.3 Minimum Temperatures

In Table 2.2.2 of this report, the minimum ambient temperature condition required to be considered for HI-STAR 100 System design is specified to be -40°F. If, conservatively, a zero decay heat load (with no solar input) is applied to the stored fuel assemblies then every component of the system at steady state would be at this minimum ambient temperature. All HI-STAR 100 System materials of construction would satisfactorily perform their intended function in the storage mode at this minimum postulated temperature condition. Structural evaluations in Chapter 3 show the acceptable performance of the overpack and MPC steel material at low temperature. Criticality and shielding functions of the HI-STAR 100 System materials (Chapters 5 and 6) are unaffected by exposure to this minimum temperature.

4.4.4 Maximum Internal Pressure

The MPC is initially filled with helium after fuel loading and drying prior to installing the MPC closure ring. During normal storage, the gas temperature within the MPC rises to its maximum operating basis temperature as determined based on the thermal analysis methodology described earlier. The gas pressure inside the MPC will also increase with rising temperature. The pressure rise is determined using the ideal gas law which states that the absolute pressure of a fixed volume of confined gas is proportional to its absolute temperature. In Tables 4.4.13 and 4.4.14, a summary of calculations for determining the net free volume in the MPC-24 and MPC-68 are presented.

The maximum gas pressure in the MPC is considered for a postulated accidental release of fission product gases caused by fuel rods rupture. For these fuel rod rupture conditions, the amounts of each of the release gas constituents in the MPC cavity are summed and the resulting total pressures determined from the Ideal Gas Law. Based on fission gases release fractions (per NUREG-1536 criteria [4.1.3]), minimum net free volume and maximum initial fill gas pressure, bounding maximum gas pressures with 1% (normal), 10% (off-normal), and 100% (accident condition) rod rupture are given in Table 4.4.15. The MPC maximum gas pressures listed in Table 4.4.15 are all below the MPC design internal pressure listed in Table 2.2.1.

The inclusion of PWR non-fuel hardware (BPRA control elements and thimble plugs) to the MPC-24 influences the internal pressure in two ways. The presence of non-fuel hardware enhances heat dissipation, thus lowering fuel temperatures and the gas filling the space between fuel rods. The gas volume displaced by the mass of non-fuel hardware lowers the cavity free volume. These two effects, namely, temperature lowering and free volume reduction, have opposing influence in the MPC cavity pressure. The first effect lowers gas pressure while the second effect raises it. In the HI-STAR thermal analysis, the computed temperature field (with non-fuel hardware excluded) provides a conservatively bounding MPC-24 temperature field. The MPC cavity free space is computed based on volume displacement by the heaviest fuel (bounding weight) with non-fuel hardware included.

During in-core irradiation of BPRAs, the B-10 isotope in the neutron absorbing material is

transformed to helium atoms. Two different forms of the neutron absorbing material are used in BPRAs: Borasilicate glass and B₄C in a refractory solid matrix (Al₂O₃). Borosilicate glass (primarily a constituent of Westinghouse BPRAs) is used in the shape of hollow pyrex glass tubes sealed within steel rods and supported on the inside by a thin walled steel liner. To accommodate helium diffusion from the glass rod into the rod internal space, a relatively high void volume (~40%) is engineered in this type of rod design. The rod internal pressure is thus designed to remain below reactor operating conditions (2,300 psia and approximately 600°F coolant temperature). The B₄C- Al₂O₃ neutron absorber material is principally used in B&W and CE fuel BPA designs. The relatively low temperature of the poison material in BPA rods (relative to fuel pellets) favor the entrapment of helium atoms in the solid matrix.

Several BPA designs are used in PWR fuel which differ in the number, diameter, and length of poison rods. The older Westinghouse fuel (W-14x14 and AW-15x15) has used 6, 12, 16, and 20 rods per assembly BPRAs and the later (W-17x17) fuel uses up to 24 rods per BPA. The BPA rods in the older fuel are much larger than the later fuel and, therefore, the B-10 isotope inventory in the 20-rod BPRAs bound the newer W-17x17 fuel. Based on bounding BPA rods internal pressure, a large hypothetical quantity of helium (7.2 g-moles/BPA) is assumed to be available for release into the MPC cavity from each fuel assembly in the MPC-24. To accommodate this quantity of helium gas* at the NUREG-1536 stipulated rods rupture assumptions, the initial helium backfill in the MPC-24 is reduced such that the final confinement boundary pressures are approximately unchanged from inclusion of non-fuel hardware. The MPC cavity pressures are summarized in Table 4.4.15

4.4.5 Maximum Thermal Stresses

Thermal expansion induced mechanical stresses due to the non-uniform temperature distribution are reported in Chapter 3. Table 4.4.16 provides a summary of HI-STAR 100 System component temperature inputs for structural evaluation.

Table 4.4.22 provides a summary of confinement boundary temperatures during normal storage conditions. Structural evaluation in Section 3.4.4 references these temperature results to demonstrate confinement boundary integrity.

4.4.6 Evaluation of System Performance for Normal Conditions of Storage

The HI-STAR 100 System thermal analysis is based on a detailed and complete heat transfer model which properly accounts for radiation, conduction and natural convection modes of heat transfer in various portions of the MPC and overpack. The thermal model incorporates many conservative features that are listed below:

1. The most severe levels of environmental factors - bounding long-term annual ambient temperature with insolation - were coincidentally imposed on the HI-STAR 100 cask. A

* 3,875 liters of helium gas at STP from 100% BPA rods rupture.

bounding solar absorptivity of 1.0 was applied to all surfaces exposed to insolation.

2. No credit was considered for the thermosiphon heat transfer which is intrinsic to the HI-STAR fuel baskets.
3. The most adversely located HI-STAR 100 System in an ISFSI array was considered for analysis.
4. No credit was considered for conduction through the radial neutron shielding material.
5. A uniform nominal radial gap between overpack-to-MPC was applied to the cask thermal model. No credit for gap reduction due to differential thermal expansion under the hot condition was considered. The MPC is considered to be in concentric alignment inside the overpack cavity. This is a worst case scenario since any eccentricity will improve conductive heat transport in this region.
6. No credit was considered for radiative heat transfer between the Boral neutron absorber panels and the Boral pocket walls, or for the presence of helium in the pocket gap.
7. Interfacial contact conductance of multilayered intermediate shell contacting layers was conservatively determined to bound surface finish, contact pressure, and base metal conductivity conditions.
8. No credit was considered for contact between fuel assemblies and the MPC basket wall or between the MPC basket and the basket supports. The fuel assemblies and MPC basket were conservatively considered to be in concentric alignment.
9. The MPC is assumed to be loaded with the SNF type which has the maximum equivalent thermal resistance of all fuel types in its category (BWR or PWR), as applicable.
10. The decay heat load, which is a function of burnup and decay time, varies in a narrow range within the group of PWR assemblies considered (Table 4.4.5) and also within the group of BWR assemblies considered (Table 4.4.6). The assembly type which gives the maximum decay heat load for a given burnup is used for defining the decay heat load vs. decay time. The B&W 15×15 is the limiting PWR SNF type (see Table 2.1.5). The governing BWR fuel is GE 7×7 (see Table 2.1.5). For other than the governing fuel types, there is a small conservatism in the decay heat load term.
11. The MPC basket axial conductivity is conservatively assumed to be equal to the lower basket cross sectional effective conductivity.
12. As discussed in Section 4.3, the NUREG-1536 endorsed DCCG [4.3.6] model yields temperature limits slightly higher (approximately 10°F) than the PNL [4.3.1] limits for

allowable peak cladding temperature during storage. For conservatism, the lower PNL value (Table 2.2.3) is used as the permissible limit.

Temperature distribution results obtained from this conservative thermal model show that the established maximum fuel cladding temperature limits are met with adequate margins. Expected margins during normal storage will be larger due to the many conservative assumptions incorporated in the analysis. The long-term impact of decay heat induced temperature levels on the HI-STAR 100 System structural and neutron shielding materials is considered to be negligible. The maximum local MPC basket temperature level is below the recommended limits for structural materials in terms of susceptibility to stress, corrosion and creep induced degradation. Furthermore, structural evaluation (Chapter 3) has demonstrated that stresses (including those induced due to imposed temperature gradients) are within ASME B&PV Code limits. The maximum local neutron shield temperature is lower than design limits. Section 4.5 provides a discussion of compliance with regulatory criteria 1 through 8 listed in Section 4.0. The above-mentioned considerations lead to the conclusion that the HI-STAR 100 System thermal design is in compliance with 10CFR72 requirements.

Table 4.4.1

CLOSED CAVITY NUSSELT NUMBER RESULTS
FOR HELIUM-FILLED MPC PERIPHERAL VOIDS

Temperature [°F]	Nusselt Number (PWR Baskets)	Nusselt Number (BWR Basket)
200	3.17	2.41
450	2.56	1.95
700	2.21	1.68

Table 4.4.2

RELATIONSHIP BETWEEN HI-STAR 100 SYSTEM REGIONS
AND MATHEMATICAL MODEL DESCRIPTIONS

<u>HI-STAR System Region</u>	<u>Mathematical Model</u>	<u>Subsections</u>
Fuel Assembly	Fuel Region Effective Thermal Conductivity	4.4.1.1.2
MPC	Effective Thermal Conductivity of Boral/Sheathing/Box Wall Sandwich	4.4.1.1.3
	Basket In-Plane Conductive Heat Transport	4.4.1.1.4
	Heat Transfer in MPC Basket Peripheral Region	4.4.1.1.5
	Effective Thermal Conductivity of Flexible MPC Basket-to-Shell Aluminum Heat Conduction Elements	4.4.1.1.10
Overpack	Effective Conductivity of Multilayered Intermediate Shell Region	4.4.1.1.6
	Effective Thermal Conductivity of Holtite Neutron Shielding Region	4.4.1.1.9
Ambient Environment	Heat Rejection from Overpack Exterior Surfaces	4.4.1.1.7
	Solar Heat Input	4.4.1.1.8
Assembled Cask Model	Overview of the Thermal Model	4.4.1.1.1
	FLUENT Model for HI-STAR 100	4.4.1.1.11

Table 4.4.3

THIS TABLE IS INTENTIONALLY DELETED.

Table 4.4.4

THIS TABLE IS INTENTIONALLY DELETED.

Table 4.4.5

SUMMARY OF PWR FUEL ASSEMBLY EFFECTIVE
THERMAL CONDUCTIVITIES

	Fuel	@ 200°F (Btu/ft-hr-°F)	@ 450°F (Btu/ft-hr-°F)	@ 700°F (Btu/ft-hr-°F)
1	W - 17×17 OFA	0.182	0.277	0.402
2	W - 17×17 Std	0.189	0.286	0.413
3	W - 17×17 Vantage	0.182	0.277	0.402
4	W - 15×15 Std	0.191	0.294	0.430
5	W - 14×14 Std	0.182	0.284	0.424
6	W - 14×14 OFA	0.175	0.275	0.413
7	B&W - 17×17	0.191	0.289	0.416
8	B&W - 15×15	0.195	0.298	0.436
9	CE - 16×16	0.183	0.281	0.411
10	CE - 14×14	0.189	0.293	0.435
11	HN [†] -15×15 SS	0.180	0.265	0.370
12	W-14×14 SS	0.170	0.254	0.361
13	B&W - 15×15	0.187	0.289	0.424
14	CE-14×14 (MP2)	0.188	0.293	0.434

Note: Boldface values denote the lowest thermal conductivity in each column.

[†] Haddam Neck B&W or Westinghouse stainless steel clad fuel assemblies.

Table 4.4.6
SUMMARY OF BWR FUEL ASSEMBLY EFFECTIVE
THERMAL CONDUCTIVITIES

	Fuel	@ 200°F (Btu/ft-hr-°F)	@ 450°F (Btu/ft-hr-°F)	@ 700°F (Btu/ft-hr-°F)
1	Dresden 1 - 8x8 [†]	0.119	0.201	0.319
2	Dresden 1 - 6x6 [†]	0.126	0.215	0.345
3	GE - 7x7	0.171	0.286	0.449
4	GE - 7x7R	0.171	0.286	0.449
5	GE - 8x8	0.168	0.278	0.433
6	GE - 8x8R	0.166	0.275	0.430
7	GE10 - 8x8	0.168	0.280	0.437
8	GE11 - 9x9	0.167	0.273	0.422
9	AC ^{††} -10x10 SS	0.152	0.222	0.309
10	Exxon-10x10 SS	0.151	0.221	0.308
11	Humboldt Bay-7x7 [†]	0.127	0.215	0.343
12	Dresden-1 Thin [†] Clad-6x6	0.124	0.212	0.343
13	Damaged Dresden-1 8x8 [†] (in a damaged fuel container)	0.107	0.169	0.254
14	Damaged [†] Dresden-1 8x8 (in TN D-1 canister)	0.107	0.168	0.252
15	8x8 QUAD ⁺ Westinghouse [†]	0.164	0.276	0.435

Note: Boldface values denote the lowest thermal conductivity in each column.

[†] Fuel cladding temperatures for low heat emitting (intact and damaged) fuel types in the HI-STAR 100 System will be bounded by design basis fuel cladding temperatures. Therefore, these fuel assembly types are excluded from the list of design basis fuel assemblies (zircaloy clad) evaluated to determine the most resistive SNF type.

^{††} Allis-Chalmers stainless steel clad fuel assemblies.

Table 4.4.7

**MPC BASKET EFFECTIVE THERMAL CONDUCTIVITY RESULTS
FROM ANSYS MODELS**

Basket	@200°F [Btu/ft-hr-°F]	@450°F [Btu/ft-hr-°F]	@700°F [Btu/ft-hr-°F]
MPC-24 (Zircaloy Clad Fuel)	1.108	1.495	1.954
MPC-68 (Zircaloy Clad Fuel)	0.959	1.188	1.432
MPC-24 (Stainless Steel Clad Fuel)	0.995	1.321	1.700 (a)
MPC-68 (Stainless Steel Clad Fuel)	0.931	1.125	1.311 (b)
MPC-68 (Dresden-1 8x8 in canister)	0.861	1.055	1.242

- (a) Conductivity is 13% less than corresponding zircaloy fueled basket.
 (b) Conductivity is 9% less than corresponding zircaloy fueled basket.

Table 4.4.8

EFFECTIVE THERMAL CONDUCTIVITY OF THE NEUTRON SHIELD/RADIAL CHANNEL LEG REGION

Condition/Temperature (°F)	Thermal Conductivity (Btu/ft-hr-°F)
Normal condition: 200 450 700	 1.953 1.812 1.645
Fire condition: 200 450 700	 3.012 2.865 2.689

Table 4.4.9

THIS TABLE IS INTENTIONALLY DELETED.

Table 4.4.10

HI-STAR 100 SYSTEM LONG-TERM NORMAL STORAGE[†]
 MAXIMUM TEMPERATURES [°F]
 (24-PWR ASSEMBLIES, MPC)

	Maximum Temperature (°F)	Normal Condition Design Temperature (°F)
Fuel Cladding	709	720
MPC Basket Centerline	675	725
MPC Basket Periphery	451	725
MPC Outer Shell Surface	332	450
MPC/Overpack Helium Gap Outer Surface	292	400
Neutron Shield Inner Surface	274	300
Overpack Outer Enclosure Surface	229	350
Overpack Bolted Closure Plate ^{††}	155	400
Overpack Bottom Plate ^{††}	241	350

† Ambient Temperature = 80°F
 Cask Array Pitch = 3 x Cask Radius = 12 ft.

†† Overpack closure plate and vent/drain port plug seals normal condition design temperature is 400°F. The maximum seals temperatures are bounded by the reported closure plate and bottom plate maximum temperatures. Consequently, a large margin of safety exists to permit safe operation of seals in the overpack helium retention boundary.

Table 4.4.11

HI-STAR 100 SYSTEM LONG-TERM NORMAL STORAGE[†]
 MAXIMUM TEMPERATURES [°F]
 (68-BWR ASSEMBLIES, MPC)

	Maximum Temperature (°F)	Normal Condition Design Temperature (°F)
Fuel Cladding	741	749
MPC Basket Centerline	725	725
MPC Basket Periphery	393	725
MPC Outer Shell Surface	331	450
MPC/Overpack Helium Gap Outer Surface	292	400
Neutron Shield Inner Surface	273	300
Overpack Outer Enclosure Surface	228	350
Overpack Bolted Closure Plate ^{††}	155	400
Overpack Bottom Plate ^{††}	213	350

† Ambient Temperature = 80°F
 Cask Array Pitch = 3 x Cask Radius = 12 ft.

†† Overpack closure plate and vent/drain port plug seals normal condition design temperature is 400°F. The maximum seals temperatures are bounded by the reported closure plate and bottom plate maximum temperatures. Consequently, a large margin of safety exists to permit safe operation of seals in the overpack helium retention boundary.

Table 4.4.12

THIS TABLE IS INTENTIONALLY DELETED.

Table 4.4.13

SUMMARY OF MPC-24 FREE VOLUME CALCULATIONS

Item	Volume (ft ³)
Cavity Volume	368.3
Basket Metal Volume	47.0
Bounding Fuel Assemblies Volume	78.8
Basket Supports and Fuel Spacers Volume	6.1
Aluminum Conduction Elements	5.9 [†]
Net Free Volume	230.5 (6529 liters)

[†] Bounding 1,000 lbs weight.

Table 4.4.14

SUMMARY OF MPC-68 FREE VOLUME CALCULATIONS

Item	Volume (ft ³)
Cavity Volume	367.3
Basket Metal Volume	45.6
Bounding Fuel Assemblies Volume	93.0
Basket Supports and Fuel Spacers Volume	11.3
Aluminum Conduction Elements	5.9 [†]
Net Free Volume	211.5 (5989 liters)

[†] Bounding 1,000 lbs weight.

Table 4.4.15

SUMMARY OF MPC CONFINEMENT BOUNDARY PRESSURES[†] FOR
NORMAL LONG-TERM STORAGE

Condition	Pressure (psig)
MPC-24:*	
Initial backfill (at 70°F)	22.2
Normal condition	43.8
With 1% rods rupture	44.3
With 10% rods rupture	49.1
With 100% rods rupture	97.3
MPC-68:	
Initial backfill (at 70°F)	28.5
Normal condition	57.5
With 1% rods rupture	57.8
With 10% rods rupture	60.2
With 100% rods rupture	84.5

[†] Pressure analysis is based on NUREG-1536 criteria (i.e., 100% of rods fill gas and 30% of radioactive gases are available for release from a ruptured rod).

* PWR fuel storage includes hypothetical BPRA rods rupture in the pressure calculations.

Table 4.4.16

SUMMARY OF HI-STAR 100 SYSTEM COMPONENTS
NORMAL STORAGE TEMPERATURES [°F]

Location	MPC-24	MPC-68
MPC Basket Top:		
Basket center	180	179
Basket periphery	168	168
MPC shell	166	167
Overpack inner shell	162	163
Overpack enclosure shell	159	160
MPC Basket Bottom:		
Basket center	251	220
Basket periphery	226	204
MPC shell	222	203
Overpack inner shell	218	201
Overpack enclosure shell	177	167

Table 4.4.17

THIS TABLE IS INTENTIONALLY DELETED.

Table 4.4.18

MPC-24 BASKET PEAK FUEL CLADDING TEMPERATURE AS A
FUNCTION OF TOTAL HEAT LOAD

Total Basket Decay Heat Load (kW)	Peak Cladding Temperature (°F)
19.0 [†]	708.8
18.5	696.9
17.0	660.1
15.5	621.9

[†] Design Basis Maximum (equivalent to 792 watts per assembly).

Table 4.4.19

MPC-68 BASKET PEAK CLADDING TEMPERATURE AS A
FUNCTION OF TOTAL DECAY HEAT LOAD

Total Basket Decay Heat Load (kW)	Peak Cladding Temperature (°F)
18.5 [†]	741.5
17.5	713.6
15.5	656.2

[†] Design Basis Maximum (equivalent to 272 watts per assembly).

Table 4.4.20

SUMMARY OF LOADED HI-STAR SYSTEM
BOUNDING COMPONENT WEIGHTS AND THERMAL INERTIAS

Component	Weight (lbs)	Heat Capacity (Btu/lb-°F)	Thermal Inertia (Btu/°F)
Holtite-A	11,000	0.39	4,290
Carbon Steel	140,000	0.1	14,000
Alloy-X MPC (empty)	35,000	0.12	4,200
Fuel	40,000	0.056	2,240
MPC Cavity Water [†]	6,500	1.0	6,500
			31,230 (Total)

[†] Based on smallest MPC-68 cavity net free volume with 50% credit for flooded water mass.

Table 4.4.21

MAXIMUM ALLOWABLE TIME DURATION FOR WET
TRANSFER OPERATIONS

Initial Temperature (°F)	Time Duration (hr)
115	46.7
120	44.3
125	41.9
130	39.5
135	37.1
140	34.6
145	32.3
150	29.8

Table 4.4.22

SUMMARY OF MPC CONFINEMENT BOUNDARY TEMPERATURE DISTRIBUTION DURING NORMAL STORAGE CONDITIONS

Location	Figure 3.4.44 Designation	MPC-24 [°F]	MPC-68 [°F]
MPC Lid Inside Surface at Centerline	A	179	178
MPC Lid Outside Surface at Centerline	B	173	172
MPC Lid Inside Surface at Periphery	C	166	167
MPC Lid Outside Surface at Periphery	D	164	164
MPC Baseplate Inside Surface at Centerline	E	249	218
MPC Baseplate Outside Surface at Centerline	F	241	213
MPC Baseplate Inside Surface at Periphery	G	222	203
MPC Baseplate Outside Surface at Periphery	H	219	200
MPC Shell Maximum	I	332	331

Table 4.4.23

SUMMARY OF 10×10 ARRAY TYPE BWR FUEL ASSEMBLY EFFECTIVE THERMAL CONDUCTIVITIES*

FUEL	@200°F [Btu/ft-hr-°F]	@450°F [Btu/ft-hr-°F]	@700°F [Btu/ft-hr-°F]
GE-12/14	0.166	0.269	0.412
Atrium-10	0.164	0.266	0.409
SVEA-96	0.164	0.269	0.416

* The conductivities reported in this table are obtained by the simplified method described in the beginning of the Subsection 4.4.1.1.2.

Table 4.4.24

COMPARISON OF ATRIUM-10 BWR FUEL ASSEMBLY CONDUCTIVITY[†] WITH THE BOUNDING^{††} BWR FUEL ASSEMBLY CONDUCTIVITY

Temperature [°F]	Atrium-10 BWR Assembly [Btu/ft-hr-°F]	Bounding BWR Assembly [Btu/ft-hr-°F]
200	0.225	0.171
450	0.345	0.271
700	0.504	0.410

[†] The reported effective conductivity has been obtained from a rigorous finite element model.

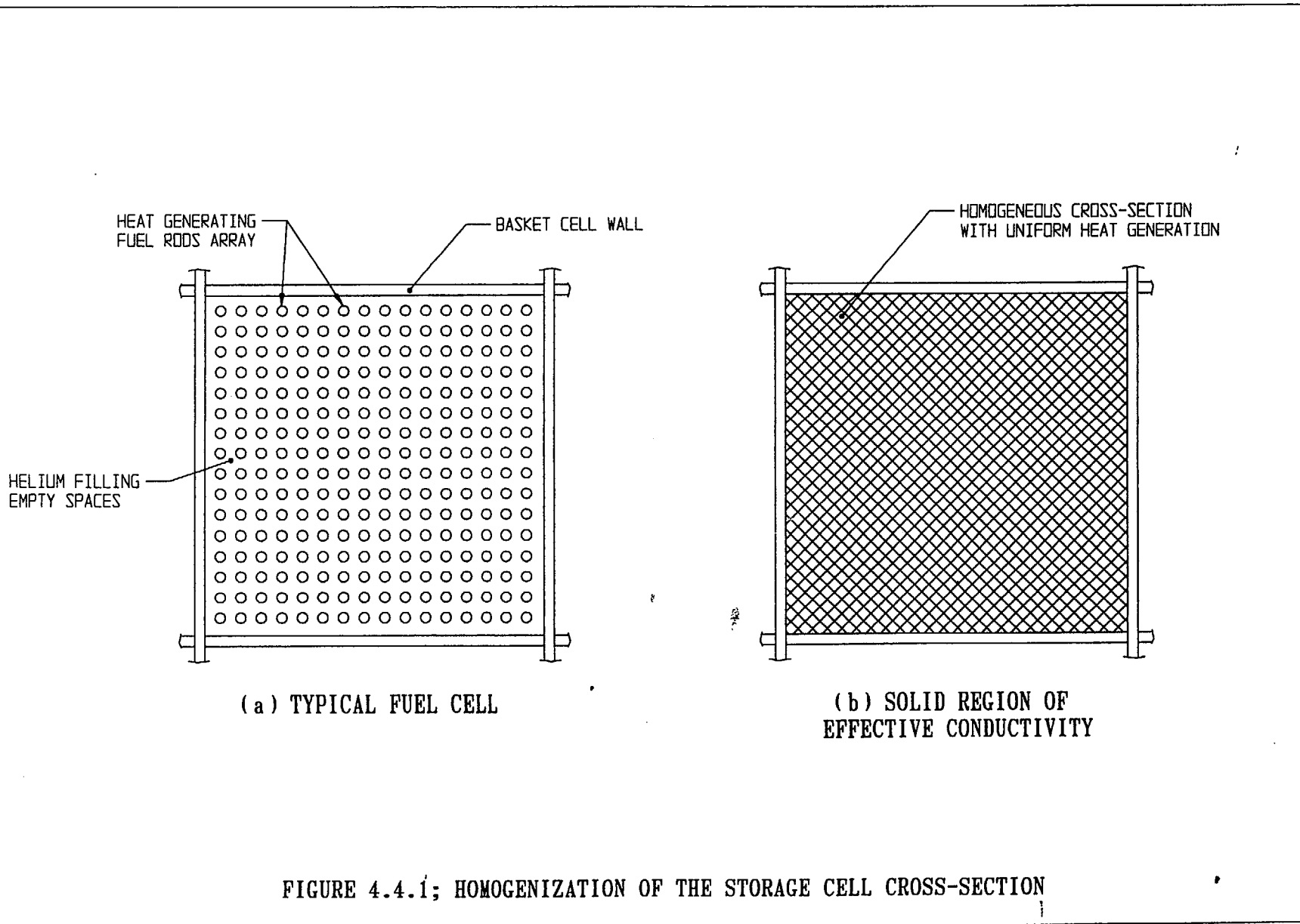
^{††} The bounding BWR fuel assembly conductivity applied in the MPC-68 basket thermal analysis.

Table 4.4.25

PLANT SPECIFIC BWR FUEL TYPES EFFECTIVE THERMAL CONDUCTIVITY*

Fuel	@200° F [Btu/ft-hr-°F]	@ 450° F [Btu/ft-hr-°F]	@ 700° F [Btu/ft-hr-°F]
Oyster Creek (7x7)	0.165	0.273	0.427
Oyster Creek (8x8)	0.162	0.266	0.413
TVA Browns Ferry (8x8)	0.160	0.264	0.411
SPC-5 (9x9)	0.149	0.245	0.380

* The conductivities reported in this table are obtained by a simplified analytical method described in Subsection 4.4.1.2.



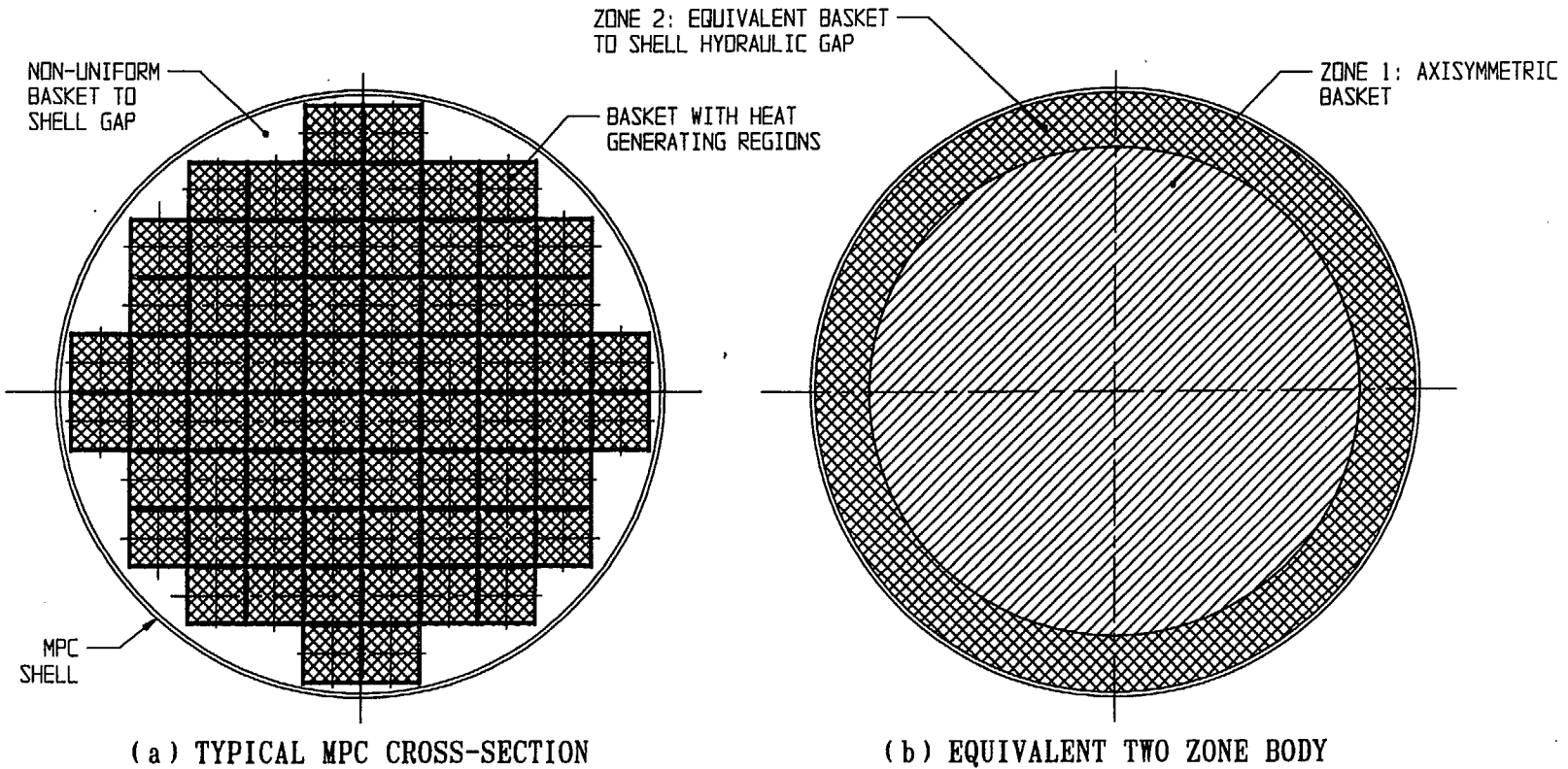


FIGURE 4.4.2; MPC CROSS-SECTION REPLACED WITH AN EQUIVALENT TWO ZONE AXISYMMETRIC BODY

HEAT CONDUCTION ELEMENTS NOT SHOWN

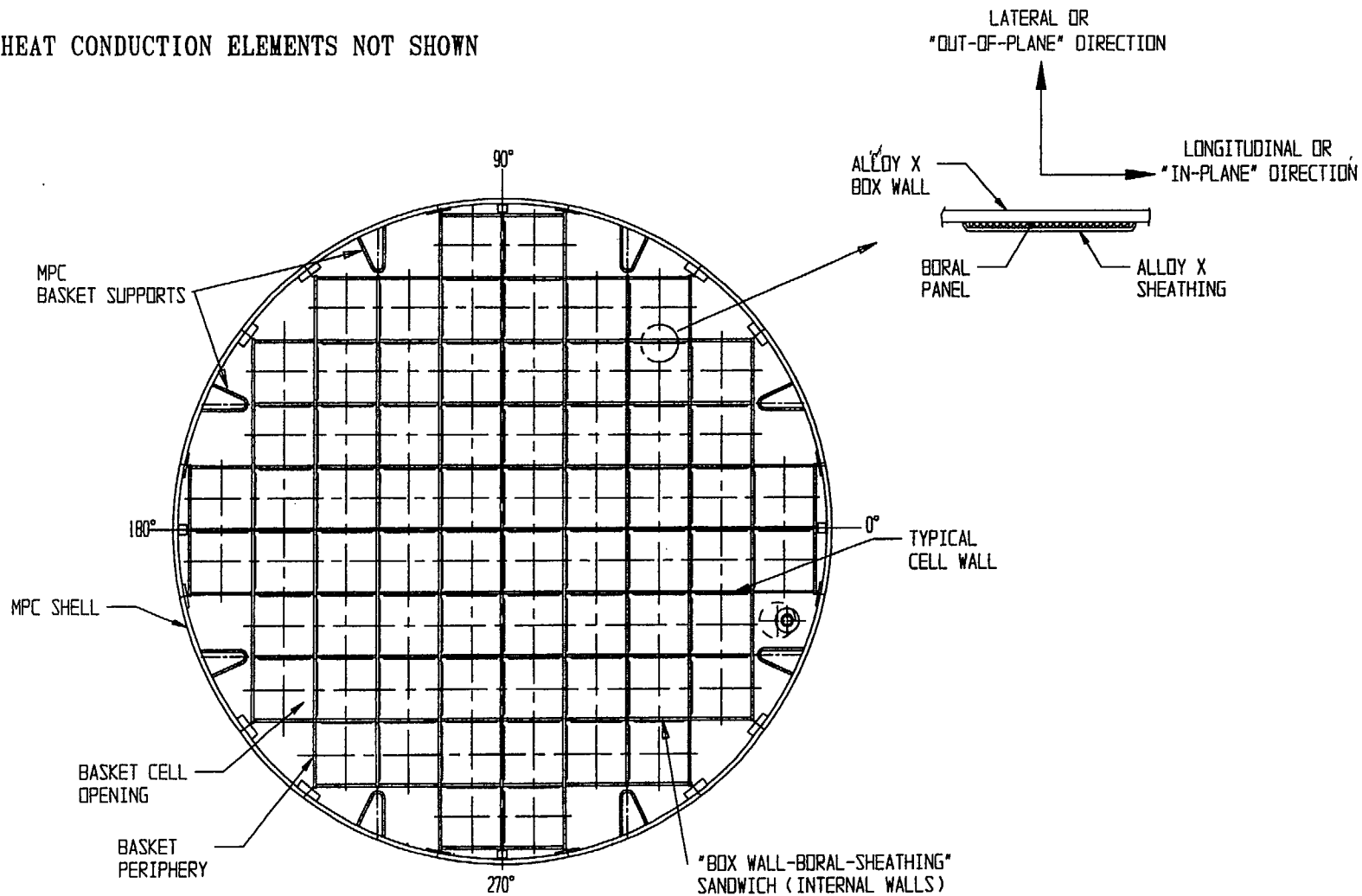


FIGURE 4.4.3; TYPICAL MPC BASKET PARTS IN A CROSS-SECTIONAL VIEW

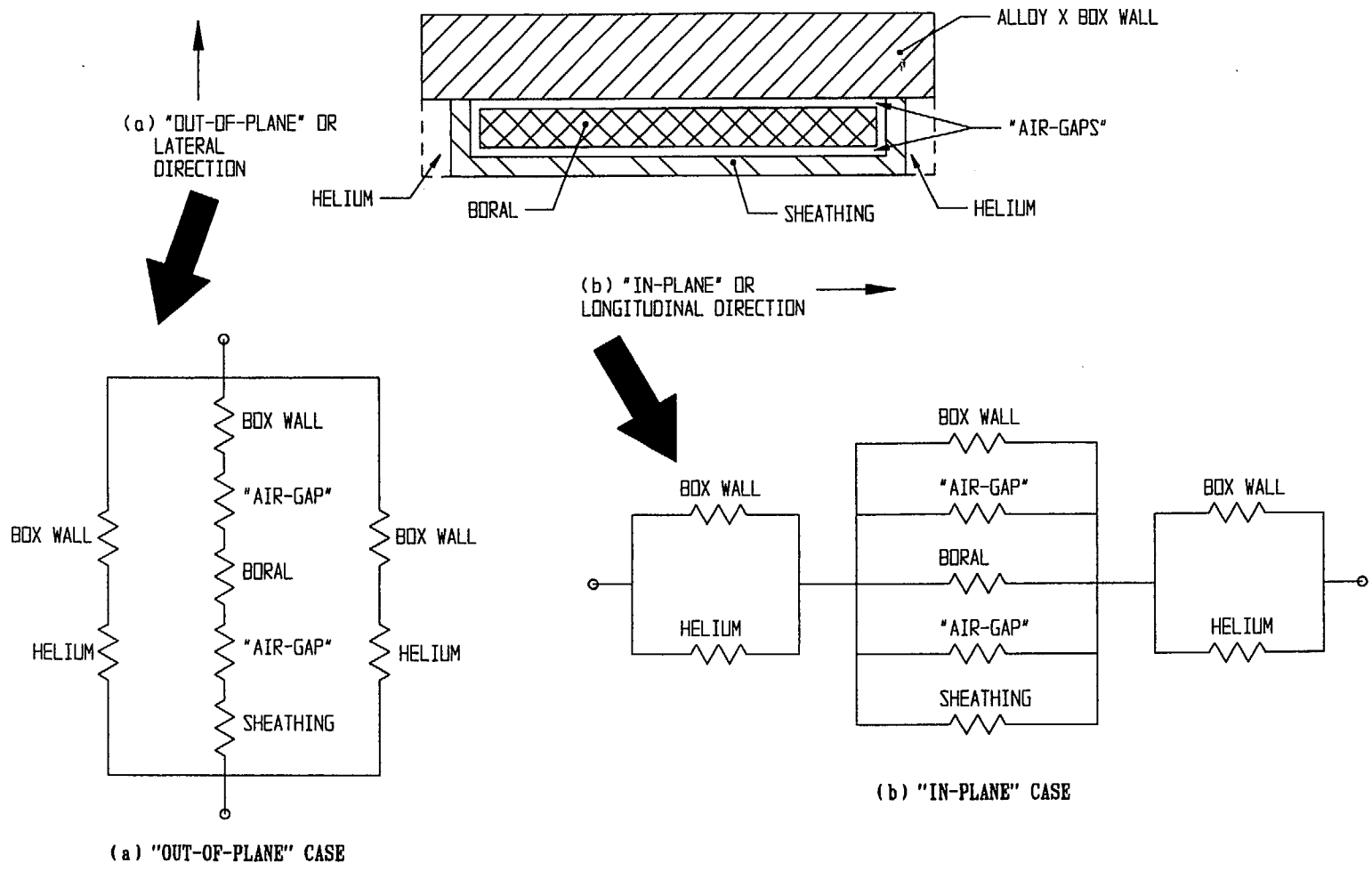
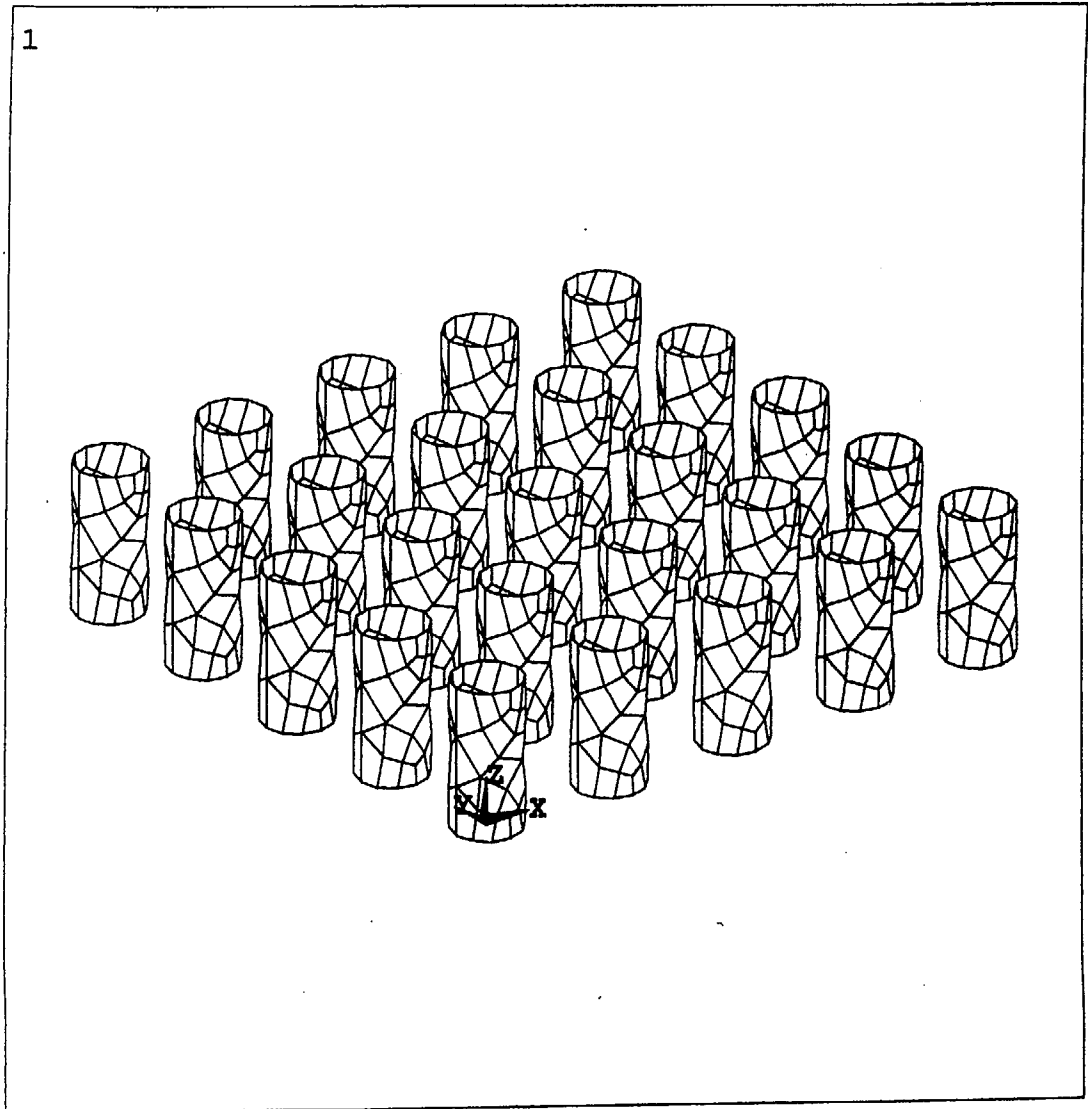


FIGURE 4.4.4; RESISTANCE NETWORK MODEL OF A "BOX WALL-BORAL-SHEATHING" SANDWICH



ANSYS 5.0 A 95
MAR 28 1995
13:56:42
PLOT NO. 1
ELEMENTS
TYPE NUM

XV = -1
YV = -1.3
ZV = 0.8
DIST=666.39
XF = 384
YF = 384
ZF = 100.125
VUP = Z
CENTROID HIDDEN

FIGURE 4.4.5; ANSYS FINITE ELEMENT MODEL FOR EVALUATION OF RADIATIVE BLOCKING FACTOR FOR A CASK ARRAY AT AN ISFSI SITE

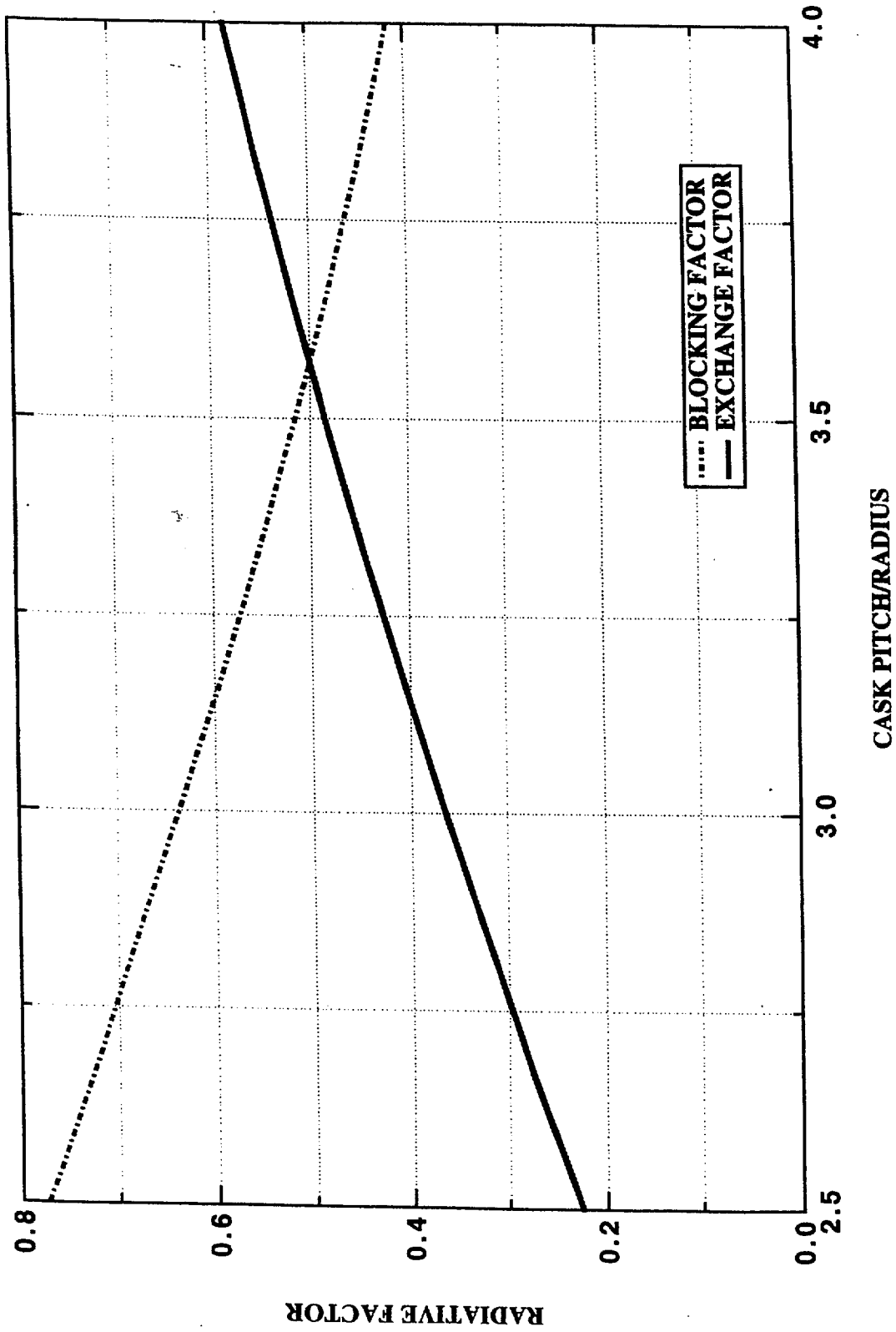


FIGURE 4.4.6; EFFECT OF ISFSI CASK ARRAY PITCH ON RADIATIVE BLOCKING AND EXCHANGE FACTORS

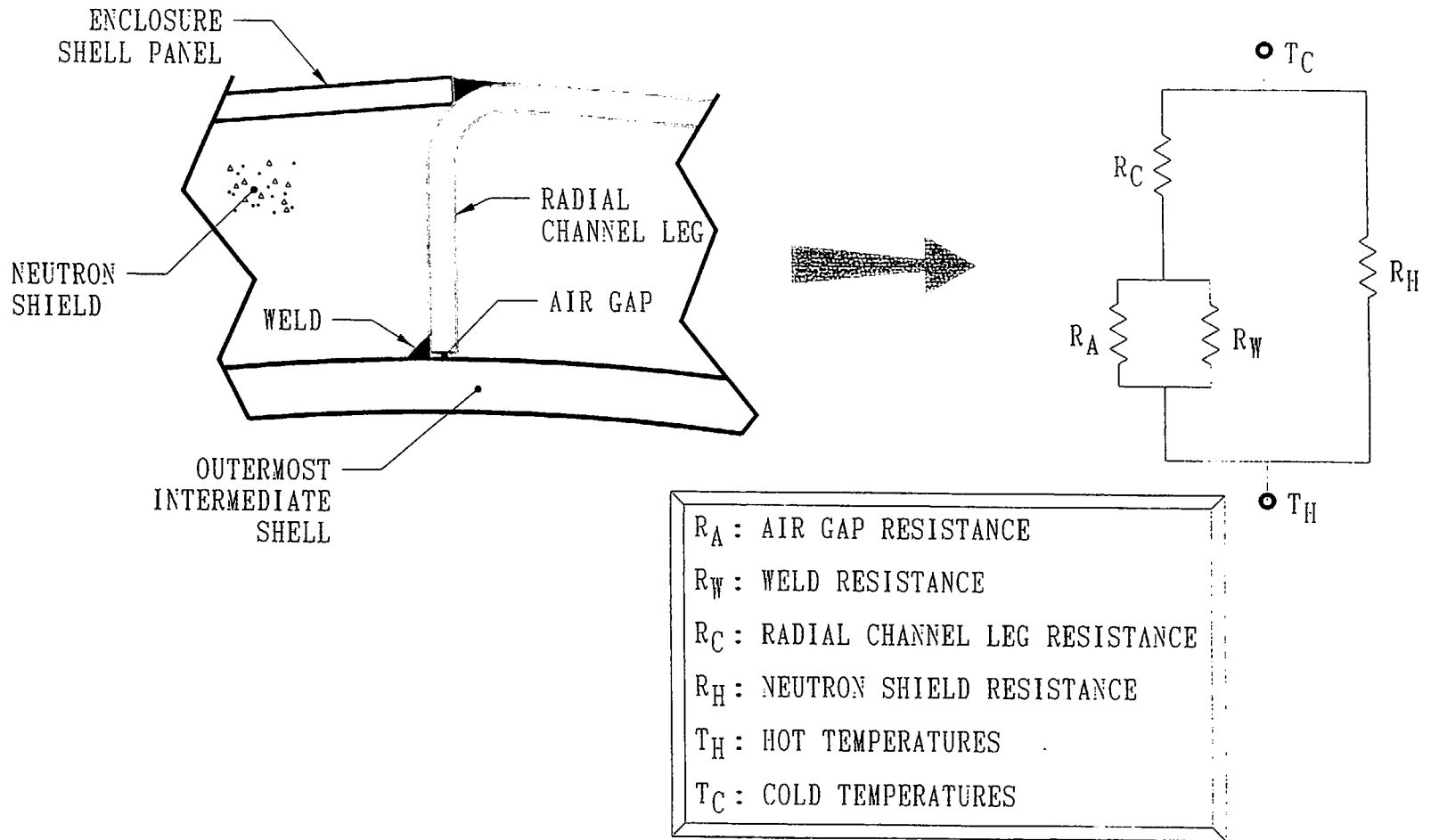
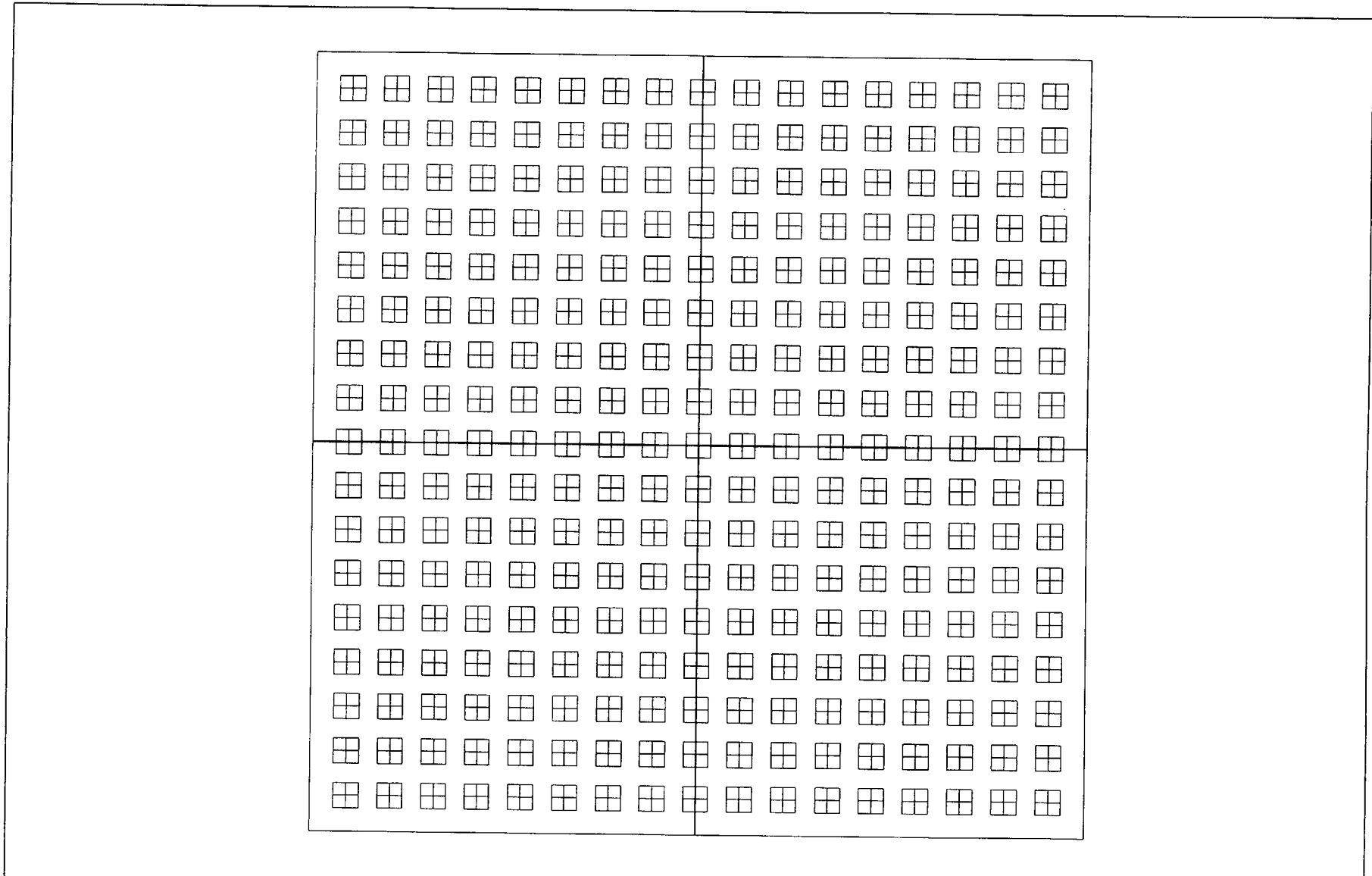


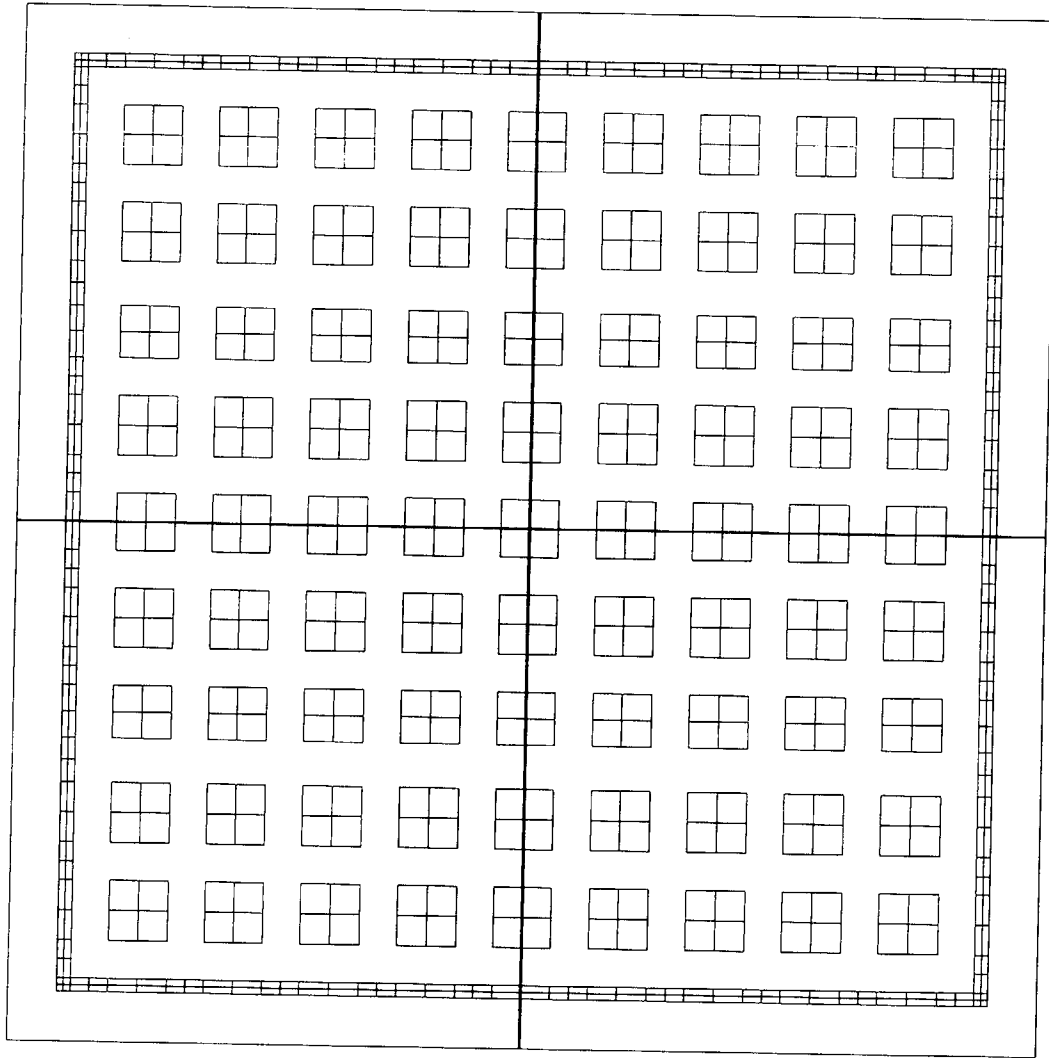
FIGURE 4.4.7; NEUTRON SHIELD REGION RESISTANCE NETWORK ANALOGY FOR EFFECTIVE CONDUCTIVITY CALCULATION



W17X17 OFA FUEL ASSEMBLY MODEL

Nov 11 1997
Fluent 4.32
Fluent Inc.

FIGURE 4.4.8: WESTINGHOUSE 17x17 OFA PWR FUEL ASSEMBLY MODEL



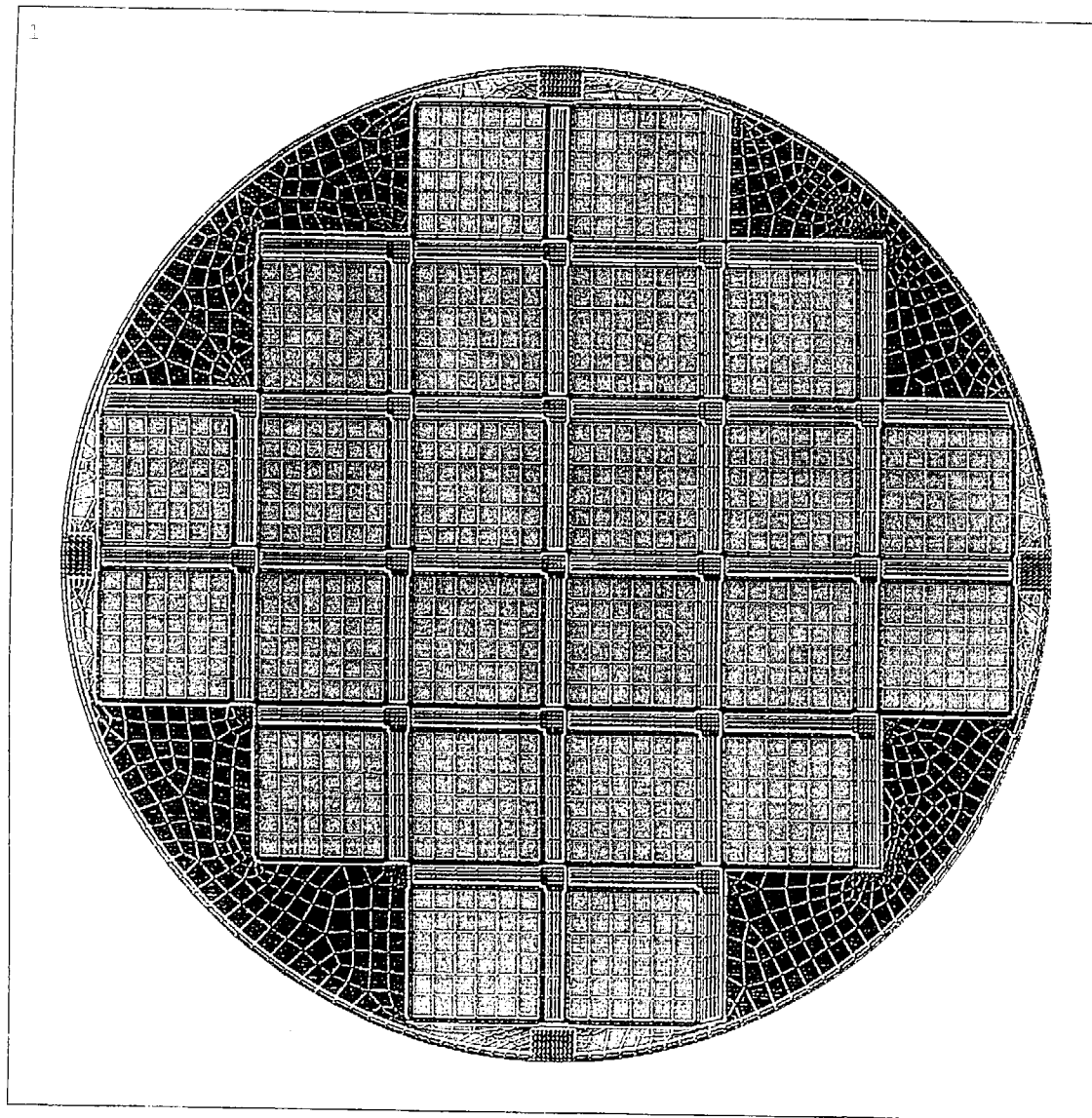
GE11-9X9 CHANNELED FUEL ASSEMBLY MODEL

Nov 11 1997
Fluent 4.32
Fluent Inc.

FIGURE 4.4.9: GENERAL ELECTRIC 9x9 BWR FUEL ASSEMBLY MODEL

FIGURE 4.4.10

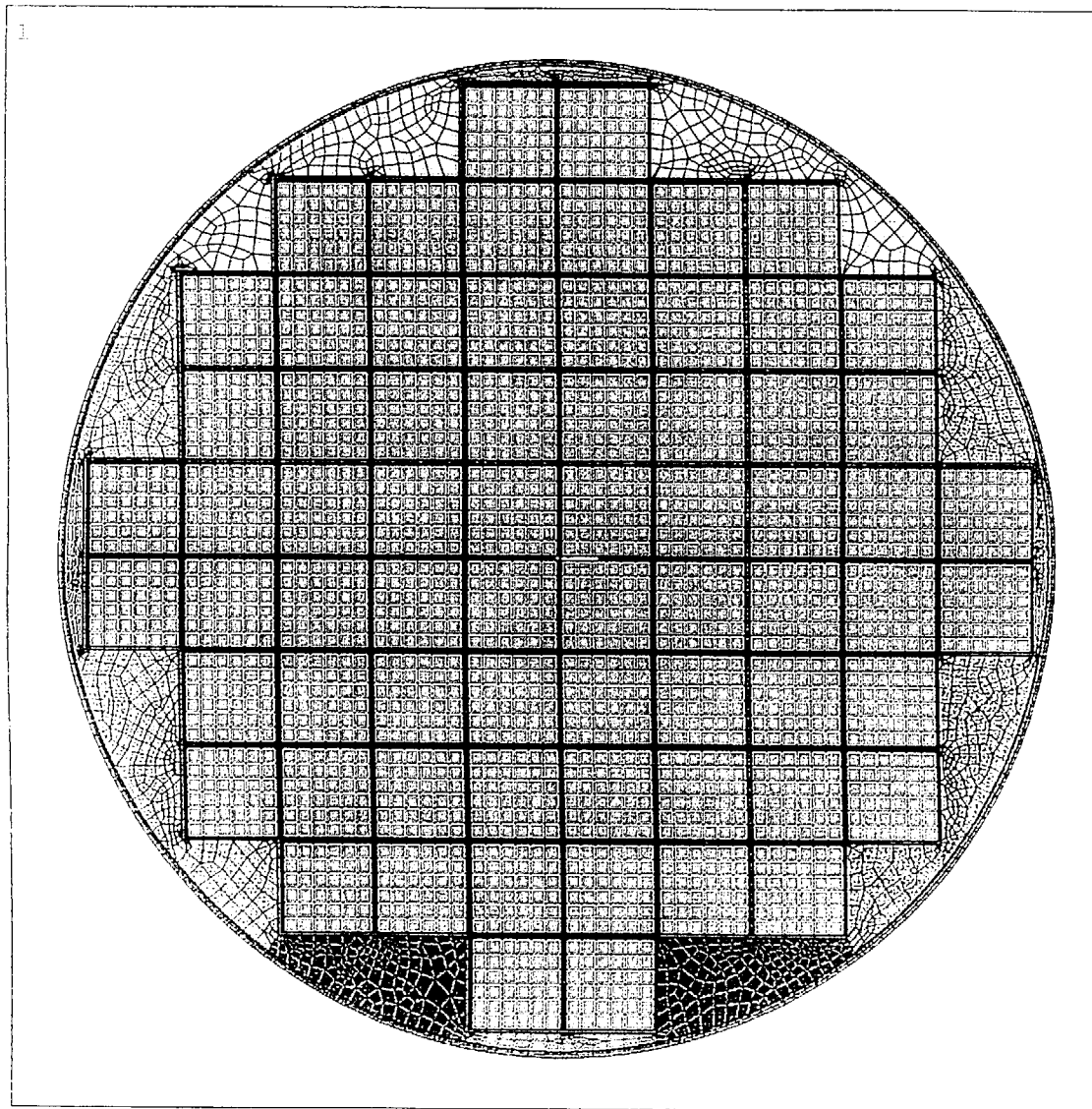
THIS FIGURE IS INTENTIONALLY DELETED



ANSYS 5.3
NOV 13 1997
11:26:52
PLOT NO. 1
ELEMENTS
MAT NUM

ZV =1
*DIST=37.606
Z-BUFFER

FIGURE 4.4.11; MPC-24 BASKET CROSS-SECTION ANSYS FINITE ELEMENT MODEL



ANSYS 5.3
NOV 13 1997
11:28:39
PLOT NO. 1
ELEMENTS
MAT NUM

ZV =1
*DIST=37.606
Z-BUFFER

FIGURE 4.4.12; MPC-68 BASKET CROSS-SECTION ANSYS FINITE ELEMENT MODEL

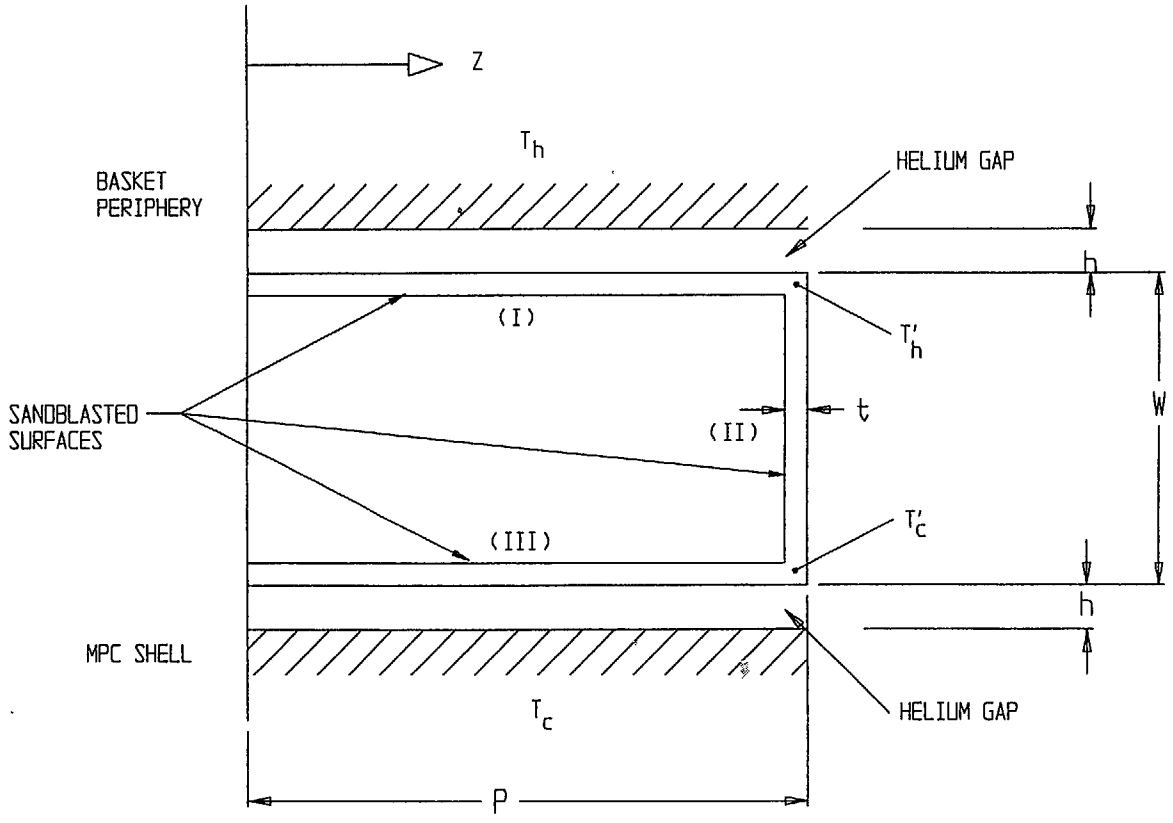
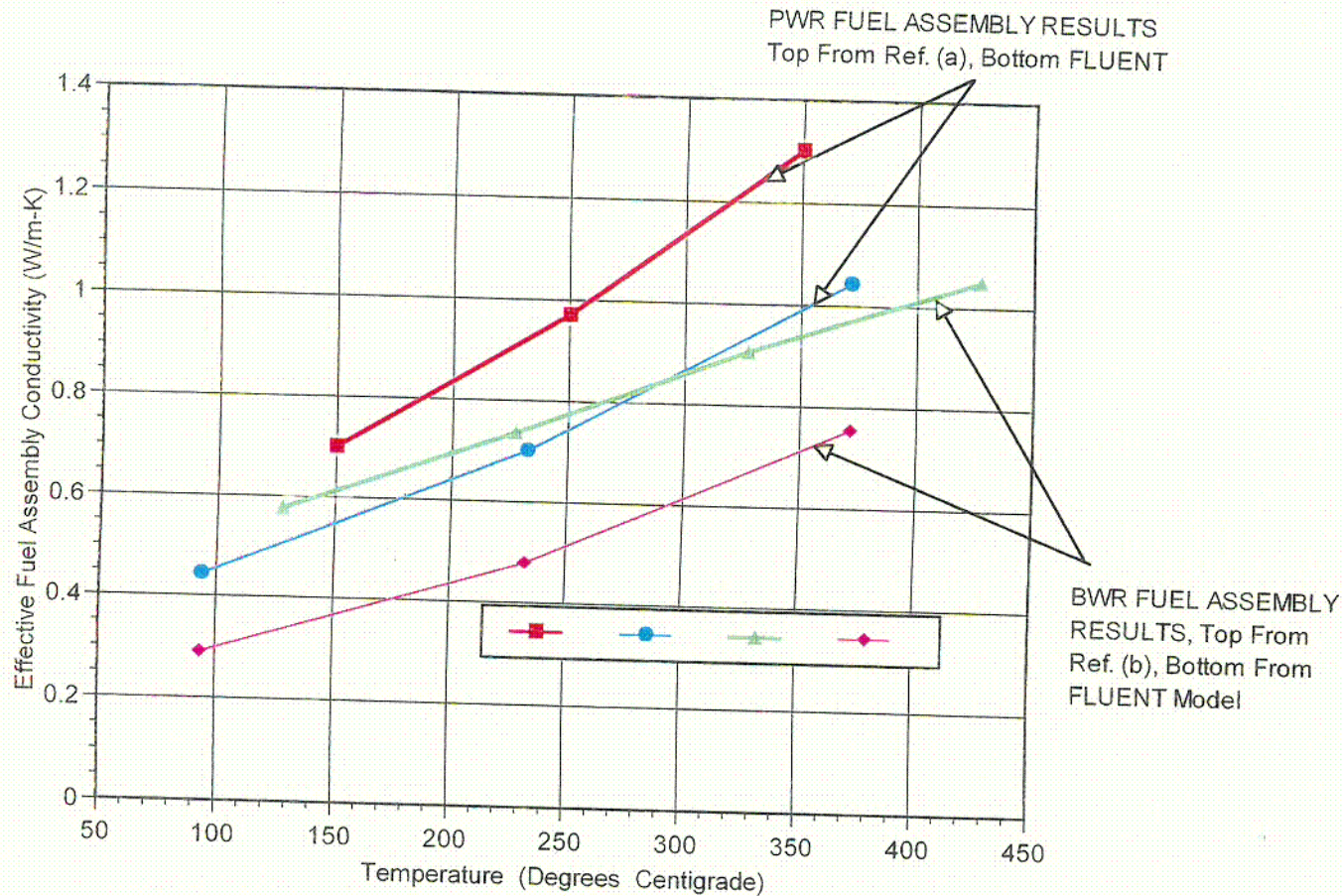


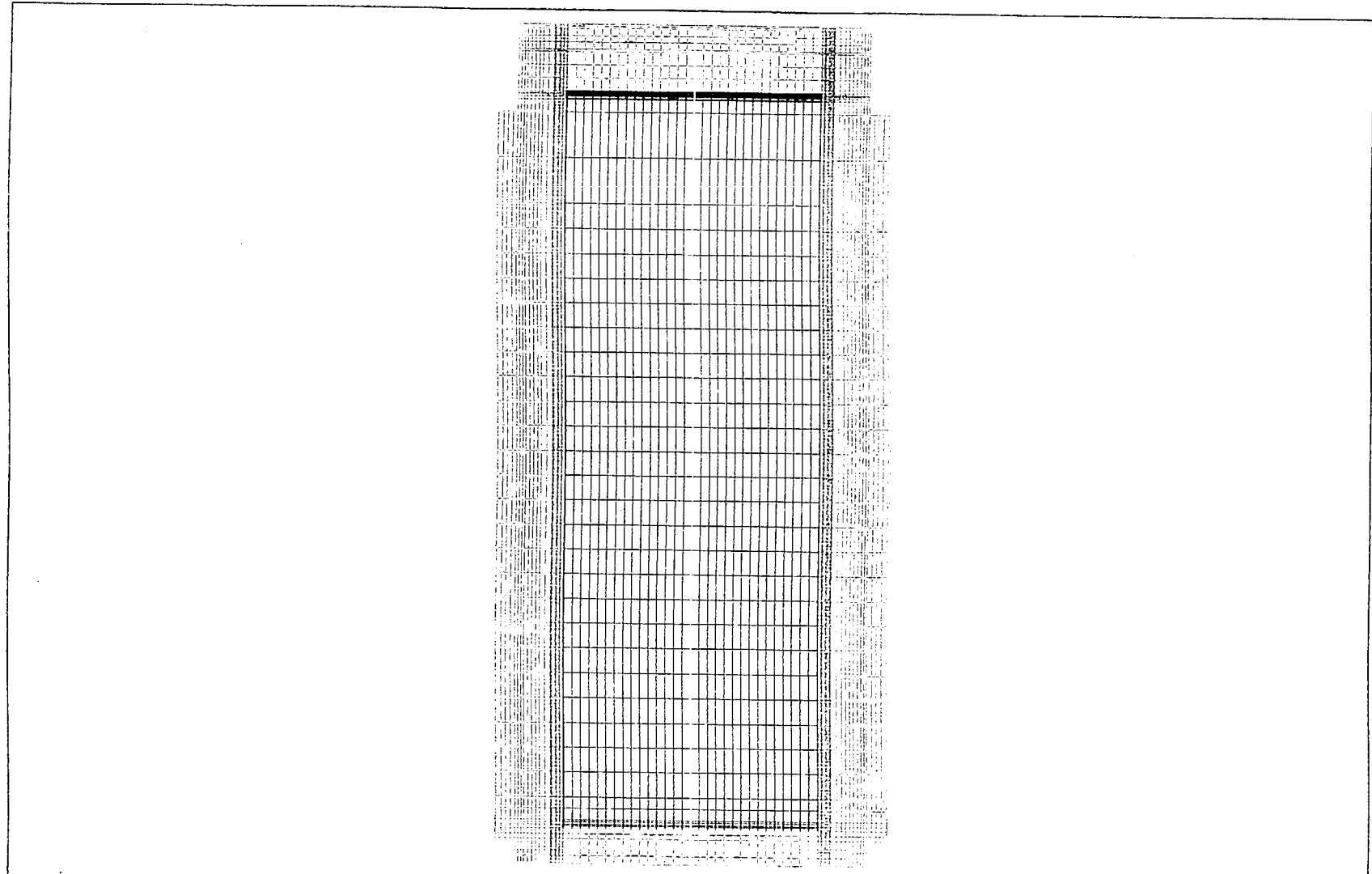
FIGURE 4.4.13; ILLUSTRATION OF AN MPC BASKET TO SHELL ALUMINUM HEAT CONDUCTION ELEMENT



(a) "Determination of SNF Peak Temperatures in the Waste Package", Bahney & Doering, *HLRWM Sixth Annual Conf.*, Pages 671-673, (April 30 - May 5, 1995)
 (b) "A Method for Determining the Spent-Fuel Contribution to Transport Cask Containment Requirements", *Sandia Report SAND90-2406*, page II-132, (1992)

FIGURE 4.4.14: COMPARISON OF FLUENT BASED FUEL ASSEMBLY EFFECTIVE CONDUCTIVITY RESULTS WITH PUBLISHED TECHNICAL DATA

C01



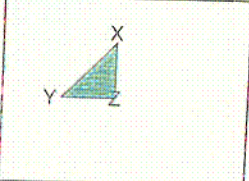
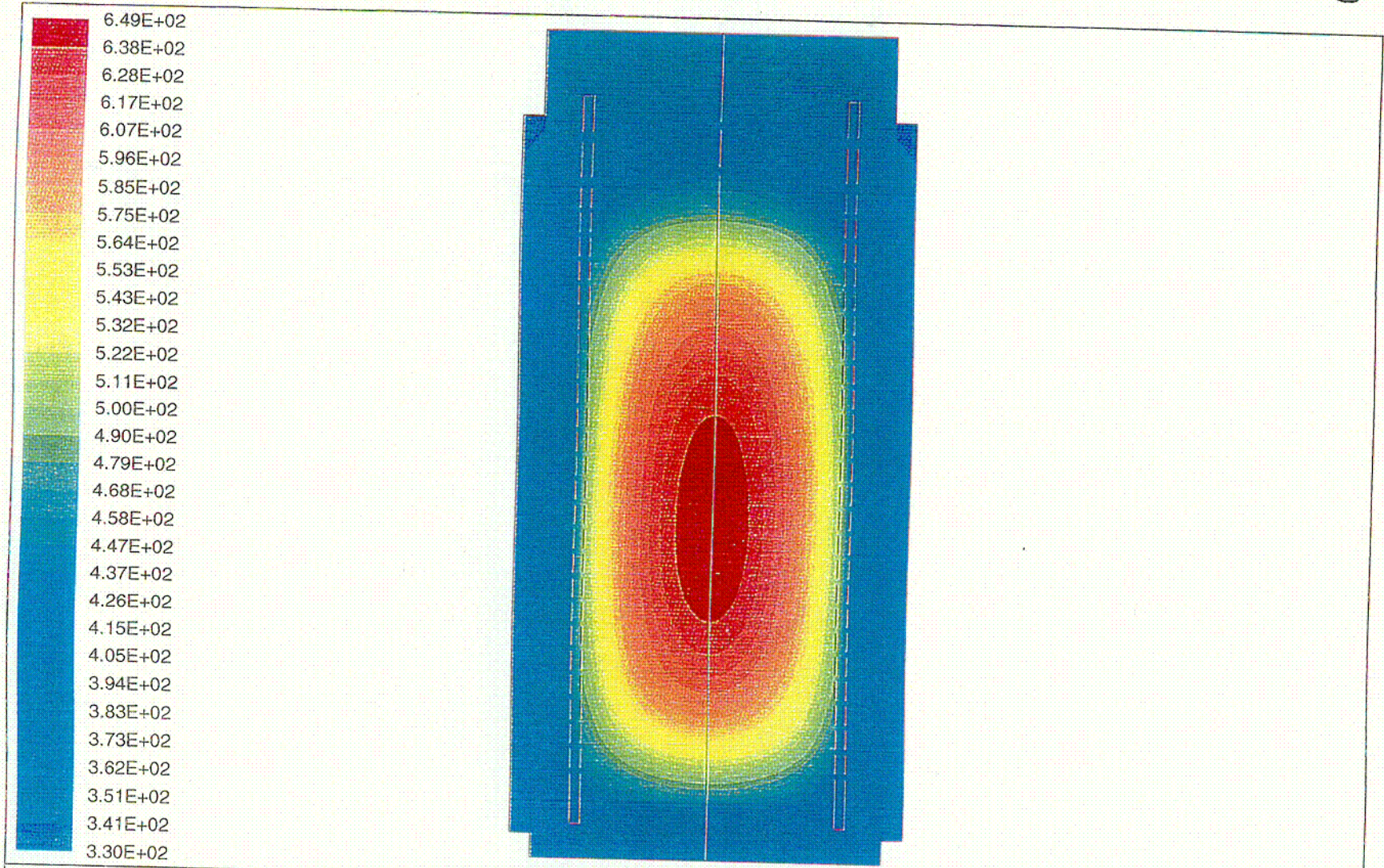
Grid (57 X 46)

Nov 18 1997
Fluent 4.32
Fluent Inc.

FIGURE 4.4.15: TYPICAL HI-STAR 100 SYSTEM FINITE ELEMENT MESH FOR THERMAL ANALYSIS

FIGURE 4.4.16

THIS FIGURE IS INTENTIONALLY DELETED



MPC-24 BASKET TEMPERATURE CONTOURS PLOT
 Temperature (Degrees Kelvin)
 Tmax = 6.491E+02 Tmin = 3.302E+02

Nov 11 1997
 Fluent 4.32
 Fluent Inc.

Rev. 0

FIGURE 4.4.17: HI-STAR 100 SYSTEM NORMAL STORAGE CONDITION TEMPERATURE CONTOURS PLOT (MPC-24 BASKET)

CO2

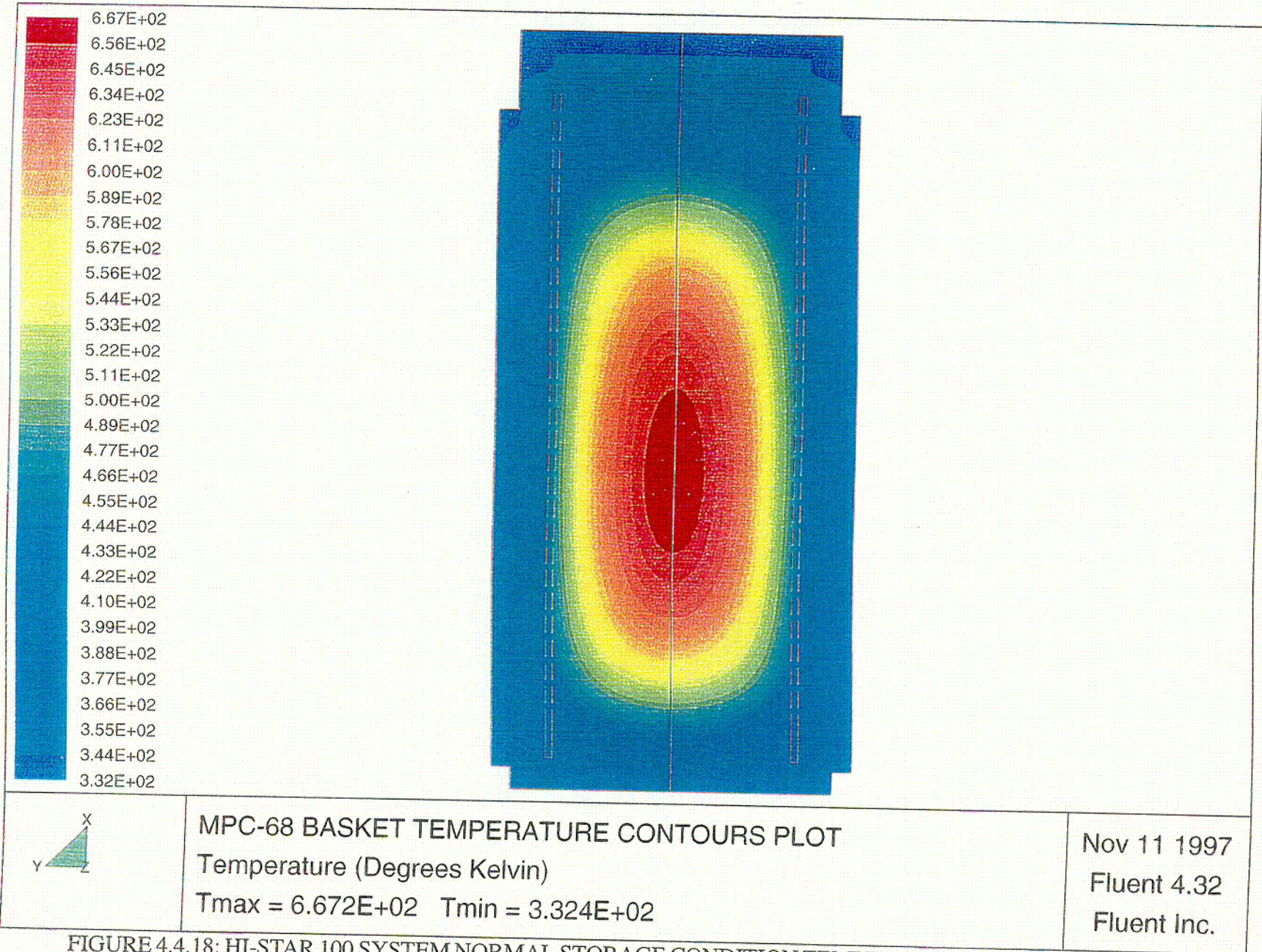


FIGURE 4.4.18: HI-STAR 100 SYSTEM NORMAL STORAGE CONDITION TEMPERATURE CONTOURS PLOT (MPC-68 BASKET)

003

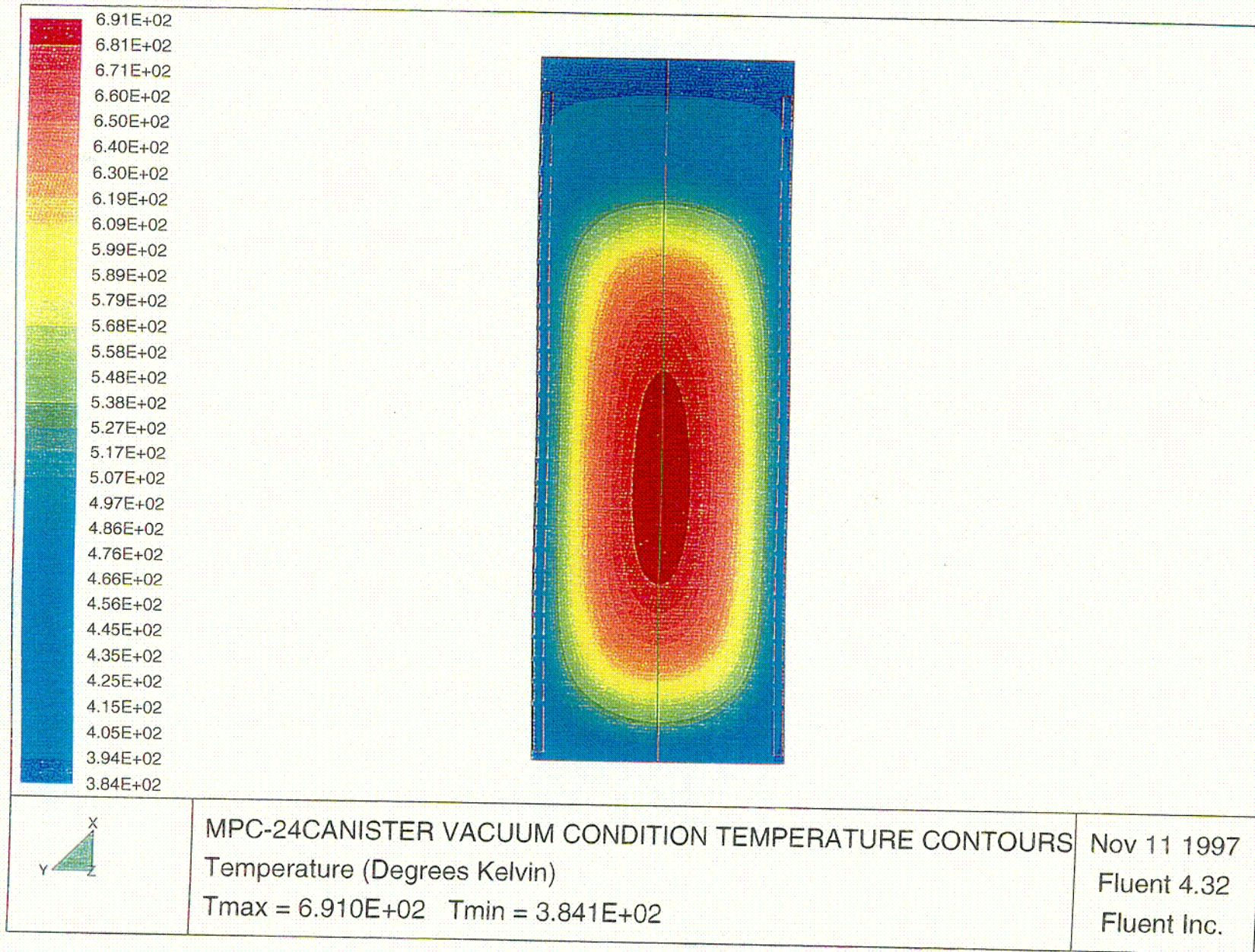


FIGURE 4.4.19: VACUUM CONDITION TEMPERATURE CONTOURS PLOT FOR BOUNDING MPC-24 BASKET

C04

FIGURE 4.4.20

THIS FIGURE IS INTENTIONALLY DELETED

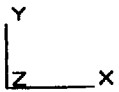
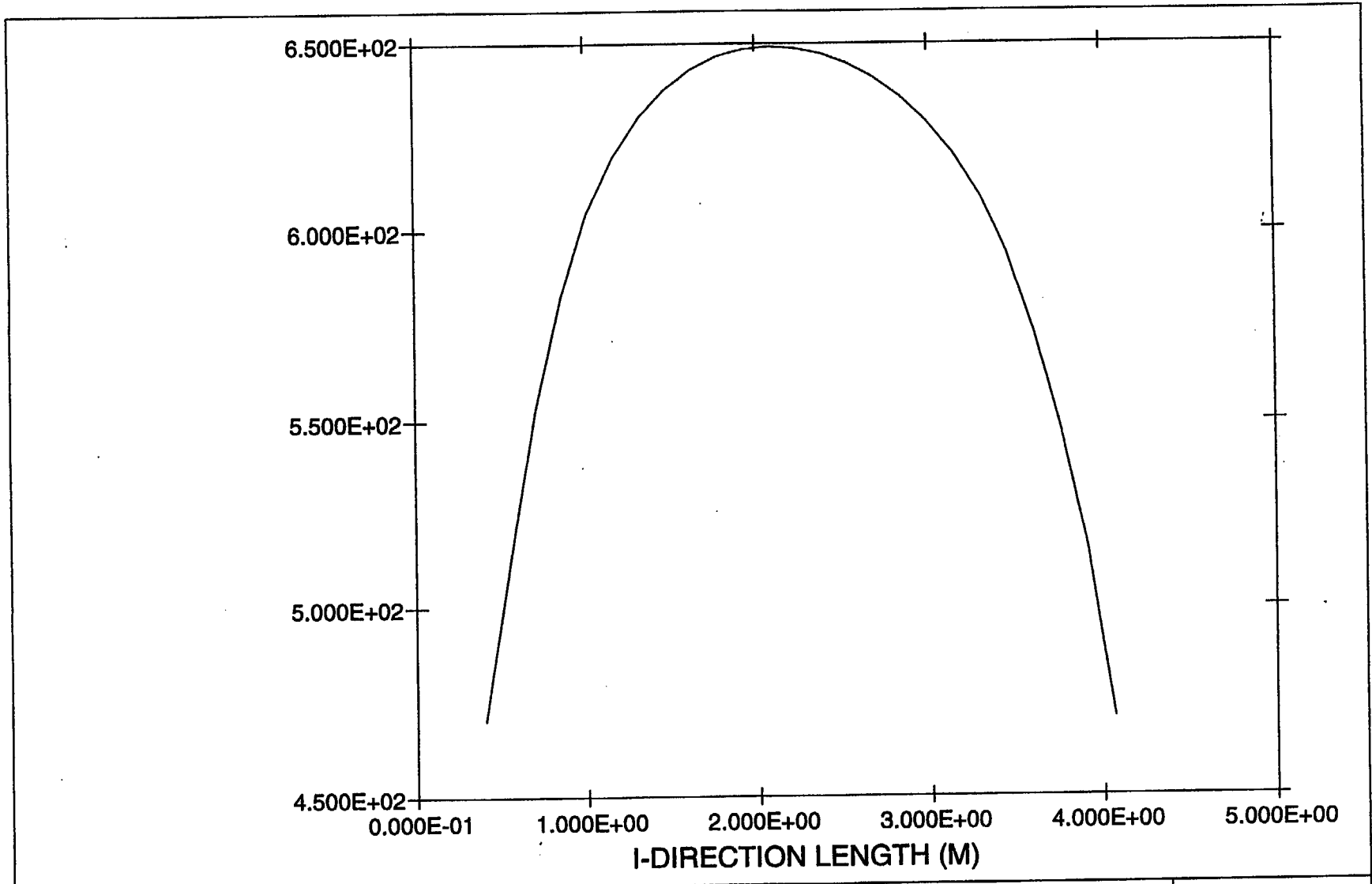


FIGURE 4.4.21: MPC-24 HOTTEST ROD TEMPERATURE PROFILE

Temperature (Kelvin) Vs. Axial Length (Meters)

May 14 1998
Fluent 4.32
Fluent Inc.

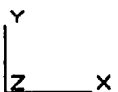
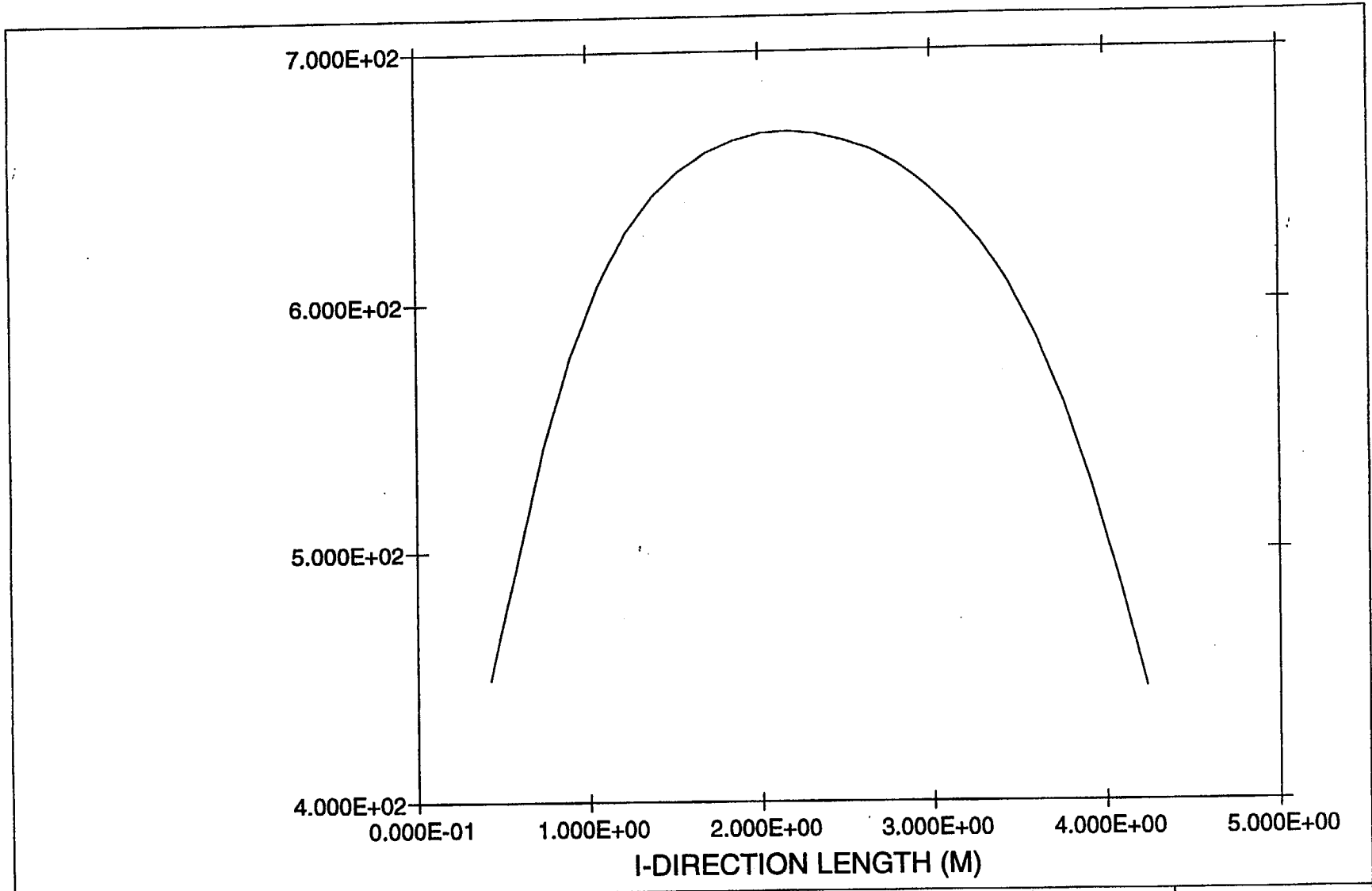


FIGURE 4.4.22: MPC-68 HOTTEST ROD TEMPERATURE PROFILE

Temperature (Kelvin) Vs. Axial Length (Meters)

May 14 1998
Fluent 4.32
Fluent Inc.

FIGURE 4.4.23

THIS FIGURE IS INTENTIONALLY DELETED

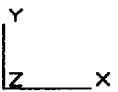
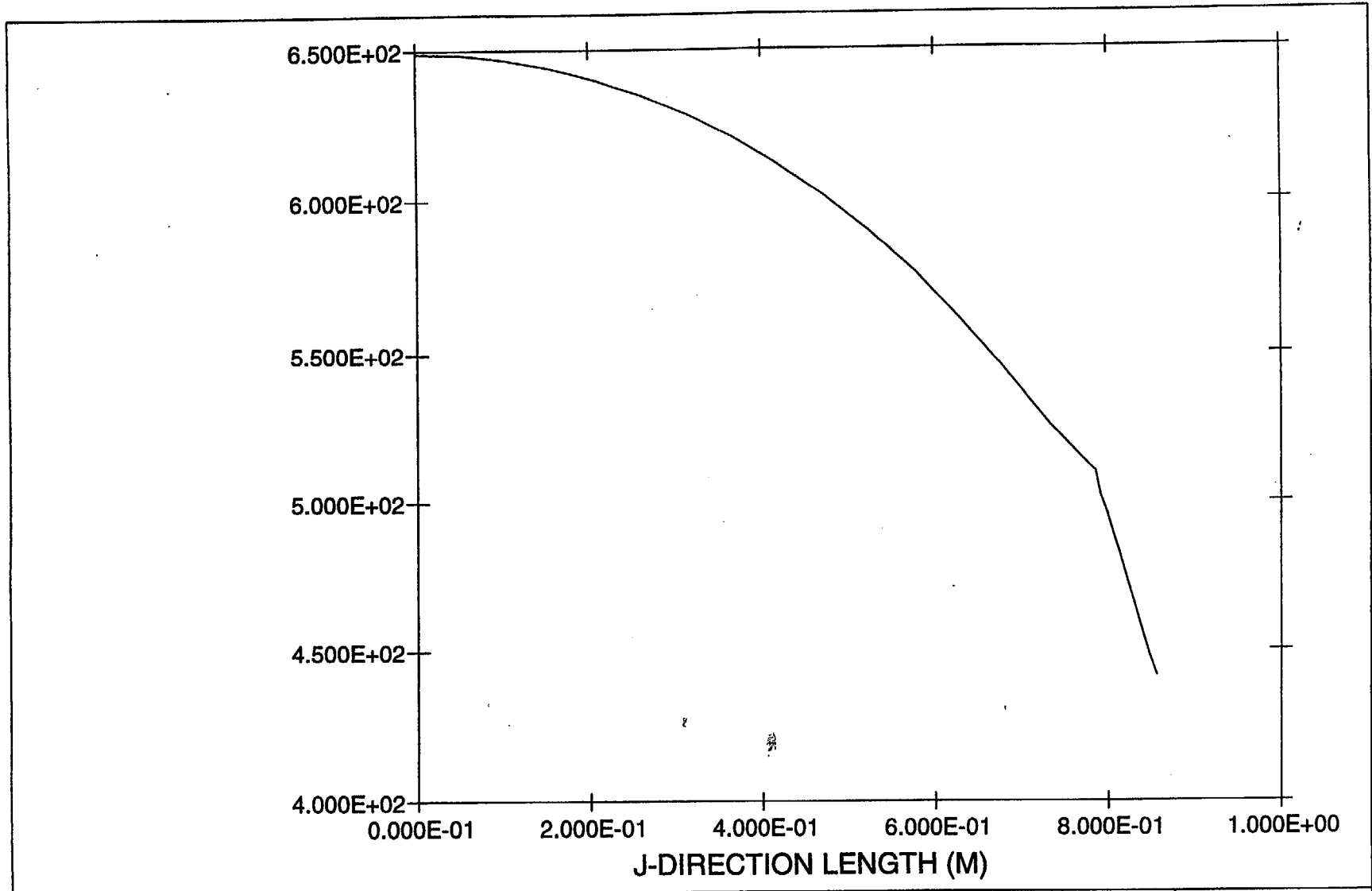


FIGURE 4.4.24: MPC-24 BASKET RADIAL TEMPERATURE PROFILE
(Hottest Basket Cross-Section)
Temperature (Kelvin) Vs. Radial Distance (Meters)

May 14 1998
Fluent 4.32
Fluent Inc.

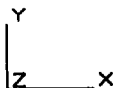
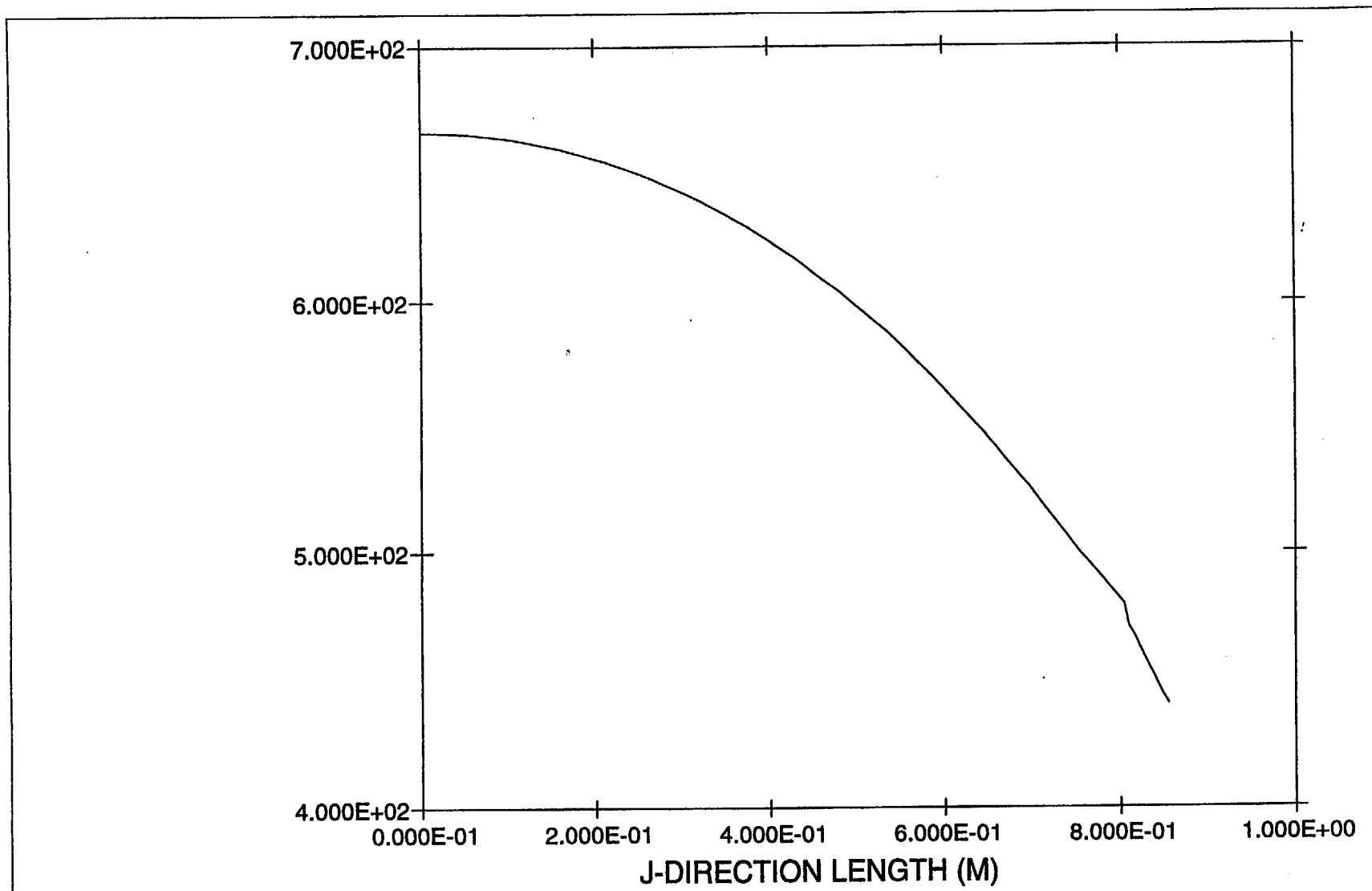


FIGURE 4.4.25: MPC-68 BASKET RADIAL TEMPERATURE PROFILE

Temperature (Kelvin) Vs. Radial Position (Meters)

May 14 1998

Fluent 4.32

Fluent Inc.

4.5 REGULATORY COMPLIANCE

NUREG-1536 ([4.1.3], IV) defines eight specific thermal acceptance criteria which are addressed in Sections 4.1 through 4.4. Each of the pertinent criteria and the conclusion of the evaluations are summarized here.

1. As required by NUREG-1536 ([4.1.3], 4.IV.1), the fuel cladding temperature at the beginning of dry cask storage is maintained below the anticipated damage-threshold temperatures for normal conditions and a minimum of 20 years of cask storage. Maximum clad temperatures for normal storage conditions are reported in Section 4.4.2.1. Anticipated damage-threshold temperatures, calculated as described in Section 4.3, are summarized in Table 2.2.3.
2. As required by NUREG-1536 ([4.1.3], 4.IV.2), the fuel cladding temperature is maintained below 570°C (1058°F) for short-term accident conditions, short-term off-normal conditions, and fuel transfer operations. Results of off-normal and accident condition evaluations presented in Chapter 11 comply with this limit. Maximum clad temperatures for vacuum drying conditions are reported in Section 4.4.2.2 which comply within this limit by large conservative margins.
3. As required by NUREG-1536 ([4.1.3], 4.IV.3), the maximum internal pressure of the cask remains within its design pressure for normal, off-normal, and accident conditions, assuming rupture of 1 percent, 10 percent, and 100 percent of the fuel rods, respectively. Assumptions for pressure calculations include release of 100 percent of the fill gas and 30 percent of the significant radioactive gases in the fuel rods. Maximum internal pressures are reported in Section 4.4.4. Design pressures are summarized in Table 2.2.1.
4. As required by NUREG-1536 ([4.1.3], 4.IV.4), all cask and fuel materials are maintained within their minimum and maximum temperatures for normal and off-normal conditions in order to enable components to perform their intended safety functions. During normal fuel handling operations (i.e., vacuum drying) the cask component temperatures are compared with short-term temperature limits (Section 4.4.2.2). Maximum and minimum temperatures for normal conditions are reported in Sections 4.4.2 and 4.4.3, respectively. Design temperature limits are summarized in Table 2.2.3. HI-STAR 100 System components defined as important to safety are listed in Table 2.2.6. Off-normal and accident condition thermal evaluations are discussed in Sections 11.1 and 11.2, respectively.
5. & 6. As required by NUREG-1536 ([4.1.3], 4.IV.5), the cask system ensures a very low probability of cladding breach during long-term storage. Further, NUREG-1536 ([4.1.3], 4.IV.6) requires that the fuel cladding damage resulting from creep cavitation should be limited to 15 percent of the original cladding cross section area during dry storage. The calculation methodology, described in Section 4.3, for determining initial dry storage fuel

clad temperature limits, ensures that both of these requirements are satisfied. Maximum fuel clad temperature limits are summarized in Table 2.2.3.

7. As required by NUREG-1536 ([4.1.3], 4.IV.7), the cask system is passively cooled. All heat rejection mechanisms described in this chapter, including conduction, natural convection, and thermal radiation, are completely passive.
8. As required by NUREG-1536 ([4.1.3], 4.IV.8), the thermal performance of the cask is within the allowable design criteria specified in FSAR Chapter 2 for normal storage and fuel handling conditions. During normal fuel handling operations (i.e., vacuum drying) the cask component temperatures are compared with short-term temperature limits. All thermal results reported in this chapter are within the design criteria allowable ranges for all normal storage and fuel handling conditions. Off-normal and fire accident condition responses are reported in Section 11.1 and 11.2, respectively.

Finally, the acceptance criteria set forth in NUREG-1536 ([4.1.3], 4.VI) can be demonstrated to have been satisfied on the strength of information provided in this FSAR. Specifically, it is noted that:

- Structures, systems, and components (SSCs) important to safety are described in sufficient detail in Chapters 1, 2 and 4 of this FSAR to enable an evaluations of their thermal effectiveness. Cask SSCs important to safety remain within their operating temperature ranges.
- The HI-STAR 100 System is designed with a heat-removal capability having verifiability and reliability consistent with its importance to safety. The cask is designed to provide adequate heat removal capacity without active cooling systems.
- The spent fuel cladding is protected against degradation leading to gross ruptures by maintaining the cladding temperature for five-year cooled fuel in an inert helium environment below 720°F for PWR fuel assemblies and below 749°F for BWR fuel assemblies. Protection of the cladding against degradation is expected to allow ready retrieval of spent fuel for further processing or disposal.

It is therefore concluded that the thermal design of the HI-STAR 100 System is in compliance with 10 CFR Part 72, and that the applicable design and acceptance criteria have been satisfied. The evaluation of the thermal design provides reasonable assurance that the HI-STAR 100 System will allow safe storage of spent fuel for its design life. This finding is reached on the basis of the technical data presented in this FSAR in conjunction with provisions of 10 CFR Part 72, appropriate regulatory guides, applicable codes and standards, and accepted engineering practices.

4.6 REFERENCES

- [4.1.1] ANSYS Finite Element Modeling Package, Swanson Analysis Systems, Inc., Houston, PA, 1993.
- [4.1.2] FLUENT Computational Fluid Dynamics Software, (Fluent, Inc., Centerra Resource Park, 10 Cavendish Court, Lebanon, NH 03766).
- [4.1.3] NUREG-1536, "Standard Review Plan for Dry Cask Storage Systems", USNRC, January 1997
- [4.1.4] "The TN-24P PWR Spent-Fuel Storage Cask: Testing and Analyses", EPRI NP-5128, (April 1987).
- [4.1.5] Deleted.
- [4.2.1] Baumeister, T., Avallone, E.A. and Baumeister III, T., "Marks' Standard Handbook for Mechanical Engineers", 8th Edition, McGraw Hill Book Co., 1978.
- [4.2.2] Rohsenow, W.M. and Hartnett, J.P., "Handbook of Heat Transfer", McGraw Hill Book Co., New York, 1973.
- [4.2.3] Creer et al., "The TN-24P Spent Fuel Storage Cask: Testing and Analyses", EPRI NP-5128, PNL-6054, UC-85, (April 1987).
- [4.2.4] Rust, J.H., "Nuclear Power Plant Engineering", Haralson Publishing Co., (1979).
- [4.2.5] Kern, D.Q., "Process Heat Transfer", McGraw Hill Kogakusha, (1950).
- [4.2.6] "A Handbook of Materials Properties for Use in the Analysis of Light Water Reactor Fuel Rod Behavior", NUREG/CR-0497, (August 1981).
- [4.2.7] "Safety Analysis Report for the NAC Storable Transport Cask", Docket No. 71-9235.
- [4.2.8] ASME Boiler and Pressure Vessel Code, Section II, Part D, (1995).
- [4.2.9] Jakob, M. and Hawkins, G.A., "Elements of Heat Transfer", John Wiley & Sons, New York, 1957.
- [4.3.1] Levy, I.S., et al., "Recommended Temperature Limits for Dry Storage of Spent Light Water Reactor Zircaloy-Clad Fuel Rods in Inert Gas", PNL-6189, (May 1987).

- [4.3.2] Deleted.
- [4.3.3] "Characteristics of Spent Fuel High-Level Waste, and Other Radioactive Wastes Which May Require Long-Term Isolation", DOE/RW-0184, (December 1987).
- [4.3.4] Johnson, Jr., A.B. and Gilbert, E.R., "Technical Basis for Storage of Zircaloy-Clad Spent Fuel in Inert Gases", PNL-4835, (September 1983).
- [4.3.5] Cunningham et. al., "Evaluation of Expected Behavior of LWR Stainless Steel-Clad Fuel in Long-Term Dry Storage", EPRI TR-106440, (April 1996).
- [4.3.6] Schwartz, M.W., Witte, M.C., "Spent Fuel Cladding Integrity During Dry Storage", LLNL, UCID-22181 (September 1987).
- [4.3.7] "Temperature Limit Determination for the Inert Dry Storage of Spent Nuclear Fuel", EPRI TR-103949, (May 1994).
- [4.4.1] Wooton, R.O. and Epstein, H.M., "Heat Transfer from a Parallel Rod Fuel Element in a Shipping Container", Battelle Memorial Institute, 1963.
- [4.4.2] Rapp, D., "Solar Energy", Prentice-Hall, Inc., Englewood Cliffs, NJ, (1981).
- [4.4.3] Deleted.
- [4.4.4] Holman, J.P., "Heat Transfer," 6th ed., McGraw Hill Book Co., (1986).
- [4.4.5] Sanders et al., "A Method for Determining the Spent-Fuel Contribution to Transport Cask Containment Requirements," Sandia Report SAND90-2406-TTC-1019UC-820, page II-127, (November 1992).
- [4.4.6] Hewitt, G.F., Shires, G.L. and Bott, T.R., "Process Heat Transfer", CRC Press, (1994).

CHAPTER 5: SHIELDING EVALUATION

5.0 INTRODUCTION

The shielding analysis of the HI-STAR 100 System is presented in this chapter. The HI-STAR 100 System is designed to accommodate different MPCs within one standard HI-STAR overpack. The MPCs are designated as MPC-24 (24 PWR fuel assemblies) and MPC-68 (68 BWR fuel assemblies).

In addition to storing intact PWR and BWR fuel assemblies, the HI-STAR 100 System is designed to store damaged BWR fuel assemblies and BWR fuel debris. Damaged fuel assemblies and fuel debris are defined in Section 2.1.3 and Appendix B to the Certificate of Compliance. Both damaged BWR fuel assemblies and BWR fuel debris are required to be loaded into Damaged Fuel Containers (DFCs) prior to being loaded into the MPC. DFCs containing fuel debris must be stored in the MPC-68F. DFCs containing damaged fuel assemblies may be stored in either the MPC-68 or the MPC-68F. Only the fuel assemblies in the Dresden 1 and Humboldt Bay fuel assembly classes identified in Table 2.1.2 are authorized as contents for storage in the HI-STAR 100 system as either damaged fuel or fuel debris.

The MPC-68 and MPC-68F are also capable of storing Dresden Unit 1 antimony-beryllium neutron sources and the single Thoria rod canister which contains 18 thoria rods that were irradiated in two separate fuel assemblies.

PWR fuel assemblies may contain burnable poison rod assemblies (BPRAs) or thimble plug devices (TPDs) or similarly named devices. These devices are an integral yet removable part of PWR fuel assemblies and therefore the HI-STAR 100 System has been designed to store PWR fuel assemblies with or without BPRAs or TPDs. Since BPRAs and TPDs occupy the same space within a fuel assembly, a single PWR fuel assembly will not contain both devices.

The sections that follow will demonstrate that the design of the HI-STAR 100 dry cask storage system fulfills the following acceptance criteria outlined in the Standard Review Plan, NUREG-1536[5.2.1]:

Acceptance Criteria

1. The minimum distance from each spent fuel handling and storage facility to the controlled area boundary must be at least 100 meters. The "controlled area" is defined in 10CFR72.3 as the area immediately surrounding an ISFSI or monitored retrievable storage (MRS) facility, for which the licensee exercises authority regarding its use and within which ISFSI operations are performed.

2. The cask vendor must show that, during both normal operations and anticipated occurrences, the radiation shielding features of the proposed dry cask storage system are sufficient to meet the radiation dose requirements in Sections 72.104(a). Specifically, the vendor must demonstrate this capability for a typical array of casks in the most bounding site configuration. For example, the most bounding configuration might be located at the minimum distance (100 meters) to the controlled area boundary, without any shielding from other structures or topography.
3. Dose rates from the cask must be consistent with a well-established "as low as reasonably achievable" (ALARA) program for activities in and around the storage site.
4. After a design-basis accident, an individual at the boundary or outside the controlled area shall not receive a dose greater than the limits specified in 10 CFR 72.106.
5. The proposed shielding features must ensure that the dry cask storage system meets the regulatory requirements for occupational and radiation dose limits for individual members of the public, as prescribed in 10 CFR Part 20, Subparts C and D.

This chapter contains the following information which demonstrates full compliance with the Standard Review Plan, NUREG-1536:

- A description of the shielding features of the HI-STAR 100 System.
- A description of the bounding source terms.
- A general description of the shielding analysis methodology.
- A description of the analysis assumptions and results for the HI-STAR 100 System.
- Analyses are presented for each MPC showing that the radiation dose rates follow As-Low-As-Reasonably-Achievable (ALARA) practices.
- The HI-STAR 100 System has been analyzed to show that the 10CFR72.104 and 10CFR72.106 controlled area boundary radiation dose limits are met during normal, off-normal, and accident conditions of storage for non-effluent radiation from illustrative ISFSI configurations at a minimum distance of 100 meters.
- Analyses are also presented which demonstrate that the storage of damaged fuel and fuel debris in the HI-STAR 100 System is bounded by the BWR intact fuel analysis during normal, off-normal, and accident conditions.

Chapter 10, Radiation Protection, contains the following information:

- A discussion of the estimated occupational exposures for the HI-STAR 100 System.
- A summary of the estimated radiation exposure to the public.

Chapter 2 contains a detailed description of structures, systems, and components important to safety.

Chapter 7 contains an analysis of the estimated dose at the controlled area boundary during normal, off-normal, and accident conditions from the release of radioactive materials. Therefore, this chapter only calculates the dose from direct neutron and gamma radiation emanating from the HI-STAR 100 System.

5.1 DISCUSSION AND RESULTS

The principal sources of radiation in the HI-STAR 100 System are:

- Gamma radiation originating from the following sources
 1. Decay of radioactive fission products
 2. Secondary photons from neutron capture in fissile and non-fissile nuclides
 3. Hardware activation products generated during core operations

- Neutron radiation originating from the following sources
 1. Spontaneous fission
 2. α, n reactions in fuel materials
 3. Secondary neutrons produced by fission from subcritical multiplication
 4. γ, n reactions (this source is negligible)
 5. Dresden Unit 1 antimony-beryllium neutron sources

Shielding from gamma radiation is provided by the steel structure of the MPC and overpack. In order for the neutron shielding to be effective, the neutrons must be thermalized and then absorbed in a material of high neutron cross section. In the HI-STAR 100 design, a neutron shielding material, Holtite-A, is used to thermalize the neutrons. Boron carbide, dispersed in the neutron shield, utilizes the high neutron absorption cross section of ^{10}B to absorb the thermalized neutrons.

The shielding analyses were performed with MCNP-4A [5.1.1] from Los Alamos National Laboratory. The source terms for the design basis fuels were calculated with the SAS2H and ORIGEN-S modules from the SCALE 4.3 system [5.1.2, 5.1.3]. A detailed description of the MCNP models and the source term calculations is presented in Sections 5.3 and 5.2, respectively.

The design basis intact zircaloy clad fuel assemblies used for calculating the dose rates presented in this chapter are B&W 15x15 and the GE 7x7, for PWR and BWR fuel types, respectively. The design basis intact 6x6, damaged, and mixed oxide (MOX) fuel assemblies are the GE 6x6. Table 2.1.6 specifies the acceptable intact zircaloy clad fuel characteristics for storage. Table 2.1.7 specifies the acceptable damaged and MOX zircaloy clad fuel characteristics for storage.

The design basis intact stainless steel clad fuels are the WE 15x15 and the A/C 10x10, for PWR and BWR fuel types, respectively. Table 2.1.11 specifies the acceptable fuel characteristics of stainless steel clad fuel for storage.

The MPC-24 and MPC-68 are qualified for storage of SNF with different combinations of maximum burnup levels and minimum cooling times. Figure 2.1.6 specifies the acceptable maximum burnup levels and minimum cooling times for storage of zircaloy clad fuel in the MPC-24 and the MPC-68 (Appendix B to the Certificate of Compliance presents this data in tabular form). Table 2.1.11 specifies the acceptable maximum burnup levels and minimum cooling times for storage of stainless steel clad fuel. The values in Figure 2.1.6 and Table 2.1.11 were chosen based on an analysis of the maximum decay heat load that could be accommodated within each MPC. The shielding analyses presented in this chapter used the burnup and cooling time combinations listed below which are either equal to or conservatively bound the acceptable burnup levels and cooling times shown in Figure 2.1.6 and Table 2.1.11.

Maximum Burnup and Minimum Cooling Times Analyzed	
Zircaloy Clad Fuel	
MPC-24	MPC-68
40,000 MWD/MTU 5 year cooling	35,000 MWD/MTU 5 year cooling
47,500 MWD/MTU 8 year cooling	45,000 MWD/MTU 9 year cooling
N/A	30,000 MWD/MTU 18 year cooling (6x6 intact, damaged and MOX fuel)
Stainless Steel Clad Fuel	
MPC-24	MPC-68
30,000 MWD/MTU 9 year cooling	22,500 MWD/MTU 10 year cooling
40,000 MWD/MTU 15 year cooling	N/A

Appendix B to the Certificate of Compliance requires that, in the MPC-24, for a minimum cooling time of 5-years, the maximum burnup is 28,700 MWD/MTU, and for 15-year cooling the maximum burnup is 42,100 MWD/MTU for PWR fuel assemblies without Burnable Poison Rod Assemblies (BPRAs). PWR fuel assemblies containing BPRAs are limited to 28,300 MWD/MTU for 5 year cooling and 41,400 MWD/MTU for 15 year cooling. Since the burnup and cooling times analyzed in this chapter for the MPC-24 were 40,000 MWD/MTU and 5-year cooling and 47,500 MWD/MTU and 8-year cooling, the shielding analysis presented is conservatively bounding for the MPC-24.

Appendix B to the Certificate of Compliance requires that, in the MPC-68, for a minimum cooling time of 5-years, the maximum burnup is 26,000 MWD/MTU, and for 15-year cooling

the maximum burnup is 37,600 MWD/MTU. Since the burnup and cooling times analyzed in this chapter for the MPC-68 were 35,000 MWD/MTU and 5-year cooling and 45,000 MWD/MTU and 9-year cooling, the shielding analysis presented is conservatively bounding for the MPC-68.

The dose rates corresponding to the burnup and cooling time combination which resulted in the highest dose rates at the midplane of the cask during normal conditions are reported in this section. Dose rates for each of the combinations are listed in Section 5.4.

5.1.1 Normal and Off-Normal Operations

Chapter 11 discusses the potential off-normal conditions and their effect on the HI-STAR 100 System. None of the off-normal conditions have any impact on the shielding analysis. Therefore, off-normal and normal conditions are identical for the purpose of the shielding evaluation.

The 10CFR72.104 criteria for radioactive materials in effluents and direct radiation during normal operations are:

1. During normal operations and anticipated occurrences, the annual dose equivalent to any real individual who is located beyond the controlled area, must not exceed 25 mrem to the whole body, 75 mrem to the thyroid and 25 mrem to any other critical organ.
2. Operational restrictions must be established to meet as low as reasonably achievable objectives for radioactive materials in effluents and direct radiation.

10CFR20 Subparts C and D specify additional requirements for occupational dose limits and radiation dose limits for individual members of the public. Chapter 10 specifically addresses these regulations.

In accordance with ALARA practices, design objective dose rates are established for the HI-STAR 100 in Section 2.3.5.2 as: 125 mrem/hour on the radial surface of the overpack, and 375 mrem/hour in areas above and below the neutron shield in the radial direction.

The dose rates presented in this section are calculated at 40,000 MWD/MTU and 5-year cooling for the MPC-24, and 35,000 MWD/MTU and 5-year cooling for the MPC-68. Based on a comparison of the normal condition dose rates at the fuel mid-plane for the various burnup and cooling time combinations analyzed, these were chosen as the worst case for the MPC-24 and the MPC-68. Section 5.4 provides a detailed list of dose rates at several cask locations for all burnup and cooling times analyzed.

Figure 5.1.1 identifies the locations of the dose points referenced in the summary tables. The bottom shield shown in this figure is temporary shielding which may be used during on-site horizontal handling operations. Dose Point #7 is located directly below the overpack bottom plate or directly below the bottom shield when it is attached. Dose Points #1, #3, and #4 are not

contact doses, but rather, in-air doses at the locations shown. The dose values reported at the locations shown on Figure 5.1.1 are averaged over a region that is approximately 1 foot in width.

Tables 5.1.2 and 5.1.3 provide the maximum dose rates adjacent to the overpack during normal conditions for each of the MPCs. Tables 5.1.5 and 5.1.6 provide the maximum dose rates at one meter from the overpack.

The dose to any real individual at or beyond the controlled area boundary is required to be below 25 mrem per year. The minimum distance to the controlled area boundary is 100 meters from the ISFSI. Only the MPC-24 was used in the calculation of the dose rates at the controlled area boundary. The MPC-24 was chosen because its dose rates are equivalent or greater than the dose rates from the MPC-68 as shown in Tables 5.1.2, 5.1.3, 5.1.5, and 5.1.6. Table 5.1.7 presents the annual dose to an individual from a single cask and various arrays of casks, assuming 100% occupancy (8760 hours). The minimum distance required for the corresponding dose is also listed. These values were calculated for the MPC-24 with a burnup of 40,000 MWD/MTU and a 5-year cooling time. It will be shown in Section 5.4.3 that this burnup and cooling time results in the highest offsite dose for the combinations of maximum burnup and minimum cooling time analyzed. It is noted that these data are provided for illustrative purposes only. A detailed site specific evaluation of dose at the controlled area boundary will be performed for each ISFSI in accordance with 10CFR72.212, as stated in Chapter 12, Operating Controls and Limits. The site specific evaluation will consider dose from other portions of the facility and will consider the specifics of the fuel being stored (burnup and cooling time).

Figure 5.1.2 is an annual dose versus distance graph for the cask configurations provided in Table 5.1.7. This curve, which is based on 100% occupancy, is provided for illustrative purposes only and will be re-evaluated on a site-specific basis.

Section 5.2 lists the gamma and neutron sources for the design basis intact and damaged fuels. Since the source strengths of the damaged fuel and the MOX fuel are significantly smaller in all energy groups than those corresponding to the intact design basis fuel source strengths, the damaged and MOX fuel dose rates for normal conditions are bounded by the MPC-68 analysis with design basis intact fuel. Therefore, no explicit analysis is required to demonstrate that the MPC-68 with damaged or MOX fuel will meet the normal condition regulatory requirements.

Section 5.2.6 lists the gamma and neutron sources from the Dresden Unit 1 Thoria rod canister and demonstrates that the Thoria rod canister is bounded by the design basis Dresden Unit 1 6x6 intact fuel.

Section 5.2.4 presents the Co-60 sources from the BPRAs and TPDs that are permitted for storage in the HI-STAR 100. Section 5.4.6 demonstrates that the maximum dose rates presented in this section bound the dose rates from fuel assemblies containing either BPRAs or TPDs.

Section 5.4.7 demonstrates that the Dresden Unit 1 fuel assemblies containing antimony-beryllium neutron sources are bounded by the shielding analysis presented in this section.

Section 5.2.3 presents the gamma and neutron source for the design basis intact stainless steel clad fuel. The dose rates from this fuel are provided in Section 5.4.5.

The analyses summarized in this section demonstrate that the HI-STAR 100 System is in compliance with the 10CFR72.104 limits and ALARA practices.

5.1.2 Accident Conditions

The 10CFR72.106 radiation dose limits at the controlled area boundary for design basis accidents are:

Any individual located on or beyond the nearest boundary of the controlled area may not receive from any design basis accident the more limiting of a total effective dose equivalent of 5 Rem, or the sum of the deep-dose equivalent and the committed dose equivalent to any individual organ or tissue (other than the lens of the eye) of 50 Rem. The lens dose equivalent shall not exceed 15 Rem and the shallow dose equivalent to skin or to any extremity shall not exceed 50 rem. The minimum distance from the spent fuel or high level radioactive waste handling and storage facilities to the nearest boundary of the controlled area shall be at least 100 meters.

The design basis accidents analyzed in Chapter 11 have one bounding consequence which affects the shielding materials. It is the damage to the neutron shield as a result of the design basis fire. Other design basis accidents result in damage to the outer enclosure shell and neutron shield; however, these accidents are localized. In a conservative fashion, the dose analysis assumes that as a result of the fire, the neutron shield is completely destroyed and replaced by a void. This is highly conservative as there will be limited sources of combustible materials stored in or around the ISFSI. Additionally, the neutron shield is assumed to be completely lost, whereas some portion of the neutron shield would be expected to remain, as the neutron shield material is fire retardant.

Throughout all design basis accident conditions the axial location of the fuel will remain fixed within the MPC because of the fuel spacers. Chapter 3 provides an analysis to show that the fuel spacers do not fail under all normal, off-normal, and accident conditions of storage. Chapter 3 also shows that the inner shell, intermediate shells, radial channels, and outer enclosure shell of the overpack remain unaltered throughout all design basis accident conditions. Localized damage of the overpack outer enclosure shell could be experienced. However, the localized deformations will have a negligible impact on the dose rate at the boundary of the controlled area.

The complete loss of the neutron shield significantly affects the dose at Dose Point #2 at the mid-height adjacent to the overpack neutron shield. Loss of the neutron shield has a small effect on the other dose points. To illustrate the impact of the design basis accident, the dose rates at Dose

Point #2 (see Figure 5.1.1) are provided in Tables 5.1.8 and 5.1.9. The normal condition dose rates are provided for reference.

Table 5.1.9 provides a comparison of the normal and accident condition dose rates at one meter from the overpack. By comparing the increase in dose rates from normal and accident conditions and the maximum normal condition controlled area dose rate, it is evident that the dose as a result of the design basis accident cannot exceed 5 Rem at the controlled area boundary for the short duration of the accident. Conservatively assuming a 1/R reduction in the dose rate, the dose rate at the 100 meter controlled area boundary would be less than 5 mrem/hr for a single HI-STAR 100 during the accident condition. At this dose rate, it would take more than 1000 hours (41 days) for the dose at the controlled area boundary to reach 5 Rem. This length of time greatly exceeds the time necessary to implement and complete the corrective actions outlined in Chapter 11 for the fire accident. Therefore, the dose requirement of 10CFR72.106 is satisfied.

The consequences of the design basis accident conditions for the MPC-68 storing damaged fuel and the MPC-68F storing damaged fuel and/or fuel debris differ slightly from those with intact fuel. It is conservatively assumed that during a drop accident (vertical, horizontal, or tip-over) the fuel collapses and the pellets rest in the bottom of the damaged fuel container. Since the damaged and MOX fuels are both Dresden 1 fuel, the MOX fuel can also be considered damaged fuel. Analysis in Section 5.4.2 demonstrates that the damaged fuel in the post-accident condition has lower source terms (both gamma and neutron) per inch than the intact BWR design basis fuel. Therefore, the damaged fuel post-accident dose rates are bounded by the BWR intact fuel post-accident dose rates.

Analyses summarized in this section demonstrate the HI-STAR 100 System's compliance with the 10CFR72.106 limits.

Table 5.1.1

DELETED

Table 5.1.2

DOSE RATES ADJACENT TO OVERPACK FOR NORMAL CONDITIONS
MPC-24 WITH DESIGN BASIS ZIRCALOY CLAD FUEL AT WORST CASE
BURNUP AND COOLING TIME
40,000 MWD/MTU AND 5-YEAR COOLING

Dose Point [†] Location	Fuel Gammas ^{††} (mrem/hr)	⁶⁰ Co Gammas (mrem/hr)	Neutrons (mrem/hr)	Totals (mrem/hr)
1	12.45	231.52	82.27	326.24
2	96.88	0.03	22.12	119.03
3	3.51	81.12	70.28	154.90
4	1.81	35.86	39.47	77.14
5	0.34	0.69	56.70	57.73
6 (dry MPC) ^{†††}	27.07	286.19	126.02	439.28
7 (no temp. shield)	100.36	1432.28	397.30	1929.94
7 (with temp. shield)	28.27	329.84	19.84	377.94

† Refer to Figure 5.1.1.

†† Gammas generated by neutron capture are included with fuel gammas.

††† Overpack closure plate not present.

Table 5.1.3

DOSE RATES ADJACENT TO OVERPACK FOR NORMAL CONDITIONS
MPC-68 WITH DESIGN BASIS ZIRCALOY CLAD FUEL AT WORST CASE
BURNUP AND COOLING TIME
35,000 MWD/MTU AND 5-YEAR COOLING

Dose Point [†] Location	Fuel Gammas ^{††} (mrem/hr)	⁶⁰ Co Gammas (mrem/hr)	Neutrons (mrem/hr)	Totals (mrem/hr)
1	10.25	297.85	65.65	373.75
2	99.95	0.03	19.40	119.39
3	0.87	117.57	29.48	147.92
4	0.40	44.36	17.04	61.81
5	0.13	0.43	24.74	25.30
6 (dry MPC) ^{†††}	5.19	204.40	59.07	268.65
7 (no temp. shield)	64.46	1794.41	327.79	2186.65
7 (with temp. shield)	20.35	381.90	14.49	416.74

† Refer to Figure 5.1.1.

†† Gammas generated by neutron capture are included with fuel gammas.

††† Overpack closure plate not present.

Table 5.1.4

DELETED

Table 5.1.5

DOSE RATES AT ONE METER FOR NORMAL CONDITIONS
MPC-24 WITH DESIGN BASIS ZIRCALOY CLAD FUEL AT WORST CASE
BURNUP AND COOLING TIME
40,000 MWD/MTU AND 5-YEAR COOLING

Dose Point [†] Location	Fuel Gammas ^{††} (mrem/hr)	⁶⁰ Co Gammas (mrem/hr)	Neutrons (mrem/hr)	TOTALS (mrem/hr)
1	10.11	25.00	8.69	43.79
2	42.67	1.06	7.74	51.47
3	7.10	14.06	9.04	30.21
4	4.59	14.69	9.33	28.61
5	0.11	0.32	16.67	17.11
7 (no temp. shield)	52.66	720.72	116.30	889.68
7 (with temp. shield)	11.46	139.22	15.19	165.87

[†] Refer to Figure 5.1.1.

^{††} Gammas generated by neutron capture are included with fuel gammas.

Table 5.1.6

DOSE RATES AT ONE METER FOR NORMAL CONDITIONS
MPC-68 WITH DESIGN BASIS ZIRCALOY CLAD FUEL AT WORST CASE
BURNUP AND COOLING TIME
35,000 MWD/MTU AND 5-YEAR COOLING

Dose Point [†] Location	Fuel Gammas ^{††} (mrem/hr)	⁶⁰ Co Gammas (mrem/hr)	Neutrons (mrem/hr)	Totals (mrem/hr)
1	10.46	34.29	7.55	52.30
2	42.83	0.58	7.46	50.87
3	4.44	20.08	4.19	28.71
4	2.59	20.47	4.01	27.08
5	0.06	0.22	7.02	7.30
7 (no temp. shield)	29.91	888.15	86.91	1004.97
7 (with temp. shield)	8.11	162.56	10.51	181.18

[†] Refer to Figure 5.1.1.

^{††} Gammas generated by neutron capture are included with fuel gammas.

Table 5.1.7

**DOSE RATES FOR ARRAYS OF MPC-24
WITH DESIGN BASIS ZIRCALOY CLAD FUEL
40,000 MWD/MTU AND 5-YEAR COOLING**

Array Configuration	1 cask	2x2	2x3	2x4	2x5
Annual Dose (mrem/year) [†]	13.55	18.60	13.84	18.45	23.06
Distance to Controlled Area Boundary (meters) ^{††, †††}	300	350	400	400	400

[†] 100% occupancy is assumed.

^{††} Dose location is at the center of the long side of the array.

^{†††} Actual controlled area boundary dose rates will be lower because the maximum permissible burnup for 5-year cooling as specified in the Technical Specifications is lower than the burnup analyzed for the design basis fuel used in this chapter .

Table 5.1.8

DOSE RATES ADJACENT TO OVERPACK FOR ACCIDENT CONDITIONS
 DESIGN BASIS ZIRCALOY CLAD FUEL
 AT WORST CASE BURNUP AND COOLING TIME

Dose Point [†] Location	Fuel Gammas ^{††} (mrem/hr)	⁶⁰ Co Gammas (mrem/hr)	Neutrons (mrem/hr)	Totals (mrem/hr)
MPC-24 (40,000 MWD/MTU AND 5-YEAR COOLING)				
2 (Accident Condition)	221.84	0.04	1149.46	1371.34
2 (Normal Condition)	96.88	0.03	22.12	119.03
MPC-68 (35,000 MWD/MTU AND 5-YEAR COOLING)				
2 (Accident Condition)	224.51	0.04	1139.45	1364.00
2 (Normal Condition)	99.95	0.03	19.40	119.39

[†] Refer to Figure 5.1.1.

^{††} Gammas generated by neutron capture are included with fuel gammas.

Table 5.1.9

DOSE RATES AT ONE METER FOR ACCIDENT CONDITIONS
 DESIGN BASIS ZIRCALOY CLAD FUEL
 AT WORST CASE BURNUP AND COOLING TIME

Dose Point [†] Location	Fuel Gammas ^{††} (mrem/hr)	⁶⁰ Co Gammas (mrem/hr)	Neutrons (mrem/hr)	Totals (mrem/hr)
MPC-24 (40,000 MWD/MTU AND 5-YEAR COOLING)				
2 (Accident Condition)	100.98	1.80	388.94	491.73
2 (Normal Condition)	42.67	1.06	7.74	51.47
MPC-68 (35,000 MWD/MTU AND 5-YEAR COOLING)				
2 (Accident Condition)	98.81	1.46	361.18	461.44
2 (Normal Condition)	42.83	0.58	7.46	50.87

[†] Refer to Figure 5.1.1.

^{††} Gammas generated by neutron capture are included with fuel gammas.

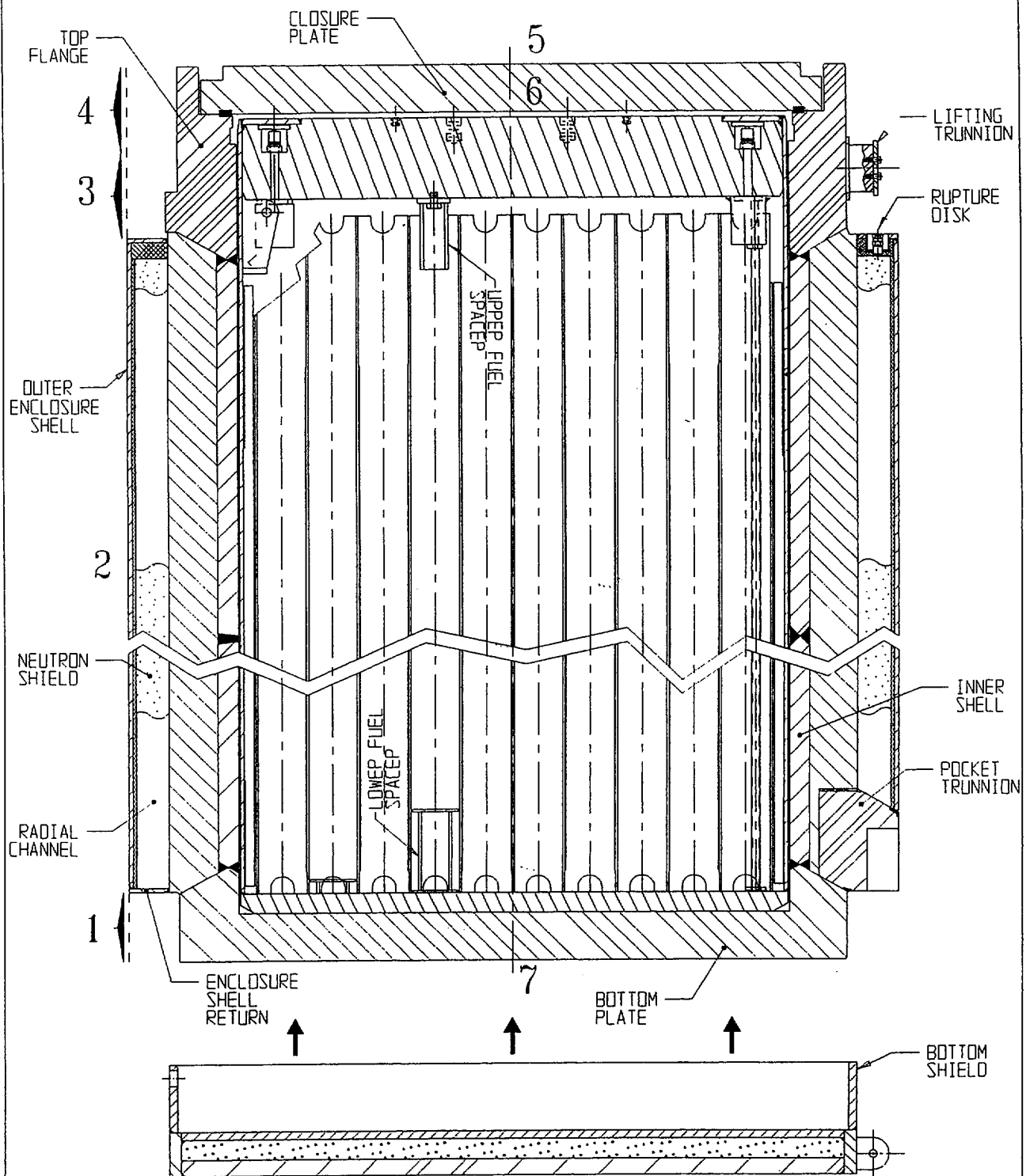


FIGURE 5.1.1; CROSS SECTION ELEVATION VIEW OF OVERPACK WITH DOSE POINT LOCATIONS

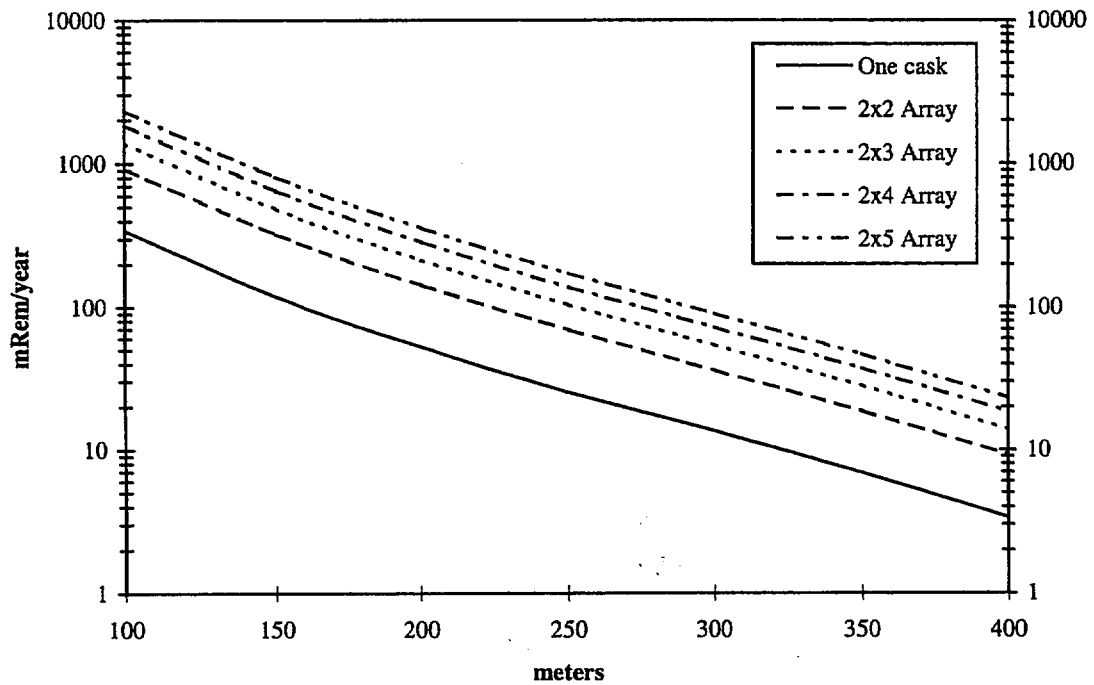


FIGURE 5.1.2; ANNUAL DOSE VERSUS DISTANCE FOR VARIOUS CONFIGURATIONS OF THE MPC-24 40,000 MWD/MTU AND 5-YEAR COOLING 100% OCCUPANCY ASSUMED

5.2 SOURCE SPECIFICATION

The neutron and gamma source terms, decay heat values, and quantities of radionuclides available for release, were calculated with the SAS2H and ORIGEN-S modules of the SCALE 4.3 system [5.1.2, 5.1.3]. Sample input files for SAS2H and ORIGEN-S are provided in Appendices 5.A and 5.B, respectively. The gamma source term is actually comprised of three distinct sources. The first is a gamma source term from the active fuel region due to decay of fission products. The second source term is from ^{60}Co activity of the steel structural material in the fuel element above and below the active fuel region. The third source is from (n,γ) reactions described below.

A description of the design basis intact zircaloy clad fuel for the source term calculations is provided in Table 5.2.1. The PWR fuel assembly described is the assembly that produces the highest neutron and gamma sources and the highest decay heat load from the following fuel assembly classes listed in Tables 2.1.1: B&W 15x15, B&W 17x17, CE 14x14, CE 16x16, WE 14x14, WE 15x15, WE 17x17, St. Lucie, and Ft. Calhoun. The BWR fuel assembly described is the assembly that produces the highest neutron and gamma sources and the highest decay heat load from the following fuel assembly classes listed in Table 2.1.2: GE BWR/2-3, GE BWR/4-6, Humboldt Bay 7x7, and Dresden 1 8x8. Multiple SAS2H and ORIGEN-S calculations were performed to confirm that the B&W 15x15 and the GE 7x7, which have the highest UO_2 mass, bound all other PWR and BWR fuel assemblies, respectively. Section 5.2.5 discusses, in detail, the determination of the design basis fuel assemblies.

The design basis Humboldt Bay and Dresden 1 6x6 fuel assembly, which is also the design basis damaged fuel assembly for the Humboldt Bay and Dresden 1 damaged fuel or fuel debris, is described in Table 5.2.2. The design basis damaged fuel assembly is also the design basis fuel assembly for fuel debris. The fuel assembly type listed produces the highest total neutron and gamma sources from the fuel assemblies at Dresden 1 and Humboldt Bay. Table 5.2.15 provides a description of the design basis Dresden 1 MOX fuel assembly used in this analysis. The design basis 6x6, damaged, and MOX fuel assemblies which are smaller than the GE 7x7, are assumed to have the same hardware characteristics as the GE 7x7. This is conservative because the larger hardware mass of the GE 7x7 results in a larger ^{60}Co activity.

The design basis stainless steel clad fuel assembly for the Haddam Neck and San Onofre 1 assembly classes is described in Table 5.2.18. This table also describes the design basis stainless steel clad LaCrosse fuel assembly.

In performing the SAS2H and ORIGEN-S calculations, a single full power cycle was used to achieve the desired burnup. This assumption, in conjunction with the above-average specific powers listed in Tables 5.2.1, 5.2.2, 5.2.15, and 5.2.18 resulted in conservative source term calculations.

Sections 5.2.1 and 5.2.2 describe the calculation of gamma and neutron source terms for zircaloy clad fuel while Section 5.2.3 discusses the calculation of the gamma and neutron source terms for the stainless steel clad fuel.

5.2.1 Gamma Source

Tables 5.2.4 through 5.2.6 provide the gamma source in MeV/s and photons/s as calculated with SAS2H and ORIGEN-S for the design bases intact fuels for the MPC-24 and MPC-68, and the design basis damaged fuel. Table 5.2.16 provides the gamma source in MeV/s and photons/s for the design basis MOX fuel. NUREG-1536 [5.2.1] states that "only gammas with energies from approximately 0.8 to 2.5 MeV will contribute significantly to the dose rate." Conservatively, only energies in the range of 0.7 MeV-3.0 MeV are used in the shielding calculations. Photons with energies below 0.7 MeV are too weak to penetrate the steel of the overpack, and photons with energies above 3.0 MeV are too few to contribute significantly to the external dose. This section provides the radiation source for each of the burnup levels and cooling times evaluated.

The primary source of activity in the non-fuel regions of an assembly arise from the activation of ^{59}Co to ^{60}Co . The primary source of ^{59}Co in a fuel assembly is the steel structural material above and below the fuel. The zircaloy in these regions is neglected since it does not have a significant ^{59}Co impurity level. Reference [5.2.2] indicates that the impurity level in steel is 800 ppm or 0.8 gm/kg. As a conservative measure, the impurity level of ^{59}Co was assumed to be 1000 ppm or 1.0 gm/kg. Therefore, Inconel and stainless steel in the non-fuel regions are both conservatively assumed to have the 1.0 gm/kg impurity level.

The gamma source from the activation of the grid spacers is negligible in comparison to the source from the active fuel. In addition, in most fuel elements that obtain high burnups, the grid spacers are manufactured from zircaloy which does not activate to produce a gamma source. Therefore, for the PWR fuel assembly, no contribution to the fuel region gamma source from activation of grid spacers is provided in the source term calculations. The BWR assembly grid spacers are zircaloy, however, some assembly designs have steel springs in conjunction with the grid spacers. The gamma source for the BWR fuel assembly includes the activation of these springs associated with the grid spacers.

The non-fuel data listed in Table 5.2.1 was taken from References [5.2.2], [5.2.4], and [5.2.5]. The BWR masses are for an 8x8 fuel assembly. These masses are also appropriate for the 7x7 assembly since the masses of the non-fuel hardware from a 7x7 and an 8x8 are approximately the same. The masses listed are those of the steel components. The zircaloy in these regions was not included because zircaloy does not produce significant activation. These masses are larger than most other fuel assemblies from other manufactures. This, in combination with the conservative ^{59}Co impurity level, results in a conservative estimate of the ^{60}Co activity.

The masses in Table 5.2.1 were used to calculate a ^{59}Co impurity level in the fuel material. The grams of impurity were then used in ORIGEN-S to calculate a ^{60}Co activity level for the desired

burnup and decay time. The methodology used to determine the activation level was developed from Reference [5.2.3] and is described here.

1. The activity of the ^{60}Co is calculated using ORIGEN-S. The flux used in the calculation was the in-core fuel region flux at full power.
2. The activity calculated in Step 1 for the region of interest was modified by the appropriate scaling factors listed in Table 5.2.7. These scaling factors were taken from Reference [5.2.3].

Tables 5.2.9 and 5.2.10 provide the ^{60}Co activity utilized in the shielding calculations in the non-fuel regions of the assemblies for the MPC-24 and the MPC-68. The design basis damaged and MOX fuel assemblies are conservatively assumed to have the same ^{60}Co source strength as the BWR intact design basis fuel. This is a conservative assumption as the design basis damaged fuel and MOX fuel are limited to a significantly lower burnup and longer cooling time than the intact design basis fuel.

In addition to the two sources already mentioned, a third source arises from (n,γ) reactions in the material of the MPC and the overpack. This source of photons is properly accounted for in MCNP when a neutron calculation is performed in a coupled neutron-gamma mode.

5.2.2 Neutron Source

It is well known that the neutron source strength increases as enrichment decreases, for a constant burnup and decay time. This is due to the increase in Pu content in the fuel which increases the inventory of other transuranium nuclides such as Cm. The gamma source also varies with enrichment, although only slightly. Because of this effect and in order to obtain conservative source terms, low initial fuel enrichments were chosen for the BWR and PWR design basis fuel assemblies. The enrichments are appropriately varied as a function of burnup. Table 5.2.23 presents the ^{235}U initial enrichments for various burnup ranges from 20,000 - 50,000 MWD/MTU for PWR and BWR zircaloy clad fuel. These enrichments are based on Reference [5.2.6]. Table 8 of this reference presents average enrichments for burnup ranges. The initial enrichments chosen in Table 5.2.23 are approximately the average enrichments for the burnup range that are 5,000 MWD/MTU less than the ranges listed in Table 5.2.23. These enrichments are below the enrichments typically required to achieve the burnups that were analyzed. Therefore, the source term calculations are conservative.

The neutron source calculated for the design basis intact fuel assemblies for the MPC-24 and MPC-68 and the design basis damaged fuel are listed in Tables 5.2.12 through 5.2.14 in neutrons/s. Table 5.2.17 provides the neutron source in neutrons/sec for the design basis MOX fuel assembly. ^{244}Cm accounts for approximately 96% of the total number of neutrons produced, with slightly over 2% originating from (α,n) reactions within the UO_2 fuel. The remaining 2% derive from spontaneous fission in various Pu and Cm radionuclides. In addition, any neutrons

generated from subcritical multiplication, (n,2n) or similar reactions are properly accounted for in the MCNP calculation.

5.2.3 Stainless Steel Clad Fuel Source

Table 5.2.18 lists the characteristics of the design basis stainless steel clad fuel. The fuel characteristics listed in this table are the input parameters that were used in the shielding calculations described in this chapter. The active fuel length listed in Table 5.2.18 is actually longer than the true active fuel length of 122 inches for the WE 15x15 and 83 inches for the A/C 10x10. Since the true active fuel length is shorter than the design basis zircaloy clad active fuel length, it would be incorrect to calculate source terms for the stainless steel fuel using the correct fuel length and compare them directly to the zircaloy clad fuel source terms because this type of approach would not reflect the potential change in dose rates at the center of the cask (center of the active fuel). As an example, if it is assumed that the source strength for both the stainless steel and zircaloy fuel is 144 photons/s and that the active fuel lengths of the stainless steel fuel and zircaloy fuel are 83 inches and 144 inches, respectively; the source strengths per inch of active fuel would be different for the two fuel types, 1.73 photons/s/inch and 1 photons/s/inch for the stainless steel and zircaloy fuel, respectively. The result would be a higher photon dose rate at the center of the cask with the stainless steel fuel than with the zircaloy clad fuel; a conclusion that would be overlooked by just comparing the source terms. This is an important consideration because the stainless steel clad fuel differs from the zircaloy clad in one important aspect: the stainless steel cladding will contain a significant photon source from Cobalt-60 which will be absent from the zircaloy clad fuel.

In order to eliminate the potential confusion when comparing source terms, the stainless steel clad fuel source terms were calculated with the same active fuel length as the design basis zircaloy clad fuel. Reference [5.2.2] indicates that the Cobalt-59 impurity level in steel is 800 ppm or 0.8 gm/kg. This impurity level was used for the stainless steel cladding in the source term calculations. It is assumed that the end fitting masses of the stainless steel clad fuel are the same as the end fitting masses of the zircaloy clad fuel. Therefore, separate source terms are not provided for the end fittings of the stainless steel fuel.

Tables 5.2.19 through 5.2.22 list the neutron and gamma source strengths for the design basis stainless steel clad fuel. It is obvious from these source terms that the neutron source strength for the stainless steel fuel is lower than for the zircaloy fuel. However, this is not true for all photon energy groups. The peak energy group is from 1.0 to 1.5 MeV which results from the large Cobalt activation in the cladding. Since some of the source strengths are higher for the stainless steel fuel, Section 5.4.5 presents the dose rates at the center of the overpack for the stainless steel fuel. The center dose location is the only location of concern since the end fittings are assumed to be the same mass as the end fittings for the zircaloy clad fuel. In addition, the burnup is lower and the cooling time is longer for the stainless steel fuel compared to the zircaloy clad fuel.

5.2.4 Control Components

Rod cluster control assemblies and axial power shaping rods are not permitted for storage in the HI-STAR 100 system. However, burnable poison rod assemblies (BPRAs) and thimble plug devices (TPDs) are permitted for storage in the HI-STAR 100 System as an integral part of a PWR fuel assembly.

5.2.4.1 BPRAs and TPDs

Burnable poison rod assemblies (BPRAs) (including wet annular burnable absorbers and similarly designed devices with different names) and thimble plug devices (TPD) (including orifice rod assemblies, guide tube plugs, and similarly designed devices with different names) are an integral, yet removable, part of a large portion of PWR fuel. The TPDs are not used in all assemblies in a reactor core but are reused from cycle to cycle. Therefore, these devices can achieve very high burnups. In contrast, BPRAs are burned with a fuel assembly in core and are not reused. In fact, many BPRAs are removed after one or two cycles before the fuel assembly is discharged. Therefore, the achieved burnup for BPRAs is not significantly different than fuel assemblies.

TPDs are made of stainless steel and contain a small amount of inconel. These devices extend down into the plenum region of the fuel assembly but do not extend into the active fuel region with the exception of the W 14x14 water displacement guide tube plugs. Since these devices are made of stainless steel, there is a significant amount of cobalt-60 produced during irradiation. This is the only significant radiation source from the activation of steel and inconel.

BPRAs are made of stainless steel in the region above the active fuel zone and may contain a small amount of inconel in this region. Within the active fuel zone the BPRAs may contain 2-24 rodlets which are burnable absorbers clad in either zircaloy or stainless steel. The stainless steel clad BPRAs create a significant radiation source (Co-60) while the zircaloy clad BPRAs create a negligible radiation source. Therefore the stainless steel clad BPRAs are bounding.

SAS2H and ORIGEN-S were used to calculate a radiation source term and decay heat level for the TPDs and BPRAs. In the ORIGEN-S calculations the cobalt-59 impurity level was conservatively assumed to be 0.8 gm/kg for stainless steel and 4.7 gm/kg for inconel. These calculations were performed by irradiating the appropriate mass of steel and inconel using the flux calculated for the design basis B&W 15x15 fuel assembly. The mass of material in the regions above the active fuel zone was scaled by the appropriate scaling factors listed in Table 5.2.10 in order to account for the reduced flux levels above the fuel assembly. The total curies of cobalt and the decay heat load were calculated for the TPDs and BPRAs as a function of burnup and cooling time. For burnups beyond 45,000 MWD/MTU, it was assumed, for the purpose of the calculation, that the burned fuel assembly was replaced with a fresh fuel assembly every 45,000 MWD/MTU. This was achieved in ORIGEN-S by resetting the flux levels and cross sections to the 0 MWD/MTU condition after every 45,000 MWD/MTU.

Since the HI-STAR 100 cask system is designed to store many varieties of PWR fuel, a bounding TPD and BPRA had to be determined for the purposes of the analysis. This was accomplished by analyzing all of the BPRAs and TPDs (Westinghouse and B&W 14x14 through 17x17) found in references [5.2.5] and [5.2.7] to determine the TPD and BPRA which produced the highest Cobalt-60 source term and decay heat for a specific burnup and cooling time. The bounding TPD was determined to be the Westinghouse 17x17 guide tube plug and the bounding BPRA was actually determined by combining the higher masses of the Westinghouse 17x17 and 15x15 BPRAs into a singly hypothetical BPRA. The masses of this TPD and BPRA are listed in Table 5.2.29. As mentioned above, reference [5.2.5] describes the Westinghouse 14x14 water displacement guide tube plug as having a steel portion which extends into the active fuel zone. This particular water displacement guide tube plug was analyzed and determined to be bounded by the design basis TPD and BPRA.

Once the bounding BPRA and TPD were determined, the allowable decay heat load and Co-60 source from the BPRA and TPD were specified: 0.77 watts and 50 curies Co-60 for each TPD, and 13.0 watts and 831 curies Co-60 for each BPRA. Table 5.2.30 shows the curies of Co-60 that were calculated for BPRAs and TPDs in each region of the fuel assembly (e.g. incore, plenum, top). The allowable decay heat load for the TPDs and BPRAs was subtracted from the allowable decay heat load per assembly to determine the allowable PWR fuel assembly burnup and cooling times listed in Table 1.1-6 of Appendix B of the Certificate of Compliance. Since the decay heat load of the TPDs is negligible the same burnup and cooling time is used for assemblies with or without TPDs. However, a different burnup and cooling time is used for assemblies that contain BPRAs to account for the allowable BPRA decay heat load of 13.0 watts. A separate allowable burnup and cooling time is used for BPRAs and TPDs. These burnup and cooling times assure that the decay heat load and Cobalt-60 activity remain below the allowable levels specified above. It should be noted that at very high burnups, greater than 200,000 MWD/MTU the TPD decay heat load for a given cooling time actually decreases as the burnup continues to increase. This is due to a decrease in the Cobalt-60 production rate as the initial Cobalt-59 impurity is being depleted. Conservatively, a constant cooling time has been specified for burnups from 180,000 to 630,000 MWD/MTU for the TPDs.

Section 5.4.6 demonstrates that the dose rates from fuel assemblies containing BPRAs or TPDs is bounded by the dose rates presented in Section 5.1.1.

5.2.5 Choice of Design Basis Assembly

The analysis presented in this chapter was performed to bound the fuel assembly classes listed in Tables 2.1.1 and 2.1.2. In order to perform a bounding analysis, a design basis fuel assembly must be chosen. Therefore, a fuel assembly from each fuel class was analyzed and a comparison of the neutrons/sec, photons/sec, and thermal power (watts) was performed. The fuel assembly which produced the highest source for a specified burnup, cooling time, and enrichment was

chosen as the design basis fuel assembly. A separate design basis assembly was chosen for the MPC-24 and the MPC-68.

5.2.5.1 PWR Design Basis Assembly

Table 2.1.1 lists the PWR fuel assembly classes that were evaluated to determine the design basis PWR fuel assembly. Within each class, the fuel assembly with the highest UO_2 mass was analyzed. Since the variations of fuel assemblies within a class are very minor (pellet diameter, clad thickness, etc.), it is conservative to choose the assembly with the highest UO_2 mass. For a given class of assemblies, the one with the highest UO_2 mass will produce the highest radiation source because, for a given burnup (MWD/MTU) and enrichment, the highest UO_2 mass will have produced the most energy and therefore the most fission products.

Table 5.2.24 presents the characteristics of the fuel assemblies analyzed to determine the design basis zircaloy clad PWR fuel assembly. The fuel assembly listed for each class is the assembly with the highest UO_2 mass. The St. Lucie and Ft. Calhoun classes are not present in Table 5.2.24. These assemblies are shorter versions of the CE 16x16 and CE 14x14 assembly classes, respectively. Therefore, these assemblies are bounded by the CE 16x16 and CE 14x14 classes and were not explicitly analyzed. Since the Haddam Neck and San Onofre 1 classes are stainless steel clad fuel, these classes were analyzed separately and are discussed below. All fuel assemblies in Table 5.2.24 were analyzed at the same burnup and cooling time. The initial enrichment used in the analysis is consistent with Table 5.2.23. The results of the comparison are provided in Table 5.2.26. These results indicate that the B&W 15x15 fuel assembly has the highest radiation source term of the zircaloy clad fuel assembly classes considered in Table 2.1.1. This fuel assembly also has the highest UO_2 mass (see Table 5.2.24) which confirms that, for a given initial enrichment, burnup, and cooling time, the assembly with the highest UO_2 mass produces the highest radiation source term.

The Haddam Neck and San Onofre 1 classes are shorter stainless steel clad versions of the WE 15x15 and WE 14x14 classes, respectively. Since these assemblies have stainless steel clad, they were analyzed separately as discussed in Section 5.2.3. Based on the results in Table 5.2.26, which show that the WE 15x15 assembly class has a higher source term than the WE 14x14 assembly class, the Haddam Neck, WE 15x15, fuel assembly was analyzed as the bounding PWR stainless steel clad fuel assembly.

5.2.5.2 BWR Design Basis Assembly

Table 2.1.2 lists the BWR fuel assembly classes that were evaluated to determine the design basis BWR fuel assembly. Since there are minor differences between the array types in the GE BWR/2-3 and GE BWR/4-6 assembly classes, these assembly classes were not considered individually but rather as a single class. Within that class, the array types, 7x7, 8x8, 9x9, and 10x10 were analyzed to determine the bounding BWR fuel assembly. Since the Humboldt Bay 7x7 and Dresden 1 8x8 are smaller versions of the 7x7 and 8x8 assemblies they are bounded by

the 7x7 and 8x8 assemblies in the GE BWR/2-3 and GE BWR/4-6 classes. Within each array type, the fuel assembly with the highest UO_2 mass was analyzed. Since the variations of fuel assemblies within an array type are very minor, it is conservative to choose the assembly with the highest UO_2 mass. For a given array type of assemblies, the one with the highest UO_2 mass will produce the highest radiation source because, for a given burnup (MWD/MTU) and enrichment, it will have produced the most energy and therefore the most fission products. The Humboldt Bay 6x6, Dresden 1 6x6, and LaCrosse assembly classes were not considered in the determination of the bounding fuel assembly. However, these assemblies were analyzed explicitly as discussed below.

Table 5.2.25 presents the characteristics of the fuel assemblies analyzed to determine the design basis zircaloy clad BWR fuel assembly. The fuel assembly listed for each array type is the assembly that has the highest UO_2 mass. All fuel assemblies in Table 5.2.25 were analyzed at the same burnup and cooling time. The initial enrichment used in these analyses is consistent with Table 5.2.23. The results of the comparison are provided in Table 5.2.27. These results indicate that the 7x7 fuel assembly has the highest radiation source term of the zircaloy clad fuel assembly classes considered in Table 2.1.2. This fuel assembly also has the highest UO_2 mass which confirms that, for a given initial enrichment, burnup, and cooling time, the assembly with the highest UO_2 mass produces the highest radiation source term. According to Reference [5.2.6], the last discharge of a 7x7 assembly was in 1985 and the maximum average burnup for a 7x7 during their operation was 29,000 MWD/MTU. This clearly indicates that the existing 7x7 assemblies have an average burnup and minimum cooling time that is well within the burnup and cooling time limits in Appendix B to the Certificate of Compliance. Therefore, the 7x7 assembly has never reached the burnup level analyzed in this chapter. However, in the interest of conservatism the 7x7 was chosen as the bounding fuel assembly array type.

Since the LaCrosse fuel assembly type is a stainless steel clad 10x10 assembly it was analyzed separately. The maximum burnup and minimum cooling times for this assembly are limited to 22,500 MWD/MTU and 10-year cooling as specified in Appendix B to the Certificate of Compliance. This assembly type is discussed further in Section 5.2.3.

The Humboldt Bay 6x6 and Dresden 1 6x6 fuel are older and shorter fuel than the other array types analyzed and therefore are considered separately. The Dresden 1 6x6 was chosen as the design basis fuel assembly for the Humboldt Bay 6x6 and Dresden 1 6x6 fuel assembly classes because it has the higher UO_2 mass. Dresden 1 also contains a few 6x6 MOX fuel assemblies which were explicitly analyzed as well.

Reference [5.2.6] indicates that the Dresden 1 6x6 fuel assembly has a higher UO_2 mass than the Dresden 1 8x8 or the Humboldt Bay fuel (6x6 and 7x7). Therefore, the Dresden 1 6x6 fuel assembly was also chosen as the bounding assembly for damaged fuel and fuel debris for the Humboldt Bay and Dresden 1 fuel assembly classes.

Since the design basis damaged fuel assembly and the design basis intact 6x6 fuel assembly are identical, the analysis presented in Section 5.4.2 for the damaged fuel assembly also demonstrates the acceptability of storing intact 6x6 fuel assemblies from the Dresden 1 and Humboldt Bay fuel assembly classes.

5.2.5.3 Decay Heat Loads

Section 2.1.5 describes the calculation of the burnup versus cooling time Technical Specification which is based on a maximum permissible decay heat per assembly. The decay heat values per assembly were calculated using the methodology described in Section 5.2. The design basis fuel assemblies, as described in Table 5.2.1, were used in the calculation of the burnup versus cooling time Technical Specification. The enrichments used in the calculation of the decay heats were consistent with Table 5.2.23. As demonstrated in Tables 5.2.26 and 5.2.27, the design basis fuel assembly produces a higher decay heat value than the other assembly types considered. This is due to the higher heavy metal mass in the design basis fuel assemblies. Conservatively, Appendix B of the Certificate of Compliance limits the heavy metal mass of the design basis fuel assembly classes to a value less than the design basis value utilized in this chapter. This provides additional assurance that the decay heat values are bounding values.

As further demonstration that the decay heat values (calculated using the design basis fuel assemblies) are conservative, a comparison between these calculated decay heats and the decay heats reported in Reference [5.2.7] are presented in Table 5.2.28. This comparison is made for a burnup of 30,000 MWD/MTU and a cooling time of 5 years. The burnup was chosen based on the limited burnup data available in Reference [5.2.7].

The heavy metal mass of the non-design basis fuel assembly classes in Appendix B of the Certificate of Compliance are limited to the masses used in Tables 5.2.24 and 5.2.25. No margin is applied between the allowable mass and the analyzed mass of heavy metal for the non-design basis fuel assemblies. This is acceptable because additional assurance that the decay heat values for the non-design basis fuel assemblies are bounding values is obtained by using the decay heat values for the design basis fuel assemblies to determine the acceptable storage criteria for all fuel assemblies. As mentioned above, Table 5.2.28 demonstrates the level of conservatism in applying the decay heat from the design basis fuel assembly to all fuel assemblies.

5.2.6 Thoria Rod Canister

Dresden Unit 1 has a single DFC containing 18 thoria rods which have obtained a relatively low burnup, 16,000 MWD/MTU. These rods were removed from two 8x8 fuel assemblies which contained 9 rods each. The irradiation of thorium produces an isotope which is not commonly found in depleted uranium fuel. Th-232 when irradiated produces U-233. The U-233 can undergo an (n,2n) reaction which produces U-232. The U-232 decays to produce Tl-208 which produces a 2.6 MeV gamma during Beta decay. This results in a significant source in the 2.5-3.0

MeV range which is not commonly present in depleted uranium fuel. Therefore, this single DFC container was analyzed to determine if it was bounded by the current shielding analysis.

A radiation source term was calculated for the 18 thoria rods using SAS2H and ORIGEN-S for a burnup of 16,000 MWD/MTU and a cooling time of 18 years. Table 5.2.31 describes the 8x8 fuel assembly that contains the thoria rods. Table 5.2.32 and 5.2.33 show the gamma and neutron source terms, respectively, that were calculated for the 18 thoria rods in the thoria rod canister. Comparing these source terms to the design basis 6x6 source terms for Dresden Unit 1 fuel in Tables 5.2.6 and 5.2.14 clearly indicates that the design basis source terms bound the thoria rods source terms in all neutron groups and in all gamma groups except the 2.5-3.0 MeV group. As mentioned above, the thoria rods have a significant source in this energy range due to the decay of Tl-208.

Section 5.4.8 provides a further discussion of the thoria rod canister and its acceptability for storage in the HI-STAR 100 System.

5.2.7 Fuel Assembly Neutron Sources

Neutron sources are used in reactors during initial startup of reactor cores. There are different types of neutron sources (e.g. californium, americium-beryllium, plutonium-beryllium, antimony-beryllium). These neutron sources are typically inserted into the water rod of a fuel assembly and are usually removable.

Dresden Unit 1 has a few antimony-beryllium neutron sources. These sources have been analyzed in Section 5.4.7 to demonstrate that they are acceptable for storage in the HI-STAR 100 System. Currently these are the only neutron source permitted for storage in the HI-STAR 100 System.

Table 5.2.1

DESCRIPTION OF DESIGN BASIS INTACT ZIRCALOY CLAD FUEL

	PWR	BWR
Assembly type/class	B&W 15x15	GE 7x7
Active fuel length (in.)	144	144
No. of fuel rods	208	49
Rod pitch (in.)	0.568	0.738
Cladding material	zircaloy-4	zircaloy-2
Rod diameter (in.)	0.428	0.570
Cladding thickness (in.)	0.0230	0.0355
Pellet diameter (in.)	0.3742	0.488
Pellet material	UO ₂	UO ₂
Pellet density (gm/cc)	10.412 (95% of theoretical)	10.412 (95% of theoretical)
Enrichment (w/o ²³⁵ U)	3.4 and 3.6	2.9 and 3.2
Burnup (MWD/MTU) [†]	40,000 and 47,500 (MPC-24)	35,000 and 45,000 (MPC-68)
Cooling Time (years) [†]	5 and 8 (MPC-24)	5 and 9 (MPC-68)
Specific power (MW/MTU)	40	30
Weight of UO ₂ (kg) ^{††}	562.029	225.177
Weight of U (kg) ^{††}	495.485	198.516

Notes:

1. The B&W 15x15 is the design basis assembly for the following fuel assembly classes listed in Table 2.1.1: B&W 15x15, B&W 17x17, CE 14x14, CE 16x16, WE 14x14, WE 15x15, WE 17x17, St. Lucie, and Ft. Calhoun.
2. The GE 7x7 is the design basis assembly for the following fuel assembly classes listed in Table 2.1.2: GE BWR/2-3, GE BWR/4-6, Humboldt Bay 7x7, and Dresden 1 8x8.

[†] Burnup and cooling time combinations conservatively bound the acceptable burnup and cooling times listed in Appendix B to the Certificate of Compliance.

^{††} Derived from parameters in this table.

Table 5.2.1 (continued)

DESCRIPTION OF DESIGN BASIS INTACT ZIRCALOY CLAD FUEL

	PWR	BWR
No. of Water Rods/Guide Tubes	17	0
Water Rod O.D. (in.)	0.53	N/A
Water Rod Thickness (in.)	0.0160	N/A
Lower End Fitting (kg)	9.46	4.8
Gas Plenum Springs (kg)	0.72176	1.1
Gas Plenum Spacer (kg)	0.82824	N/A
Expansion Springs (kg)	N/A	0.4
Upper End Fitting (kg)	9.28	2.0
Handle (kg)	N/A	0.5
Fuel Grid Spacer Springs (kg of steel)	N/A	0.33

Table 5.2.2

DESCRIPTION OF DESIGN BASIS DAMAGED ZIRCALOY CLAD FUEL

	BWR
Fuel type	GE 6x6
Active fuel length (in.)	110
No. of fuel rods	36
Rod pitch (in.)	0.694
Cladding material	zircaloy-2
Rod diameter (in.)	0.5645
Cladding thickness (in.)	0.035
Pellet diameter (in.)	0.494
Pellet material	UO ₂
Pellet density (gm/cc)	10.412 (95% of theoretical)
Enrichment (w/o ²³⁵ U)	2.24
Burnup (MWD/MTU)	30,000
Cooling Time (years)	18
Specific power (MW/MTU)	16.5
Weight of UO ₂ (kg) [†]	129.5
Weight of U (kg) [†]	114.2

Notes:

1. The 6x6 is the design basis damaged fuel assembly for the Humboldt Bay (all array types) and the Dresden 1 (all array types) damaged fuel assembly classes. It is also the design basis fuel assembly for the intact Humboldt Bay 6x6 and Dresden 1 6x6 fuel assembly classes.
2. This design basis damaged fuel assembly is also the design basis fuel assembly for fuel debris.

[†] Derived from parameters in this table.

Table 5.2.3

DELETED

Table 5.2.4

CALCULATED MPC-24 PWR FUEL GAMMA SOURCE PER ASSEMBLY
 FOR DESIGN BASIS ZIRCALOY CLAD FUEL
 FOR VARYING BURNUPS AND COOLING TIMES

Lower Energy (MeV)	Upper Energy (MeV)	40,000 MWD/MTU 5-Year Cooling		47,500 MWD/MTU 8-Year Cooling	
		(MeV/s)	(Photons/s)	(MeV/s)	(Photons/s)
7.0e-01	1.0	5.96e+14	7.01e+14	3.06e+14	3.60e+14
1.0	1.5	1.38e+14	1.11e+14	9.68e+13	7.74e+13
1.5	2.0	8.94e+12	5.11e+12	4.61e+12	2.64e+12
2.0	2.5	6.85e+12	3.05e+12	6.28e+11	2.79e+11
2.5	3.0	2.67e+11	9.71e+10	3.96e+10	1.44e+10
Totals		7.50e+14	8.20e+14	4.08e+14	4.40e+14

Table 5.2.5

CALCULATED MPC-68 BWR FUEL GAMMA SOURCE PER ASSEMBLY
 FOR DESIGN BASIS ZIRCALOY CLAD FUEL
 FOR VARYING BURNUPS AND COOLING TIMES

Lower Energy (MeV)	Upper Energy (MeV)	35,000 MWD/MTU 5-Year Cooling		45,000 MWD/MTU 9-Year Cooling	
		(MeV/s)	(Photons/s)	(MeV/s)	(Photons/s)
7.0e-01	1.0	1.84e+14	2.17e+14	7.92e+13	9.32e+13
1.0	1.5	4.28e+13	3.43e+13	2.85e+13	2.28e+13
1.5	2.0	2.81e+12	1.60e+12	1.37e+12	7.83e+11
2.0	2.5	2.13e+12	9.48e+11	9.25e+10	4.11e+10
2.5	3.0	8.50e+10	3.09e+10	6.78e+9	2.47e+9
Totals		2.32e+14	2.54e+14	1.09e+14	1.17e+14

Table 5.2.6

CALCULATED MPC-68 and MPC-68F BWR FUEL GAMMA
SOURCE PER ASSEMBLY FOR DESIGN BASIS
ZIRCALOY CLAD DAMAGED FUEL

Lower Energy (MeV)	Upper Energy (MeV)	30,000 MWD/MTU 18-Year Cooling	
		(MeV/s)	(Photons/s)
7.0e-01	1.0	3.97e+12	4.67e+12
1.0	1.5	3.67e+12	2.94e+12
1.5	2.0	2.20e+11	1.26e+11
2.0	2.5	1.35e+9	5.99e+8
2.5	3.0	7.30e+7	2.66e+7
Totals		7.86e+12	7.74e+12

Table 5.2.7

SCALING FACTORS USED IN CALCULATING THE ⁶⁰Co SOURCE

Region	PWR	BWR
Handle	N/A	0.05
Upper end fitting	0.1	0.1
Gas plenum spacer	0.1	N/A
Expansion springs	N/A	0.1
Gas plenum springs	0.2	0.2
Grid spacer springs	N/A	1.0
Lower end fitting	0.2	0.15

Table 5.2.8

DELETED

Table 5.2.9

CALCULATED MPC-24 ⁶⁰Co SOURCE PER ASSEMBLY
 FOR DESIGN BASIS ZIRCALOY CLAD FUEL
 AT VARYING BURNUP AND COOLING TIMES

Location	40,000 MWD/MTU 5-Year Cooling (curies)	47,500 MWD/MTU 8-Year Cooling (curies)
Lower end fitting	154.95	118.06
Gas plenum springs	11.82	9.01
Gas plenum spacer	6.78	5.17
Expansion springs	N/A	N/A
Grid spacer springs	N/A	N/A
Upper end fitting	76.00	57.91
Handle	N/A	N/A

Table 5.2.10

CALCULATED MPC-68 ⁶⁰Co SOURCE PER ASSEMBLY
 FOR DESIGN BASIS ZIRCALOY CLAD FUEL
 AT VARYING BURNUP AND COOLING TIMES

Location	35,000 MWD/MTU 5-Year Cooling (curies)	45,000 MWD/MTU 9-Year Cooling (curies)
Lower end fitting	57.38	40.15
Gas plenum springs	17.53	12.27
Gas plenum spacer	N/A	N/A
Expansion springs	3.19	2.23
Grid spacer springs	26.30	18.40
Upper end fitting	15.94	11.15
Handle	1.99	1.39

Table 5.2.11

DELETED

Table 5.2.12

CALCULATED MPC-24 PWR NEUTRON SOURCE PER ASSEMBLY
 FOR DESIGN BASIS ZIRCALOY CLAD FUEL
 FOR VARYING BURNUP AND COOLING TIMES

Lower Energy (MeV)	Upper Energy (MeV)	40,000 MWD/MTU 5-Year Cooling (Neutrons/s)	47,500 MWD/MTU 8-Year Cooling (Neutrons/s)
1.0e-01	4.0e-01	1.11e+7	1.80e+7
4.0e-01	9.0e-01	5.69e+7	9.19e+7
9.0e-01	1.4	5.21e+7	8.41e+7
1.4	1.85	3.85e+7	6.20e+7
1.85	3.0	6.80e+7	1.10e+8
3.0	6.43	6.16e+7	9.94e+7
6.43	20.0	5.45e+6	8.81e+6
Totals		2.94e+8	4.74e+8

Table 5.2.13

CALCULATED MPC-68 BWR NEUTRON SOURCE PER ASSEMBLY
 FOR DESIGN BASIS ZIRCALOY CLAD FUEL
 FOR VARYING BURNUP AND COOLING TIMES

Lower Energy (MeV)	Upper Energy (MeV)	35,000 MWD/MTU 5-Year Cooling (Neutrons/s)	45,000 MWD/MTU 9-Year Cooling (Neutrons/s)
1.0e-01	4.0e-01	3.05e+6	6.23e+6
4.0e-01	9.0e-01	1.56e+7	3.18e+7
9.0e-01	1.4	1.43e+7	2.91e+7
1.4	1.85	1.06e+7	2.15e+7
1.85	3.0	1.87e+7	3.79e+7
3.0	6.43	1.69e+7	3.44e+7
6.43	20.0	1.49e+6	3.05e+6
Totals		8.06e+7	1.64e+8

Table 5.2.14

CALCULATED MPC-68 and MPC-68F BWR NEUTRON SOURCE PER ASSEMBLY
FOR DESIGN BASIS DAMAGED ZIRCALOY CLAD FUEL

Lower Energy (MeV)	Upper Energy (MeV)	30,000 MWD/MTU 18-Year Cooling (Neutrons/s)
1.0e-01	4.0e-01	8.22e+5
4.0e-01	9.0e-01	4.20e+6
9.0e-01	1.4	3.87e+6
1.4	1.85	2.88e+6
1.85	3.0	5.18e+6
3.0	6.43	4.61e+6
6.43	20.0	4.02e+5
Totals		2.20e+7

Table 5.2.15

DESCRIPTION OF DESIGN BASIS ZIRCALOY CLAD MIXED OXIDE FUEL

	BWR
Fuel type	GE 6x6
Active fuel length (in.)	110
No. of fuel rods	36
Rod pitch (in.)	0.696
Cladding material	zircaloy-2
Rod diameter (in.)	0.5645
Cladding thickness (in.)	0.036
Pellet diameter (in.)	0.482
Pellet material	UO ₂ and PuUO ₂
No. of UO ₂ Rods	27
No. of PuUO ₂ rods	9
Pellet density (gm/cc)	10.412 (95% of theoretical)
Enrichment (w/o ²³⁵ U) [†]	2.24 (UO ₂ rods) 0.711 (PuUO ₂ rods)
Burnup (MWD/MTU)	30,000
Cooling Time (years)	18
Specific power (MW/MTU)	16.5
Weight of UO ₂ ,PuUO ₂ (kg) ^{††}	123.3
Weight of U,Pu (kg) ^{††}	108.7

[†] See Table 5.3.3 for detailed composition of PuUO₂ rods.

^{††} Derived from parameters in this table.

Table 5.2.16

**CALCULATED MPC-68 BWR FUEL GAMMA SOURCE PER ASSEMBLY
FOR DESIGN BASIS ZIRCALOY CLAD MIXED OXIDE FUEL**

Lower Energy	Upper Energy	30,000 MWD/MTU 18-Year Cooling	
		(MeV/s)	(Photons/s)
7.0e-01	1.0	3.87e+12	4.56e+12
1.0	1.5	3.72e+12	2.98e+12
1.5	2.0	2.18e+11	1.25e+11
2.0	2.5	1.17e+9	5.22e+8
2.5	3.0	9.25e+7	3.36e+7
Totals		7.81e+12	7.67e+12

Table 5.2.17

**CALCULATED MPC-68 BWR NEUTRON SOURCE PER ASSEMBLY
FOR DESIGN BASIS ZIRCALOY CLAD MIXED OXIDE FUEL**

Lower Energy (MeV)	Upper Energy (MeV)	30,000 MWD/MTU 18-Year Cooling (Neutrons/s)
1.0e-01	4.0e-01	1.24e+6
4.0e-01	9.0e-01	6.36e+6
9.0e-01	1.4	5.88e+6
1.4	1.85	4.43e+6
1.85	3.0	8.12e+6
3.0	6.43	7.06e+6
6.43	20.0	6.07e+5
Totals		3.37e+7

Table 5.2.18

DESCRIPTION OF DESIGN BASIS INTACT STAINLESS STEEL CLAD FUEL

	PWR	BWR
Fuel type	WE 15x15	A/C 10x10
Active fuel length (in.)	144	144
No. of fuel rods	204	100
Rod pitch (in.)	0.563	0.565
Cladding material	304 SS	348H SS
Rod diameter (in.)	0.422	0.396
Cladding thickness (in.)	0.0165	0.02
Pellet diameter (in.)	0.3825	0.35
Pellet material	UO ₂	UO ₂
Pellet density (gm/cc)	10.412 (95% of theoretical)	10.412 (95% of theoretical)
Enrichment (w/o ²³⁵ U)	3.5	3.5
Burnup (MWD/MTU)	30,000 @ 9 yr (MPC-24) 40,000 @ 15 yr (MPC-24)	22,500 (MPC-68)
Cooling Time (years)	9 (MPC-24) 15 (MPC-24)	10 (MPC-68)
Specific power (MW/MTU)	37.96	29.17
No. of Water Rods	21	0
Water Rod O.D. (in.)	0.546	N/A
Water Rod Thickness (in.)	0.017	N/A

Notes:

1. The WE 15x15 is the design basis assembly for the following fuel assembly classes listed in Table 2.1.1: Haddam Neck and San Onofre 1.
2. The A/C 10x10 is the design basis assembly for the following fuel assembly class listed in Table 2.1.2: LaCrosse.

Table 5.2.19

CALCULATED BWR FUEL GAMMA SOURCE PER ASSEMBLY
FOR STAINLESS STEEL CLAD FUEL

Lower Energy (MeV)	Upper Energy (MeV)	22,500 MWD/MTU 10-Year Cooling	
		(MeV/s)	(Photons/s)
7.0e-01	1.0	1.97e+13	2.31e+13
1.0	1.5	7.93e+13	6.34e+13
1.5	2.0	4.52e+11	2.58e+11
2.0	2.5	3.28e+10	1.46e+10
2.5	3.0	1.69e+9	6.14e+8
Totals		9.95e+13	8.68e+13

Note:

These source terms were calculated for a 144 inch active fuel length. The actual active fuel length is 83 inches.

Table 5.2.20

CALCULATED PWR FUEL GAMMA SOURCE PER ASSEMBLY
FOR STAINLESS STEEL CLAD FUEL

Lower Energy (MeV)	Upper Energy (MeV)	30,000 MWD/MTU 9-Year Cooling		40,000 MWD/MTU 15-Year Cooling	
		(MeV/s)	(Photons/s)	(MeV/s)	(Photons/s)
7.0e-01	1.0	1.18e+14	1.39e+14	4.79e+13	5.63e+13
1.0	1.5	3.00e+14	2.40e+14	1.88e+14	1.50e+14
1.5	2.0	2.28e+12	1.30e+12	2.07e+12	1.18e+12
2.0	2.5	2.34e+11	1.04e+11	1.28e+10	5.71e+9
2.5	3.0	1.33e+10	4.83e+9	9.59e+8	3.49e+8
Totals		4.21e+14	3.80e+14	2.38e+14	2.07e+14

Note:

These source terms were calculated for a 144 inch active fuel length. The actual active fuel length is 122 inches.

Table 5.2.21

CALCULATED BWR NEUTRON SOURCE PER ASSEMBLY
FOR STAINLESS STEEL CLAD FUEL

Lower Energy (MeV)	Upper Energy (MeV)	22,500 MWD/MTU 10-Year Cooling (Neutrons/s)
1.0e-01	4.0e-01	2.23e+5
4.0e-01	9.0e-01	1.14e+6
9.0e-01	1.4	1.07e+6
1.4	1.85	8.20e+5
1.85	3.0	1.56e+6
3.0	6.43	1.30e+6
6.43	20.0	1.08e+5
Total		6.22e+6

Note:

These source terms were calculated for a 144 inch active fuel length. The actual active fuel length is 83 inches.

Table 5.2.22

**CALCULATED PWR NEUTRON SOURCE PER ASSEMBLY
FOR STAINLESS STEEL CLAD FUEL**

Lower Energy (MeV)	Upper Energy (MeV)	30,000 MWD/MTU 9-Year Cooling (Neutrons/s)	40,000 MWD/MTU 15-Year Cooling (Neutrons/s)
1.0e-01	4.0e-01	3.05e+6	8.02e+6
4.0e-01	9.0e-01	1.56e+7	4.10e+7
9.0e-01	1.4	1.44e+7	3.77e+7
1.4	1.85	1.07e+7	2.79e+7
1.85	3.0	1.93e+7	4.98e+7
3.0	6.43	1.71e+7	4.47e+7
6.43	20.0	1.49e+6	3.93e+6
Totals		8.16e+7	2.13e+8

Note:

These source terms were calculated for a 144 inch active fuel length. The actual active fuel length is 122 inches.

Table 5.2.23

INITIAL ENRICHMENTS USED IN THE SOURCE TERM CALCULATIONS

Burnup Range (MWD/MTU)	Initial Enrichment (wt. % ²³⁵ U)
BWR Fuel	
20,000-25,000	2.1
25,000-30,000	2.4
30,000-35,000	2.6
35,000-40,000	2.9
40,000-45,000	3.0
45,000-50,000	3.2
PWR Fuel	
20,000-25,000	2.3
25,000-30,000	2.6
30,000-35,000	2.9
35,000-40,000	3.2
40,000-45,000	3.4
45,000-50,000	3.6

Note: The burnup ranges do not overlap. Therefore, 20,000-25,000 MWD/MTU means 20,000-24,999.9 MWD/MTU, etc.

Table 5.2.24

DESCRIPTION OF EVALUATED INTACT ZIRCALOY CLAD PWR FUEL

Assembly class	WE 14x14	WE 15x15	WE 17x17	CE 14x14	CE 16x16	B&W 15x15	B&W 17x17
Active fuel length (in.)	144	144	144	144	150	144	144
No. of fuel rods	179	204	264	176	236	208	264
Rod pitch (in.)	0.556	0.563	0.496	0.580	0.5063	0.568	0.502
Cladding material	Zr-4						
Rod diameter (in.)	0.422	0.422	0.374	0.440	0.382	0.428	0.377
Cladding thickness (in.)	0.0243	0.0245	0.0225	0.0280	0.0250	0.0230	0.0220
Pellet diameter (in.)	0.3659	0.366	0.3225	0.377	0.3255	0.3742	0.3252
Pellet material	UO ₂						
Pellet density (gm/cc) (95% of theoretical)	10.412	10.412	10.412	10.412	10.412	10.412	10.412
Enrichment (wt.% ²³⁵ U)	3.4	3.4	3.4	3.4	3.4	3.4	3.4
Burnup (MWD/MTU)	40,000	40,000	40,000	40,000	40,000	40,000	40,000
Cooling time (years)	5	5	5	5	5	5	5
Specific power (MW/MTU)	40	40	40	40	40	40	40
Weight of UO ₂ (kg) [†]	462.451	527.327	529.848	482.706	502.609	562.029	538.757
Weight of U (kg) [†]	407.697	464.891	467.114	425.554	443.100	495.485	474.968
No. of Guide Tubes	17	21	25	5	5	17	25
Guide Tube O.D. (in.)	0.539	0.546	0.474	1.115	0.98	0.53	0.564
Guide Tube Thickness (in.)	0.0170	0.0170	0.0160	0.0400	0.0400	0.0160	0.0175

[†] Derived from parameters in this table.

Table 5.2.25

DESCRIPTION OF EVALUATED INTACT ZIRCALOY CLAD BWR FUEL

Array Type	7×7	8×8	9×9	10×10
Active fuel length (in.)	144	144	144	144
No. of fuel rods	49	63	74	92
Rod pitch (in.)	0.738	0.640	0.566	0.510
Cladding material	Zr-2	Zr-2	Zr-2	Zr-2
Rod diameter (in.)	0.570	0.493	0.440	0.404
Cladding thickness (in.)	0.0355	0.0340	0.0280	0.0260
Pellet diameter (in.)	0.488	0.416	0.376	0.345
Pellet material	UO ₂	UO ₂	UO ₂	UO ₂
Pellet density (gm/cc) (95% of theoretical)	10.412	10.412	10.412	10.412
Enrichment (wt.% ²³⁵ U)	3.0	3.0	3.0	3.0
Burnup (MWD/MTU)	40,000	40,000	40,000	40,000
Cooling time (years)	5	5	5	5
Specific power (MW/MTU)	30	30	30	30
Weight of UO ₂ (kg) [†]	225.177	210.385	201.881	211.307
Weight of U (kg) [†]	198.516	185.475	177.978	186.288
No. of Water Rods	0	1	2	2
Water Rod O.D. (in.)	n/a	0.493	0.980	0.980
Water Rod Thickness (in.)	n/a	0.0340	0.0300	0.0300

[†] Derived from parameters in this table.

Table 5.2.26

COMPARISON OF SOURCE TERMS FOR INTACT ZIRCALOY CLAD PWR FUEL
 3.4 wt.% ²³⁵U - 40,000 MWD/MTU - 5 years cooling

Assembly class	WE 14x14	WE 15x15	WE 17x17	CE 14x14	CE 16x16	B&W 15x15	B&W 17x17
Neutrons/sec	2.29e+8 / 2.28e+8	2.63e+8 / 2.65e+8	2.62e+8	2.31e+8	2.34e+8	2.94e+8	2.64e+8
Photons/sec (0.7-3.0 MeV)	6.64e+14/ .09e+14	7.54e+14/ 8.12e+14	7.60e+14	6.77e+14	7.06e+14	8.20e+14	7.71e+14
Thermal power (watts)	926.6 / 934.9	1056 / 1068	1062	956.6	995.7	1137	1077

Note:

The WE 14x14 and WE 15x15 have both zircaloy and stainless steel guide tubes. The first value presented is for the assembly with zircaloy guide tubes and the second value is for the assembly with stainless steel guide tubes.

Table 5.2.27

COMPARISON OF SOURCE TERMS FOR INTACT ZIRCALOY CLAD BWR FUEL
 3.0 wt.% ²³⁵U - 40,000 MWD/MTU - 5 years cooling

Assembly class	7x7	8x8	9x9	10x10
Neutrons/sec	1.33e+8	1.17e+8	1.11e+8	1.22e+8
Photons/sec (0.7-3.0 MeV)	3.10e+14	2.83e+14	2.71e+14	2.89e+14
Thermal power (watts)	435.5	402.3	385.3	407.4

Table 5.2.28

**COMPARISON OF CALCULATED DECAY HEATS FOR DESIGN BASIS FUEL
AND VALUES REPORTED IN THE
DOE CHARACTERISTICS DATABASE [†] FOR
30,000 MWD/MTU AND 5-YEAR COOLING**

Fuel Assembly Class	Decay Heat from the DOE Database (watts/assembly)	Decay Heat from Design Basis Fuel (watts/assembly)
PWR Fuel		
B&W 15x15	752.0	827.5
B&W 17x17	732.9	827.5
CE 16x16	653.7	827.5
CE 14x14	601.3	827.5
WE 17x17	742.5	827.5
WE 15x15	762.2	827.5
WE 14x14	649.6	827.5
BWR Fuel		
7x7	310.9	315.7
8x8	296.6	315.7
9x9	275.0	315.7

Notes:

1. The PWR and BWR design basis fuels are the B&W 15x15 and the GE 7x7, respectively.
2. The decay heat values from the database include contributions from in-core material (e.g. spacer grids).
3. Information on the 10x10 was not available in the DOE database. However, based on the results in Table 5.2.27, the actual decay heat values from the 10x10 would be very similar to the values shown above for the 8x8.

[†] Reference [5.2.7].

Table 5.2.29

DESCRIPTION OF DESIGN BASIS BURNABLE POISON ROD ASSEMBLY
AND THIMBLE PLUG DEVICE

Region	BPRA	TPD
Upper End Fitting (kg of steel)	2.62	2.3
Upper End Fitting (kg of inconel)	0.42	0.42
Gas Plenum Spacer (kg of steel)	0.77488	1.71008
Gas Plenum Springs (kg of steel)	0.67512	1.48992
In-core (kg of steel)	13.2	N/A

Table 5.2.30

DESIGN BASIS COBALT-60 ACTIVITIES FOR BURNABLE POISON ROD
ASSEMBLIES AND THIMBLE PLUG DEVICES

Region	BPRA	TPD
Upper End Fitting (curies Co-60)	30.4	25.21
Gas Plenum Spacer (curies Co-60)	4.6	9.04
Gas Plenum Springs (curies Co-60)	8.2	15.75
In-core (curies Co-60)	787.8	N/A

Table 5.2.31

DESCRIPTION OF FUEL ASSEMBLY USED TO ANNALYZE
THORIA RODS IN THE THORIA ROD CANISTER

	BWR
Fuel type	8x8
Active fuel length (in.)	110.5
No. of UO ₂ fuel rods	55
No. of UO ₂ /ThO ₂ fuel rods	9
Rod pitch (in.)	0.523
Cladding material	zircaloy
Rod diameter (in.)	0.412
Cladding thickness (in.)	0.025
Pellet diameter (in.)	0.358
Pellet material	98.2% ThO ₂ and 1.8% UO ₂ for UO ₂ /ThO ₂ rods
Pellet density (gm/cc)	10.412
Enrichment (w/o ²³⁵ U)	93.5 in UO ₂ for UO ₂ /ThO ₂ rods and 1.8 for UO ₂ rods
Burnup (MWD/MTIHM)	16,000
Cooling Time (years)	18
Specific power (MW/MTIHM)	16.5
Weight of ThO ₂ and UO ₂ (kg) [†]	121.46
Weight of U (kg) [†]	92.29
Weight of Th (kg) [†]	14.74

[†] Derived from parameters in this table.

Table 5.2.32

CALCULATED FUEL GAMMA SOURCE FOR THORIA ROD
CANISTER CONTAINING EIGHTEEN THORIA RODS

Lower Energy (MeV)	Upper Energy (MeV)	16,000 MWD/MTIHM 18-Year Cooling	
		(MeV/s)	(Photons/s)
7.0e-01	1.0	5.79e+11	6.81e+11
1.0	1.5	3.79e+11	3.03e+11
1.5	2.0	4.25e+10	2.43e+10
2.0	2.5	4.16e+8	1.85e+8
2.5	3.0	2.31e+11	8.39e+10
Totals		1.23e+12	1.09e+12

Table 5.2.33

CALCULATED FUEL NEUTRON SOURCE FOR THORIA ROD
CANISTER CONTAINING EIGHTEEN THORIA RODS

Lower Energy (MeV)	Upper Energy (MeV)	16,000 MWD/MTIHM 18-Year Cooling (Neutrons/s)
1.0e-01	4.0e-01	5.65e+2
4.0e-01	9.0e-01	3.19e+3
9.0e-01	1.4	6.79e+3
1.4	1.85	1.05e+4
1.85	3.0	3.68e+4
3.0	6.43	1.41e+4
6.43	20.0	1.60e+2
Totals		7.21e+4

The shielding analysis of the HI-STAR 100 System was performed with MCNP-4A [5.1.1]. MCNP is a Monte Carlo transport code that offers a full three-dimensional combinatorial geometry modeling capability including such complex surfaces as cones and tori. This means that no gross approximations were required to represent the HI-STAR 100 System in the shielding analysis. A sample input file for MCNP is provided in Appendix 5.C.

As discussed in Section 5.1.1, off-normal conditions do not have any implications for the shielding analysis. Therefore, the MCNP models and results developed for the normal conditions also represent the off-normal condition. Section 5.1.2 discussed the accident conditions and stated that the only accident that would impact the shielding analysis would be a loss of the neutron shield. Therefore, the MCNP models of the HI-STAR 100 System normal condition have the neutron shield in place while the accident condition replaces the neutron shield with void.

5.3.1 Description of the Radial and Axial Shielding Configuration

Section 1.5 provides the Design Drawings that describe the HI-STAR 100 System. These drawings were used to create the MCNP models used in the radiation transport calculations. Figures 5.3.2 and 5.3.3 show cross sectional views of the HI-STAR 100 overpack and MPC as it was modeled in MCNP for each of the MPCs. These figures were created with the MCNP two-dimensional plotter and are drawn to scale. The figures clearly illustrate the radial steel fins and pocket trunnions in the neutron shield region. Since the fins and pocket trunnions were modeled explicitly, neutron streaming through these components is accounted for in the calculations of the dose adjacent to the overpack and 1 meter dose. In Section 5.4.1, the dose effect of localized streaming through these compartments is analyzed. Figures 5.3.5 and 5.3.6 show the MCNP models of the MPC-24 and MPC-68 fuel baskets including the as-modeled dimensions. Figure 5.3.9 shows a cross sectional view of the HI-STAR 100 overpack with the as-modeled thickness of the various materials. Figure 5.3.10 is an axial representation of the HI-STAR 100 overpack with the various as-modeled dimensions indicated. As Figure 5.3.10 indicates, the thickness of the MPC-68 lid and the thickness of the MPC-24 lid are 10.0 and 9.5 inches, respectively. Correspondingly, the MPC-internal cavity heights differ by 0.5 inch. In the MCNP models of the MPC-24 and MPC-68, the actual lid thickness and internal cavity height for that particular MPC was used.

Calculations were performed to determine the acceptability of homogenizing the fuel assembly versus explicit modeling. Based on these calculations it was concluded that it was acceptable to homogenize the fuel assembly without loss of accuracy. The PWR fuel assembly modeled was the design basis fuel assembly, the B&W 15x15. The width of this homogenized fuel assembly in MCNP is equal to 15 times the pitch. The BWR fuel assembly modeled was an 8x8 fuel assembly. This is different from the 7x7 design basis fuel assembly used for the source term calculations. However, it is conservative to use an 8x8 fuel assembly in the MCNP model since it contains less fuel and therefore less shielding than the 7x7 fuel assembly. The width of the BWR

homogenized fuel assembly is equal to 8 times the pitch. Homogenization of the fuel assemblies resulted in a noticeable decrease in run time.

Several conservative approximations were made in modeling the MPC. The conservative approximations are listed below.

1. The basket material in the top and bottom 0.9 inches where the MPC basket flow holes are located is not modeled. The length of the basket not modeled (0.9 inches) was determined by calculating the equivalent area removed by the flow holes. This method of approximation is conservative because no material for the basket shielding is provided in the 0.9 inch area at the top and bottom of the MPC basket.
2. The upper and lower fuel spacers are not modeled. The fuel spacers are not needed on all fuel assembly types. However, most PWR fuel assemblies will have upper and lower fuel spacers. The positioning of the fuel assembly for the shielding analysis is determined by the fuel spacer length for the design basis fuel assembly type, but the fuel spacer materials are not modeled. This is conservative since it removes steel which would provide a small amount of additional shielding.
3. For the MPC-24 and the MPC-68, the MPC basket supports are not modeled. This is conservative since it removes steel which would provide a small increase in shielding. The aluminum heat conduction elements are also conservatively not modeled.
4. The MPC-24 basket is fabricated from 5/16 inch thick cell plates and 9/32 inch thick angles. It is conservatively assumed for modeling purposes that the structural portion of the MPC-24 basket is uniformly fabricated from 9/32 inch thick steel. The Boral and sheathing are modeled explicitly. This is conservative since it removes steel which would provide a small amount of additional shielding.
5. In the modeling of the BWR fuel assemblies, the zircaloy flow channel was not represented. This was done because it cannot be guaranteed that all BWR fuel assemblies will have an associated flow channel when placed in the MPC. The flow channel does not contribute to the source, but does provide some small amount of shielding. However, no credit is taken for this additional shielding.
6. In the MPC-24, 12 of the 24 Boral panels on the periphery have a reduced width. Conservatively, all Boral panels on the periphery were modeled with a reduced width of 5 inches.

5.3.1.1 Fuel Configuration

As described above, the active fuel region is modeled as a homogenous zone. The end fittings and the plenum regions are also modeled as homogenous regions of steel. The masses of steel used in these regions are shown in Table 5.2.1. The axial description of the design basis fuel assemblies is provided in Table 5.3.1. Figures 5.3.7 and 5.3.8 graphically depict the location of the PWR and BWR fuel assemblies within the HI-STAR 100 System. The axial locations of the Boral, basket, pocket trunnion, and transition areas are shown in these figures.

5.3.1.2 Streaming Considerations

The streaming from the radial steel fins and pocket trunnions in the neutron shield is evaluated in Section 5.4.1. The MCNP model of the HI-STAR 100 completely describes the radial steel fins and pocket trunnions, thereby properly accounting for the streaming effect. This is discussed further in Section 5.4.1.

The design of the HI-STAR 100 System, as described in the Design Drawings in Section 1.5, has eliminated all other possible streaming paths. Therefore, the MCNP model does not represent any additional streaming paths. A brief justification of this assumption is provided for each penetration.

- The lifting trunnions will remain installed in the overpack top flange. No credit is taken for any part of the trunnion that extends outside of the overpack.
- The pocket trunnions are modeled as solid blocks of steel. The pocket trunnion will be filled with a solid steel rotation trunnion attached to the transport frame during handling and a shield plug when located at the ISFSI pad.
- The threaded holes in the MPC lid are plugged with solid plugs during storage and, therefore, do not create a void in the MPC lid.
- The drain and vent ports in the MPC lid are designed to eliminate streaming paths. The steel lost in the MPC lid at the port location is replaced with a block of steel approximately 6 inches thick below the port opening and attached to the underside of the lid. This design feature is shown on the Design Drawings in Section 1.5. The MCNP model did not explicitly represent this arrangement but, rather, modeled the MPC lid as a solid piece.
- The penetrations in the overpack are filled with bolts that extend into the penetration when in storage operations, thereby eliminating any potential direct streaming paths. Cover plates are also designed in such a way as to maintain the thickness of the overpack

to the maximum extent practical. Therefore, the MCNP model does not represent any streaming paths due to penetrations in the overpack.

5.3.2 Regional Densities

Composition and densities of the various materials used in the HI-STAR 100 System shielding analyses are given in Tables 5.3.2 and 5.3.3. All of the materials and their actual geometries are represented in the MCNP model.

Sections 4.4 and 4.5 demonstrate that all materials used in the HI-STAR 100 System remain below their design temperatures as specified in Table 2.2.3 during all normal conditions. Therefore, the shielding analysis does not address changes in the material density or composition as a result of temperature changes.

Chapter 11 discusses the effect of the various accident conditions on the temperatures of the shielding materials and the resultant impact on their shielding effectiveness. As stated in Section 5.1.2, there is only one accident that has any significant impact on the shielding configuration. This accident is the loss of the neutron shield in the HI-STAR 100 System as a result of fire or other damage. The change in the neutron shield was conservatively analyzed by assuming that the entire volume of the neutron shield was replaced by void.

Table 5.3.1

DESCRIPTION OF THE AXIAL MCNP MODEL OF THE FUEL ASSEMBLIES[†]

Region	Start (in.)	Finish (in.)	Length (in.)	Actual Material	Modeled Material
PWR					
Lower End Fitting	0.0	7.375	7.375	SS304	SS304
Space	7.375	8.375	1.0	zircaloy	void
Fuel	8.375	152.375	144	fuel & zircaloy	fuel
Gas Plenum Springs	152.375	156.1875	3.8125	SS304 & zircaloy	SS304
Gas Plenum Spacer	156.1875	160.5625	4.375	SS304 & zircaloy	SS304
Upper End Fitting	160.5625	165.625	5.0625	SS304	SS304
BWR					
Lower End Fitting	0.0	7.385	7.385	SS304	SS304
Fuel	7.385	151.385	144	fuel & zircaloy	fuel
Space	151.385	157.385	6	zircaloy	void
Gas Plenum Springs	157.385	166.865	9.48	SS304 & zircaloy	SS304
Expansion Springs	166.865	168.215	1.35	SS304	SS304
Upper End Fitting	168.215	171.555	3.34	SS304	SS304
Handle	171.555	176	4.445	SS304	SS304

[†] All dimensions start at the bottom of the fuel assembly. The length of the lower fuel spacer must be added to the distances to determine the distance from the top of the MPC baseplate.

Table 5.3.2

COMPOSITION OF THE MATERIALS IN THE HI-STAR 100 SYSTEM

Component	Density (g/cm ³)	Elements	Mass Fraction (%)
Uranium Oxide	10.412	²³⁵ U	2.9971(BWR) 3.2615(PWR)
		²³⁸ U	85.1529(BWR) 84.8885(PWR)
		O	11.85
Boral	2.644	¹⁰ B	4.4226 (MPC-68) 4.367 (MPC-24)
		¹¹ B	20.1474 (MPC-68) 19.893 (MPC-24)
		Al	68.61 (MPC-68) 69.01 (MPC-24)
		C	6.82 (MPC-68) 6.73 (MPC-24)
SS304	7.92	Cr	19
		Mn	2
		Fe	69.5
		Ni	9.5
Carbon Steel	7.82	C	0.5
		Fe	99.5
Zircaloy	6.55	Zr	100

Table 5.3.2 (continued)

COMPOSITION OF THE MATERIALS IN THE HI-STAR 100 SYSTEM

Component	Density (g/cm ³)	Elements	Mass Fraction (%)
Neutron Shield Holtite-A	1.61	C	27.66039
		H	5.92
		Al	21.285
		N	1.98
		O	42.372
		¹⁰ B	0.14087
		¹¹ B	0.64174
BWR Fuel Region Mixture	3.979996	²³⁵ U	2.4483
		²³⁸ U	69.5601
		O	9.6801
		Zr	18.3115
PWR Fuel Region Mixture	3.853705	²³⁵ U	2.6944
		²³⁸ U	70.1276
		O	9.7895
		Zr	17.3885
Lower End Fitting (PWR)	1.0783	SS304	100
Gas Plenum Springs (PWR)	0.1591	SS304	100
Gas Plenum Spacer (PWR)	0.1591	SS304	100

Table 5.3.2 (continued)

COMPOSITION OF THE MATERIALS IN THE HI-STAR 100 SYSTEM

Component	Density (g/cm³)	Elements	Mass Fraction (%)
Upper End Fitting (PWR)	1.5410	SS304	100
Lower End Fitting (BWR)	1.5130	SS304	100
Gas Plenum Springs (BWR)	0.2701	SS304	100
Expansion Springs (BWR)	0.6897	SS304	100
Upper End Fitting (BWR)	1.3939	SS304	100
Handle (BWR)	0.2619	SS304	100

Table 5.3.3

COMPOSITION OF THE FUEL IN THE MIXED OXIDE FUEL
ASSEMBLIES IN THE MPC-68 OF THE HI-STAR 100 SYSTEM

Component	Density (g/cm ³)	Elements	Mass Fraction (%)
Mixed Oxide Pellets	10.412	²³⁸ U	84.498
		²³⁵ U	0.612
		²³⁸ Pu	0.421
		²³⁹ Pu	1.455
		²⁴⁰ Pu	0.034
		²⁴¹ Pu	0.123
		²⁴² Pu	0.007
		O	11.85
Uranium Oxide Pellets	10.412	²³⁸ U	86.175
		²³⁵ U	1.975
		O	11.85

FIGURE 5.3.1

DELETED

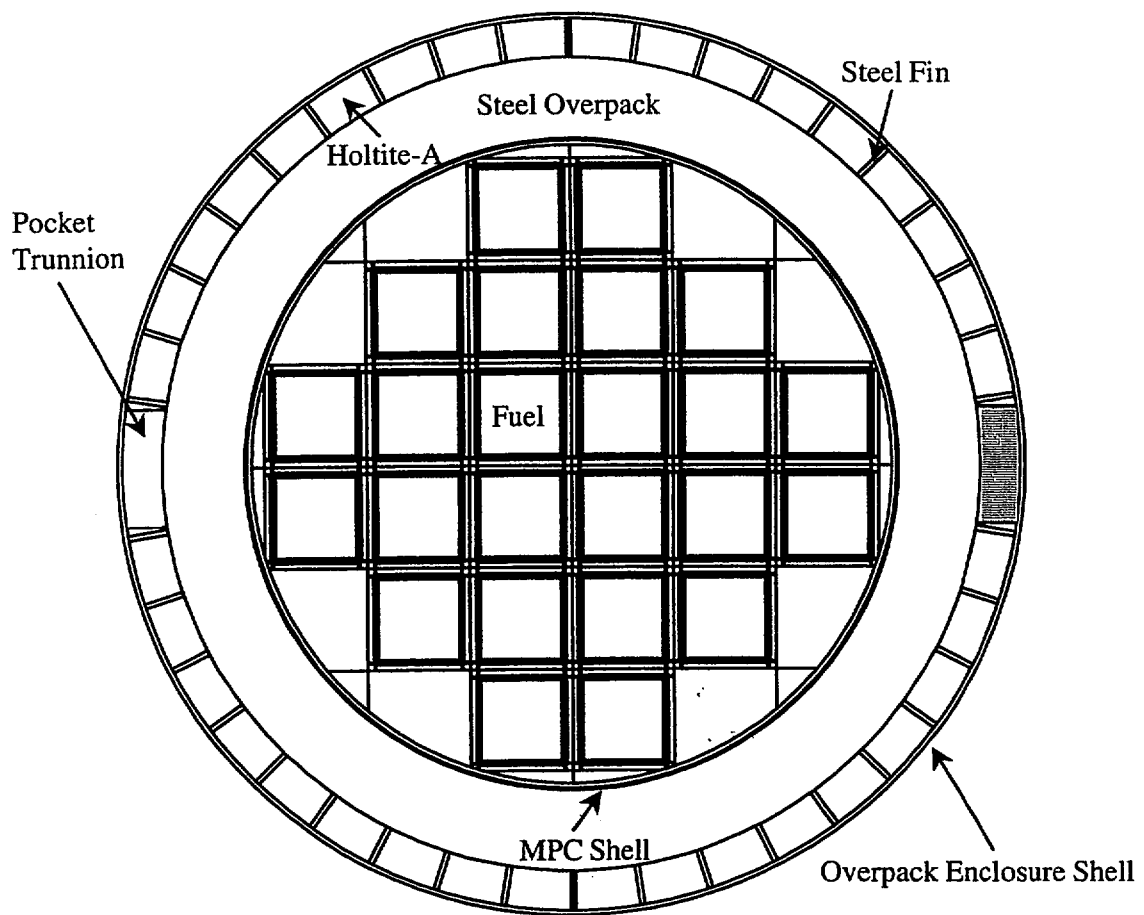


FIGURE 5.3.2; HI-STAR 100 OVERPACK WITH MPC-24 CROSS SECTIONAL VIEW AS MODELLED IN MCNP[†]

[†] This figure is drawn to scale using the MCNP plotter.

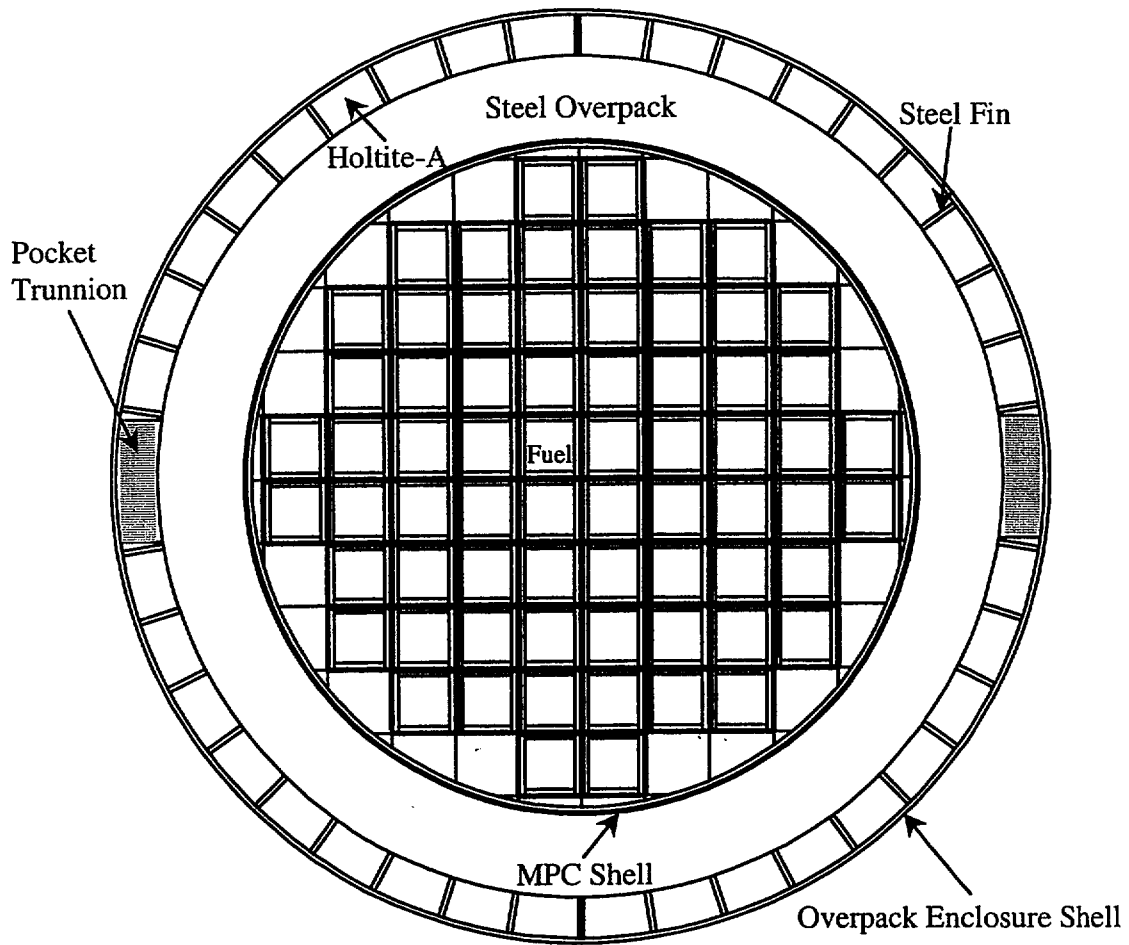


FIGURE 5.3.3; HI-STAR 100 OVERPACK WITH MPC-68 CROSS SECTIONAL VIEW AS MODELLED IN MCNP[†]

[†] This figure is drawn to scale using the MCNP plotter.

FIGURE 5.3.4

DELETED

**FIGURE WITHHELD AS SENSITIVE
UNCLASSIFIED INFORMATION**

FIGURE 5.3.5; CROSS SECTIONAL VIEW OF AN MPC-24 BASKET CELL AS MODELED
IN MCNP

**FIGURE WITHHELD AS SENSITIVE
UNCLASSIFIED INFORMATION**

FIGURE 5.3.6; CROSS SECTIONAL VIEW OF AN MPC-68 BASKET CELL AS MODELED
IN MCNP

**FIGURE WITHHELD AS SENSITIVE
UNCLASSIFIED INFORMATION**

FIGURE 5.3.6; CROSS SECTIONAL VIEW OF AN MPC-68 BASKET CELL AS MODELED
IN MCNP

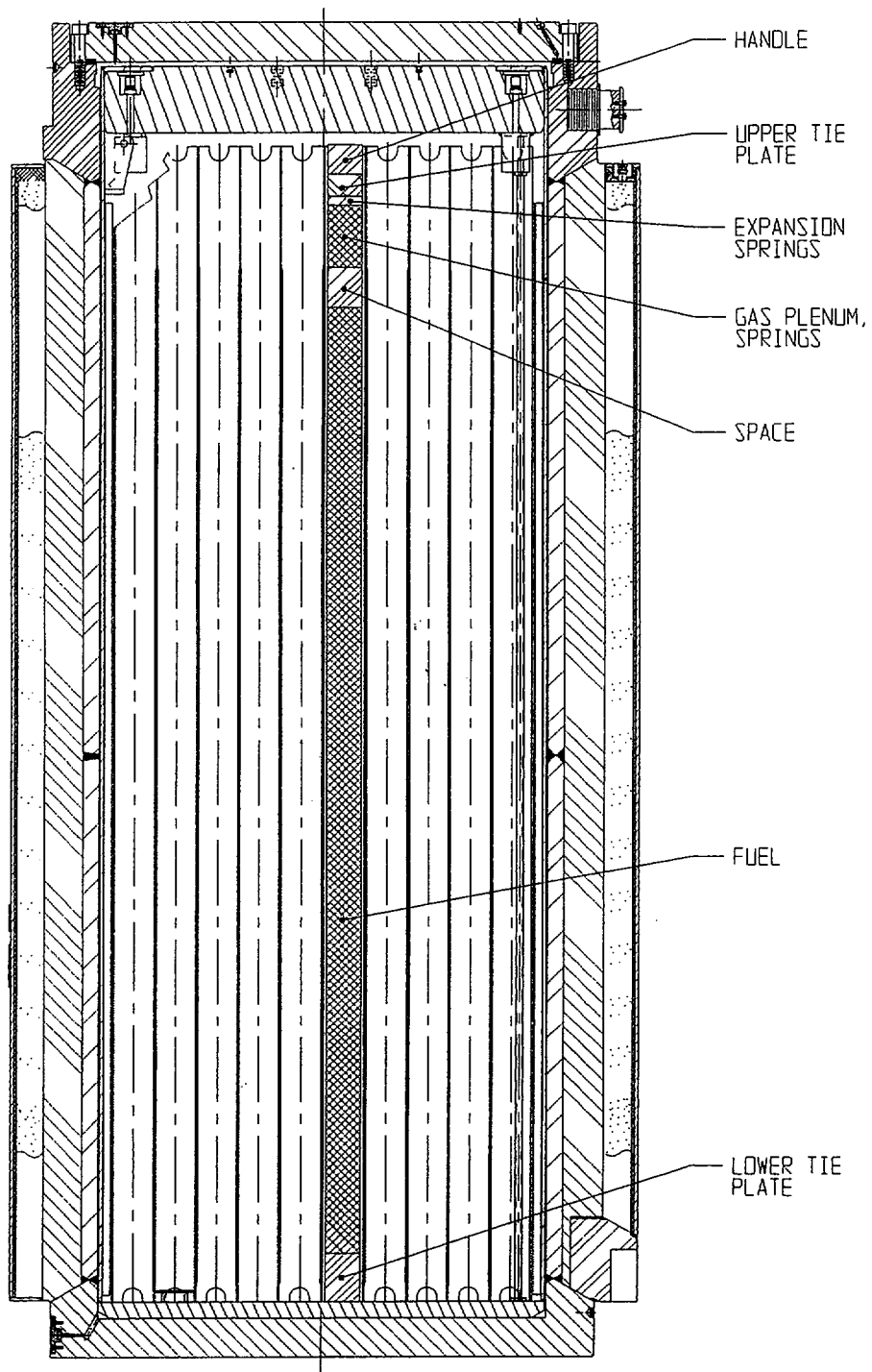


FIGURE 5.3.8; AXIAL LOCATION OF BWR DESIGN BASIS FUEL IN THE HI-STAR 100 SYSTEM

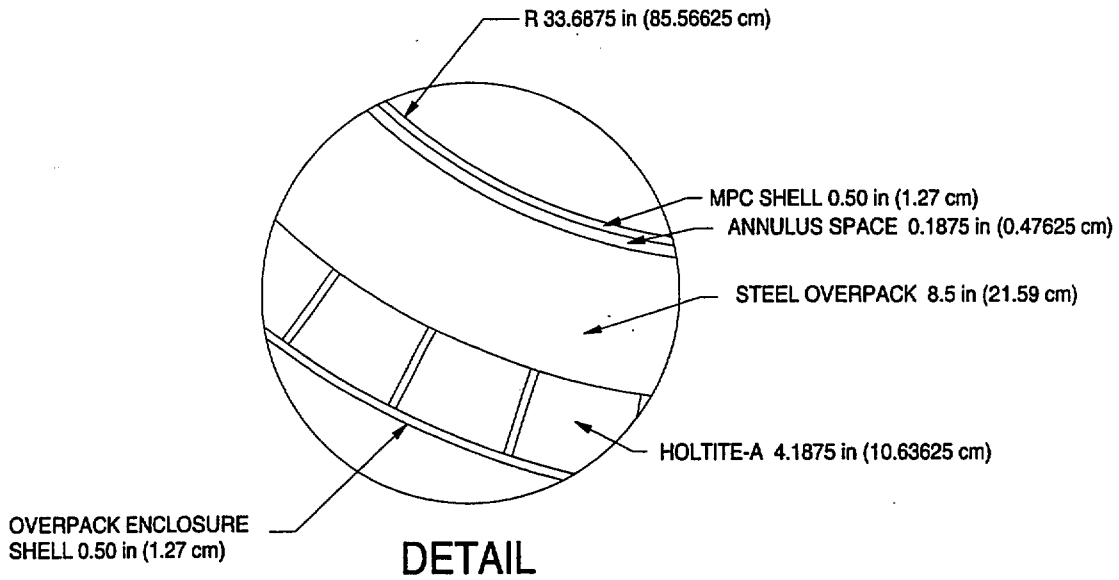
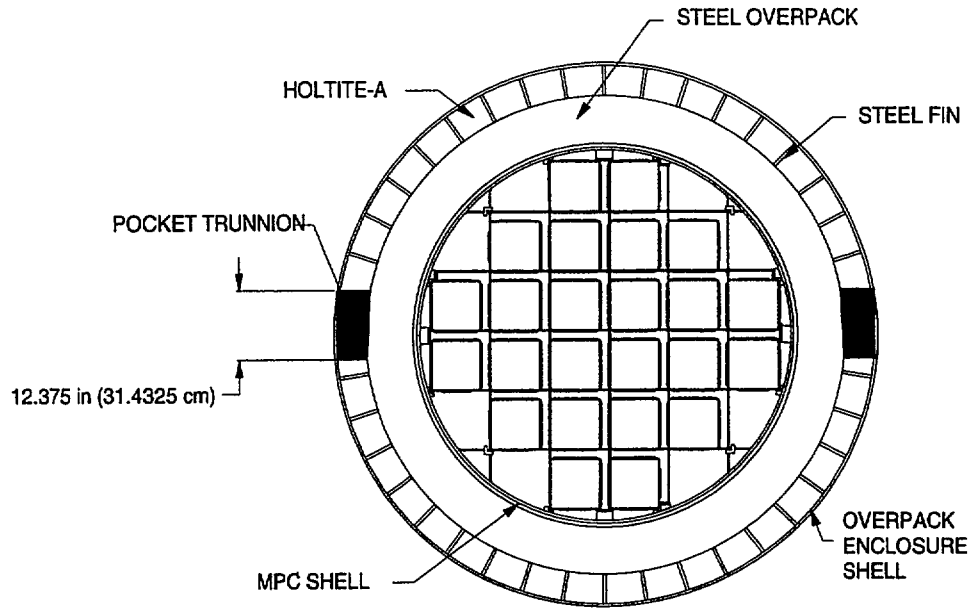


FIGURE 5.3.9; HI-STAR 100 OVERPACK WITH MPC-24 CROSS SECTIONAL VIEW SHOWING THE THICKNESS OF THE MPC SHELL AND OVERPACK AS MODELED IN MCNP

**FIGURE WITHHELD AS SENSITIVE
UNCLASSIFIED INFORMATION**

FIGURE 5.3.10; AXIAL VIEW OF IHI-STAR 100 OVERPACK AND MPC WITH AXIAL DIMENSIONS SHOWN AS MODELED IN MCNP

The MCNP-4A code[5.1.1] was used for all of the shielding analyses. MCNP is a continuous energy, three-dimensional, coupled neutron-photon-electron Monte Carlo transport code. Continuous energy cross-section data is represented with sufficient energy points to permit linear-linear interpolation between these points. The individual cross-section libraries used for each nuclide are those recommended by the MCNP manual. All of these data are based on ENDF/B-V data. MCNP has been extensively benchmarked against experimental data by the large user community. References [5.4.2], [5.4.3], and [5.4.4] are three examples of the benchmarking that has been performed.

The energy distribution of the source term, as described earlier, is used explicitly in the MCNP model. A different MCNP calculation is performed for each of the three source terms (neutron, decay gamma, and ^{60}Co). The axial distribution of the fuel source term is described in Table 2.1.8 and Figures 2.1.3 and 2.1.4. The PWR and BWR axial burnup distributions were obtained from References [5.4.5] and [5.4.6] respectively. These axial distributions were obtained from operating plants and are representative of PWR and BWR fuel with burnups greater than 30,000 MWD/MTU. The ^{60}Co source in the activated hardware was assumed to be uniformly distributed over the appropriate regions.

It has been shown that the neutron source strength varies as the burnup level raised by the power of 4.2. Since this relationship is non-linear and since the burnup in the axial center of a fuel assembly is greater than the average burnup, the neutron source strength in the axial center of the assembly is greater than the relative burnup times the average neutron source strength. In order to account for this effect, the neutron source strength in each of the 10 axial nodes listed in Table 2.1.8 was determined by multiplying the average source strength by the relative burnup level raised to the power of 4.2. The peak relative burnups listed in Table 2.1.8 for the PWR and BWR fuels are 1.105 and 1.195 respectively. Using the power of 4.2 relationship results in a 37.6% ($1.105^{4.2}/1.105$) and 76.8% ($1.195^{4.2}/1.195$) increase in the neutron source strength in the peak nodes for the PWR and BWR fuel respectively. The total neutron source strength increases by 15.6% for the PWR fuel assemblies and 36.9% for the BWR fuel assemblies.

MCNP was used to calculate dose at the various desired locations. MCNP calculates neutron or photon flux which can be converted into dose by the use of dose response functions. This is done internally in MCNP and the dose response functions are listed in the input file. The response functions used in these calculations are listed in Table 5.4.1 and were taken from ANSI/ANS 6.1.1, 1977 [5.4.1].

Tables 5.4.2 through 5.4.7 list the normal condition dose rates (from each of the three radiation sources) adjacent to the overpack for each of the burnup levels and cooling times evaluated for the MPC-24 and MPC-68. Tables 5.4.8 and 5.4.9 provide the total dose rate for each burnup level and cooling time for the MPC-24 and MPC-68, respectively. This information was used to determine the worst case burnup level and cooling time and corresponding maximum dose rates

reported in Section 5.1. A detailed discussion of the normal, off-normal, and accident condition dose rates was provided in Sections 5.1.1 and 5.1.2.

Since MCNP is a statistical code, there is an uncertainty associated with the calculated values. In MCNP the uncertainty is expressed as the relative error which is defined as the standard deviation of the mean divided by the mean. Therefore, the standard deviation is represented as a percentage of the mean. The relative error for the total dose rates presented in this chapter were typically less than 3% and the relative error for the individual dose components was typically less than 5%.

5.4.1 Streaming Through Radial Steel Fins and Pocket Trunnions

The HI-STAR 100 overpack utilizes 0.5 inch thick radial steel fins for structural support and cooling. The attenuation of neutrons through steel is substantially less than the attenuation of neutrons through the Holtite-A. Therefore, it is possible to have neutron streaming through the fins which could result in a localized dose peak. The reverse is true for photons which would result in a localized reduction in the photon dose. Analyses were performed to determine the magnitude of the dose peaks and depressions and the impact on localized dose as compared to average total dose. This effect was evaluated at the radial surface of the cask and a distance of one meter from the cask.

In addition to the fins, the pocket trunnions are essentially blocks of steel that are approximately 12 inches wide and 12 inches high. The effect of the pocket trunnion on neutron streaming and photon transmission will be more substantial than the effect of a single fin. Therefore, analyses were performed to quantify this effect. Figure 5.1.1 illustrates the location of the pocket trunnion and its axial position relative to the active fuel. This position will be important in the discussion that follows.

The effect of streaming through the pocket trunnion and the fins was analyzed using MCNP. The model used was an infinite height radial model which consisted of the MPC and the surrounding overpack. The active fuel region of the fuel assemblies was represented in the MPC basket when the neutron source was used and the lower steel regions of the fuel elements were presented in the MPC basket when the cobalt source was used. The pocket trunnion was represented in this infinite model as being axially adjacent to the active fuel. A calculation was not performed with the photon source. Any depression of the gamma dose due to the steel will be evident when using the cobalt source and this will conservatively bound the effects due to the photon source. This is because the average energy of the photons from ^{60}Co is higher than the average energy of decay gammas.

The MPC-24 and the MPC-68 were analyzed. Figure 5.4.1 shows a quarter of the HI-STAR 100 overpack with 91 azimuthal bins drawn. There is one bin per steel fin and 8 bins in each Holtite-A region. This azimuthal binning structure was used in an infinite height two-dimensional model of the MPC and overpack. The dose was calculated in each of these bins and then compared to

the average dose calculated over the surface to determine a peak-to-average ratio for the dose in that bin. The location of the pocket trunnion is shown in Figure 5.4.1. The pocket trunnion was modeled as solid steel. During storage, a shield plug shall be placed in the pocket trunnion recess, and during handling operations a steel rotation trunnion shall be placed in the pocket trunnion recess. To conservatively evaluate the peak-to-average ratio, the pocket trunnion is assumed to be solid steel. The peak-to-average ratio was calculated for the entire pocket trunnion which would correspond to the first seven azimuthal bins.

Table 5.4.10 provides the peak-to-average ratios that were calculated for the various dose components and locations. The peak-to-average ratios were essentially the same for all MPCs, therefore, only one set of values is shown. The values presented for the pocket trunnions are very conservative since the two-dimensional model represented the trunnion as infinite in height whereas the actual height is approximately 12 inches. In addition, the pocket trunnion was represented as being axially adjacent to the active fuel which is not completely accurate for the design basis fuel. The infinite two-dimensional model therefore does not represent any leakage out of the pocket trunnion in the axial direction which would reduce the peaking effect.

Table 5.4.11 presents the dose rates at Dose Point #2 (see Figure 5.1.1) and the adjusted dose rates at this point to account for the streaming effects. An additional dose point labeled 2a is listed in this table. This location is axially adjacent to the pocket trunnion and approximately 6 feet below Dose Point #2. Based on these results it can be concluded that the streaming effect is noticeable but is not of significant concern.

5.4.2 Damaged Fuel Post-Accident Shielding Evaluation

As discussed in Section 5.2.5.2, the analysis presented below, even though it is for damaged fuel, demonstrates the acceptability of storing intact Humboldt Bay 6x6 and intact Dresden 1 6x6 fuel assemblies.

For the damaged fuel and fuel debris accident condition, it is conservatively assumed that the damaged fuel cladding ruptures and all the fuel pellets fall and collect at the bottom of the damaged fuel container. The inner dimension of the damaged fuel container, specified in the Design Drawings of Section 1.5, and the design basis damaged fuel and fuel debris assembly dimensions in Table 5.2.2 are used to calculate the axial height of the rubble in the damaged fuel container assuming 50% compaction. Neglecting the fuel pellet to cladding inner diameter gap, the volume of cladding and fuel pellets available for deposit is calculated assuming the fuel rods are solid. Using the volume in conjunction with the damaged fuel container, the axial height of rubble is calculated to be 80 inches.

Dividing the total fuel gamma source for damaged fuel in Table 5.2.6 by the 80 inch rubble height provides a gamma source per inch of $9.68e+10$ photon/s. Dividing the total neutron source for damaged fuel in Table 5.2.14 by 80 inches provides a neutron source per inch of $2.75e+5$ neutron/s. These values are both bounded by the BWR design basis fuel gamma source

per inch and neutron source per inch values of 1.76×10^{12} photon/s and 5.60×10^5 neutron/s. These BWR design basis values were calculated by dividing the total source strengths in Tables 5.2.5 and 5.2.13 by the active fuel length of 144 inches. Therefore, the design basis damaged fuel assembly is bounded by the design basis intact BWR fuel assembly for accident conditions. No explicit analysis of the damaged fuel dose rates are provided as they are bounded by the intact fuel analysis.

5.4.3 Site Boundary Evaluation

Since NUREG-1536 [5.2.1] states that detailed calculations need not be presented, Chapter 12 assigns ultimate compliance responsibilities to the site licensee. Therefore, this subsection describes, by example, the general methodology for performing site boundary dose calculations. The site-specific fuel characteristics, burnup, cooling time, and the site layout and boundary characteristics would be factored into the evaluation performed by the licensee.

As an example of the methodology, the dose from a single MPC-24 cask and various arrays of MPC-24 casks at a distance greater than 100 meters was evaluated with MCNP. In the model the casks were placed on an infinite slab of concrete to account for earth-shine effects. The atmosphere was represented as dry air at a uniform density corresponding to 20 degrees C. The height of air modeled was 800 meters. This is more than sufficient to properly account for skyshine effects.

The annual dose, assuming 100% occupancy (8760 hours), at 300 meters from one cask is presented in Table 5.4.12 at the varying maximum burnup and minimum cooling times analyzed. This table indicates that the 40,000 MWD/MTU and 5-year cooling is the bounding case for these combinations.

This table also indicates that the dose due to neutrons is 21% of the total dose. This is an important observation because it implies that simplistic analytical methods such as point kernel techniques may not properly account for the neutron transmission and could lead to low estimates of the site boundary dose.

One of the features of MCNP is the ability to calculate the dose from particles that have passed through certain geometrical regions (referred to as surface or cell flagging). This technique was used to estimate the fraction of the dose at distance from particles, both neutron and gamma, passing through the upper flange region of the overpack. This region is referred to as 3 and 4 on Figure 5.1.1. It was found that, for one cask, approximately 9% of the dose comes from this upper flange region. This is a significant fraction of the total dose and one that is only accounted for using three-dimensional analysis, such as MCNP, which properly includes the effects of neutron and gamma skyshine.

Since the upper flange region is located at the top of the cask, it is reasonable to conclude that this contribution to total dose would be unaffected by placing the cask in an array configuration.

The annual dose, assuming 100% occupancy, at distance from an array of casks was calculated in three steps.

1. The annual dose from the radiation leaving the side of a single HI-STAR 100 overpack was calculated at the distance desired. The side of the HI-STAR 100 overpack is defined as any surface between the bottom of the bottom plate and the top of the closure plate including the upper flange area. Dose value = A.
2. The annual dose from the radiation leaving the top of a single HI-STAR 100 overpack was calculated at the distance desired. The top of the HI-STAR 100 overpack is defined as the top of the closure plate. Dose value = B.
3. The annual dose from the radiation leaving the side of a HI-STAR 100 overpack, when it is in the center of a 3x3 array of casks, was calculated at the distance desired. The casks in the array have a 12 foot pitch. Dose value = C.

The annual dose calculated in each of these three steps was averaged over a cylindrical surface at various distances from the source cask for ease of calculation. In step 3, the dose at the cylindrical surface included contributions from radiation that traveled between the surrounding casks and from radiation that traveled above the surrounding casks and scattered in air to reach the dose location. Therefore, the average dose values from step 3 include all possible paths for radiation to reach the dose location. The values from step 3 represent the dose from a cask in the second row of an array which is shielded by casks in the front row.

The doses calculated in the steps above are listed in Table 5.4.13 for 40,000 MWD/MTU and 5-year cooling. Using these values, the annual dose (at the center of the long side) from an arbitrary 2 by Z array of HI-STAR 100 overpacks can easily be calculated. The following formula describes the method.

Z = number of casks along long side

$$\text{Dose} = ZA + 2ZB + ZC$$

As an example, the dose from a 2x3 array at 250 meters is presented.

1. The annual dose from the side of a single cask: Dose A = 24.53
2. The annual dose from the top of a single cask: Dose B = 0.63
3. The annual dose from the side of a cask in the center of a 3x3 array: Dose C = 8.81

Using the formula shown above (Z=3) the total dose at 250 meters from a 2x3 array of filled HI-STAR 100 overpacks is 103.80 mrem/year, assuming 100% occupancy.

An important point to notice here is that the dose from the side of the back row of casks is approximately 25% of the total dose. This is a significant contribution and one that would probably not be accounted for properly by simpler methods of analysis.

The results for various arrays of filled HI-STAR 100 overpacks can be found in Section 5.1.1.

5.4.4 Mixed Oxide Fuel Evaluation

The source terms calculated for the Dresden 1 GE 6x6 MOX fuel assemblies can be compared to the design basis source terms for the GE 7x7 assemblies which demonstrates that the MOX fuel source terms are bounded by the design basis source terms and no additional shielding analysis is needed.

Since the active fuel length of the MOX fuel assemblies is shorter than the active fuel length of the design basis fuel, the source terms must be compared on a per inch basis. Dividing the total fuel gamma source for the MOX fuel in Table 5.2.16 by the 110 inch active fuel height provides a gamma source per inch of $6.97e+10$ photons/s. Dividing the total neutron source for the MOX fuel assemblies in Table 5.2.17 by 110 inches provides a neutron source strength per inch of $3.06e+5$ neutrons/s. These values are both bounded by the BWR design basis fuel gamma source per inch and neutron source per inch values of $1.76e+12$ photons/s and $5.60e+5$ neutrons/s. These BWR design basis values were calculated by dividing the total source strength in Tables 5.2.5 and 5.2.13 by the active fuel length of 144 inches. This comparison shows that the MOX fuel source terms are bound by the design basis source terms. Therefore, no explicit analysis of dose rates is provided for MOX fuel.

Since the MOX fuel assemblies are Dresden 1 6x6 assemblies, they can also be considered as damaged fuel or fuel debris. Using the same methodology as described in Section 5.4.2, the source term for the MOX fuel is calculated on a per inch basis assuming a post accident rubble height of 80 inches. The resulting gamma and neutron source strengths are $9.59e+10$ photons/s and $4.21e+5$ neutrons/s. These values are also bounded by the design basis fuel gamma source per inch and neutron source per inch. Therefore, no explicit analysis of dose rates is provided for MOX fuel in a post accident configuration.

5.4.5 Stainless Steel Clad Fuel Evaluation

Table 5.4.14 presents the dose rates at the center of the HI-STAR 100 overpack, adjacent and at one meter distance, for the stainless steel clad fuel. These dose rates, when compared to Tables 5.1.2, 5.1.3, 5.1.5, and 5.1.6, are very close to the dose rates from the design basis zircaloy clad fuel indicating that these fuel assemblies are acceptable for storage.

As described in Section 5.2.3, it would be incorrect to compare the total source strength from the stainless steel clad fuel assemblies to the source strength from the design basis zircaloy clad fuel assemblies since these assemblies do not have the same active fuel length and since there is a

significant gamma source from Cobalt-60 activation in the stainless steel. Therefore it is necessary to calculate the dose rates from the stainless steel clad fuel and compare them to the dose rates from the zircaloy clad fuel. In calculating the dose rates, the source term for the stainless steel fuel was calculated with an artificial active fuel length of 144 inches to permit a simple comparison of dose rates from stainless steel clad fuel and zircaloy clad fuel at the center of the HI-STAR 100 overpack. Since the true active fuel length is shorter than 144 inches and since the end fitting masses of the stainless steel clad fuel are assumed to be identical to the end fitting masses of the zircaloy clad fuel, the dose rates at the other locations on the overpack are bounded by the dose rates from the design basis zircaloy clad fuel, and therefore, no additional dose rates are presented.

5.4.6 BPRAs and TPDs

In order to verify that the BPRAs and TPDs do not affect the shielding analysis, the total dose rates were calculated for the HI-STAR 100 assuming all fuel assemblies in the MPC contained either BPRAs or TPDs. For this calculation, three separate burnups, slightly higher than the allowable burnups listed in Appendix B of the Certificate of Compliance were used with the corresponding cooling time. Tables 5.4.16 and 5.4.17 present the comparison of the total dose rates around the HI-STAR 100 overpack for PWR fuel with and without BPRAs or TPDs. The design basis dose rates are provided in these tables for easy comparison. A comparison of accident condition dose rates is only performed for assemblies with BPRAs since the TPDs, which are in the upper portion of the fuel assembly, will not have a noticeable impact on the accident dose rates at the centerline of the overpack. These tables illustrate that the dose rates for fuel assemblies containing BPRAs and TPDs are bounded by the design basis 40,000 MWD/MTU and 5 year cooling dose rates listed in Section 5.1.1 and Section 5.1.2. Therefore, the addition of BPRAs and TPDs to the MPC-24 is bounded by the shielding analysis presented in this chapter.

5.4.7 Dresden Unit 1 Antimony-Beryllium Neutron Sources

Dresden Unit 1 has antimony-beryllium neutron sources which are placed in the water rod location of their fuel assemblies. These sources are steel rods which contain a cylindrical antimony-beryllium source which is 77.25 inches in length. The steel rod is approximately 95 inches in length. Information obtained from Dresden Unit 1 characterizes these sources in the following manner: "About one-quarter pound of beryllium will be employed as a special neutron source material. The beryllium produces neutrons upon gamma irradiation. The gamma rays for the source at initial start-up will be provided by neutron-activated antimony (about 865 curies). The source strength is approximately $1E+8$ neutrons/second."

As stated above, beryllium produces neutrons through gamma irradiation and in this particular case antimony is used as the gamma source. The threshold gamma energy for producing neutrons from beryllium is 1.666 MeV. The outgoing neutron energy increases as the incident gamma energy increases. Sb-124, which decays by Beta decay with a half life of 60.2 days, produces a

gamma of energy 1.69 MeV which is just energetic enough to produce a neutron from beryllium. Approximately 54% of the Beta decays for Sb-124 produce gammas with energies greater than or equal to 1.69 MeV. Therefore, the neutron production rate in the neutron source can be specified as $5.8E-6$ neutrons per gamma ($1E+8/865/3.7e+10/0.54$) with energy greater than 1.666 MeV or $1.16E+5$ neutrons/curie ($1E+8/865$) of Sb-124.

With the short half life of 60.2 days all of the initial Sb-124 is decayed and any Sb-124 that was produced while the neutron source was in the reactor is also decayed since these neutron sources are assumed to have the same minimum cooling time as the Dresden 1 fuel assemblies (array classes 6x6A, 6x6B, 6x6C, and 8x8A) of 18 years. Therefore, there are only two possible gamma sources which can produce neutrons from this antimony-beryllium source. The first is the gammas from the decay of fission products in the fuel assemblies in the MPC. The second gamma source is from Sb-124 which is being produced in the MPC from neutron activation from neutrons from the decay of fission products.

MCNP calculations were performed to determine the gamma source as a result of decay gammas from fuel assemblies and Sb-124 activation. The calculations explicitly modeled the 6x6 fuel assembly described in Table 5.2.2. A single fuel rod was removed and replaced by a guide tube. In order to determine the amount of Sb-124 that is being activated from neutrons in the MPC it was necessary to estimate the amount of antimony in the neutron source. The O.D. of the source was assumed to be the I.D. of the steel rod encasing the source (0.345 in.). The length of the source is 77.25 inches. The beryllium is assumed to be annular in shape encompassing the antimony. Using the assumed O.D. of the beryllium and the mass and length, the I.D. of the beryllium was calculated to be 0.24 inches. The antimony is assumed to be a solid cylinder with an O.D. equal to the I.D. of the beryllium. These assumptions are conservative since the antimony and beryllium are probably encased in another material which would reduce the mass of antimony. A larger mass of antimony is conservative since the calculated activity of Sb-124 is directly proportional to the initial mass of antimony.

The number of gammas from fuel assemblies with energies greater than 1.666 MeV entering the 77.25 inch long neutron source was calculated to be $1.04E+8$ gammas/sec which would produce a neutron source of 603.2 neutrons/sec ($1.04E+8 * 5.8E-6$). The steady state amount of Sb-124 activated in the antimony was calculated to be 39.9 curies. This activity level would produce a neutron source of $4.63E+6$ neutrons/sec ($39.9 * 1.16E+5$) or $6.0E+4$ neutrons/sec/inch ($4.63E+6/77.25$). These calculations conservatively neglect the reduction in antimony and beryllium which would have occurred while the neutron sources were in the core and being irradiated at full reactor power.

Since this is a localized source (77.25 inches in length) it is appropriate to compare the neutron source per inch from the design basis Dresden Unit 1 fuel assembly, 6x6, containing an Sb-Be neutron source to the design basis fuel neutron source per inch. This comparison, presented in Table 5.4.15, demonstrates that a Dresden Unit 1 fuel assembly containing an Sb-Be neutron source is bounded by the design basis fuel.

As stated above, the Sb-Be source is encased in a steel rod. Therefore, the gamma source from the activation of the steel was considered assuming a burnup of 120,000 MWD/MTU which is the maximum burnup assuming the Sb-Be source was in the reactor for the entire 18 year life of Dresden Unit 1. The cooling time assumed was 18 years which is the minimum cooling time for Dresden Unit 1 fuel. The source from the steel was bounded by the design basis fuel assembly. In conclusion, storage of a Dresden Unit 1 Sb-Be neutron source in a Dresden Unit 1 fuel assembly is acceptable and bounded by the current analysis.

5.4.8 Thoria Rod Canister

Based on a comparison of the gamma spectra from Tables 5.2.32 and 5.2.6 for the thoria rod canister and design basis 6x6 fuel assembly, respectively, it is difficult to determine if the thoria rods will be bounded by the 6x6 fuel assemblies. However, it is obvious that the neutron spectra from the 6x6, Table 5.2.14, bounds the thoria rod neutron spectra, Table 5.2.33, with a significant margin. In order to demonstrate that the gamma spectrum from the single thoria rod canister is bounded by the gamma spectrum from the design basis 6x6 fuel assembly, the gamma dose rate on the outer radial surface of the overpack was estimated conservatively assuming an MPC full of thoria rod canisters. This gamma dose rate was compared to an estimate of the dose rate from an MPC full of design basis 6x6 fuel assemblies. The gamma dose rate from the 6x6 fuel was higher than the dose rate from an MPC full of thoria rod canisters. This in conjunction with the significant margin in neutron spectrum and the fact that there is only one thoria rod canister clearly demonstrates that the thoria rod canister is acceptable for storage in the MPC-68 or the MPC-68F.

Table 5.4.1

FLUX-TO-DOSE CONVERSION FACTORS
(FROM [5.4.1])

Gamma Energy (MeV)	(rem/hr)/ (photon/cm²-s)
0.01	3.96E-06
0.03	5.82E-07
0.05	2.90E-07
0.07	2.58E-07
0.1	2.83E-07
0.15	3.79E-07
0.2	5.01E-07
0.25	6.31E-07
0.3	7.59E-07
0.35	8.78E-07
0.4	9.85E-07
0.45	1.08E-06
0.5	1.17E-06
0.55	1.27E-06
0.6	1.36E-06
0.65	1.44E-06
0.7	1.52E-06
0.8	1.68E-06
1.0	1.98E-06
1.4	2.51E-06
1.8	2.99E-06
2.2	3.42E-06

Table 5.4.1 (continued)

FLUX-TO-DOSE CONVERSION FACTORS
(FROM [5.4.1])

Gamma Energy (MeV)	(rem/hr)/ (photon/cm²-s)
2.6	3.82E-06
2.8	4.01E-06
3.25	4.41E-06
3.75	4.83E-06
4.25	5.23E-06
4.75	5.60E-06
5.0	5.80E-06
5.25	6.01E-06
5.75	6.37E-06
6.25	6.74E-06
6.75	7.11E-06
7.5	7.66E-06
9.0	8.77E-06
11.0	1.03E-05
13.0	1.18E-05
15.0	1.33E-05

Table 5.4.1 (continued)

FLUX-TO-DOSE CONVERSION FACTORS
(FROM [5.4.1])

Neutron Energy (MeV)	Quality Factor	(rem/hr) [†] /(n/cm ² -s)
2.5E-8	2.0	3.67E-6
1.0E-7	2.0	3.67E-6
1.0E-6	2.0	4.46E-6
1.0E-5	2.0	4.54E-6
1.0E-4	2.0	4.18E-6
1.0E-3	2.0	3.76E-6
1.0E-2	2.5	3.56E-6
0.1	7.5	2.17E-5
0.5	11.0	9.26E-5
1.0	11.0	1.32E-4
2.5	9.0	1.25E-4
5.0	8.0	1.56E-4
7.0	7.0	1.47E-4
10.0	6.5	1.47E-4
14.0	7.5	2.08E-4
20.0	8.0	2.27E-4

[†] Includes the Quality Factor.

Table 5.4.2

**DOSE RATES FROM FUEL GAMMAS
DOSE LOCATION ADJACENT TO OVERPACK
NORMAL CONDITIONS
MPC-24 DESIGN BASIS ZIRCALOY CLAD FUEL AT VARYING BURNUP
AND COOLING TIMES[†]**

Dose Point^{††} Location	40,000 MWD/MTU 5-Year Cooling (mrem/hr)	47,500 MWD/MTU 8-Year Cooling (mrem/hr)
1	12.45	6.93
2	96.88	54.98
3	3.51	2.20
4	1.81	1.11
5	0.34	0.42
6 (dry MPC) ^{†††}	27.07	14.36
7 (no temp. shield)	100.36	50.68
7 (with temp. shield)	28.27	19.59

[†] Gammas generated by neutron capture are included with fuel gammas.

^{††} Refer to Figure 5.1.1.

^{†††} Overpack closure plate not present.

Table 5.4.3

DOSE RATES FROM ^{60}Co GAMMAS
DOSE LOCATION ADJACENT TO OVERPACK
NORMAL CONDITIONS
MPC-24 DESIGN BASIS ZIRCALOY CLAD FUEL AT VARYING BURNUP
AND COOLING TIMES

Dose Point [†] Location	40,000 MWD/MTU 5-Year Cooling (mrem/hr)	47,500 MWD/MTU 8-Year Cooling (mrem/hr)
1	231.52	176.39
2	0.03	0.02
3	81.12	61.80
4	35.86	27.32
5	0.69	0.53
6 (dry MPC) ^{††}	286.19	218.05
7 (no temp. shield)	1432.28	1091.26
7 (with temp. shield)	329.84	251.30

[†] Refer to Figure 5.1.1.

^{††} Overpack closure plate not present.

Table 5.4.4

DOSE RATES FROM NEUTRONS
DOSE LOCATION ADJACENT TO OVERPACK
NORMAL CONDITIONS
MPC-24 DESIGN BASIS ZIRCALOY CLAD FUEL AT VARYING BURNUP
AND COOLING TIMES

Dose Point[†] Location	40,000 MWD/MTU 5-Year Cooling (mrem/hr)	47,500 MWD/MTU 8-Year Cooling (mrem/hr)
1	82.27	132.74
2	22.12	35.69
3	70.28	113.40
4	39.47	63.68
5	56.70	91.48
6 (dry MPC) ^{††}	126.02	203.29
7 (no temp. shield)	397.30	641.02
7 (with temp. shield)	19.84	32.01

[†] Refer to Figure 5.1.1.

^{††} Overpack closure plate not included.

Table 5.4.5

DOSE RATES FROM FUEL GAMMAS
DOSE LOCATION ADJACENT TO OVERPACK
NORMAL CONDITIONS
MPC-68 DESIGN BASIS ZIRCALOY CLAD FUEL AT VARYING BURNUP
AND COOLING TIMES[†]

Dose Point^{††} Location	35,000 MWD/MTU 5-Year Cooling (mrem/hr)	45,000 MWD/MTU 9-Year Cooling (mrem/hr)
1	10.25	5.48
2	99.95	52.19
3	0.87	0.77
4	0.40	0.32
5	0.13	0.22
6 (dry MPC) ^{†††}	5.19	2.82
7 (no temp. shield)	64.46	31.28
7 (with temp. shield)	20.35	16.02

[†] Gammas generated by neutron capture are included with fuel gammas.

^{††} Refer to Figure 5.1.1.

^{†††} Overpack closure plate not included.

Table 5.4.6

DOSE RATES FROM ⁶⁰Co GAMMAS
DOSE LOCATION ADJACENT TO OVERPACK
NORMAL CONDITIONS
MPC-68 DESIGN BASIS ZIRCALOY CLAD FUEL AT VARYING BURNUP
AND COOLING TIMES

Dose Point [†] Location	35,000 MWD/MTU 5-Year Cooling (mrem/hr)	45,000 MWD/MTU 9-Year Cooling (mrem/hr)
1	297.85	208.39
2	0.03	0.01
3	117.57	82.25
4	44.36	31.04
5	0.43	0.30
6 (dry MPC) ^{††}	204.40	143.00
7 (no temp. shield)	1794.41	1255.40
7 (with temp. shield)	381.90	267.18

[†] Refer to Figure 5.1.1.

^{††} Overpack closure plate not included.

Table 5.4.7

DOSE RATES FROM NEUTRONS
DOSE LOCATION ADJACENT TO OVERPACK
NORMAL CONDITIONS
MPC-68 DESIGN BASIS ZIRCALOY CLAD FUEL AT VARYING BURNUP
AND COOLING TIMES

Dose Point [†] Location	35,000 MWD/MTU 5-Year Cooling (mrem/hr)	45,000 MWD/MTU 9-Year Cooling (mrem/hr)
1	65.65	133.60
2	19.40	43.11
3	29.48	60.00
4	17.04	34.68
5	24.74	50.34
6 (dry MPC) ^{††}	59.07	120.19
7 (no temp. shield)	327.79	667.01
7 (with temp. shield)	14.49	29.48

[†] Refer to Figure 5.1.1.

^{††} Overpack closure plate not included.

Table 5.4.8

TOTAL DOSE RATES
DOSE LOCATION ADJACENT TO OVERPACK
NORMAL CONDITIONS
MPC-24 DESIGN BASIS ZIRCALOY CLAD FUEL AT VARYING BURNUP
AND COOLING TIMES

Dose Point[†] Location	40,000 MWD/MTU 5-Year Cooling (mrem/hr)	47,500 MWD/MTU 8-Year Cooling (mrem/hr)
1	326.24	316.06
2	119.03	90.69
3	154.90	177.40
4	77.14	92.12
5	57.73	92.43
6 (dry MPC) ^{††}	439.28	435.70
7 (no temp. shield)	1929.94	1782.95
7 (with temp. shield)	377.94	302.90

[†] Refer to Figure 5.1.1.

^{††} Overpack closure plate not included.

Table 5.4.9

TOTAL DOSE RATES
DOSE LOCATION ADJACENT TO OVERPACK
NORMAL CONDITIONS
MPC-68 DESIGN BASIS ZIRCALOY CLAD FUEL AT VARYING BURNUP
AND COOLING TIMES

Dose Point [†] Location	35,000 MWD/MTU 5-Year Cooling (mrem/hr)	45,000 MWD/MTU 9-Year Cooling (mrem/hr)
1	373.75	347.46
2	119.39	95.32
3	147.92	143.02
4	61.81	66.04
5	25.30	50.86
6 (dry MPC) ^{††}	268.65	266.01
7 (no temp. shield)	2186.65	1953.70
7 (with temp. shield)	416.74	312.69

[†] Refer to Figure 5.1.1.

^{††} Overpack closure plate not included.

Table 5.4.10

**PEAK-TO-AVERAGE RATIOS FOR THE DOSE COMPONENTS
AT VARIOUS LOCATIONS**

Location	Fuel Gammas	Gammas from Neutrons	⁶⁰Co Gammas	Neutron
Pocket Trunnion (surface)	0.06	0.33	0.06	7.94
Steel Fin (surface)	0.74	0.95	0.74	2.16
Holtite-A (surface)	1.17	1.05	1.17	0.71
Pocket Trunnion (1 meter)	0.6	0.86	0.6	2.82
Steel Fin (1 meter)	1.0	1.0	1.0	1.05
Holtite-A (1 meter)	1.0	1.0	1.0	0.92

Table 5.4.11

DOSE RATES FOR NORMAL CONDITIONS SHOWING THE
EFFECT OF PEAKING
MPC-24 DESIGN BASIS ZIRCALOY CLAD FUEL
40,000 MWD/MTU 5-YEAR COOLING

Dose Point [†] Location	Fuel Gammas (mrem/hr)	Gammas from Neutrons (mrem/hr)	⁶⁰ Co Gammas (mrem/hr)	Neutrons (mrem/hr)	Total (mrem/hr)
SURFACE					
2	90.55	6.33	0.03	22.12	119.03
2 (fin)	67.01	6.01	0.02	47.78	120.82
2 (Holtite)	105.94	6.65	0.04	15.71	128.34
2a (Holtite) ^{††}	12.35	1.49	77.43	10.08	101.35
2a (pocket trunnion) ^{††}	0.63	0.47	3.97	112.75	117.82
ONE METER					
2	40.47	2.20	1.06	7.74	51.47
2 (fin)	40.47	2.20	1.06	8.13	51.86
2 (Holtite)	40.47	2.20	1.06	7.12	50.85
2a (Holtite) ^{††}	14.67	0.93	16.58	6.90	39.08
2a (pocket trunnion) ^{††}	8.80	0.80	9.95	21.14	40.69

[†] Refer to Figure 5.1.1.

^{††} Dose point #2a is axially located next to either the Holtite (neutron shield) or pocket trunnion and approximately 6 feet below Dose point #2.

Table 5.4.12

ANNUAL DOSE AT 300 METERS FROM A SINGLE CASK[†]

	40,000 MWD/MTU 5-Year Cooling (mrem/yr)	47,500 MWD/MTU 8-Year Cooling (mrem/yr)
Fuel gammas ^{††}	8.15	4.34
⁶⁰ Co Gammas	2.46	1.88
Neutrons	2.94	4.74
Total	13.55	10.96

[†] 100% occupancy (8760 hours) is assumed.

^{††} Gammas generated by neutron capture are included with fuel gammas.

Table 5.4.13

DOSE VALUES USED IN CALCULATING ANNUAL DOSE FROM
 VARIOUS ISFSI CONFIGURATIONS
 40,000 MWD/MTU AND 5-YEAR COOLING[†]

	A Side of Overpack (mrem/yr)	B Top of Overpack (mrem/yr)	C Side of Shielded Overpack (mrem/yr)
100 meters	337.58	7.40	110.31
150 meters	115.93	3.07	40.56
200 meters	51.52	1.35	17.54
250 meters	24.53	0.63	8.81
300 meters	13.28	0.27	4.15
350 meters	6.76	0.15	2.23
400 meters	3.28	0.09	1.16

[†] 100% occupancy (8760 hours) is assumed.

Table 5.4.14

DOSE RATES AT THE CENTERLINE OF THE OVERPACK FOR
DESIGN BASIS STAINLESS STEEL CLAD FUEL

Dose Point [†] Location	Fuel Gammas ^{††} (mrem/hr)	⁶⁰ Co Gammas (mrem/hr)	Neutrons (mrem/hr)	Totals (mrem/hr)
MPC-24 (30,000 MWD/MTU AND 9-YEAR COOLING)				
2 (Adjacent)	101.34	0.06	5.13	106.53
2 (One Meter)	43.64	0.40	2.16	46.20
MPC-24 (40,000 MWD/MTU AND 15-YEAR COOLING)				
2 (Adjacent)	64.26	0.01	16.06	80.33
2 (One Meter)	28.38	0.19	5.63	34.19
MPC-68 (22,500 MWD/MTU AND 10-YEAR COOLING)				
2 (Adjacent)	80.71	0.01	1.51	82.23
2 (One Meter)	34.70	0.30	0.58	35.59

[†] Refer to Figure 5.1.1.

^{††} Gammas generated by neutron capture are included with fuel gammas.

Table 5.4.15

COMPARISON OF NEUTRON SOURCE PER INCH PER SECOND FOR
DESIGN BASIS 7X7 FUEL AND DESIGN BASIS DRESDEN UNIT 1 FUEL

Assembly	Active fuel length (inch)	Neutrons per sec per inch	Neutrons per sec per inch with Sb-Be source	Reference for neutrons per sec per inch
7x7 design basis	144	5.60E+5	N/A	Table 5.2.13 - 35 GWD/MTU and 5 year cooling
6x6 design basis	110	2.0e+5	2.6E+5	Table 5.2.14
6x6 design basis MOX	110	3.06E+5	3.66E+5	Table 5.2.17

Table 5.4.16

**COMPARISON OF TOTAL DOSE RATES FOR DESIGN BASIS PWR FUEL
AND PWR FUEL WITH BPRAS
MPC-24 NORMAL AND ACCIDENT CONDITIONS**

Dose Point[†] Location	40 GWD/MTU 5 year cooling DESIGN BASIS (mrem/hr)	29 GWD/MTU 5 year cooling (mrem/hr)	39 GWD/MTU 10 year cooling (mrem/hr)	42.5 GWD/MTU 15 year cooling (mrem/hr)
BPRAs ?	NO	YES	YES	YES
SURFACE - NORMAL CONDITION				
1	326.24	244.72	195.95	143.2
2	119.03	99.66	69.57	61.70
3	154.90	136.39	136.84	120.32
4	77.14	64.13	67.66	60.70
5	57.73	25.15	48.25	50.53
6 (dry MPC) ^{††}	439.28	445.46	389.94	324.45
7 (no temp. shield)	1929.94	1557.87	1165.15	810.77
ONE METER - NORMAL CONDITION				
1	43.79	34.47	25.62	19.12
2	51.47	44.42	29.32	25.50
3	30.21	28.68	24.86	21.27
4	28.61	27.06	24.19	20.68
5	17.11	7.55	14.3	14.95
7 (no temp. shield)	889.68	717.64	501.61	329.5
SURFACE - ACCIDENT CONDITION				
2	1371.34	699.45	1074.98	1101.53
ONE METER - ACCIDENT CONDITION				
2	491.73	263.82	378.91	384.75

† Refer to Figure 5.1.1.

†† Overpack closure plate not present.

Table 5.4.17

COMPARISON OF TOTAL DOSE RATES FOR DESIGN BASIS PWR FUEL
AND PWR FUEL WITH TPDS
MPC-24 NORMAL CONDITIONS

Dose Point [†] Location	40 GWD/MTU 5 year cooling DESIGN BASIS (mrem/hr)	29 GWD/MTU 5 year cooling (mrem/hr)	39 GWD/MTU 10 year cooling (mrem/hr)	42.5 GWD/MTU 15 year cooling (mrem/hr)
TPDs ?	NO	YES	YES	YES
SURFACE - NORMAL CONDITION				
1	326.24	241.88	193.11	140.36
2	119.03	78.00	47.91	40.04
3	154.90	134.01	134.47	117.95
4	77.14	63.09	66.62	59.66
5	57.73	25.12	48.22	50.51
6 (dry MPC) ^{††}	439.28	439.39	383.86	318.38
7 (no temp. shield)	1929.94	1531.39	1138.67	784.28
ONE METER - NORMAL CONDITION				
1	43.79	32.23	23.39	16.88
2	51.47	34.70	19.61	15.78
3	30.21	27.55	23.74	20.15
4	28.61	26.11	23.25	19.73
5	17.11	7.54	14.29	14.94
7 (no temp. shield)	889.68	703.89	487.86	315.76

[†] Refer to Figure 5.1.1.

^{††} Overpack closure plate not present.

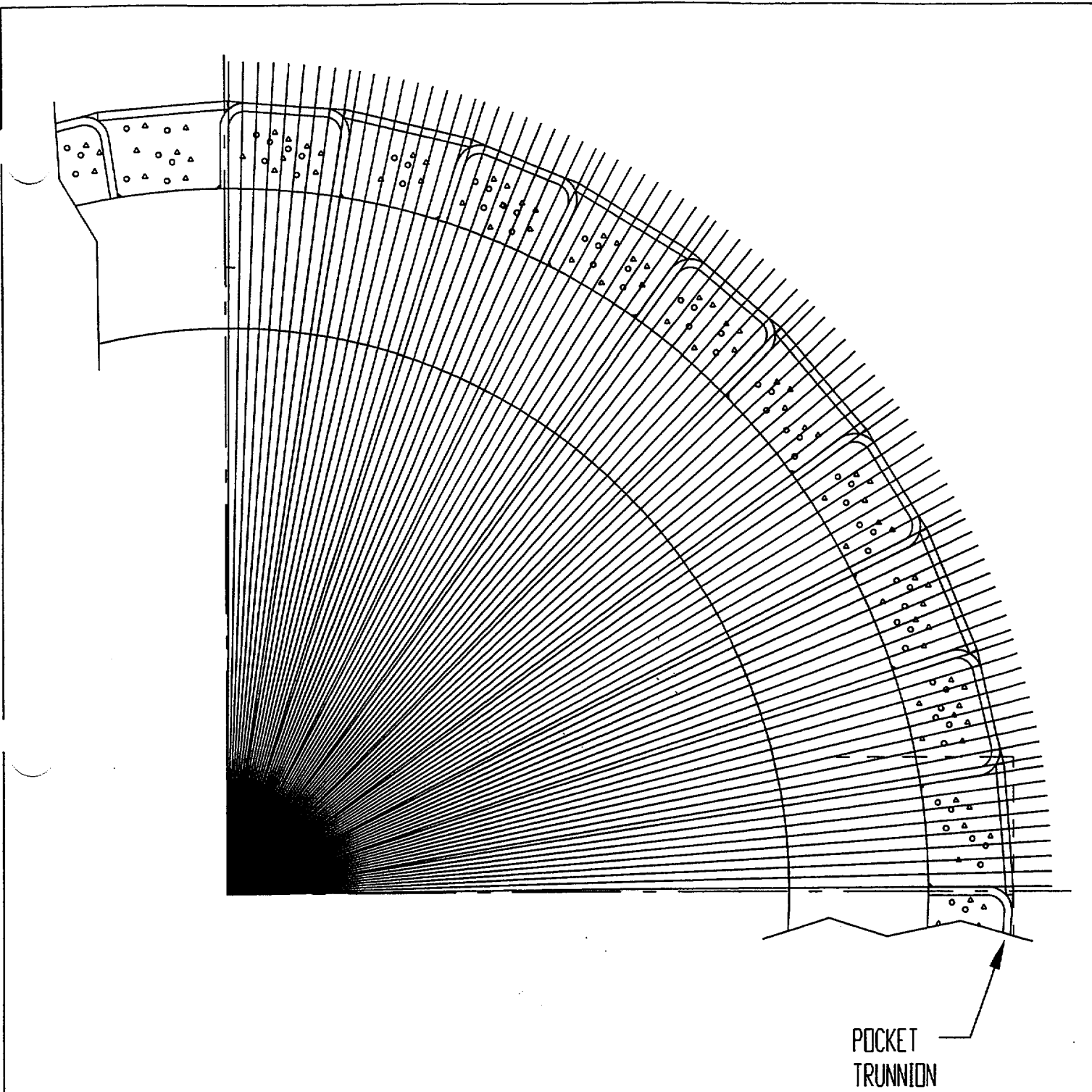


FIGURE 5.4.1; DEPICTION OF THE AZIMUTHAL SEGMENTATION OF THE OVERPACK USED IN ANALYZING NEUTRON AND PHOTON STREAMING

5.5 REGULATORY COMPLIANCE

Chapters 1 and 2 and this chapter of this FSAR describe in detail the shielding structures, systems, and components (SSCs) important to safety.

This chapter has evaluated these shielding SSCs important to safety and has assessed the impact on health and safety resulting from operation of an independent spent fuel storage installation (ISFSI) utilizing the HI-STAR 100 System.

It has been shown that the design of the shielding system of the HI-STAR 100 System is in compliance with 10CFR72 and that the applicable design and acceptance criteria including 10CFR20 have been satisfied. Thus, this shielding evaluation provides reasonable assurance that the HI-STAR 100 System will allow safe storage of spent fuel.

5.6 REFERENCES

- [5.1.1] J.F. Briesmeister, Ed., "MCNP - A General Monte Carlo N-Particle Transport Code, Version 4A." Los Alamos National Laboratory, LA-12625-M (1993).
- [5.1.2] O.W. Hermann, C.V. Parks, "SAS2H: A Coupled One-Dimensional Depletion and Shielding Analysis Module," NUREG/CR-0200, Revision 5, (ORNL/NUREG/CSD-2/V2/R5), Oak Ridge National Laboratory, September 1995.
- [5.1.3] O.W. Hermann, R.M. Westfall, "ORIGEN-S: SCALE System Module to Calculate Fuel Depletion, Actinide Transmutation, Fission Product Buildup and Decay, and Associated Radiation Source Terms," NUREG/CR-0200, Revision 5, (ORNL/NUREG/CSD-2/V2/R5), Oak Ridge National Laboratory, September 1995.
- [5.2.1] NUREG-1536, SRP for Dry Cask Storage Systems, USNRC, Washington, DC, January 1997.
- [5.2.2] A.G. Croff, M.A. Bjerke, G.W. Morrison, L.M. Petrie, "Revised Uranium-Plutonium Cycle PWR and BWR Models for the ORIGEN Computer Code," ORNL/TM-6051, Oak Ridge National Laboratory, September 1978.
- [5.2.3] A. Luksic, "Spent Fuel Assembly Hardware: Characterization and 10CFR 61 Classification for Waste Disposal," PNL-6906-vol. 1, Pacific Northwest Laboratory, June 1989.
- [5.2.4] J.W. Roddy et al., "Physical and Decay Characteristics of Commercial LWR Spent Fuel," ORNL/TM-9591/V1&R1, Oak Ridge National Laboratory, January 1996.
- [5.2.5] "Characteristics of Spent Fuel, High Level Waste, and Other Radioactive Wastes Which May Require Long-Term Isolation," DOE/RW-0184, U.S. Department of Energy, December 1987.
- [5.2.6] "Spent Nuclear Fuel Discharges from U.S. Reactors 1994," SR/CNEAF/96-01, Energy Information Administration, U.S. Department of Energy, February 1996.

- [5.2.7] "Characteristics Database System LWR Assemblies Database," DOE/RW-0184-R1, U.S. Department of Energy, July 1992.
- [5.4.1] "American National Standard Neutron and Gamma-Ray Flux-to-Dose Rate Factors", ANSI/ANS-6.1.1-1977.
- [5.4.2] D. J. Whalen, et al., "MCNP: Photon Benchmark Problems," LA-12196, Los Alamos National Laboratory, September 1991.
- [5.4.3] D. J. Whalen, et al., "MCNP: Neutron Benchmark Problems," LA-12212, Los Alamos National Laboratory, November 1991.
- [5.4.4] J. C. Wagner, et al., "MCNP: Criticality Safety Benchmark Problems," LA-12415, Los Alamos National Laboratory, October 1992.
- [5.4.5] S. E. Turner, "Uncertainty Analysis - Axial Burnup Distribution Effects," presented in "Proceedings of a Workshop on the Use of Burnup Credit in Spent Fuel Transport Casks," SAND-89-0018, Sandia National Laboratory, Oct. 1989.
- [5.4.6] Commonwealth Edison Company, Letter No. NFS-BND-95-083, Chicago, Illinois.

APPENDIX 5.A

SAMPLE INPUT FILE FOR SAS2H

(Total number of pages in this appendix : 3)

```

=SAS2H   PARM='halt08,skipshipdata'
bw 15x15 PWR assembly
' fuel temp 923
44groupndf5   LATTICECELL
UO2 1 0.95 923 92234 0.03026 92235 3.4 92236 0.01564
    92238 96.5541 END
'
' Zirc 4 composition
ARBM-ZIRC4 6.55 4 1 0 0 50000 1.7 26000 0.24 24000 0.13 40000 97.93
    2 1.0 595 END
'
' water with 652.5 ppm boron
H2O      3 DEN=0.7135 1 579 END
ARBM-BORMOD 0.7135 1 1 0 0 5000 100 3 652.5E-6 579 END
'
co-59 3 0 1-20 579 end
kr-83 1 0 1-20 923 end
kr-84 1 0 1-20 923 end
kr-85 1 0 1-20 923 end
kr-86 1 0 1-20 923 end
sr-90 1 0 1-20 923 end
y-89 1 0 1-20 923 end
zr-94 1 0 1-20 923 end
zr-95 1 0 1-20 923 end
mo-94 1 0 1-20 923 end
mo-95 1 0 1-20 923 end
nb-94 1 0 1-20 923 end
nb-95 1 0 1-20 923 end
tc-99 1 0 1-20 923 end
ru-106 1 0 1-20 923 end
rh-103 1 0 1-20 923 end
rh-105 1 0 1-20 923 end
sb-124 1 0 1-20 923 end
sn-126 1 0 1-20 923 end
xe-131 1 0 1-20 923 end
xe-132 1 0 1-20 923 end
xe-134 1 0 1-20 923 end
'
xe-135 1 0 1-09 923 end
'
xe-136 1 0 1-20 923 end
cs-133 1 0 1-20 923 end
cs-134 1 0 1-20 923 end
cs-135 1 0 1-20 923 end
cs-137 1 0 1-20 923 end
ba-136 1 0 1-20 923 end
la-139 1 0 1-20 923 end
ce-144 1 0 1-20 923 end
pr-143 1 0 1-20 923 end
nd-143 1 0 1-20 923 end
nd-144 1 0 1-20 923 end
nd-145 1 0 1-20 923 end
nd-146 1 0 1-20 923 end
nd-147 1 0 1-20 923 end
nd-148 1 0 1-20 923 end
nd-150 1 0 1-20 923 end
pm-147 1 0 1-20 923 end
pm-148 1 0 1-20 923 end
pm-149 1 0 1-20 923 end

```

```
sm-147 1 0 1-20 923 end
sm-148 1 0 1-20 923 end
sm-149 1 0 1-20 923 end
sm-150 1 0 1-20 923 end
sm-151 1 0 1-20 923 end
sm-152 1 0 1-20 923 end
eu-151 1 0 1-20 923 end
eu-153 1 0 1-20 923 end
eu-154 1 0 1-20 923 end
eu-155 1 0 1-20 923 end
gd-154 1 0 1-20 923 end
gd-155 1 0 1-20 923 end
gd-157 1 0 1-20 923 end
gd-158 1 0 1-20 923 end
gd-160 1 0 1-20 923 end
```

```
END COMP
```

```
-----
FUEL-PIN-CELL GEOMETRY:
```

```
SQUAREPITCH 1.44272 0.950468 1 3 1.08712 2 0.97028 0 END
```

```
-----
MTU in this model is 0.495485 based on fuel dimensions provided
```

```
1 power cycle will be used and a library will be generated every
2500 MWD/MTU power level is 40 MW/MTU
therefore 62.5 days per 2500 MWD/MTU
```

```
Below
```

```
BURN=62.5*NLIB/CYC
```

```
POWER=MTU*40
```

```
Number of libraries is 17 which is 42,500 MWD/MTU burnup (17*2500)
```

```
ASSEMBLY AND CYCLE PARAMETERS:
```

```
NPIN/ASSM=208 FUELNGTH=365.76 NCYCLES=1 NLIB/CYC=17
```

```
PRINTLEVEL=1
```

```
LIGHTEL=5 INPLEVEL=1 NUMHOLES=17
```

```
NUMINStr= 0 ORTUBE= 0.6731 SRTUBE=0.63246 END
```

```
POWER=19.81938 BURN=1062.5 END
```

```
O 66.54421
```

```
FE 0.24240868
```

```
ZR 98.78151 CR 0.1311304 SN 1.714782
```

```
END
```

```
=SAS2H PARM='restarts, halt17, skipshipdata'
```

```
bw 15x15 PWR assembly
```

```
END
```

APPENDIX 5.B

SAMPLE INPUT FILE FOR ORIGEN-S

(Total number of pages in this appendix : 6)

#ORIGENS

0\$\$ A4 33 A8 26 A11 71 E
1\$\$ 1 T
bw 15x15 FUEL -- FT33F001 -

' SUBCASE 1 LIBRARY POSITION 1

' lib pos grms photon group
3\$\$ 33 A3 1 0 A16 2 E T
35\$\$ 0 T
56\$\$ 5 5 A6 3 A10 0 A13 9 A15 3 A19 1 E
57** 0.0 A3 1.E-5 0.0625 E T
FUEL 3.4
BW 15x15 0.495485 MTU
58** 19.81938 19.81938 19.81938 19.81938 19.81938
60** 1.0000 3.0000 15.0000 30.0000 62.5
66\$\$ A1 2 A5 2 A9 2 E
73\$\$ 922350 922340 922360 922380 80000 500000
260000 240000 400000
74** 16846.48 149.9336 77.49379 478410.7 66544.21 1714.782
242.0868 131.1304 98781.51
75\$\$ 2 2 2 2 4 4 4 4 4 T

' SUBCASE 2 LIBRARY POSITION 2

' 3\$\$ 33 A3 2 0 A16 2 A33 0 E T
35\$\$ 0 T
56\$\$ 3 3 A6 3 A10 5 A15 3 A19 1 E
57** 0.0 A3 1.E-5 0.0625 E T
fuel
BW 15X15
58** 19.81938 19.81938 19.81938
60** 18.5 37.0 62.5
66\$\$ A1 2 A5 2 A9 2 E T

' SUBCASE 3 LIBRARY POSITION 3

' 3\$\$ 33 A3 3 0 A16 2 A33 0 E T
35\$\$ 0 T
56\$\$ 3 3 A6 3 A10 3 A15 3 A19 1 E
57** 0.0 A3 1.E-5 0.0625 E T
fuel
BW 15X15
58** 19.81938 19.81938 19.81938
60** 18.5 37.0 62.5
66\$\$ A1 2 A5 2 A9 2 E T

' SUBCASE 4 LIBRARY POSITION 4

' 3\$\$ 33 A3 4 0 A16 2 A33 0 E T
35\$\$ 0 T
56\$\$ 3 3 A6 3 A10 3 A15 3 A19 1 E
57** 0.0 A3 1.E-5 0.0625 E T
fuel
BW 15X15
58** 19.81938 19.81938 19.81938
60** 18.5 37.0 62.5
66\$\$ A1 2 A5 2 A9 2 E T

' SUBCASE 5 LIBRARY POSITION 5
,
3\$\$ 33 A3 5 0 A16 2 A33 0 E T
35\$\$ 0 T
56\$\$ 3 3 A6 3 A10 3 A15 3 A19 1 E
57** 0.0 A3 1.E-5 0.0625 E T
fuel
BW 15X15
58** 19.81938 19.81938 19.81938
60** 18.5 37.0 62.5
66\$\$ A1 2 A5 2 A9 2 E T
,

' SUBCASE 6 LIBRARY POSITION 6
,
3\$\$ 33 A3 6 0 A16 2 A33 0 E T
35\$\$ 0 T
56\$\$ 3 3 A6 3 A10 3 A15 3 A19 1 E
57** 0.0 A3 1.E-5 0.0625 E T
fuel
BW 15X15
58** 19.81938 19.81938 19.81938
60** 18.5 37.0 62.5
66\$\$ A1 2 A5 2 A9 2 E T
,

' SUBCASE 7 LIBRARY POSITION 7
,
3\$\$ 33 A3 7 0 A16 2 A33 0 E T
35\$\$ 0 T
56\$\$ 3 3 A6 3 A10 3 A15 3 A19 1 E
57** 0.0 A3 1.E-5 0.0625 E T
fuel
BW 15X15
58** 19.81938 19.81938 19.81938
60** 18.5 37.0 62.5
66\$\$ A1 2 A5 2 A9 2 E T
,

' SUBCASE 8 LIBRARY POSITION 8
,
3\$\$ 33 A3 8 0 A16 2 A33 0 E T
35\$\$ 0 T
56\$\$ 3 3 A6 3 A10 3 A15 3 A19 1 E
57** 0.0 A3 1.E-5 0.0625 E T
fuel
BW 15X15
58** 19.81938 19.81938 19.81938
60** 18.5 37.0 62.5
66\$\$ A1 2 A5 2 A9 2 E T
,

' SUBCASE 9 LIBRARY POSITION 9
,
3\$\$ 33 A3 9 0 A16 2 A33 0 E T
35\$\$ 0 T
56\$\$ 3 3 A6 3 A10 3 A15 3 A19 1 E
57** 0.0 A3 1.E-5 0.0625 E T
fuel
BW 15X15
58** 19.81938 19.81938 19.81938
60** 18.5 37.0 62.5
66\$\$ A1 2 A5 2 A9 2 E T

' SUBCASE 10 LIBRARY POSITION 10
,

3\$\$ 33 A3 10 0 A16 2 A33 0 E T
35\$\$ 0 T
56\$\$ 3 3 A6 3 A10 3 A15 3 A19 1 E
57** 0.0 A3 1.E-5 0.0625 E T
fuel
BW 15X15
58** 19.81938 19.81938 19.81938
60** 18.5 37.0 62.5
66\$\$ A1 2 A5 2 A9 2 E T

' SUBCASE 11 LIBRARY POSITION 11
,

3\$\$ 33 A3 11 0 A16 2 A33 0 E T
35\$\$ 0 T
56\$\$ 3 3 A6 3 A10 3 A15 3 A19 1 E
57** 0.0 A3 1.E-5 0.0625 E T
fuel
BW 15X15
58** 19.81938 19.81938 19.81938
60** 18.5 37.0 62.5
66\$\$ A1 2 A5 2 A9 2 E T

' SUBCASE 12 LIBRARY POSITION 12
,

3\$\$ 33 A3 12 0 A16 2 A33 0 E T
35\$\$ 0 T
56\$\$ 3 3 A6 3 A10 3 A15 3 A19 1 E
57** 0.0 A3 1.E-5 0.0625 E T
fuel
BW 15X15
58** 19.81938 19.81938 19.81938
60** 18.5 37.0 62.5
66\$\$ A1 2 A5 2 A9 2 E T

' SUBCASE 13 LIBRARY POSITION 13
,

3\$\$ 33 A3 13 0 A16 2 A33 0 E T
35\$\$ 0 T
56\$\$ 3 3 A6 3 A10 3 A15 3 A19 1 E
57** 0.0 A3 1.E-5 0.0625 E T
fuel
BW 15X15
58** 19.81938 19.81938 19.81938
60** 18.5 37.0 62.5
66\$\$ A1 2 A5 2 A9 2 E T

' SUBCASE 14 LIBRARY POSITION 14
,

3\$\$ 33 A3 14 0 A16 2 A33 0 E T
35\$\$ 0 T
56\$\$ 3 3 A6 3 A10 3 A15 3 A19 1 E
57** 0.0 A3 1.E-5 0.0625 E T
fuel
BW 15X15
58** 19.81938 19.81938 19.81938
60** 18.5 37.0 62.5

66\$\$ A1 2 A5 2 A9 2 E T

' SUBCASE 15 LIBRARY POSITION 15

3\$\$ 33 A3 15 0 A16 2 A33 0 E T

35\$\$ 0 T

56\$\$ 3 3 A6 3 A10 3 A15 3 A19 1 E

57** 0.0 A3 1.E-5 0.0625 E T

fuel

BW 15X15

58** 19.81938 19.81938 19.81938

60** 18.5 37.0 62.5

66\$\$ A1 2 A5 2 A9 2 E T

' SUBCASE 16 LIBRARY POSITION 16

3\$\$ 33 A3 16 A4 7 0 A16 2 A33 18 E T

35\$\$ 0 T

56\$\$ 3 3 A6 1 A10 3 A15 3 A19 1 E

57** 0.0 A3 1.E-5 0.0625 E T

fuel

BW 15X15

58** 19.81938 19.81938 19.81938

60** 18.5 37.0 62.5

66\$\$ A1 2 A5 2 A9 2 E T

' SUBCASE - decay

54\$\$ A8 1 E

56\$\$ 0 9 A6 1 A10 3 A14 3 A15 1 A19 1 E

57** 0.0 0 1.E-5 E T

fuel enrichment above

60** 0.5 0.75 1.0 4.0 8.0 12.0 24.0 48.0 96.0

61** F0.1

65\$\$

GRAM-ATOMS	GRAMS	CURIES	WATTS-ALL	WATTS-GAMMA	
3Z	0 1 0	0 0 0	1 0 0	3Z	6Z
3Z	0 1 0	0 0 0	1 0 0	3Z	6Z
3Z	0 1 0	0 0 0	1 0 0	3Z	6Z T

' SUBCASE - decay

54\$\$ A8 1 E

56\$\$ 0 9 A6 1 A10 9 A14 4 A15 1 A19 1 E

57** 4.0 0 1.E-5 E T

fuel enrichment above

60** 10.0 20.0 30.0 60.0 90.0 120.0 180.0 240.0 365.0

61** F0.1

65\$\$

GRAM-ATOMS	GRAMS	CURIES	WATTS-ALL	WATTS-GAMMA	
3Z	0 1 0	0 0 0	1 0 0	3Z	6Z
3Z	0 1 0	0 0 0	1 0 0	3Z	6Z
3Z	0 1 0	0 0 0	1 0 0	3Z	6Z T

' SUBCASE - decay

54\$\$ A8 0 E

56\$\$ 0 9 A6 1 A10 9 A14 5 A15 1 A19 1 E

57** 1.0 0 1.E-5 E T

fuel enrichment above
60** 1.5 3.0 4.0 5.0 6.0 7.0 8.0 9.0 10.0

61** F1.0e-5

65\$\$

'GRAM-ATOMS	GRAMS	CURIES	WATTS-ALL	WATTS-GAMMA
3Z	0 1 0	1 0 0	1 0 0	3Z 6Z
3Z	0 1 0	1 0 0	1 0 0	3Z 6Z
3Z	0 1 0	1 0 0	1 0 0	3Z 6Z

81\$\$ 2 0 26 1 E

82\$\$ 0 2 2 2 2 2 2 2 2

83** 1.1E+7 8.0E+6 6.0E+6 4.0E+6 3.0E+6 2.5E+6 2.0E+6 1.5E+6
1.0E+6 7.0E+5 4.5E+5 3.0E+5 1.5E+5 1.0E+5 7.0E+4 4.5E+4
3.0E+4 2.0E+4 1.0E+4

84** 20.0E+6 6.43E+6 3.0E+6 1.85E+6 1.40E+6 9.00E+5 4.00E+5 1.0E+5 T

SUBCASE - decay

54\$\$ A8 0 E

56\$\$ 0 10 A6 1 A10 9 A14 5 A15 1 A19 1 E

57** 10.0 0 1.E-5 E T

fuel enrichment above

60** 11.0 12.0 13.0 14.0 15.0 16.0 17.0 18.0 19.0 20.0

61** F1.0e-5

65\$\$

'GRAM-ATOMS	GRAMS	CURIES	WATTS-ALL	WATTS-GAMMA
3Z	0 1 0	1 0 0	1 0 0	3Z 6Z
3Z	0 1 0	1 0 0	1 0 0	3Z 6Z
3Z	0 1 0	1 0 0	1 0 0	3Z 6Z

81\$\$ 2 0 26 1 E

82\$\$ 2 2 2 2 2 2 2 2 2 2

83** 1.1E+7 8.0E+6 6.0E+6 4.0E+6 3.0E+6 2.5E+6 2.0E+6 1.5E+6
1.0E+6 7.0E+5 4.5E+5 3.0E+5 1.5E+5 1.0E+5 7.0E+4 4.5E+4
3.0E+4 2.0E+4 1.0E+4

84** 20.0E+6 6.43E+6 3.0E+6 1.85E+6 1.40E+6 9.00E+5 4.00E+5 1.0E+5 T

END

56\$\$ F0 T

END

APPENDIX 5.C

SAMPLE INPUT FILE FOR MCNP

(Total number of pages in this appendix : 35)


```

348 0      30 -31 23 -32 410 -435 u=-1
349 0      30 -31 33 -26 410 -435 u=-1
350 0      15 -30 23 -28 435 -460 u=-1
351 0      31 -20 23 -28 435 -460 u=-1
352 0      30 -31 33 -28 435 -460 u=-1
353 0      30 -31 23 -32 435 -460 u=-1
c      fuel element
354 5 -1.51304 30 -31 32 -33      -420 u=1
355 2 -3.979996 30 -31 32 -33 420 -425 u=-1
356 0      30 -31 32 -33 425 -430 u=-1
357 5 -0.270112 30 -31 32 -33 430 -440 u=-1
358 5 -0.689740 30 -31 32 -33 440 -445 u=-1
359 5 -1.393935 30 -31 32 -33 445 -450 u=-1
360 5 -0.261853 30 -31 32 -33 450 -670 u=-1
361 5 -0.261853 30 -31 32 -33 670 -455 u=-1
362 0      30 -31 32 -33 455 u=1
363 0      -30      460 u=1
364 0      31      460 u=1
365 0      30 -31 -32      460 u=1
366 0      30 -31 33      460 u=1
c
c      universe 2
c
c      egg crate
401 0      -30      -400 u=2
402 0      31      -400 u=2
403 0      30 -31 -32      -400 u=2
404 0      30 -31 33      -400 u=2
405 5 -7.92      28      400 -420 u=2
406 5 -7.92      -23 400 -420 u=2
407 5 -7.92      -15 23 -28 400 -420 u=2
408 5 -7.92 20      23 -28 400 -420 u=2
409 5 -7.92      28      420 -430 u=2
410 5 -7.92      -23 420 -430 u=2
411 5 -7.92      -15 23 -28 420 -430 u=2
412 5 -7.92 20      23 -28 420 -430 u=2
413 5 -7.92      28      430 -440 u=2
414 5 -7.92      -23 430 -440 u=2
415 5 -7.92      -15 23 -28 430 -440 u=2
416 5 -7.92 20      23 -28 430 -440 u=2
417 5 -7.92      28      440 -670 u=2
418 5 -7.92      -23 440 -670 u=2
419 5 -7.92      -15 23 -28 440 -670 u=2
420 5 -7.92 20      23 -28 440 -670 u=2
421 5 -7.92      28      670 -460 u=2
422 5 -7.92      -23 670 -460 u=2
423 5 -7.92      -15 23 -28 670 -460 u=2
424 5 -7.92 20      23 -28 670 -460 u=2
c      boral and inside of egg crate and outside of fuel
426 0      15 -30 23 -28 400 -460 u=-2
427 0      31 -20 23 -28 400 -460 u=-2
428 0      30 -31 33 -28 400 -460 u=-2
429 0      30 -31 23 -32 400 -460 u=-2
c      fuel element
454 5 -1.51304 30 -31 32 -33      -420 u=2
455 2 -3.979996 30 -31 32 -33 420 -425 u=-2
456 0      30 -31 32 -33 425 -430 u=-2
457 5 -0.270112 30 -31 32 -33 430 -440 u=-2
458 5 -0.689740 30 -31 32 -33 440 -445 u=-2
459 5 -1.393935 30 -31 32 -33 445 -450 u=-2
460 5 -0.261853 30 -31 32 -33 450 -670 u=-2
461 5 -0.261853 30 -31 32 -33 670 -455 u=-2
462 0      30 -31 32 -33 455 u=2
463 0      -30      460 u=2
464 0      31      460 u=2
465 0      30 -31 -32      460 u=2
466 0      30 -31 33      460 u=2
c
c      universe 3

```

```

c
c   egg crate
501 0          -30          -400 u=3
502 0          31          -400 u=3
503 0          30 -31 -32    -400 u=3
504 0          30 -31 33     -400 u=3
505 5 -7.92    28          400 -420 u=3
506 5 -7.92    -23 400 -420 u=3
507 5 -7.92    -15 23 -28 400 -420 u=3
508 5 -7.92    20 23 -28 400 -420 u=3
509 5 -7.92    28          420 -430 u=3
510 5 -7.92    -23 420 -430 u=3
511 5 -7.92    -15 23 -28 420 -430 u=3
512 5 -7.92    20 23 -28 420 -430 u=3
513 5 -7.92    28          430 -440 u=3
514 5 -7.92    -23 430 -440 u=3
515 5 -7.92    -15 23 -28 430 -440 u=3
516 5 -7.92    20 23 -28 430 -440 u=3
517 5 -7.92    28          440 -670 u=3
518 5 -7.92    -23 440 -670 u=3
519 5 -7.92    -15 23 -28 440 -670 u=3
520 5 -7.92    20 23 -28 440 -670 u=3
521 5 -7.92    28          670 -460 u=3
522 5 -7.92    -23 670 -460 u=3
523 5 -7.92    -15 23 -28 670 -460 u=3
524 5 -7.92    20 23 -28 670 -460 u=3
c   borol and inside of egg crate and outside of fuel
526 0          15 -30 23 -28 400 -410 u=-3
527 0          31 -20 23 -28 400 -410 u=-3
528 0          30 -31 33 -28 400 -410 u=-3
529 0          30 -31 23 -32 400 -410 u=-3
530 0          15 -18 26 -28 410 -435 u=-3
531 0          19 -20 26 -28 410 -435 u=-3
534 6 -2.644 18 -19 27 -28 410 -420 u=-3
535 5 -7.92 18 -19 26 -27 410 -420 u=-3
538 6 -2.644 18 -19 27 -28 420 -430 u=-3
539 5 -7.92 18 -19 26 -27 420 -430 u=-3
542 6 -2.644 18 -19 27 -28 430 -435 u=-3
543 5 -7.92 18 -19 26 -27 430 -435 u=-3
546 0          15 -30 23 -26 410 -435 u=-3
547 0          31 -20 23 -26 410 -435 u=-3
548 0          30 -31 23 -32 410 -435 u=-3
549 0          30 -31 33 -26 410 -435 u=-3
550 0          15 -30 23 -28 435 -460 u=-3
551 0          31 -20 23 -28 435 -460 u=-3
552 0          30 -31 33 -28 435 -460 u=-3
553 0          30 -31 23 -32 435 -460 u=-3
c   fuel element
554 5 -1.51304 30 -31 32 -33    -420 u=3
555 2 -3.979996 30 -31 32 -33 420 -425 u=-3
556 0          30 -31 32 -33 425 -430 u=-3
557 5 -0.270112 30 -31 32 -33 430 -440 u=-3
558 5 -0.689740 30 -31 32 -33 440 -445 u=-3
559 5 -1.393935 30 -31 32 -33 445 -450 u=-3
560 5 -0.261853 30 -31 32 -33 450 -670 u=-3
561 5 -0.261853 30 -31 32 -33 670 -455 u=-3
562 0          30 -31 32 -33 455 u=3
563 0          -30          460 u=3
564 0          31          460 u=3
565 0          30 -31 -32    460 u=3
566 0          30 -31 33     460 u=3
c
c   universe 4
c
c   egg crate
601 0          -30          -400 u=4
602 0          31          -400 u=4
603 0          30 -31 -32    -400 u=4
604 0          30 -31 33     -400 u=4

```

605	5	-7.92		28		400	-420	u=4	
606	5	-7.92			-23	400	-420	u=4	
607	5	-7.92	-15	23	-28	400	-420	u=4	
608	5	-7.92	20		23	-28	400	-420	u=4
609	5	-7.92			28		420	-430	u=4
610	5	-7.92				-23	420	-430	u=4
611	5	-7.92	-15	23	-28	420	-430	u=4	
612	5	-7.92	20		23	-28	420	-430	u=4
613	5	-7.92			28		430	-440	u=4
614	5	-7.92				-23	430	-440	u=4
615	5	-7.92	-15	23	-28	430	-440	u=4	
616	5	-7.92	20		23	-28	430	-440	u=4
617	5	-7.92			28		440	-670	u=4
618	5	-7.92				-23	440	-670	u=4
619	5	-7.92	-15	23	-28	440	-670	u=4	
620	5	-7.92	20		23	-28	440	-670	u=4
621	5	-7.92			28		670	-460	u=4
622	5	-7.92				-23	670	-460	u=4
623	5	-7.92	-15	23	-28	670	-460	u=4	
624	5	-7.92	20		23	-28	670	-460	u=4
c	boral and inside of egg crate and outside of fuel								
626	0		15	-30	23	-28	400	-410	u=-4
627	0		31	-20	23	-28	400	-410	u=-4
628	0		30	-31	33	-28	400	-410	u=-4
629	0		30	-31	23	-32	400	-410	u=-4
632	0		15	-17	23	-24	410	-435	u=-4
633	0		15	-17	25	-28	410	-435	u=-4
636	6	-2.644	15	-16	24	-25	410	-420	u=-4
637	5	-7.92	16	-17	24	-25	410	-420	u=-4
640	6	-2.644	15	-16	24	-25	420	-430	u=-4
641	5	-7.92	16	-17	24	-25	420	-430	u=-4
644	6	-2.644	15	-16	24	-25	430	-435	u=-4
645	5	-7.92	16	-17	24	-25	430	-435	u=-4
646	0		17	-30	23	-28	410	-435	u=-4
647	0		31	-20	23	-28	410	-435	u=-4
648	0		30	-31	23	-32	410	-435	u=-4
649	0		30	-31	33	-28	410	-435	u=-4
650	0		15	-30	23	-28	435	-460	u=-4
651	0		31	-20	23	-28	435	-460	u=-4
652	0		30	-31	33	-28	435	-460	u=-4
653	0		30	-31	23	-32	435	-460	u=-4
c	fuel element								
654	5	-1.51304	30	-31	32	-33		-420	u=4
655	2	-3.979996	30	-31	32	-33	420	-425	u=-4
656	0		30	-31	32	-33	425	-430	u=-4
657	5	-0.270112	30	-31	32	-33	430	-440	u=-4
658	5	-0.689740	30	-31	32	-33	440	-445	u=-4
659	5	-1.393935	30	-31	32	-33	445	-450	u=-4
660	5	-0.261853	30	-31	32	-33	450	-670	u=-4
661	5	-0.261853	30	-31	32	-33	670	-455	u=-4
662	0		30	-31	32	-33	455		u=4
663	0		-30					460	u=4
664	0		31					460	u=4
665	0		30	-31	-32			460	u=4
666	0		30	-31	33			460	u=4
c	universe 5								
c									
701	0							-400	u=5
702	5	-7.92	20	400				-420	u=5
703	5	-7.92	20	420				-430	u=5
704	5	-7.92	20	430				-440	u=5
705	5	-7.92	20	440				-670	u=5
706	5	-7.92	20	670				-460	u=5
707	0		-20	400				-460	u=5
708	0			460					u=5
c	universe 6								
c									


```

c
811 0 -28 400 -460 u=11
822 0 -400 u=11
823 5 -7.92 28 400 -420 u=11
824 5 -7.92 28 420 -430 u=11
825 5 -7.92 28 430 -440 u=11
826 5 -7.92 28 440 -670 u=11
827 5 -7.92 28 670 -460 u=11
828 0 460 u=11

```

```

c
c universe 12

```

```

c
830 0 -20 -28 400 -460 u=12
841 0 -400 u=12
842 5 -7.92 -20 28 400 -420 u=12
843 5 -7.92 20 400 -420 u=12
844 5 -7.92 -20 28 420 -430 u=12
845 5 -7.92 20 420 -430 u=12
846 5 -7.92 -20 28 430 -440 u=12
847 5 -7.92 20 430 -440 u=12
848 5 -7.92 -20 28 440 -670 u=12
849 5 -7.92 20 440 -670 u=12
850 5 -7.92 -20 28 670 -460 u=12
851 5 -7.92 20 670 -460 u=12
852 0 460 u=12

```

```

c
c universe 13

```

```

c
c 810 0 -420 u=13
c 811 0 420 -430 u=13
c 812 0 430 -440 u=13
c 813 0 440 -670 u=13
c 814 0 670 u=13

```

```

c
c storage locations

```

```

c
201 0 -301 -106 212 620 -675
202 0 -301 106 -107 212 620 -675
fill=6 (-8.2423 90.6653 0.0)
203 0 -301 107 -108 212 620 -675
fill=6 ( 8.2423 90.6653 0.0)
204 0 -301 108 212 620 -675
c
205 0 -301 -104 211 620 -675
206 0 -301 104 -105 211 620 -675
fill=6 (-41.2115 74.1807 0.0)
207 0 -301 105 -106 211 -212 620 -675
fill=7 (-24.7269 74.1807 0.0)
c
101 0 106 -107 211 -212 620 -675
fill=2 (-8.2423 74.1807 0.0)
102 0 107 -108 211 -212 620 -675
fill=4 ( 8.2423 74.1807 0.0)
c
208 0 -301 108 -109 211 -212 620 -675
fill=9 (24.7269 74.1807 0.0)
209 0 -301 109 -110 211 620 -675
fill=6 (41.2115 74.1807 0.0)
210 0 -301 110 211 620 -675
c
211 0 -301 -103 210 620 -675
212 0 -301 103 -104 210 -211 620 -675
fill=7 (-57.6961 57.6961 0.0)
c
103 0 104 -105 210 -211 620 -675
fill=2 (-41.2115 57.6961 0.0)
104 0 105 -106 210 -211 620 -675
fill=4 (-24.7269 57.6961 0.0)
105 0 106 -107 210 -211 620 -675
fill=1 (-8.2423 57.6961 0.0)

```

```

106 0 107 -108 210 -211 620 -675
      fill=1 ( 8.2423 57.6961 0.0)
107 0 108 -109 210 -211 620 -675
      fill=4 ( 24.7269 57.6961 0.0)
108 0 109 -110 210 -211 620 -675
      fill=4 ( 41.2115 57.6961 0.0)
c
213 0 -301 110 -111 210 -211 620 -675
      fill=9 ( 57.6961 57.6961 0.0)
214 0 -301 111 210 620 -675
c
215 0 -301 -103 209 -210 620 -675
      fill=5 (-74.1807 41.2115 0.0)
c
109 0 103 -104 209 -210 620 -675
      fill=2 (-57.6961 41.2115 0.0)
110 0 104 -105 209 -210 620 -675
      fill=1 (-41.2115 41.2115 0.0)
111 0 105 -106 209 -210 620 -675
      fill=1 (-24.7269 41.2115 0.0)
112 0 106 -107 209 -210 620 -675
      fill=1 (-8.2423 41.2115 0.0)
113 0 107 -108 209 -210 620 -675
      fill=1 ( 8.2423 41.2115 0.0)
114 0 108 -109 209 -210 620 -675
      fill=1 ( 24.7269 41.2115 0.0)
115 0 109 -110 209 -210 620 -675
      fill=1 ( 41.2115 41.2115 0.0)
116 0 110 -111 209 -210 620 -675
      fill=4 ( 57.6961 41.2115 0.0)
c
216 0 -301 111 209 -210 620 -675
      fill=8 (74.1807 41.2115 0.0)
c
217 0 -301 -102 208 620 -675
218 0 -301 102 -103 208 -209 620 -675
      fill=7 (-74.1807 24.7269 0.0)
c
117 0 103 -104 208 -209 620 -675
      fill=3 (-57.6961 24.7269 0.0)
118 0 104 -105 208 -209 620 -675
      fill=1 (-41.2115 24.7269 0.0)
119 0 105 -106 208 -209 620 -675
      fill=1 (-24.7269 24.7269 0.0)
120 0 106 -107 208 -209 620 -675
      fill=1 (-8.2423 24.7269 0.0)
121 0 107 -108 208 -209 620 -675
      fill=1 ( 8.2423 24.7269 0.0)
122 0 108 -109 208 -209 620 -675
      fill=1 ( 24.7269 24.7269 0.0)
123 0 109 -110 208 -209 620 -675
      fill=1 ( 41.2115 24.7269 0.0)
124 0 110 -111 208 -209 620 -675
      fill=1 ( 57.6961 24.7269 0.0)
c
219 0 -301 111 -112 208 -209 620 -675
      fill=9 (74.1807 24.7269 0.0)
220 0 -301 112 208 620 -675
c
221 0 -301 -102 207 -208 620 -675
      fill=5 (-90.6653 8.2423 0.0)
c
125 0 102 -103 207 -208 620 -675
      fill=2 (-74.1807 8.2423 0.0)
126 0 103 -104 207 -208 620 -675
      fill=1 (-57.6961 8.2423 0.0)
127 0 104 -105 207 -208 620 -675
      fill=1 (-41.2115 8.2423 0.0)
128 0 105 -106 207 -208 620 -675

```

```

    fill=1 (-24.7269 8.2423 0.0)
129 0 106 -107 207 -208 620 -675
    fill=1 (-8.2423 8.2423 0.0)
130 0 107 -108 207 -208 620 -675
    fill=1 ( 8.2423 8.2423 0.0)
131 0 108 -109 207 -208 620 -675
    fill=1 ( 24.7269 8.2423 0.0)
132 0 109 -110 207 -208 620 -675
    fill=1 ( 41.2115 8.2423 0.0)
133 0 110 -111 207 -208 620 -675
    fill=1 ( 57.6961 8.2423 0.0)
134 0 111 -112 207 -208 620 -675
    fill=4 ( 74.1807 8.2423 0.0)
c
222 0 -301 112 207 -208 620 -675
    fill=8 (90.6653 8.2423 0.0)
c
223 0 -301 -102 206 -207 620 -675
    fill=5 (-90.6653 -8.2423 0.0)
c
135 0 102 -103 206 -207 620 -675
    fill=3 (-74.1807 -8.2423 0.0)
136 0 103 -104 206 -207 620 -675
    fill=1 (-57.6961 -8.2423 0.0)
137 0 104 -105 206 -207 620 -675
    fill=1 (-41.2115 -8.2423 0.0)
138 0 105 -106 206 -207 620 -675
    fill=1 (-24.7269 -8.2423 0.0)
139 0 106 -107 206 -207 620 -675
    fill=1 (-8.2423 -8.2423 0.0)
140 0 107 -108 206 -207 620 -675
    fill=1 ( 8.2423 -8.2423 0.0)
141 0 108 -109 206 -207 620 -675
    fill=1 ( 24.7269 -8.2423 0.0)
142 0 109 -110 206 -207 620 -675
    fill=1 ( 41.2115 -8.2423 0.0)
143 0 110 -111 206 -207 620 -675
    fill=1 ( 57.6961 -8.2423 0.0)
144 0 111 -112 206 -207 620 -675
    fill=1 ( 74.1807 -8.2423 0.0)
c
224 0 -301 112 206 -207 620 -675
    fill=8 (90.6653 -8.2423 0.0)
c
225 0 -301 -102 -206 620 -675
226 0 -301 102 -103 205 -206 620 -675
    fill=12 (-74.1807 -24.7269 0.0)
c
145 0 103 -104 205 -206 620 -675
    fill=3 (-57.6961 -24.7269 0.0)
146 0 104 -105 205 -206 620 -675
    fill=1 (-41.2115 -24.7269 0.0)
147 0 105 -106 205 -206 620 -675
    fill=1 (-24.7269 -24.7269 0.0)
148 0 106 -107 205 -206 620 -675
    fill=1 (-8.2423 -24.7269 0.0)
149 0 107 -108 205 -206 620 -675
    fill=1 ( 8.2423 -24.7269 0.0)
150 0 108 -109 205 -206 620 -675
    fill=1 ( 24.7269 -24.7269 0.0)
151 0 109 -110 205 -206 620 -675
    fill=1 ( 41.2115 -24.7269 0.0)
152 0 110 -111 205 -206 620 -675
    fill=1 ( 57.6961 -24.7269 0.0)
c
227 0 -301 111 -112 205 -206 620 -675
    fill=10 (74.1807 -24.7269 0.0)
228 0 -301 112 -206 620 -675
c

```

```

229 0 -301 -103 204 -205 620 -675
    fill=5 (-74.1807 -41.2115 0.0)
c
153 0 103 -104 204 -205 620 -675
    fill=3 (-57.6961 -41.2115 0.0)
154 0 104 -105 204 -205 620 -675
    fill=1 (-41.2115 -41.2115 0.0)
155 0 105 -106 204 -205 620 -675
    fill=1 (-24.7269 -41.2115 0.0)
156 0 106 -107 204 -205 620 -675
    fill=1 (-8.2423 -41.2115 0.0)
157 0 107 -108 204 -205 620 -675
    fill=1 ( 8.2423 -41.2115 0.0)
158 0 108 -109 204 -205 620 -675
    fill=1 ( 24.7269 -41.2115 0.0)
159 0 109 -110 204 -205 620 -675
    fill=1 ( 41.2115 -41.2115 0.0)
160 0 110 -111 204 -205 620 -675
    fill=1 ( 57.6961 -41.2115 0.0)
c
230 0 -301 111 204 -205 620 -675
    fill=8 (74.1807 -41.2115 0.0)
c
231 0 -301 -103 -204 620 -675
232 0 -301 103 -104 203 -204 620 -675
    fill=12 (-57.6961 -57.6961 0.0)
c
161 0 104 -105 203 -204 620 -675
    fill=3 (-41.2115 -57.6961 0.0)
162 0 105 -106 203 -204 620 -675
    fill=1 (-24.7269 -57.6961 0.0)
163 0 106 -107 203 -204 620 -675
    fill=1 (-8.2423 -57.6961 0.0)
164 0 107 -108 203 -204 620 -675
    fill=1 ( 8.2423 -57.6961 0.0)
165 0 108 -109 203 -204 620 -675
    fill=1 ( 24.7269 -57.6961 0.0)
166 0 109 -110 203 -204 620 -675
    fill=1 ( 41.2115 -57.6961 0.0)
c
233 0 -301 110 -111 203 -204 620 -675
    fill=10 ( 57.6961 -57.6961 0.0)
234 0 -301 111 -204 620 -675
c
235 0 -301 -104 -203 620 -675
236 0 -301 104 -105 -203 620 -675
    fill=11 (-41.2115 -74.1807 0.0)
237 0 -301 105 -106 202 -203 620 -675
    fill=12 (-24.7269 -74.1807 0.0)
c
167 0 106 -107 202 -203 620 -675
    fill=3 (-8.2423 -74.1807 0.0)
168 0 107 -108 202 -203 620 -675
    fill=1 ( 8.2423 -74.1807 0.0)
c
238 0 -301 108 -109 202 -203 620 -675
    fill=10 (24.7269 -74.1807 0.0)
239 0 -301 109 -110 -203 620 -675
    fill=11 (41.2115 -74.1807 0.0)
240 0 -301 110 -203 620 -675
c
241 0 -301 -106 -202 620 -675
242 0 -301 106 -107 -202 620 -675
    fill=11 (-8.2423 -90.6653 0.0)
243 0 -301 107 -108 -202 620 -675
    fill=11 ( 8.2423 -90.6653 0.0)
244 0 -301 108 -202 620 -675
c
1821 5 -7.92 301 -302 610 -615 $ MPC shell

```

1822	0		302	-501	610	-615	\$	Air gap
1823	5	-7.92	301	-302	615	-630	\$	MPC shell
1824	0		302	-501	615	-630	\$	Air gap
1825	5	-7.92	301	-302	630	-420	\$	MPC shell
1826	0		302	-501	630	-420	\$	Air gap
1827	5	-7.92	301	-302	420	-430	\$	MPC shell
1828	0		302	-501	420	-430	\$	Air gap
1829	5	-7.92	301	-302	430	-440	\$	MPC shell
1830	0		302	-501	430	-440	\$	Air gap
1831	5	-7.92	301	-302	440	-670	\$	MPC shell
1832	0		302	-501	440	-670	\$	Air gap
1833	5	-7.92	301	-302	670	-675	\$	MPC shell
1834	0		302	-501	670	-675	\$	Air gap
1835	5	-7.92	301	-302	675	-651	\$	MPC shell
1836	0		302	-501	675	-651	\$	Air gap
1837	5	-7.92	301	-302	651	-652	\$	MPC shell
1838	0		302	-501	651	-652	\$	Air gap
1839	5	-7.92	301	-302	652	-653	\$	MPC shell
1840	0		302	-501	652	-653	\$	Air gap
1841	5	-7.92	301	-302	653	-654	\$	MPC shell
1842	0		302	-501	653	-654	\$	Air gap
1843	5	-7.92	301	-302	654	-655	\$	MPC shell
1844	0		302	-501	654	-655	\$	Air gap
1845	5	-7.92	301	-302	655	-656	\$	MPC shell
1846	0		302	-501	655	-656	\$	Air gap
1847	5	-7.92	301	-302	656	-657	\$	MPC shell
1848	0		302	-501	656	-657	\$	Air gap
1849	5	-7.92	301	-302	657	-680	\$	MPC shell
1850	0		301	-302	680	-685	\$	Air gap
1851	0		302	-501	657	-685	\$	Air gap
c								
1854	5	-7.92		-301	610	-615	\$	MPC baseplate
1855	5	-7.92		-301	615	-620	\$	MPC baseplate
1860	5	-7.92		-301	675	-651	\$	MPC lid (both)
1861	5	-7.92		-301	651	-652	\$	MPC lid (both)
1862	5	-7.92		-301	652	-653	\$	MPC lid (both)
1863	5	-7.92		-301	653	-654	\$	MPC lid (both)
1864	5	-7.92		-301	654	-655	\$	MPC lid (both)
1865	5	-7.92		-301	655	-656	\$	MPC lid (both)
1866	5	-7.92		-301	656	-657	\$	MPC lid (both)
1867	5	-7.92		-301	657	-680	\$	MPC lid (both)
1868	0			-301	680	-685	\$	Air gap
c								
				OVERPACK	\\	\\	\\	\\
c								
1001	8	-7.82	501	-508	630	-420	\$	steel shell
1002	8	-7.82	501	-508	420	-430	\$	steel shell
1003	8	-7.82	501	-508	430	-440	\$	steel shell
1004	8	-7.82	501	-508	440	-670	\$	steel shell
1005	0			508	-512	630	-420	fill=20
1006	0			508	-512	420	-430	fill=20
1007	0			508	-512	430	-440	fill=20
1008	0			508	-512	440	-670	fill=20
1009	8	-7.82	512	-513	630	-420	\$	outer steel shell
1010	8	-7.82	512	-513	420	-430	\$	outer steel shell
1011	8	-7.82	512	-513	430	-440	\$	outer steel shell
1012	8	-7.82	512	-513	440	-670	\$	outer steel shell
c				512	-513	640	-670	\$ outer steel shell
c				512	-513	630	-640	1103 -1102 \$ air in pocket trun.
c				512	-513	630	-640	2103 -2102 \$ air in pocket trun.
c				512	-513	630	-640	1102 2102 \$ outer steel shell
c				512	-513	630	-640	1102 -2103 \$ outer steel shell
c				512	-513	630	-640	-1103 -2103 \$ outer steel shell
c				512	-513	630	-640	-1103 2102 \$ outer steel shell
c								
				steel spines and holtite				
10101	8	-7.82	2000	-2002	645	-660	1000	u=20 \$ steel spine
10102	7	-1.61	2002	-2011	645	-660	2000	u=20 \$ holtite
10103	8	-7.82	2011	-2012	645	-660	2000	u=20 \$ steel spine
10104	7	-1.61	2012	-2021	645	-660	2000	u=20 \$ holtite

10105	8	-7.82	2021	-2022	645	-660	2000	u=20	\$	steel spine
10106	7	-1.61	2022	-2031	645	-660	2000	u=20	\$	holtite
10107	8	-7.82	2031	-2032	645	-660	2000	u=20	\$	steel spine
10108	7	-1.61	2032	-2041	645	-660	2000	u=20	\$	holtite
10109	8	-7.82	2041	-2042	645	-660	2000	u=20	\$	steel spine
10110	7	-1.61	2042	-2051	645	-660	2000	u=20	\$	holtite
10111	8	-7.82	2051	-2052	645	-660	2000	u=20	\$	steel spine
10112	7	-1.61	2052	-2061	645	-660	2000	u=20	\$	holtite
10113	8	-7.82	2061	-2062	645	-660	2000	u=20	\$	steel spine
10114	7	-1.61	2062	-2071	645	-660	2000	u=20	\$	holtite
10115	8	-7.82	2071	-2072	645	-660	2000	u=20	\$	steel spine
10116	7	-1.61	2072	-2081	645	-660	2000	u=20	\$	holtite
10117	8	-7.82	2081	-2082	645	-660	2000	u=20	\$	steel spine
10118	7	-1.61	2082	-2091	645	-660	2000	u=20	\$	holtite
10119	8	-7.82	2091	-2092	645	-660	2000	u=20	\$	steel spine
10120	7	-1.61	2092	1002	645	-660	2000	u=20	\$	holtite
10121	8	-7.82	1000	-1002	645	-660	2000	u=20	\$	steel spine
c										
10122	8	-7.82	1001	-1000	645	-660	2000	u=20	\$	steel spine
10123	7	-1.61	1012	-1001	645	-660	2000	u=20	\$	holtite
10124	8	-7.82	1011	-1012	645	-660	2000	u=20	\$	steel spine
10125	7	-1.61	1022	-1011	645	-660	2000	u=20	\$	holtite
10126	8	-7.82	1021	-1022	645	-660	2000	u=20	\$	steel spine
10127	7	-1.61	1032	-1021	645	-660	2000	u=20	\$	holtite
10128	8	-7.82	1031	-1032	645	-660	2000	u=20	\$	steel spine
10129	7	-1.61	1042	-1031	645	-660	2000	u=20	\$	holtite
10130	8	-7.82	1041	-1042	645	-660	2000	u=20	\$	steel spine
10131	7	-1.61	1052	-1041	645	-660	2000	u=20	\$	holtite
10132	8	-7.82	1051	-1052	645	-660	2000	u=20	\$	steel spine
10133	7	-1.61	1062	-1051	645	-660	2000	u=20	\$	holtite
10134	8	-7.82	1061	-1062	645	-660	2000	u=20	\$	steel spine
10135	7	-1.61	1072	-1061	645	-660	2000	u=20	\$	holtite
10136	8	-7.82	1071	-1072	645	-660	2000	u=20	\$	steel spine
10137	7	-1.61	1082	-1071	645	-660	2000	u=20	\$	holtite
10138	8	-7.82	1081	-1082	645	-660	2000	u=20	\$	steel spine
10139	7	-1.61	1092	-1081	645	-660	2000	u=20	\$	holtite
10140	8	-7.82	1091	-1092	645	-660	2000	u=20	\$	steel spine
10141	7	-1.61	2002	-1091	645	-660	2000	u=20	\$	holtite
10142	8	-7.82	2000	-2002	645	-660	-1000	u=20	\$	steel spine
c										
10143	8	-7.82	2001	-2000	645	-660	-1000	u=20	\$	steel spine
10144	7	-1.61	2012	-2001	645	-660	-2000	u=20	\$	holtite
10145	8	-7.82	2011	-2012	645	-660	-2000	u=20	\$	steel spine
10146	7	-1.61	2022	-2011	645	-660	-2000	u=20	\$	holtite
10147	8	-7.82	2021	-2022	645	-660	-2000	u=20	\$	steel spine
10148	7	-1.61	2032	-2021	645	-660	-2000	u=20	\$	holtite
10149	8	-7.82	2031	-2032	645	-660	-2000	u=20	\$	steel spine
10150	7	-1.61	2042	-2031	645	-660	-2000	u=20	\$	holtite
10151	8	-7.82	2041	-2042	645	-660	-2000	u=20	\$	steel spine
10152	7	-1.61	2052	-2041	645	-660	-2000	u=20	\$	holtite
10153	8	-7.82	2051	-2052	645	-660	-2000	u=20	\$	steel spine
10154	7	-1.61	2062	-2051	645	-660	-2000	u=20	\$	holtite
10155	8	-7.82	2061	-2062	645	-660	-2000	u=20	\$	steel spine
10156	7	-1.61	2072	-2061	645	-660	-2000	u=20	\$	holtite
10157	8	-7.82	2071	-2072	645	-660	-2000	u=20	\$	steel spine
10158	7	-1.61	2082	-2071	645	-660	-2000	u=20	\$	holtite
10159	8	-7.82	2081	-2082	645	-660	-2000	u=20	\$	steel spine
10160	7	-1.61	2092	-2081	645	-660	-2000	u=20	\$	holtite
10161	8	-7.82	2091	-2092	645	-660	-2000	u=20	\$	steel spine
10162	7	-1.61	-1001	-2091	645	-660	-2000	u=20	\$	holtite
10163	8	-7.82	1001	-1000	645	-660	-2000	u=20	\$	steel spine
c										
10164	8	-7.82	1000	-1002	645	-660	-2000	u=20	\$	steel spine
10165	7	-1.61	1002	-1011	645	-660	-2000	u=20	\$	holtite
10166	8	-7.82	1011	-1012	645	-660	-2000	u=20	\$	steel spine
10167	7	-1.61	1012	-1021	645	-660	-2000	u=20	\$	holtite
10168	8	-7.82	1021	-1022	645	-660	-2000	u=20	\$	steel spine
10169	7	-1.61	1022	-1031	645	-660	-2000	u=20	\$	holtite
10170	8	-7.82	1031	-1032	645	-660	-2000	u=20	\$	steel spine

10171	7	-1.61	1032	-1041	645	-660	-2000	u=20	\$ holtite
10172	8	-7.82	1041	-1042	645	-660	-2000	u=20	\$ steel spine
10173	7	-1.61	1042	-1051	645	-660	-2000	u=20	\$ holtite
10174	8	-7.82	1051	-1052	645	-660	-2000	u=20	\$ steel spine
10175	7	-1.61	1052	-1061	645	-660	-2000	u=20	\$ holtite
10176	8	-7.82	1061	-1062	645	-660	-2000	u=20	\$ steel spine
10177	7	-1.61	1062	-1071	645	-660	-2000	u=20	\$ holtite
10178	8	-7.82	1071	-1072	645	-660	-2000	u=20	\$ steel spine
10179	7	-1.61	1072	-1081	645	-660	-2000	u=20	\$ holtite
10180	8	-7.82	1081	-1082	645	-660	-2000	u=20	\$ steel spine
10181	7	-1.61	1082	-1091	645	-660	-2000	u=20	\$ holtite
10182	8	-7.82	1091	-1092	645	-660	-2000	u=20	\$ steel spine
10183	7	-1.61	1092	-2001	645	-660	-2000	u=20	\$ holtite
10184	8	-7.82	2001	-2000	645	-660	1000	u=20	\$ steel spine
c									
c	10201	8	-7.82	2000	-2002	635	-645	1000	u=20 \$ steel spine
c	10202	7	-1.61	2002	-2011	635	-645	2000	u=20 \$ holtite
10202	7	-1.61	2101	-2011	635	-645	2000	u=20	\$ holtite
10203	8	-7.82	2011	-2012	635	-645	2000	u=20	\$ steel spine
10204	7	-1.61	2012	-2021	635	-645	2000	u=20	\$ holtite
10205	8	-7.82	2021	-2022	635	-645	2000	u=20	\$ steel spine
10206	7	-1.61	2022	-2031	635	-645	2000	u=20	\$ holtite
10207	8	-7.82	2031	-2032	635	-645	2000	u=20	\$ steel spine
10208	7	-1.61	2032	-2041	635	-645	2000	u=20	\$ holtite
10209	8	-7.82	2041	-2042	635	-645	2000	u=20	\$ steel spine
10210	7	-1.61	2042	-2051	635	-645	2000	u=20	\$ holtite
10211	8	-7.82	2051	-2052	635	-645	2000	u=20	\$ steel spine
10212	7	-1.61	2052	-2061	635	-645	2000	u=20	\$ holtite
10213	8	-7.82	2061	-2062	635	-645	2000	u=20	\$ steel spine
10214	7	-1.61	2062	-2071	635	-645	2000	u=20	\$ holtite
10215	8	-7.82	2071	-2072	635	-645	2000	u=20	\$ steel spine
10216	7	-1.61	2072	-2081	635	-645	2000	u=20	\$ holtite
10217	8	-7.82	2081	-2082	635	-645	2000	u=20	\$ steel spine
10218	7	-1.61	2082	-2091	635	-645	2000	u=20	\$ holtite
10219	8	-7.82	2091	-2092	635	-645	2000	u=20	\$ steel spine
c	10220	7	-1.61	2092	1101	635	-645	2000	u=20 \$ holtite
10220	7	-1.61	2092	1002	635	-645	2000	u=20	\$ holtite
10221	8	-7.82	1000	-1002	635	-645	2000	u=20	\$ steel spine
c									
10222	8	-7.82	1001	-1000	635	-645	2000	u=20	\$ steel spine
10223	7	-1.61	1012	-1001	635	-645	2000	u=20	\$ holtite
c	10223	7	-1.61	1012	-1104	635	-645	2000	u=20 \$ holtite
10224	8	-7.82	1011	-1012	635	-645	2000	u=20	\$ steel spine
10225	7	-1.61	1022	-1011	635	-645	2000	u=20	\$ holtite
10226	8	-7.82	1021	-1022	635	-645	2000	u=20	\$ steel spine
10227	7	-1.61	1032	-1021	635	-645	2000	u=20	\$ holtite
10228	8	-7.82	1031	-1032	635	-645	2000	u=20	\$ steel spine
10229	7	-1.61	1042	-1031	635	-645	2000	u=20	\$ holtite
10230	8	-7.82	1041	-1042	635	-645	2000	u=20	\$ steel spine
10231	7	-1.61	1052	-1041	635	-645	2000	u=20	\$ holtite
10232	8	-7.82	1051	-1052	635	-645	2000	u=20	\$ steel spine
10233	7	-1.61	1062	-1051	635	-645	2000	u=20	\$ holtite
10234	8	-7.82	1061	-1062	635	-645	2000	u=20	\$ steel spine
10235	7	-1.61	1072	-1061	635	-645	2000	u=20	\$ holtite
10236	8	-7.82	1071	-1072	635	-645	2000	u=20	\$ steel spine
10237	7	-1.61	1082	-1071	635	-645	2000	u=20	\$ holtite
10238	8	-7.82	1081	-1082	635	-645	2000	u=20	\$ steel spine
10239	7	-1.61	1092	-1081	635	-645	2000	u=20	\$ holtite
10240	8	-7.82	1091	-1092	635	-645	2000	u=20	\$ steel spine
10241	7	-1.61	2101	-1091	635	-645	2000	u=20	\$ holtite
c	10241	7	-1.61	2002	-1091	635	-645	2000	u=20 \$ holtite
c	10242	8	-7.82	2000	-2002	635	-645	-1000	u=20 \$ steel spine
c									
c	10243	8	-7.82	2001	-2000	635	-645	-1000	u=20 \$ steel spine
c	10244	7	-1.61	2012	-2001	635	-645	-2000	u=20 \$ holtite
10244	7	-1.61	2012	-2104	635	-645	-2000	u=20	\$ holtite
10245	8	-7.82	2011	-2012	635	-645	-2000	u=20	\$ steel spine
10246	7	-1.61	2022	-2011	635	-645	-2000	u=20	\$ holtite
10247	8	-7.82	2021	-2022	635	-645	-2000	u=20	\$ steel spine


```

2002 8 -7.82      -501 602 -603
2003 8 -7.82      -501 603 -604
2004 8 -7.82      -501 604 -610
c
2010 8 -7.82 501 -515 600 -601
2011 8 -7.82 501 -515 601 -602
2012 8 -7.82 501 -515 602 -603
2013 8 -7.82 501 -515 603 -604
2014 8 -7.82 501 -515 604 -610
2015 8 -7.82 501 -515 610 -615
2016 8 -7.82 501 -515 615 -630
2020 0  515 -513 600 -601
2021 0  515 -513 601 -602
2022 0  515 -513 602 -603
2023 0  515 -513 603 -604
2024 0  515 -513 604 -610
2025 0  515 -513 610 -615
2026 0  515 -513 615 -630
c
c      overpack lid
c
3000 8 -7.82      -506 685 -686
3001 8 -7.82      -506 686 -687
3002 8 -7.82      -506 687 -688
3003 8 -7.82      -506 688 -689
3004 8 -7.82      -506 689 -695
3010 0  506 -513 685 -686
3011 0  506 -513 686 -687
3012 0  506 -513 687 -688
3013 0  506 -513 688 -689
3014 0  506 -513 689 -695
c
3020 8 -7.82 501 -517 675 -676
3021 8 -7.82 501 -516 676 -651
3022 8 -7.82 501 -516 651 -652
3023 8 -7.82 501 -516 652 -653
3024 8 -7.82 501 -516 653 -654
3025 8 -7.82 501 -516 654 -655
3026 8 -7.82 501 -516 655 -656
3027 8 -7.82 501 -516 656 -677
3028 8 -7.82 501 -506 677 -657
3029 8 -7.82 501 -506 657 -685
3030 0  517 -513 675 -676
3031 0  516 -513 676 -651
3032 0  516 -513 651 -652
3033 0  516 -513 652 -653
3034 0  516 -513 653 -654
3035 0  516 -513 654 -655
3036 0  516 -513 655 -656
3037 0  516 -513 656 -677
3038 0  506 -513 677 -657
3039 0  506 -513 657 -685
c
3042 8 -7.82 501 -517 670 -675
3047 0  517 -513 670 -675
c
c      surrounding air regions
c
9000 9 -1.17e-3      -506 695 -830
9001 9 -1.17e-3      -506 830 -831
9002 9 -1.17e-3      -506 831 -832
9003 9 -1.17e-3      -506 832 -833
9004 9 -1.17e-3      -506 833 -837
9010 0  506 -527 695 -830
9011 0  506 -527 830 -831
9012 0  506 -527 831 -832
9013 0  506 -527 832 -833
9014 0  506 -527 833 -837
c
9100 9 -1.17e-3      -515 810 -600

```

```

9101 9 -1.17e-3      -515 811 -810
9102 9 -1.17e-3      -515 812 -811
9103 9 -1.17e-3      -515 813 -812
9104 9 -1.17e-3      -515 817 -813
9110 0 515 -527 810 -600
9111 0 515 -527 811 -810
9112 0 515 -527 812 -811
9113 0 515 -527 813 -812
9114 0 515 -527 817 -813
c
9200 0 513 -527 600 -601
9201 0 513 -527 601 -602
9202 0 513 -527 602 -603
9203 0 513 -527 603 -604
9204 0 513 -527 604 -610
9205 0 513 -527 610 -615
9206 0 513 -527 615 -630
9207 0 513 -527 630 -420
9208 0 513 -527 420 -430
9209 0 513 -527 430 -440
9210 0 513 -527 440 -670
9211 0 513 -527 670 -675
9212 0 513 -527 675 -651
9213 0 513 -527 651 -652
9214 0 513 -527 652 -653
9215 0 513 -527 653 -654
9216 0 513 -527 654 -655
9217 0 513 -527 655 -656
9218 0 513 -527 656 -657
9219 0 513 -527 657 -685
9220 0 513 -527 685 -686
9221 0 513 -527 686 -687
9222 0 513 -527 687 -688
9223 0 513 -527 688 -689
9224 0 513 -527 689 -695
c
c
c
9999 0 527:-817:837
c
c BLANK LINE
c
c BLANK LINE
c
c MPC surfaces\ / \ / \ / \ / \ /
c
1 cz 0.52832
2 cz 0.53213
3 cz 0.61341
4 cz 0.67437
5 cz 0.75057
6 px 0.8128
7 px -0.8128
8 py 0.8128
9 py -0.8128
10 px -4.445
11 px 4.445
12 py -4.445
13 py 4.445
c 14 px -8.2423
14 px -8.242301
15 px -7.9248
16 px -7.66826
17 px -7.47776
18 px -6.0325
19 px 6.0325
20 px 7.9248
c 21 px 8.2423
c 22 py -8.2423

```

21	px	8.242301		
22	py	-8.242301		
23	py	-7.9248		
24	py	-6.0325		
25	py	6.0325		
26	py	7.47776		
27	py	7.66826		
28	py	7.9248		
c				
29	py	8.2423		
29	py	8.242301		
c				
30	px	-6.5024		
31	px	6.5024		
32	py	-6.5024		
33	py	6.5024		
c				
101	px	-98.9076		
102	px	-82.423		
103	px	-65.9384		
104	px	-49.4538		
105	px	-32.9692		
106	px	-16.4846		
107	px	0.0		
108	px	16.4846		
109	px	32.9692		
110	px	49.4538		
111	px	65.9384		
112	px	82.423		
113	px	98.9076		
c				
201	py	-98.9076		
202	py	-82.423		
203	py	-65.9384		
204	py	-49.4538		
205	py	-32.9692		
206	py	-16.4846		
207	py	0.0		
208	py	16.4846		
209	py	32.9692		
210	py	49.4538		
211	py	65.9384		
212	py	82.423		
213	py	98.9076		
c				
301	cz	85.4075		
302	cz	86.6775		
c				
c	620	pz	21.59	\$ MPC baseplate - 2.5 inches
c	400	pz	24.765	\$ start of egg crate
400	pz	23.876		\$ start of egg crate
410	pz	33.9725		\$ start of boral
420	pz	40.3479		\$ beginning of fuel
425	pz	406.1079		\$ end of fuel
430	pz	421.3479		\$ space
435	pz	430.2125		\$ end of boral
440	pz	445.4271		\$ plenum
445	pz	448.8561		\$ expansion springs
450	pz	457.3397		\$ top end fitting
455	pz	468.63		\$ top of element
460	pz	466.344		\$ top of egg crate
c				
c				MPC surfaces \ / \ / \ / \ / \ /
c				
c				OVERPACK survaces \ / \ / \ / \ / \ /
c				
501	cz	87.3125		\$ IR for overpack
502	cz	90.4875		\$ item 2 1.25 inch
503	cz	93.6625		\$ item 2 1.25 inch

504	cz	96.8375	\$ item 12 1.25 inch
505	cz	100.0125	\$ item 13 1.25 inch
506	cz	103.1875	\$ item 14 1.25 inch
507	cz	106.3625	\$ item 15 1.25 inch
508	cz	108.9025	\$ item 16 1 inch
509	cz	111.521875	\$ holtite
510	cz	114.14125	\$ holtite
511	cz	116.760625	\$ holtite
512	cz	119.53875	\$ holtite - total 4.1875 inches
513	cz	120.80875	\$ outer steel shell - 0.5 inches
c	512	cz 119.38	\$ holtite - total 4.125 inches
c	513	cz 120.65	\$ outer steel shell - 0.5 inches
514	cz	111.54	\$ hole in pocket trunion
515	cz	105.7275	\$ flange bottom of overpack
516	cz	105.7275	\$ flange top of overpack
517	cz	109.5375	\$ shear ring
518	cz	103.1875	\$ item 14 1.25 inch
519	cz	108.2675	\$ impact limiter - 2 inch steel
c			
521	cz	162.56	\$ surface of impact limiters
522	cz	203.1875	\$ 1 meter from 506 - upper and lower part overpack
523	cz	220.80875	\$ 1 meter from 513 - outer steel
524	cz	303.1875	\$ 2 meter from 506 - upper and lower part overpack
525	cz	320.80875	\$ 2 meter from 513 - outer steel
526	cz	362.56	\$ 2 meter from 521 - edge of impact limiters
527	cz	400.00	
c			
600	pz	0.0	\$ bottom of overpack
601	pz	3.048	
602	pz	6.096	
603	pz	9.144	
604	pz	12.192	
610	pz	15.24	\$ overpack baseplate - 6 inches
615	pz	18.415	
620	pz	21.59	\$ MPC baseplate - 2.5 inches
630	pz	22.225	\$ beginning of item 17 - 0.25 inches
635	pz	23.495	\$ item 17 - 0.5 inches
640	pz	41.75125	\$ hole in pocket trun - 7.6875 inches from 630
645	pz	54.61	\$ top of pocket trun - 12.75 inches from 630
660	pz	455.6125	\$ top of holtite - 170.125 inches from 635
665	pz	460.6925	\$ top of foam - 2 inches
670	pz	461.9625	\$ top of item 17 on top - 0.5 inches
675	pz	473.71	\$ bottom of MPC in lid - 178 inches from 620
676	pz	476.5675	\$ top of shear ring
677	pz	494.03	\$ top of add steel
651	pz	476.885	
652	pz	480.06	
653	pz	483.235	
654	pz	486.41	
655	pz	489.585	
656	pz	492.76	
657	pz	495.935	
680	pz	499.11	\$ top of MPC outer lid
685	pz	500.6975	\$ bot of overpack lid - 5/8 inch
686	pz	503.7455	
687	pz	506.7935	
688	pz	509.8415	
689	pz	512.8895	
695	pz	515.9375	\$ top of overpack lid - 6 inches
c			
c			
c			
c			
701	pz	-121.92	
702	pz	-91.44	
703	pz	-60.96	
704	pz	-30.48	
c	600	pz 0.0	\$ bottom of overpack
c	630	pz 22.225	\$ beginning of item 17 - 0.25 inches
705	pz	51.5408	

706	pz	80.8567	
707	pz	110.1725	
708	pz	139.4883	
709	pz	168.8042	
710	pz	198.1200	
711	pz	227.4358	
712	pz	256.7517	
713	pz	286.0675	
714	pz	315.3833	
715	pz	344.6992	
716	pz	374.0150	
717	pz	403.3308	
718	pz	432.6467	
c	670	pz	461.9625 \$ top of item 17 on top- 0.5 inches
719	pz	488.3150	
c	695	pz	514.6675 \$ top of overpack lid - 6 inches
720	pz	545.1475	
721	pz	575.6275	
722	pz	606.1075	
723	pz	636.5875	
c			
740	cz	15.24	
741	cz	45.72	
742	cz	76.2	
743	cz	106.68	
744	cz	137.16	
745	cz	167.64	
746	cz	198.12	
747	cz	228.6	
748	cz	259.08	
749	cz	289.56	
750	cz	320.04	
751	cz	350.52	
752	cz	381.0	
c			
801	pz	-2.54	\$ steel disk
802	pz	-5.715	\$ holtite
803	pz	-8.89	\$ holtite
804	pz	-9.2075	\$ cover over holtite
805	pz	-53.34	\$ item 2 on impact limiters
810	pz	-100.0	\$ 1 meter from surface overpack
811	pz	-105.7275	\$ edge of impact limiter
812	pz	-200.0	\$ 2 meter from surface overpack
813	pz	-305.7275	\$ 2 meter from surface impact limiter
814	pz	-427.6475	\$ 2 meter + 4 feet
815	pz	-488.6075	\$ 2 meter + 6 feet
816	pz	-671.4875	\$ 2 meter + 12 feet
817	pz	-700.00	
c			
821	pz	518.4775	\$ steel disk
822	pz	521.6525	\$ holtite
823	pz	524.8275	\$ holtite
824	pz	525.145	\$ cover over holtite
825	pz	569.2775	\$ item 2 on impact limiters
830	pz	615.9375	\$ 1 meter from surface overpack
831	pz	621.6650	\$ edge of impact limiter
832	pz	715.9375	\$ 2 meter from surface overpack
833	pz	821.6650	\$ 2 meter from surface impact limiter
834	pz	943.5850	\$ 2 meter + 4 feet
835	pz	1004.545	\$ 2 meter + 6 feet
836	pz	1187.425	\$ 2 meter + 12 feet
837	pz	1200.00	
c			
c			steel spine and holtite cells
c			
1000	px	0.0	
1001	px	-0.635	
1002	px	0.635	
1011	1 px	-0.635	

```

1012 1 px 0.635
1021 2 px -0.635
1022 2 px 0.635
1031 3 px -0.635
1032 3 px 0.635
1041 4 px -0.635
1042 4 px 0.635
1051 5 px -0.635
1052 5 px 0.635
1061 6 px -0.635
1062 6 px 0.635
1071 7 px -0.635
1072 7 px 0.635
1081 8 px -0.635
1082 8 px 0.635
1091 9 px -0.635
1092 9 px 0.635
c
1101 px 15.71625 $ pocket trunion
1102 px 8.09625 $ pocket trunion opening
1103 px -8.09625 $ pocket trunion opening 6 3/8 inches thick
1104 px -15.71625 $ pocket trunion - 9 3/8 inches thick
c
2000 py 0.0
2001 py -0.635
2002 py 0.635
2011 1 py -0.635
2012 1 py 0.635
2021 2 py -0.635
2022 2 py 0.635
2031 3 py -0.635
2032 3 py 0.635
2041 4 py -0.635
2042 4 py 0.635
2051 5 py -0.635
2052 5 py 0.635
2061 6 py -0.635
2062 6 py 0.635
2071 7 py -0.635
2072 7 py 0.635
2081 8 py -0.635
2082 8 py 0.635
2091 9 py -0.635
2092 9 py 0.635
c
2101 py 15.71625 $ pocket trunion
2102 py 8.09625 $ pocket trunion opening
2103 py -8.09625 $ pocket trunion opening 6 3/8 inches thick
2104 py -15.71625 $ pocket trunion - 9 3/8 inches thick
c
c OVERPACK surfaces \ / \ / \ / \ / \ /
c
c BLANK LINE
c
c BLANK LINE
c
*tr1 0 0 0 9 279 90 99 9 90 90 90 0
*tr2 0 0 0 18 288 90 108 18 90 90 90 0
*tr3 0 0 0 27 297 90 117 27 90 90 90 0
*tr4 0 0 0 36 306 90 126 36 90 90 90 0
*tr5 0 0 0 45 315 90 135 45 90 90 90 0
*tr6 0 0 0 54 324 90 144 54 90 90 90 0
*tr7 0 0 0 63 333 90 153 63 90 90 90 0
*tr8 0 0 0 72 342 90 162 72 90 90 90 0
*tr9 0 0 0 81 351 90 171 81 90 90 90 0
c
c PHOTON MATERIALS
c
c fuel 3.4 w/o U235 10.412 gm/cc

```



```

c
phys:n 20 0.0
phys:p 100 0
c imp:n 1 228r 0
c imp:p 1 228r 0
nps 500000
prtmp j -30 1 2
c print 10 110 160 161 20 170
print
mode n p
c
sdef par=1 erg=d1 axs=0 0 1 x=d4 y=fx d5 z=d3
c
c energy dist for gammas in the fuel
c
c sil h 0.7 1.0 1.5 2.0 2.5 3.0
c spl 0 0.31 0.31 0.15 0.15 0.08
c
c energy dist for neutrons in the fuel
c
c sil h 0.1 0.4 0.9 1.4 1.85 3.0 6.43 20.0
c spl 0 0.03787 0.1935 0.1773 0.1310 0.2320 0.2098 0.01853
c
c energy dist for Co60 gammas
c
c sil d 1.3325 1.1732
c spl 0.5 0.5
c
c axial dist for neut and phot in fuel
c
c si3 h 40.3479 55.5879 70.8279 101.3079 162.2679 223.2279
c 284.1879 345.1479 375.6279 390.8679 406.1079
c sp3 0 0.00005 0.00961 0.07031 0.23323 0.25719 0.22907
c 0.16330 0.03309 0.00409 0.00005
c sb3 0 1 1 1 1 1 1 1 1 1
c
c axial dist for Co60 - a zero prob is in the fuel
c
c si3 h 21.59 40.3479 421.3479 445.4271 448.8561 457.3397 468.63
c sp3 0 0.547 0.0 0.125 0.045 0.227 0.056
c
c si4 s
c 15 16
c 13 14 15 16 17 18
c 12 13 14 15 16 17 18 19
c 12 13 14 15 16 17 18 19
c 11 12 13 14 15 16 17 18 19 20
c 11 12 13 14 15 16 17 18 19 20
c 12 13 14 15 16 17 18 19
c 12 13 14 15 16 17 18 19
c 13 14 15 16 17 18
c 15 16
c
c sp4 1 67r
c
c ds5 s
c 30 30
c 29 29 29 29 29 29
c 28 28 28 28 28 28 28 28
c 27 27 27 27 27 27 27 27
c 26 26 26 26 26 26 26 26 26
c 25 25 25 25 25 25 25 25 25
c 24 24 24 24 24 24 24 24
c 23 23 23 23 23 23 23 23
c 22 22 22 22 22 22
c 21 21
c
c
si11 -80.6831 -67.6783
si12 -64.1985 -51.1937
si13 -47.7139 -34.7091
si14 -31.2293 -18.2245
si15 -14.7447 -1.7399

```

si16	1.7399	14.7447
si17	18.2245	31.2293
si18	34.7091	47.7139
si19	51.1937	64.1985
si20	67.6783	80.6831

c

si21	-80.6831	-67.6783
si22	-64.1985	-51.1937
si23	-47.7139	-34.7091
si24	-31.2293	-18.2245
si25	-14.7447	-1.7399
si26	1.7399	14.7447
si27	18.2245	31.2293
si28	34.7091	47.7139
si29	51.1937	64.1985
si30	67.6783	80.6831

sp11	0	1
sp12	0	1
sp13	0	1
sp14	0	1
sp15	0	1
sp16	0	1
sp17	0	1
sp18	0	1
sp19	0	1
sp20	0	1
sp21	0	1
sp22	0	1
sp23	0	1
sp24	0	1
sp25	0	1
sp26	0	1
sp27	0	1
sp28	0	1
sp29	0	1
sp30	0	1

c

#	imp:n	imp:p
301	1	1
302	1	1
303	1	1
304	1	1
305	2	1
306	2	1
307	2	1
308	2	1
309	1	1
310	1	1
311	1	1
312	1	1
313	2	1
314	2	1
315	2	1
316	2	1
317	4	1
318	4	1
319	4	1
320	4	1
321	4	1
322	4	1
323	4	1
324	4	1
326	1	1
327	1	1
328	1	1
329	1	1
330	1	1
331	1	1
332	1	1

333	1	1
334	2	1
335	2	1
336	2	1
337	2	1
338	1	1
339	1	1
340	1	1
341	1	1
342	2	1
343	2	1
344	2	1
345	2	1
346	1	1
347	1	1
348	1	1
349	1	1
350	1	1
351	1	1
352	1	1
353	1	1
354	2	1
355	1	1
356	1	1
357	2	1
358	4	1
359	4	1
360	4	1
361	4	1
362	1	1
363	1	1
364	1	1
365	1	1
366	1	1
401	1	1
402	1	1
403	1	1
404	1	1
405	2	1
406	2	1
407	2	1
408	2	1
409	1	1
410	1	1
411	1	1
412	1	1
413	2	1
414	2	1
415	2	1
416	2	1
417	4	1
418	4	1
419	4	1
420	4	1
421	4	1
422	4	1
423	4	1
424	4	1
426	1	1
427	1	1
428	1	1
429	1	1
454	2	1
455	1	1
456	1	1
457	2	1
458	4	1
459	4	1
460	4	1

461	4	1
462	1	1
463	1	1
464	1	1
465	1	1
466	1	1
501	1	1
502	1	1
503	1	1
504	1	1
505	2	1
506	2	1
507	2	1
508	2	1
509	1	1
510	1	1
511	1	1
512	1	1
513	2	1
514	2	1
515	2	1
516	2	1
517	4	1
518	4	1
519	4	1
520	4	1
521	4	1
522	4	1
523	4	1
524	4	1
526	1	1
527	1	1
528	1	1
529	1	1
530	1	1
531	1	1
534	2	1
535	2	1
538	1	1
539	1	1
542	2	1
543	2	1
546	1	1
547	1	1
548	1	1
549	1	1
550	1	1
551	1	1
552	1	1
553	1	1
554	2	1
555	1	1
556	1	1
557	2	1
558	4	1
559	4	1
560	4	1
561	4	1
562	1	1
563	1	1
564	1	1
565	1	1
566	1	1
601	1	1
602	1	1
603	1	1
604	1	1
605	2	1
606	2	1

607	2	1
608	2	1
609	1	1
610	1	1
611	1	1
612	1	1
613	2	1
614	2	1
615	2	1
616	2	1
617	4	1
618	4	1
619	4	1
620	4	1
621	4	1
622	4	1
623	4	1
624	4	1
626	1	1
627	1	1
628	1	1
629	1	1
632	1	1
633	1	1
636	2	1
637	2	1
640	1	1
641	1	1
644	2	1
645	2	1
646	1	1
647	1	1
648	1	1
649	1	1
650	1	1
651	1	1
652	1	1
653	1	1
654	2	1
655	1	1
656	1	1
657	2	1
658	4	1
659	4	1
660	4	1
661	4	1
662	1	1
663	1	1
664	1	1
665	1	1
666	1	1
701	1	1
702	2	1
703	1	1
704	2	1
705	4	1
706	4	1
707	1	1
708	1	1
710	1	1
711	2	1
712	1	1
713	2	1
714	4	1
715	4	1
716	1	1
717	1	1
720	1	1
721	2	1

722	2	1
723	1	1
724	1	1
725	2	1
726	2	1
727	4	1
728	4	1
729	4	1
730	4	1
731	1	1
732	1	1
735	1	1
736	1	1
747	2	1
748	1	1
749	2	1
750	4	1
751	4	1
752	1	1
755	1	1
766	1	1
767	2	1
768	2	1
769	1	1
770	1	1
771	2	1
772	2	1
773	4	1
774	4	1
775	4	1
776	4	1
777	1	1
780	1	1
799	1	1
800	2	1
801	2	1
802	1	1
803	1	1
804	2	1
805	2	1
806	4	1
807	4	1
808	4	1
809	4	1
810	1	1
811	1	1
822	1	1
823	2	1
824	1	1
825	2	1
826	4	1
827	4	1
828	1	1
830	1	1
841	1	1
842	2	1
843	2	1
844	1	1
845	1	1
846	2	1
847	2	1
848	4	1
849	4	1
850	4	1
851	4	1
852	1	1
201	1	1
202	1	1
203	1	1

204	1	1
205	1	1
206	1	1
207	1	1
101	1	1
102	1	1
208	1	1
209	1	1
210	1	1
211	1	1
212	1	1
103	1	1
104	1	1
105	1	1
106	1	1
107	1	1
108	1	1
213	1	1
214	1	1
215	1	1
109	1	1
110	1	1
111	1	1
112	1	1
113	1	1
114	1	1
115	1	1
116	1	1
216	1	1
217	1	1
218	1	1
117	1	1
118	1	1
119	1	1
120	1	1
121	1	1
122	1	1
123	1	1
124	1	1
219	1	1
220	1	1
221	1	1
125	1	1
126	1	1
127	1	1
128	1	1
129	1	1
130	1	1
131	1	1
132	1	1
133	1	1
134	1	1
222	1	1
223	1	1
135	1	1
136	1	1
137	1	1
138	1	1
139	1	1
140	1	1
141	1	1
142	1	1
143	1	1
144	1	1
224	1	1
225	1	1
226	1	1
145	1	1
146	1	1

147	1	1
148	1	1
149	1	1
150	1	1
151	1	1
152	1	1
227	1	1
228	1	1
229	1	1
153	1	1
154	1	1
155	1	1
156	1	1
157	1	1
158	1	1
159	1	1
160	1	1
230	1	1
231	1	1
232	1	1
161	1	1
162	1	1
163	1	1
164	1	1
165	1	1
166	1	1
233	1	1
234	1	1
235	1	1
236	1	1
237	1	1
167	1	1
168	1	1
238	1	1
239	1	1
240	1	1
241	1	1
242	1	1
243	1	1
244	1	1
1821	4	1
1822	4	1
1823	4	1
1824	4	1
1825	2	1
1826	2	1
1827	1	1
1828	1	1
1829	2	1
1830	2	1
1831	4	1
1832	4	1
1833	4	1
1834	4	1
1835	8	1
1836	8	1
1837	8	1
1838	8	1
1839	16	1
1840	16	1
1841	16	1
1842	16	1
1843	32	1
1844	32	1
1845	32	1
1846	32	1
1847	64	1
1848	64	1
1849	64	1

1850	64	1
1851	64	1
1854	4	1
1855	4	1
1860	8	1
1861	8	1
1862	16	1
1863	16	1
1864	32	1
1865	32	1
1866	64	1
1867	64	1
1868	64	1
1001	2	1
1002	1	1
1003	2	1
1004	4	1
1005	2	1
1006	1	1
1007	2	1
1008	4	1
1009	2	1
1010	1	1
1011	2	1
1012	4	1
10101	1	1
10102	1	1
10103	1	1
10104	1	1
10105	1	1
10106	1	1
10107	1	1
10108	1	1
10109	1	1
10110	1	1
10111	1	1
10112	1	1
10113	1	1
10114	1	1
10115	1	1
10116	1	1
10117	1	1
10118	1	1
10119	1	1
10120	1	1
10121	1	1
10122	1	1
10123	1	1
10124	1	1
10125	1	1
10126	1	1
10127	1	1
10128	1	1
10129	1	1
10130	1	1
10131	1	1
10132	1	1
10133	1	1
10134	1	1
10135	1	1
10136	1	1
10137	1	1
10138	1	1
10139	1	1
10140	1	1
10141	1	1
10142	1	1
10143	1	1
10144	1	1

10145	1	1
10146	1	1
10147	1	1
10148	1	1
10149	1	1
10150	1	1
10151	1	1
10152	1	1
10153	1	1
10154	1	1
10155	1	1
10156	1	1
10157	1	1
10158	1	1
10159	1	1
10160	1	1
10161	1	1
10162	1	1
10163	1	1
10164	1	1
10165	1	1
10166	1	1
10167	1	1
10168	1	1
10169	1	1
10170	1	1
10171	1	1
10172	1	1
10173	1	1
10174	1	1
10175	1	1
10176	1	1
10177	1	1
10178	1	1
10179	1	1
10180	1	1
10181	1	1
10182	1	1
10183	1	1
10184	1	1
10202	1	1
10203	1	1
10204	1	1
10205	1	1
10206	1	1
10207	1	1
10208	1	1
10209	1	1
10210	1	1
10211	1	1
10212	1	1
10213	1	1
10214	1	1
10215	1	1
10216	1	1
10217	1	1
10218	1	1
10219	1	1
10220	1	1
10221	1	1
10222	1	1
10223	1	1
10224	1	1
10225	1	1
10226	1	1
10227	1	1
10228	1	1
10229	1	1
10230	1	1

10231	1	1
10232	1	1
10233	1	1
10234	1	1
10235	1	1
10236	1	1
10237	1	1
10238	1	1
10239	1	1
10240	1	1
10241	1	1
10244	1	1
10245	1	1
10246	1	1
10247	1	1
10248	1	1
10249	1	1
10250	1	1
10251	1	1
10252	1	1
10253	1	1
10254	1	1
10255	1	1
10256	1	1
10257	1	1
10258	1	1
10259	1	1
10260	1	1
10261	1	1
10262	1	1
10263	1	1
10264	1	1
10265	1	1
10266	1	1
10267	1	1
10268	1	1
10269	1	1
10270	1	1
10271	1	1
10272	1	1
10273	1	1
10274	1	1
10275	1	1
10276	1	1
10277	1	1
10278	1	1
10279	1	1
10280	1	1
10281	1	1
10282	1	1
10283	1	1
11000	1	1
11001	1	1
11002	1	1
11003	1	1
11111	1	1
11112	1	1
11113	1	1
11114	1	1
11115	1	1
2000	32	1
2001	16	1
2002	16	1
2003	8	1
2004	8	1
2010	32	1
2011	16	1
2012	16	1
2013	8	1

2014	8	1
2015	4	1
2016	4	1
2020	1	1
2021	1	1
2022	1	1
2023	1	1
2024	1	1
2025	1	1
2026	1	1
3000	128	1
3001	128	1
3002	256	1
3003	256	1
3004	512	1
3010	1	1
3011	1	1
3012	1	1
3013	1	1
3014	1	1
3020	8	1
3021	8	1
3022	8	1
3023	16	1
3024	16	1
3025	32	1
3026	32	1
3027	64	1
3028	64	1
3029	64	1
3030	1	1
3031	1	1
3032	1	1
3033	1	1
3034	1	1
3035	1	1
3036	1	1
3037	1	1
3038	1	1
3039	1	1
3042	4	1
3047	1	1
9000	512	1
9001	512	1
9002	512	1
9003	512	1
9004	512	1
9010	1	1
9011	1	1
9012	1	1
9013	1	1
9014	1	1
9100	32	1
9101	32	1
9102	32	1
9103	32	1
9104	32	1
9110	1	1
9111	1	1
9112	1	1
9113	1	1
9114	1	1
9200	1	1
9201	1	1
9202	1	1
9203	1	1
9204	1	1
9205	1	1
9206	1	1

```

9207      1      1
9208      1      1
9209      1      1
9210      1      1
9211      1      1
9212      1      1
9213      1      1
9214      1      1
9215      1      1
9216      1      1
9217      1      1
9218      1      1
9219      1      1
9220      1      1
9221      1      1
9222      1      1
9223      1      1
9224      1      1
9999      0      0
c
c      neutron dose factors
c
c      2.5e-8  1.0e-7  1.0e-6  1.0e-5  1.0e-4  1.0e-3  1.0e-2  0.1
c      0.5    1.0    2.5    5.0    7.0    10.0   14.0   20.0
c      3.67e-6 3.67e-6 4.46e-6 4.54e-6 4.18e-6 3.76e-6 3.56e-6 2.17e-5
c      9.26e-5 1.32e-4 1.25e-4 1.56e-4 1.47e-4 1.47e-4 2.08e-4 2.27e-4
c
c      photon dose factors
c
c      0.01 0.03 0.05 0.07 0.1 0.15 0.2 0.25 0.3 0.35 0.4 0.45
c      0.5 0.55 0.6 0.65 0.7 0.8 1.0 1.4 1.8 2.2 2.6 2.8 3.25
c      3.75 4.25 4.75 5.0 5.25 5.75 6.25 6.75 7.5 9.0 11.0
c      13.0 15.0
c      3.96e-06 5.82e-07 2.90e-07 2.58e-07 2.83e-07 3.79e-07 5.01e-07
c      6.31e-07 7.59e-07 8.78e-07 9.85e-07 1.08e-06 1.17e-06 1.27e-06
c      1.36e-06 1.44e-06 1.52e-06 1.68e-06 1.98e-06 2.51e-06 2.99e-06
c      3.42e-06 3.82e-06 4.01e-06 4.41e-06 4.83e-06 5.23e-06 5.60e-06
c      5.80e-06 6.01e-06 6.37e-06 6.74e-06 7.11e-06 7.66e-06 8.77e-06
c      1.03e-05 1.18e-05 1.33e-05
c
f2:n      600 810 811 812 813
fs2      -740 -741 -742 -743 -744 -745 -746 -747 -748 -749 -750 -751 -752 t
fc2      1ft all
ft2      scx 1
de2      2.5e-8  1.0e-7  1.0e-6  1.0e-5  1.0e-4  1.0e-3  1.0e-2  0.1
c      0.5    1.0    2.5    5.0    7.0    10.0   14.0   20.0
df2      3.67e-6 3.67e-6 4.46e-6 4.54e-6 4.18e-6 3.76e-6 3.56e-6 2.17e-5
c      9.26e-5 1.32e-4 1.25e-4 1.56e-4 1.47e-4 1.47e-4 2.08e-4 2.27e-4
fq2      u s
tf2      3j 2
c
f12:n     695 830 831 832 833
fs12     -740 -741 -742 -743 -744 -745 -746 -747 -748 -749 -750 -751 -752 t
fc12     1ft all
ft12     scx 1
de12     2.5e-8  1.0e-7  1.0e-6  1.0e-5  1.0e-4  1.0e-3  1.0e-2  0.1
c      0.5    1.0    2.5    5.0    7.0    10.0   14.0   20.0
df12     3.67e-6 3.67e-6 4.46e-6 4.54e-6 4.18e-6 3.76e-6 3.56e-6 2.17e-5
c      9.26e-5 1.32e-4 1.25e-4 1.56e-4 1.47e-4 1.47e-4 2.08e-4 2.27e-4
fq12     u s
tf12     3j 2
c
c      PHOTON TALLIES
c
f102:p   600 810 811 812 813
fs102    -740 -741 -742 -743 -744 -745 -746 -747 -748 -749 -750 -751 -752 t
fc102    1ft all
ft102    scx 1
de102    0.01 0.03 0.05 0.07 0.1 0.15 0.2 0.25 0.3 0.35 0.4 0.45

```

	0.5	0.55	0.6	0.65	0.7	0.8	1.0	1.4	1.8	2.2	2.6	2.8	3.25
	3.75	4.25	4.75	5.0	5.25	5.75	6.25	6.75	7.5	9.0	11.0		
	13.0	15.0											
df102	3.96e-06	5.82e-07	2.90e-07	2.58e-07	2.83e-07	3.79e-07	5.01e-07						
	6.31e-07	7.59e-07	8.78e-07	9.85e-07	1.08e-06	1.17e-06	1.27e-06						
	1.36e-06	1.44e-06	1.52e-06	1.68e-06	1.98e-06	2.51e-06	2.99e-06						
	3.42e-06	3.82e-06	4.01e-06	4.41e-06	4.83e-06	5.23e-06	5.60e-06						
	5.80e-06	6.01e-06	6.37e-06	6.74e-06	7.11e-06	7.66e-06	8.77e-06						
	1.03e-05	1.18e-05	1.33e-05										
fq102	u	s											
tf102	3j	2											
c													
f112:p	695	830	831	832	833								
fs112	-740	-741	-742	-743	-744	-745	-746	-747	-748	-749	-750	-751	-752 t
fc112	lft	all											
ft112	scx	1											
del12	0.01	0.03	0.05	0.07	0.1	0.15	0.2	0.25	0.3	0.35	0.4	0.45	
	0.5	0.55	0.6	0.65	0.7	0.8	1.0	1.4	1.8	2.2	2.6	2.8	3.25
	3.75	4.25	4.75	5.0	5.25	5.75	6.25	6.75	7.5	9.0	11.0		
	13.0	15.0											
df112	3.96e-06	5.82e-07	2.90e-07	2.58e-07	2.83e-07	3.79e-07	5.01e-07						
	6.31e-07	7.59e-07	8.78e-07	9.85e-07	1.08e-06	1.17e-06	1.27e-06						
	1.36e-06	1.44e-06	1.52e-06	1.68e-06	1.98e-06	2.51e-06	2.99e-06						
	3.42e-06	3.82e-06	4.01e-06	4.41e-06	4.83e-06	5.23e-06	5.60e-06						
	5.80e-06	6.01e-06	6.37e-06	6.74e-06	7.11e-06	7.66e-06	8.77e-06						
	1.03e-05	1.18e-05	1.33e-05										
fq112	u	s											
tf112	3j	2											

CHAPTER 6: CRITICALITY EVALUATION

This chapter documents the criticality evaluation of the HI-STAR 100 System for the storage of spent nuclear fuel in accordance with 10CFR72.124. The results of this evaluation demonstrate that the HI-STAR 100 System is in full compliance with the Standard Review Plan for Dry Cask Storage Systems, NUREG-1536, and thus, fulfills the following acceptance criteria:

1. The multiplication factor (k_{eff}), including all biases and uncertainties at a 95-percent confidence level, should not exceed 0.95 under all credible normal, off-normal, and accident conditions.
2. At least two unlikely, independent, and concurrent or sequential changes to the conditions essential to criticality safety, under normal, off-normal, and accident conditions, should occur before an accidental criticality is deemed to be possible.
3. When practicable, criticality safety of the design should be established on the basis of favorable geometry, permanent fixed neutron-absorbing materials (poisons), or both. Where solid neutron absorbing materials are used, the design should provide for a positive means to verify their continued efficacy during the storage period.
4. Criticality safety of the cask system should not rely on use of the following credits:
 - a. burnup of the fuel
 - b. fuel-related burnable neutron absorbers
 - c. more than 75 percent for fixed neutron absorbers when subject to standard acceptance test.

In addition to demonstrating that the criticality safety acceptance criteria are satisfied, this chapter describes the HI-STAR 100 System design structures and components important to criticality safety and defines the limiting fuel characteristics.

DISCUSSION AND RESULTS

In conformance with the principles established in NUREG-1536 [6.1.1], 10CFR72.124 [6.1.2], and NUREG-0800 Section 9.1.2 [6.1.3], the results in this chapter demonstrate that the effective multiplication factor (k_{eff}) of the HI-STAR 100 System, including all biases and uncertainties evaluated with a 95% probability at the 95% confidence level, does not exceed 0.95 under all credible normal, off-normal, and accident conditions. Moreover, these results demonstrate that the HI-STAR 100 System is designed and maintained such that at least two unlikely, independent, and concurrent or sequential changes must occur to the conditions essential to criticality safety before a nuclear criticality accident is possible. These criteria provide a large subcritical margin, sufficient to assure the criticality safety of the HI-STAR 100 System when fully loaded with fuel of the highest permissible reactivity.

Criticality safety of the HI-STAR 100 System depends on the following three principal design parameters:

1. The inherent geometry of the fuel basket designs within the MPC (and the flux-trap water gaps in the MPC-24);
2. The incorporation of permanent fixed neutron-absorbing panels (Boral) in the fuel basket structure; and
3. An administrative limit on the maximum enrichment for PWR fuel and maximum planar-average enrichment for BWR fuel.

The normal conditions for loading/unloading, handling, packaging, transfer, and storage of the HI-STAR 100 System conservatively include: full flooding with ordinary water corresponding to the highest reactivity, and the worst case (most conservative) combination of manufacturing and fabrication tolerances. The off-normal and accident conditions defined in Chapter 2 and considered in Chapter 11 have no adverse effect on the design parameters important to criticality safety, and thus, the off-normal and accident conditions are identical to those for normal conditions.

The HI-STAR 100 System is designed such that the fixed neutron absorber (Boral) will remain effective for a storage period greater than 20 years, and there are no credible means to lose it. Therefore, in accordance with 10CFR72.124(b), there is no need to provide a surveillance or monitoring program to verify the continued efficacy of the neutron absorber.

Criticality safety of the HI-STAR 100 System does not rely on the use of any of the following credits:

- burnup of fuel
- fuel-related burnable neutron absorbers
- more than 75 percent of the B-10 content for the fixed neutron absorber (Boral).

The following two interchangeable basket designs are available for use in the HI-STAR 100 System:

- a 24-cell basket (MPC-24), designed for intact PWR fuel assemblies with a specified maximum enrichment
- a 68-cell basket (MPC-68), designed for both intact and damaged BWR fuel assemblies with a specified maximum planar-average enrichment. Additionally, a variation in the MPC-68, designated MPC-68F, is designed for damaged BWR fuel assemblies and BWR fuel debris with a specified maximum planar-average enrichment.

The HI-STAR 100 System for storage is dry (no moderator), and thus, the reactivity is very low ($k_{\text{eff}} < 0.40$). However, the HI-STAR 100 System for loading and unloading operations is flooded, and thus, represents the limiting case in terms of reactivity.

Confirmation of the criticality safety of the HI-STAR 100 System under flooded conditions, when filled with fuel of the maximum permissible reactivity for which they are designed, was accomplished with the three-dimensional Monte Carlo code MCNP4a [6.1.4]. Independent confirmatory calculations were made with NITAWL-KENO5a from the SCALE-4.3 package. KENO5a [6.1.5] calculations used the 238-group SCALE cross-section library compiled with the NITAWL-II program [6.1.6], which adjusts the uranium-238 cross sections to compensate for resonance self-shielding effects. The Dancoff factors required by NITAWL-II were calculated with the CELLDAN code [6.1.13]; which includes the SUPERDAN code [6.1.7] as a subroutine. K-factors for one-sided statistical tolerance limits with 95% probability at the 95% confidence level were obtained from the National Bureau of Standards (now NIST) Handbook 91 [6.1.8].

CASMO-3, a two-dimensional transport theory code [6.1.9-6.1.12] for fuel assemblies, was used to assess the incremental reactivity effects due to manufacturing tolerances. The CASMO-3 calculations identify those tolerances that cause a positive reactivity effect, enabling the Monte Carlo code input to define the worst case (most conservative) conditions. CASMO-3 was not used for quantitative information, but only to qualitatively indicate the direction and approximate magnitude of the reactivity effects of the manufacturing tolerances.

Benchmark calculations were made to compare the primary code packages (MCNP4a and KENO5a) with experimental data, using critical experiments selected to encompass, insofar as practical, the design parameters of the HI-STAR 100 System. The most important parameters are (1) the enrichment, (2) the water-gap size (MPC-24) or cell spacing (MPC-68), and (3) the ^{10}B loading of the neutron absorber panels. Benchmark calculations are presented in Appendix 6.A.

Applicable codes, standards, and regulations, or pertinent sections thereof, include the following:

- NUREG-1536, Standard Review Plan for Dry Cask Storage Systems, USNRC, Washington D.C., January 1997.
- 10CFR72.124, Criteria For Nuclear Criticality Safety.
- Code of Federal Regulations, Title 10, Part 50, Appendix A, General Design Criterion 62, Prevention of Criticality in Fuel Storage and Handling.
- USNRC Standard Review Plan, NUREG-0800, Section 9.1.2, Spent Fuel Storage, Rev. 3, July 1981.

To assure the true reactivity will always be less than the calculated reactivity, the following conservative assumptions were made:

- The MPCs are assumed to contain the most reactive fresh fuel authorized to be loaded into a specific basket design.
- In accordance with NUREG-1536, no credit for fuel burnup is assumed, either in depleting the quantity of fissile nuclides or in producing fission product poisons.
- In accordance with NUREG-1536, the criticality analyses assume 75% of the manufacturer's minimum Boron-10 content for the Boral neutron absorber.
- The fuel stack density is conservatively assumed to be 96% of theoretical (10.522 g/cm^3) for all criticality analyses. No credit is taken for fuel pellet dishing or chamfering.
- No credit is taken for the ^{234}U and ^{236}U in the fuel.
- When flooded, the moderator is assumed to be pure, unborated water at a temperature corresponding to the highest reactivity within the expected operating range (i.e., water density of 1.000 g/cc).

- Neutron absorption in minor structural members and heat conduction elements is neglected, i.e., spacer grids, basket supports, and aluminum heat conduction elements are replaced by water.
- In compliance with NUREG-1536, the worst hypothetical combination of tolerances (most conservative values within the range of acceptable values), as identified in Section 6.3, is assumed.
- When flooded, the fuel rod pellet-to-clad gap regions are assumed to be flooded.
- Planar-averaged enrichments are assumed for BWR fuel. (In accordance with NUREG-1536, analysis is presented in Appendix 6.B to demonstrate that the use of planar-average enrichments produces conservative results.)
- In accordance with NUREG-1536, fuel-related burnable neutron absorbers, such as the Gadolinia normally used in BWR fuel and IFBA normally used in PWR fuel, are neglected.
- Higher temperatures of the fuel and moderator resulting from decay heat are neglected.
- For evaluation of the bias, all benchmark calculations that result in a k_{eff} greater than 1.0 are conservatively truncated to 1.0000, in accordance with NUREG-1536.
- The water reflector above and below the fuel is assumed to be unborated water.
- For fuel assemblies that contain low-enriched axial blankets, the governing enrichment is that of the highest planar average, and the blankets are not included in determining the average enrichment.
- For intact fuel assemblies, as defined in Appendix B to the Certificate of Compliance, missing fuel rods are assumed to be replaced with dummy rods that displace an amount of water greater than or equal to the original rods.

Results of the design basis criticality safety calculations for single unreflected, internally flooded casks (limiting cases) are listed in Tables 6.1.1 through 6.1.3, conservatively evaluated for the worst combination of manufacturing tolerances (as identified in Section 6.3), and including the calculational bias, uncertainties, and calculational statistics. For each of the MPC designs and

fuel assembly classes[†], Tables 6.1.1 through 6.1.3 list the bounding maximum k_{eff} value and the associated maximum allowable enrichment. The maximum allowed enrichments are defined in Appendix B to the Certificate of Compliance. Maximum k_{eff} values for each of the candidate fuel assemblies and basket configurations, that are bounded by those listed in Tables 6.1.1 through 6.1.3, are given in Section 6.2.

A table listing the maximum k_{eff} (including bias, uncertainties, and calculational statistics), calculated k_{eff} , standard deviation, and energy of the average lethargy causing fission (EALF) for each of the candidate fuel assemblies and basket configurations is provided in Appendix 6.C. These results confirm that the maximum k_{eff} values for the HI-STAR 100 System are below the limiting design criteria ($k_{\text{eff}} < 0.95$) when fully flooded and loaded with any of the candidate fuel assemblies and basket configurations. Analyses for the various conditions of flooding that support the conclusion that the fully flooded condition corresponds to the highest reactivity, and thus is most limiting, are presented in Section 6.4. The capability of the HI-STAR 100 System to safely accommodate damaged fuel and fuel debris is demonstrated in Subsection 6.4.4.

Accident conditions have also been considered and no credible accident has been identified that would result in exceeding the design criteria limit on reactivity. After the MPC is loaded with spent fuel, it is seal-welded and cannot be internally flooded. The HI-STAR 100 System for storage is dry (no moderator) and the reactivity is very low. For arrays of HI-STAR 100 casks, the radiation shielding and the physical separation between overpacks due to the large diameter and cask pitch preclude any significant neutronic coupling between the casks.

[†] For each array size (e.g., 6x6, 7x7, 14x14, etc.), the fuel assemblies have been subdivided into a number of assembly classes, where an assembly class is defined in terms of the (1) number of fuel rods; (2) pitch; (3) number and location of guide tubes (PWR) or water rods (BWR); and (4) cladding material. The assembly classes for BWR and PWR fuel are defined in Section 6.2.

Table 6.1.1

BOUNDED MAXIMUM k_{eff} VALUES FOR EACH ASSEMBLY CLASS IN THE MPC-24

Fuel Assembly Class	Maximum Allowable Enrichment (wt% ^{235}U)	Maximum [†] k_{eff}
14x14A	4.6	0.9383
14x14B	4.6	0.9323
14x14C	4.6	0.9400
14x14D	4.0	0.8576
15x15A	4.1	0.9301
15x15B	4.1	0.9473
15x15C	4.1	0.9444
15x15D	4.1	0.9440
15x15E	4.1	0.9475
15x15F	4.1	0.9478 ^{††}
15x15G	4.0	0.8986
15x15H	3.8	0.9411
16x16A	4.6	0.9383
17x17A	4.0	0.9452
17x17B	4.0	0.9436
17x17C	4.0	0.9427

Note: These calculations are for single unreflected, fully flooded casks. However, comparable reactivities were obtained for fully reflected casks and for arrays of casks.

† The term "maximum k_{eff} " as used here, and elsewhere in this document, means the highest possible k-effective, including bias, uncertainties, and calculational statistics, evaluated for the worst case combination of manufacturing tolerances.

†† KENO5a verification calculation resulted in a maximum k_{eff} of 0.9466.

Table 6.1.2

BOUNDING MAXIMUM k_{eff} VALUES FOR EACH ASSEMBLY CLASS IN THE MPC-68

Fuel Assembly Class	Maximum Allowable Planar-Average Enrichment (wt% ^{235}U)	Maximum [†] k_{eff}
6x6A	2.7 ^{††}	0.7888 ^{†††}
6x6B [‡]	2.7 ^{††}	0.7824 ^{†††}
6x6C	2.7 ^{††}	0.8021 ^{†††}
7x7A	2.7 ^{††}	0.7974 ^{†††}
7x7B	4.2	0.9386
8x8A	2.7 ^{††}	0.7697 ^{†††}
8x8B	4.2	0.9416
8x8C	4.2	0.9425
8x8D	4.2	0.9403
8x8E	4.2	0.9312
8x8F	3.6	0.9153

Note: These calculations are for single unreflected, fully flooded casks. However, comparable reactivities were obtained for fully reflected casks and for arrays of casks.

† The term "maximum k_{eff} " as used here, and elsewhere in this document, means the highest possible k-effective, including bias, uncertainties, and calculational statistics, evaluated for the worst case combination of manufacturing tolerances.

†† This calculation was performed for 3.0% planar-average enrichment, however, the actual fuel is limited, as specified in Appendix B to the CoC, to a maximum planar-average enrichment of 2.7%. Therefore, the listed maximum k_{eff} value is conservative.

††† This calculation was performed for a ^{10}B loading of 0.0067 g/cm², which is 75% of a minimum ^{10}B loading of 0.0089 g/cm². The minimum ^{10}B loading in the MPC-68 is 0.0372 g/cm². Therefore, the listed maximum k_{eff} value is conservative.

‡ Assemblies in this class contain both MOX and UO₂ pins. The composition of the MOX fuel pins is given in Table 6.3.4. The maximum allowable planar-average enrichment for the MOX pins is given in the Appendix B to the Certificate of Compliance.

Table 6.1.2 (continued)

BOUNDING MAXIMUM k_{eff} VALUES FOR EACH ASSEMBLY CLASS IN THE MPC-68

Fuel Assembly Class	Maximum Allowable Planar-Average Enrichment (wt% ^{235}U)	Maximum [†] k_{eff}
9x9A	4.2	0.9417
9x9B	4.2	0.9422
9x9C	4.2	0.9395
9x9D	4.2	0.9394
9x9E	4.1	0.9424
9x9F	4.1	0.9424
10x10A	4.2	0.9457 ^{††}
10x10B	4.2	0.9436
10x10C	4.2	0.9021
10x10D	4.0	0.9376
10x10E	4.0	0.9185

Note: These calculations are for single unreflected, fully flooded casks. However, comparable reactivities were obtained for fully reflected casks and for arrays of casks.

† The term "maximum k_{eff} " as used here, and elsewhere in this document, means the highest possible k-effective, including bias, uncertainties, and calculational statistics, evaluated for the worst case combination of manufacturing tolerances.

†† KENO5a verification calculation resulted in a maximum k_{eff} of 0.9453.

Table 6.1.3

BOUNDING MAXIMUM k_{eff} VALUES FOR EACH ASSEMBLY CLASS IN THE MPC-68F

Fuel Assembly Class	Maximum Allowable Planar-Average Enrichment (wt% ^{235}U)	Maximum [†] k_{eff}
6x6A	2.7 ^{††}	0.7888
6x6B ^{†††}	2.7	0.7824
6x6C	2.7	0.8021
7x7A	2.7	0.7974
8x8A	2.7	0.7697

Note:

1. These calculations are for single unreflected, fully flooded casks. However, comparable reactivities were obtained for fully reflected casks and for arrays of casks.
2. These calculations were performed for a ^{10}B loading of 0.0067 g/cm^2 , which is 75% of a minimum ^{10}B loading of 0.0089 g/cm^2 . The minimum ^{10}B loading in the MPC-68F is 0.010 g/cm^2 . Therefore, the listed maximum k_{eff} values are conservative.

† The term "maximum k_{eff} " as used here, and elsewhere in this document, means the highest possible k-effective, including bias, uncertainties, and calculational statistics, evaluated for the worst case combination of manufacturing tolerances.

†† These calculations were performed for 3.0% planar-average enrichment, however, the actual fuel is limited, as specified in Appendix B to the CoC, to a maximum planar-average enrichment of 2.7%. Therefore, the listed maximum k_{eff} values are conservative.

††† Assemblies in this class contain both MOX and UO_2 pins. The composition of the MOX fuel pins is given in Table 6.3.4. The maximum allowable planar-average enrichment for the MOX pins is specified in Appendix B to the Certificate of Compliance.

6.2 SPENT FUEL LOADING

Specifications for the BWR and PWR fuel assemblies that were analyzed in this criticality evaluation are given in Tables 6.2.1 and 6.2.2, respectively. For the BWR fuel characteristics, the number and dimensions for the water rods are the actual number and dimensions. For the PWR fuel characteristics, the actual number and dimensions of the control rod guide tubes and thimbles are used. Table 6.2.1 lists 56 unique BWR assemblies while Table 6.2.2 lists 41 unique PWR assemblies, all of which were explicitly analyzed for this evaluation. Examination of Tables 6.2.1 and 6.2.2 reveals that there are a large number of minor variations in fuel assembly dimensions.

Due to the large number of minor variations in the fuel assembly dimensions, the use of explicit dimensions in the Certificate of Compliance could limit the applicability of the HI-STAR 100 System. To resolve this limitation, bounding criticality analyses are presented in this section for a number of defined fuel assembly classes for both fuel types (PWR and BWR). The results of the bounding criticality analyses justify using bounding specifications for fuel dimensions in the Certificate of Compliance.

6.2.1 Definition of Assembly Classes

For each array size (e.g., 6x6, 7x7, 15x15, etc.), the fuel assemblies have been subdivided into a number of defined classes, where a class is defined in terms of (1) the number of fuel rods; (2) pitch; (3) number and locations of guide tubes (PWR) or water rods (BWR); and (4) cladding material. The assembly classes for BWR and PWR fuel are defined in Tables 6.2.1 and 6.2.2, respectively. It should be noted that these assembly classes are unique to this evaluation and are not known to be consistent with any class designations in the open literature.

For each assembly class, calculations have been performed for all of the dimensional variations for which data is available (i.e., all data in Tables 6.2.1 and 6.2.2). These calculations demonstrate that the maximum reactivity corresponds to:

- maximum active fuel length,
- maximum fuel pellet diameter,
- minimum cladding outside diameter (OD),
- maximum cladding inside diameter (ID),
- minimum guide tube/water rod thickness, and
- maximum channel thickness (for BWR assemblies only).

Therefore, for each assembly class, a bounding assembly was defined based on the above characteristics and a calculation for the bounding assembly was performed to demonstrate compliance with the regulatory requirement of $k_{\text{eff}} < 0.95$. In some assembly classes this

bounding assembly corresponds directly to one of the actual (real) assemblies; while in most assembly classes, the bounding assembly is artificial (i.e., based on bounding dimensions from more than one of the actual assemblies). In classes where the bounding assembly is artificial, the reactivity of the actual (real) assemblies is typically much less than that of the bounding assembly; thereby providing additional conservatism. As a result of these analyses, the Certificate of Compliance will define acceptability in terms of the bounding assembly parameters for each class.

To demonstrate that the aforementioned characteristics are bounding, a parametric study was performed for a reference BWR assembly, designated herein as 8x8C04 (identified generally as a GE8x8R). The results of this study are shown in Table 6.2.3, and verify the positive reactivity effect associated with (1) increasing the pellet diameter, (2) maximizing the cladding ID (while maintaining a constant cladding OD), (3) minimizing the cladding OD (while maintaining a constant cladding ID), (4) decreasing the water rod thickness, (5) artificially replacing the Zircaloy water rod tubes with water, and (6) maximizing the channel thickness. These results, and the many that follow, justify the approach for using bounding dimensions in the Certificate of Compliance. Where margins permit, the Zircaloy water rod tubes (BWR assemblies) are artificially replaced by water in the bounding cases to remove the requirement for water rod thickness from the Certificate of Compliance.

As mentioned, the bounding approach used in these analyses often results in a maximum k_{eff} value for a given class of assemblies that is much greater than the reactivity of any of the actual (real) assemblies within the class, and yet, is still below the 0.95 regulatory limit.

6.2.2 PWR Fuel Assemblies in the MPC-24

For PWR fuel assemblies (specifications listed in Table 6.2.2) the 15x15F01 fuel assembly at 4.1% enrichment has the highest reactivity (maximum k_{eff} of 0.9478). The 17x17A01 assembly (otherwise known as a Westinghouse 17x17 OFA) has a similar reactivity (see Table 6.2.16) and was used throughout this criticality evaluation as a reference PWR assembly. The 17x17A01 assembly is a representative PWR fuel assembly in terms of design and reactivity and is useful for the reactivity studies presented in Sections 6.3 and 6.4. Calculations for the various PWR fuel assemblies in the MPC-24 are summarized in Tables 6.2.4 through 6.2.19 for the fully flooded condition.

Tables 6.2.4 through 6.2.19 show the maximum k_{eff} values for the assembly classes that are acceptable for storage in the MPC-24. All maximum k_{eff} values include the bias, uncertainties, and calculational statistics, evaluated for the worst combination of manufacturing tolerances. All calculations for the MPC-24 were performed for a ^{10}B loading of 0.020 g/cm^2 , which is 75% of the minimum loading, 0.0267 g/cm^2 , specified on BM-1478, Bill of Materials for 24-Assembly HI-STAR 100 PWR MPC, in Section 1.5. The maximum allowable enrichment in the MPC-24 varies from 4.0 to 4.6 wt% ^{235}U , depending on the assembly class, and is defined in Tables 6.2.4

through 6.2.19. It should be noted that the maximum allowable enrichment does not vary within an assembly class. Table 6.1.1 summarizes the maximum allowable enrichments for each of the assembly classes that are acceptable for storage in the MPC-24.

Tables 6.2.4 through 6.2.19 are formatted with the assembly class information in the top row, the unique assembly designations, dimensions, and k_{eff} values in the following rows above the bold double lines, and the bounding dimensions selected for the Certificate of Compliance and corresponding bounding k_{eff} values in the final rows. Where the bounding assembly corresponds directly to one of the actual assemblies, the fuel assembly designation is listed in the bottom row in parentheses (e.g., Table 6.2.4). Otherwise, the bounding assembly is given a unique designation. For an assembly class that contains only a single assembly (e.g., 14x14D, see Table 6.2.7), the Certificate of Compliance dimensions are based on the assembly dimensions from that single assembly. All of the maximum k_{eff} values corresponding to the selected bounding dimensions are greater than or equal to those for the actual assembly dimensions and are below the 0.95 regulatory limit.

6.2.3 BWR Fuel Assemblies in the MPC-68

For BWR fuel assemblies (specifications listed in Table 6.2.1) the artificial bounding assembly for the 10x10A assembly class at 4.2% enrichment has the highest reactivity (maximum k_{eff} of 0.9457). Calculations for the various BWR fuel assemblies in the MPC-68 are summarized in Tables 6.2.20 through 6.2.36 for the fully flooded condition. In all cases, the gadolinia (Gd_2O_3) normally incorporated in BWR fuel was conservatively neglected.

For calculations involving BWR assemblies, the use of a uniform (planar-average) enrichment, as opposed to the distributed enrichments normally used in BWR fuel, produces conservative results. Calculations confirming this statement are presented in Appendix 6.B for several representative BWR fuel assembly designs. These calculations justify the specification of planar-average enrichments to define acceptability of BWR fuel for loading into the MPC-68.

Tables 6.2.20 through 6.2.36 show the maximum k_{eff} values for assembly classes that are acceptable for storage in the MPC-68. All maximum k_{eff} values include the bias, uncertainties, and calculational statistics, evaluated for the worst combination of manufacturing tolerances. With the exception of assembly classes 6x6A, 6x6B, 6x6C, 7x7A, and 8x8A, which will be discussed in Section 6.2.4, all calculations for the MPC-68 were performed with a ^{10}B loading of 0.0279 g/cm^2 , which is 75% of the minimum loading, 0.0372 g/cm^2 , specified on BM-1479, Bill of Materials for 68-Assembly HI-STAR 100 BWR MPC, in Section 1.5. Calculations for assembly classes 6x6A, 6x6B, 6x6C, 7x7A, and 8x8A were conservatively performed with a ^{10}B loading of 0.0067 g/cm^2 . The maximum allowable enrichment in the MPC-68 varies from 2.7 to 4.2 wt% ^{235}U , depending on the assembly class. It should be noted that the maximum allowable enrichment does not vary within an assembly class. Table 6.1.2 summarizes the maximum allowable enrichments for all assembly classes that are acceptable for storage in the MPC-68.

Tables 6.2.20 through 6.2.36 are formatted with the assembly class information in the top row, the unique assembly designations, dimensions, and k_{eff} values in the following rows above the bold double lines, and the bounding dimensions selected for the Certificate of Compliance and corresponding bounding k_{eff} values in the final rows. Where an assembly class contains only a single assembly (e.g., 8x8E, see Table 6.2.24), the Certificate of Compliance dimensions are based on the assembly dimensions from that single assembly. For assembly classes that are suspected to contain assemblies with thicker channels (e.g., 120 mils), bounding calculations are also performed to qualify the thicker channels (e.g. 7x7B, see Table 6.2.20). All of the maximum k_{eff} values corresponding to the selected bounding dimensions are shown to be greater than or equal to those for the actual assembly dimensions and are below the 0.95 regulatory limit.

For assembly classes that contain partial length rods (i.e., 9x9A, 10x10A, and 10x10B), calculations were performed for the actual (real) assembly configuration and for the axial segments (assumed to be full length) with and without the partial length rods. In all cases, the axial segment with only the full length rods present (where the partial length rods are absent) is bounding. Therefore, the bounding maximum k_{eff} values reported for assembly classes that contain partial length rods bound the reactivity regardless of the active fuel length of the partial length rods. As a result, the Certificate of Compliance have no minimum requirement for the active fuel length of the partial length rods.

For BWR fuel assembly classes where margins permit, the Zircaloy water rod tubes are artificially replaced by water in the bounding cases to remove the requirement for water rod thickness from the Certificate of Compliance. For these cases, the bounding water rod thickness is listed as zero.

As mentioned, the highest observed maximum k_{eff} value is 0.9457, corresponding to the artificial bounding assembly in the 10x10A assembly class. This assembly has the following bounding characteristics: (1) the partial length rods are assumed to be zero length (most reactive configuration); (2) the channel is assumed to be 120 mils thick; and (3) the active fuel length of the full length rods is 155 inches. Therefore, the maximum reactivity value is bounding compared to any of the real BWR assemblies listed.

6.2.4 Damaged BWR Fuel Assemblies and BWR Fuel Debris

In addition to storing intact PWR and BWR fuel assemblies, the HI-STAR 100 System is designed to store damaged BWR fuel assemblies and BWR fuel debris. Damaged fuel assemblies and fuel debris are defined in Section 2.1.3 and Appendix B to the Certificate of Compliance. Both damaged BWR fuel assemblies and BWR fuel debris are required to be loaded into Damaged Fuel Containers (DFCs) prior to being loaded into the MPC. Two different DFC types with slightly different cross sections are considered. DFCs containing fuel debris must be stored in the MPC-68F. DFCs containing damaged fuel assemblies may be stored in either the MPC-68

or MPC-68F. The criticality evaluation of various possible damaged conditions of the fuel is presented in Subsection 6.4.4 for both DFC types.

Tables 6.2.37 through 6.2.41 show the maximum k_{eff} values for the six assembly classes that may be stored as damaged fuel or fuel debris. All maximum k_{eff} values include the bias, uncertainties, and calculational statistics, evaluated for the worst combination of manufacturing tolerances. All calculations were performed for a ^{10}B loading of 0.0067 g/cm^2 , which is 75% of a minimum loading, 0.0089 g/cm^2 . However, because the practical manufacturing lower limit for minimum ^{10}B loading is 0.01 g/cm^2 , the minimum ^{10}B loading of 0.01 g/cm^2 is specified on BM-1479, Bill of Materials for 68-Assembly HI-STAR 100 BWR MPC, in Section 1.5, for the MPC-68F. As an additional level of conservatism in the analyses, the calculations were performed for an enrichment of 3.0 wt% ^{235}U , while the maximum allowable enrichment for these assembly classes is limited to 2.7 wt% ^{235}U in the Certificate of Compliance. Therefore, the maximum k_{eff} values for damaged BWR fuel assemblies and fuel debris are conservative. Calculations for the various BWR fuel assemblies in the MPC-68F are summarized in Tables 6.2.37 through 6.2.41 for the fully flooded condition.

For the assemblies that may be stored as damaged fuel or fuel debris, the 6x6C01 assembly at 3.0 wt% ^{235}U enrichment has the highest reactivity (maximum k_{eff} of 0.8021). Considering all of the conservatism built into this analysis (e.g., higher than allowed enrichment and lower than actual ^{10}B loading), the actual reactivity will be lower.

Because the analysis for the damaged BWR fuel assemblies and fuel debris was performed for a ^{10}B loading of 0.0089 g/cm^2 , which conservatively bounds damaged BWR fuel assemblies in a standard MPC-68 with a minimum ^{10}B loading of 0.0372 g/cm^2 , damaged BWR fuel assemblies may also be stored in the standard MPC-68. However, fuel debris is limited to the MPC-68F by Appendix B to the Certificate of Compliance.

Tables 6.2.37 through 6.2.41 are formatted with the assembly class information in the top row, the unique assembly designations, dimensions, and k_{eff} values in the following rows above the bold double lines, and the bounding dimensions selected for the Certificate of Compliance and corresponding bounding k_{eff} values in the final rows. Where an assembly class contains only a single assembly (e.g., 6x6C, see Table 6.2.39), the Certificate of Compliance dimensions are based on the assembly dimensions from that single assembly. All of the maximum k_{eff} values corresponding to the selected bounding dimensions are greater than or equal to those for the actual assembly dimensions and are well below the 0.95 regulatory limit.

6.2.5 Thoria Rod Canister

Additionally, the HI-STAR 100 System is designed to store a Thoria Rod Canister in the MPC68 or MPC68F. The canister is similar to a DFC and contains 18 intact Thoria Rods placed in a separator assembly. The reactivity of the canister in the MPC68 or MPC68F is very low compared to the reactivity of the approved fuel assemblies (The ^{235}U content of these rods

corresponds to UO₂ rods with an initial enrichment of approximately 1.7 wt% ²³⁵U). It is therefore permissible to store the Thoria Rod Canister together with any other approved content in a MPC68 or MPC68F. Specifications of the canister and the Thoria Rods that are used in the criticality evaluation are given in Table 6.2.42. The criticality evaluation is presented in Subsection 6.4.6.

Table 6.2.1 (page 1 of 6)
BWR FUEL CHARACTERISTICS AND ASSEMBLY CLASS DEFINITIONS
(all dimensions are in inches)

Fuel Assembly Designation	Clad Material	Pitch	Number of Fuel Rods	Cladding OD	Cladding Thickness	Pellet Diameter	Active Fuel Length	Number of Water Rods	Water Rod OD	Water Rod ID	Channel Thickness	Channel ID
6x6A Assembly Class												
6x6A01	Zr	0.694	36	0.5645	0.0350	0.4940	110.0	0	n/a	n/a	0.060	4.290
6x6A02	Zr	0.694	36	0.5645	0.0360	0.4820	110.0	0	n/a	n/a	0.060	4.290
6x6A03	Zr	0.694	36	0.5645	0.0350	0.4820	110.0	0	n/a	n/a	0.060	4.290
6x6A04	Zr	0.694	36	0.5550	0.0350	0.4820	110.0	0	n/a	n/a	0.060	4.290
6x6A05	Zr	0.696	36	0.5625	0.0350	0.4820	110.0	0	n/a	n/a	0.060	4.290
6x6A06	Zr	0.696	35	0.5625	0.0350	0.4820	110.0	1	0.0	0.0	0.060	4.290
6x6A07	Zr	0.700	36	0.5555	0.03525	0.4780	110.0	0	n/a	n/a	0.060	4.290
6x6A08	Zr	0.710	36	0.5625	0.0260	0.4980	110.0	0	n/a	n/a	0.060	4.290
6x6B (MOX) Assembly Class												
6x6B01	Zr	0.694	36	0.5645	0.0350	0.4820	110.0	0	n/a	n/a	0.060	4.290
6x6B02	Zr	0.694	36	0.5625	0.0350	0.4820	110.0	0	n/a	n/a	0.060	4.290
6x6B03	Zr	0.696	36	0.5625	0.0350	0.4820	110.0	0	n/a	n/a	0.060	4.290
6x6B04	Zr	0.696	35	0.5625	0.0350	0.4820	110.0	1	0.0	0.0	0.060	4.290
6x6B05	Zr	0.710	35	0.5625	0.0350	0.4820	110.0	1	0.0	0.0	0.060	4.290
6x6C Assembly Class												
6x6C01	Zr	0.740	36	0.5630	0.0320	0.4880	77.5	0	n/a	n/a	0.060	4.542
7x7A Assembly Class												
7x7A01	Zr	0.631	49	0.4860	0.0328	0.4110	80	0	n/a	n/a	0.060	4.542

Table 6.2.1 (page 2 of 6)
 BWR FUEL CHARACTERISTICS AND ASSEMBLY CLASS DEFINITIONS
 (all dimensions are in inches)

Fuel Assembly Designation	Clad Material	Pitch	Number of Fuel Rods	Cladding OD	Cladding Thickness	Pellet Diameter	Active Fuel Length	Number of Water Rods	Water Rod OD	Water Rod ID	Channel Thickness	Channel ID
7x7B Assembly Class												
7x7B01	Zr	0.738	49	0.5630	0.0320	0.4870	150	0	n/a	n/a	0.080	5.278
7x7B02	Zr	0.738	49	0.5630	0.0370	0.4770	150	0	n/a	n/a	0.102	5.291
7x7B03	Zr	0.738	49	0.5630	0.0370	0.4770	150	0	n/a	n/a	0.080	5.278
7x7B04	Zr	0.738	49	0.5700	0.0355	0.4880	150	0	n/a	n/a	0.080	5.278
7x7B05	Zr	0.738	49	0.5630	0.0340	0.4775	150	0	n/a	n/a	0.080	5.278
7x7B06	Zr	0.738	49	0.5700	0.0355	0.4910	150	0	n/a	n/a	0.080	5.278
8x8A Assembly Class												
8x8A01	Zr	0.523	64	0.4120	0.0250	0.3580	110	0	n/a	n/a	0.100	4.290
8x8A02	Zr	0.523	63	0.4120	0.0250	0.3580	120	0	n/a	n/a	0.100	4.290

Table 6.2.1 (page 3 of 6)
 BWR FUEL CHARACTERISTICS AND ASSEMBLY CLASS DEFINITIONS
 (all dimensions are in inches)

Fuel Assembly Designation	Clad Material	Pitch	Number of Fuel Rods	Cladding OD	Cladding Thickness	Pellet Diameter	Active Fuel Length	Number of Water Rods	Water Rod OD	Water Rod ID	Channel Thickness	Channel ID
8x8B Assembly Class												
8x8B01	Zr	0.641	63	0.4840	0.0350	0.4050	150	1	0.484	0.414	0.100	5.278
8x8B02	Zr	0.636	63	0.4840	0.0350	0.4050	150	1	0.484	0.414	0.100	5.278
8x8B03	Zr	0.640	63	0.4930	0.0340	0.4160	150	1	0.493	0.425	0.100	5.278
8x8B04	Zr	0.642	64	0.5015	0.0360	0.4195	150	0	n/a	n/a	0.100	5.278
8x8C Assembly Class												
8x8C01	Zr	0.641	62	0.4840	0.0350	0.4050	150	2	0.484	0.414	0.100	5.278
8x8C02	Zr	0.640	62	0.4830	0.0320	0.4100	150	2	0.591	0.531	0.000	no channel
8x8C03	Zr	0.640	62	0.4830	0.0320	0.4100	150	2	0.591	0.531	0.080	5.278
8x8C04	Zr	0.640	62	0.4830	0.0320	0.4100	150	2	0.591	0.531	0.100	5.278
8x8C05	Zr	0.640	62	0.4830	0.0320	0.4100	150	2	0.591	0.531	0.120	5.278
8x8C06	Zr	0.640	62	0.4830	0.0320	0.4110	150	2	0.591	0.531	0.100	5.278
8x8C07	Zr	0.640	62	0.4830	0.0340	0.4100	150	2	0.591	0.531	0.100	5.278
8x8C08	Zr	0.640	62	0.4830	0.0320	0.4100	150	2	0.493	0.425	0.100	5.278
8x8C09	Zr	0.640	62	0.4930	0.0340	0.4160	150	2	0.493	0.425	0.100	5.278
8x8C10	Zr	0.640	62	0.4830	0.0340	0.4100	150	2	0.591	0.531	0.120	5.278
8x8C11	Zr	0.640	62	0.4830	0.0340	0.4100	150	2	0.591	0.531	0.120	5.215
8x8C12	Zr	0.636	62	0.4830	0.0320	0.4110	150	2	0.591	0.531	0.120	5.215

Table 6.2.1 (page 4 of 6)
 BWR FUEL CHARACTERISTICS AND ASSEMBLY CLASS DEFINITIONS
 (all dimensions are in inches)

Fuel Assembly Designation	Clad Material	Pitch	Number of Fuel Rods	Cladding OD	Cladding Thickness	Pellet Diameter	Active Fuel Length	Number of Water Rods	Water Rod OD	Water Rod ID	Channel Thickness	Channel ID
8x8D Assembly Class												
8x8D01	Zr	0.640	60	0.4830	0.0320	0.4110	150	2 large/ 2 small	0.591/ 0.483	0.531/ 0.433	0.100	5.278
8x8D02	Zr	0.640	60	0.4830	0.0320	0.4110	150	4	0.591	0.531	0.100	5.278
8x8D03	Zr	0.640	60	0.4830	0.0320	0.4110	150	4	0.483	0.433	0.100	5.278
8x8D04	Zr	0.640	60	0.4830	0.0320	0.4110	150	1	1.34	1.26	0.100	5.278
8x8D05	Zr	0.640	60	0.4830	0.0320	0.4100	150	1	1.34	1.26	0.100	5.278
8x8D06	Zr	0.640	60	0.4830	0.0320	0.4110	150	1	1.34	1.26	0.120	5.278
8x8D07	Zr	0.640	60	0.4830	0.0320	0.4110	150	1	1.34	1.26	0.080	5.278
8x8D08	Zr	0.640	61	0.4830	0.0300	0.4140	150	3	0.591	0.531	0.080	5.278
8x8E Assembly Class												
8x8E01	Zr	0.640	59	0.4930	0.0340	0.4160	150	5	0.493	0.425	0.100	5.278
8x8F Assembly Class.												
8x8F01	Zr	0.609	64	0.4576	0.0290	0.3913	150	4 [†]	0.291 [†]	0.228 [†]	0.055	5.390
9x9A Assembly Class												
9x9A01	Zr	0.566	74	0.4400	0.0280	0.3760	150	2	0.98	0.92	0.100	5.278
9x9A02	Zr	0.566	66	0.4400	0.0280	0.3760	150	2	0.98	0.92	0.100	5.278
9x9A03	Zr	0.566	74/66	0.4400	0.0280	0.3760	150/90	2	0.98	0.92	0.100	5.278
9x9A04	Zr	0.566	74/66	0.4400	0.0280	0.3760	150/90	2	0.98	0.92	0.120	5.278

[†] Four rectangular water cross segments dividing the assembly into four quadrants

Table 6.2.1 (page 5 of 6)
BWR FUEL CHARACTERISTICS AND ASSEMBLY CLASS DEFINITIONS
(all dimensions are in inches)

Fuel Assembly Designation	Clad Material	Pitch	Number of Fuel Rods	Cladding OD	Cladding Thickness	Pellet Diameter	Active Fuel Length	Number of Water Rods	Water Rod OD	Water Rod ID	Channel Thickness	Channel ID
9x9B Assembly Class												
9x9B01	Zr	0.569	72	0.4330	0.0262	0.3737	150	1	1.516	1.459	0.100	5.278
9x9B02	Zr	0.569	72	0.4330	0.0260	0.3737	150	1	1.516	1.459	0.100	5.278
9x9B03	Zr	0.572	72	0.4330	0.0260	0.3737	150	1	1.516	1.459	0.100	5.278
9x9C Assembly Class												
9x9C01	Zr	0.572	80	0.4230	0.0295	0.3565	150	1	0.512	0.472	0.100	5.278
9x9D Assembly Class												
9x9D01	Zr	0.572	79	0.4240	0.0300	0.3565	150	2	0.424	0.364	0.100	5.278
9x9E Assembly Class [†]												
9x9E01	Zr	0.572	76	0.4170	0.0265	0.3530	150	5	0.546	0.522	0.120	5.215
9x9E02	Zr	0.572	48 28	0.4170 0.4430	0.0265 0.0285	0.3530 0.3745	150	5	0.546	0.522	0.120	5.215
9x9F Assembly Class [†]												
9x9F01	Zr	0.572	76	0.4430	0.0285	0.3745	150	5	0.546	0.522	0.120	5.215
9x9F02	Zr	0.572	48 28	0.4170 0.4430	0.0265 0.0285	0.3530 0.3745	150	5	0.546	0.522	0.120	5.215

[†] The 9x9E and 9x9F fuel assembly classes represent a single fuel type containing fuel rods with different dimensions (SPC 9x9-5). In addition to the actual configuration (9x9E02 and 9x9F02), the 9x9E class contains a hypothetical assembly with only small fuel rods (9x9E01), and the 9x9F class contains a hypothetical assembly with only large rods (9x9F01). This was done in order to simplify the specification of this assembly in the CoC.

Table 6.2.1 (page 6 of 6)
 BWR FUEL CHARACTERISTICS AND ASSEMBLY CLASS DEFINITIONS
 (all dimensions are in inches)

Fuel Assembly Designation	Clad Material	Pitch	Number of Fuel Rods	Cladding OD	Cladding Thickness	Pellet Diameter	Active Fuel Length	Number of Water Rods	Water Rod OD	Water Rod ID	Channel Thickness	Channel ID
10x10A Assembly Class												
10x10A01	Zr	0.510	92	0.4040	0.0260	0.3450	155	2	0.980	0.920	0.100	5.278
10x10A02	Zr	0.510	78	0.4040	0.0260	0.3450	155	2	0.980	0.920	0.100	5.278
10x10A03	Zr	0.510	92/78	0.4040	0.0260	0.3450	155/90	2	0.980	0.920	0.100	5.278
10x10B Assembly Class												
10x10B01	Zr	0.510	91	0.3957	0.0239	0.3413	155	1	1.378	1.321	0.100	5.278
10x10B02	Zr	0.510	83	0.3957	0.0239	0.3413	155	1	1.378	1.321	0.100	5.278
10x10B03	Zr	0.510	91/83	0.3957	0.0239	0.3413	155/90	1	1.378	1.321	0.100	5.278
10x10C Assembly Class												
10x10C01	Zr	0.488	96	0.3780	0.0243	0.3224	150	5	1.227	1.165	0.055	5.457
10x10D Assembly Class												
10x10D01	SS	0.565	100	0.3960	0.0200	0.3500	83	0	n/a	n/a	0.08	5.663
10x10E Assembly Class												
10x10E01	SS	0.557	96	0.3940	0.0220	0.3430	83	4	0.3940	0.3500	0.08	5.663

Table 6.2.2 (page 1 of 3)
PWR FUEL CHARACTERISTICS AND ASSEMBLY CLASS DEFINITIONS
(all dimensions are in inches)

Fuel Assembly Designation	Clad Material	Pitch	Number of Fuel Rods	Cladding OD	Cladding Thickness	Pellet Diameter	Active Fuel Length	Number of Guide Tubes	Guide Tube OD	Guide Tube ID	Guide Tube Thickness
14x14A Assembly Class											
14x14A01	Zr	0.556	179	0.400	0.0243	0.3444	150	17	0.527	0.493	0.0170
14x14A02	Zr	0.556	179	0.400	0.0243	0.3444	150	17	0.528	0.490	0.0190
14x14A03	Zr	0.556	179	0.400	0.0243	0.3444	150	17	0.526	0.492	0.0170
14x14B Assembly Class											
14x14B01	Zr	0.556	179	0.422	0.0243	0.3659	150	17	0.539	0.505	0.0170
14x14B02	Zr	0.556	179	0.417	0.0295	0.3505	150	17	0.541	0.507	0.0170
14x14B03	Zr	0.556	179	0.424	0.0300	0.3565	150	17	0.541	0.507	0.0170
14x14B04	Zr	0.556	179	0.426	0.0310	0.3565	150	17	0.541	0.507	0.0170
14x14C Assembly Class											
14x14C01	Zr	0.580	176	0.440	0.0280	0.3765	150	5	1.115	1.035	0.0400
14x14C02	Zr	0.580	176	0.440	0.0280	0.3770	150	5	1.115	1.035	0.0400
14x14C03	Zr	0.580	176	0.440	0.0260	0.3805	150	5	1.111	1.035	0.0380
14x14D Assembly Class											
14x14D01	SS	0.556	180	0.422	0.0165	0.3835	144	16	0.543	0.514	0.0145
15x15A Assembly Class											
15x15A01	Zr	0.550	204	0.418	0.0260	0.3580	150	21	0.533	0.500	0.0165

Table 6.2.2 (page 2 of 3)
PWR FUEL CHARACTERISTICS AND ASSEMBLY CLASS DEFINITIONS
(all dimensions are in inches)

Fuel Assembly Designation	Clad Material	Pitch	Number of Fuel Rods	Cladding OD	Cladding Thickness	Pellet Diameter	Active Fuel Length	Number of Guide Tubes	Guide Tube OD	Guide Tube ID	Guide Tube Thickness
15x15B Assembly Class											
15x15B01	Zr	0.563	204	0.422	0.0245	0.3660	150	21	0.533	0.499	0.0170
15x15B02	Zr	0.563	204	0.422	0.0245	0.3660	150	21	0.546	0.512	0.0170
15x15B03	Zr	0.563	204	0.422	0.0243	0.3660	150	21	0.533	0.499	0.0170
15x15B04	Zr	0.563	204	0.422	0.0243	0.3659	150	21	0.545	0.515	0.0150
15x15B05	Zr	0.563	204	0.422	0.0242	0.3659	150	21	0.545	0.515	0.0150
15x15B06	Zr	0.563	204	0.420	0.0240	0.3671	150	21	0.544	0.514	0.0150
15x15C Assembly Class											
15x15C01	Zr	0.563	204	0.424	0.0300	0.3570	150	21	0.544	0.493	0.0255
15x15C02	Zr	0.563	204	0.424	0.0300	0.3570	150	21	0.544	0.511	0.0165
15x15C03	Zr	0.563	204	0.424	0.0300	0.3565	150	21	0.544	0.511	0.0165
15x15C04	Zr	0.563	204	0.417	0.0300	0.3565	150	21	0.544	0.511	0.0165
15x15D Assembly Class											
15x15D01	Zr	0.568	208	0.430	0.0265	0.3690	150	17	0.530	0.498	0.0160
15x15D02	Zr	0.568	208	0.430	0.0265	0.3686	150	17	0.530	0.498	0.0160
15x15D03	Zr	0.568	208	0.430	0.0265	0.3700	150	17	0.530	0.499	0.0155
15x15D04	Zr	0.568	208	0.430	0.0250	0.3735	150	17	0.530	0.500	0.0150
15x15E Assembly Class											
15x15E01	Zr	0.568	208	0.428	0.0245	0.3707	150	17	0.528	0.500	0.0140
15x15F Assembly Class											
15x15F01	Zr	0.568	208	0.428	0.0230	0.3742	150	17	0.528	0.500	0.0140

Table 6.2.2 (page 3 of 3)
PWR FUEL CHARACTERISTICS AND ASSEMBLY CLASS DEFINITIONS
(all dimensions are in inches)

Fuel Assembly Designation	Clad Material	Pitch	Number of Fuel Rods	Cladding OD	Cladding Thickness	Pellet Diameter	Active Fuel Length	Number of Guide Tubes	Guide Tube OD	Guide Tube ID	Guide Tube Thickness
15x15G Assembly Class											
15x15G01	SS	0.563	204	0.422	0.0165	0.3825	144	21	0.543	0.514	0.0145
15x15H Assembly Class											
15x15H01	Zr	0.568	208	0.414	0.0220	0.3622	150	17	0.528	0.500	0.0140
16x16A Assembly Class											
16x16A01	Zr	0.506	236	0.382	0.0250	0.3255	150	5	0.980	0.900	0.0400
16x16A02	Zr	0.506	236	0.382	0.0250	0.3250	150	5	0.980	0.900	0.0400
17x17A Assembly Class											
17x17A01	Zr	0.496	264	0.360	0.0225	0.3088	144	25	0.474	0.442	0.0160
17x17A02	Zr	0.496	264	0.360	0.0225	0.3088	150	25	0.474	0.442	0.0160
17x17A03	Zr	0.496	264	0.360	0.0250	0.3030	150	25	0.480	0.448	0.0160
17x17B Assembly Class											
17x17B01	Zr	0.496	264	0.374	0.0225	0.3225	150	25	0.482	0.450	0.0160
17x17B02	Zr	0.496	264	0.374	0.0225	0.3225	150	25	0.474	0.442	0.0160
17x17B03	Zr	0.496	264	0.376	0.0240	0.3215	150	25	0.480	0.448	0.0160
17x17B04	Zr	0.496	264	0.372	0.0205	0.3232	150	25	0.427	0.399	0.0140
17x17B05	Zr	0.496	264	0.374	0.0240	0.3195	150	25	0.482	0.450	0.0160
17x17B06	Zr	0.496	264	0.372	0.0205	0.3232	150	25	0.480	0.452	0.0140
17x17C Assembly Class											
17x17C01	Zr	0.502	264	0.379	0.0240	0.3232	150	25	0.472	0.432	0.0200
17x17C02	Zr	0.502	264	0.377	0.0220	0.3252	150	25	0.472	0.432	0.0200

Table 6.2.3
 REACTIVITY EFFECT OF ASSEMBLY PARAMETER VARIATIONS
 (all dimensions are in inches)

Fuel Assembly/ Parameter Variation	reactivity effect	calculated k_{eff}	standard deviation	cladding OD	cladding ID	cladding thickness	pellet OD	water rod thickness	channel thickness
8x8C04 (GE8x8R)	reference	0.9307	0.0007	0.483	0.419	0.032	0.410	0.030	0.100
increase pellet OD (+0.001)	+0.0005	0.9312	0.0007	0.483	0.419	0.032	0.411	0.030	0.100
decrease pellet OD (-0.001)	-0.0008	0.9299	0.0009	0.483	0.419	0.032	0.409	0.030	0.100
increase clad ID (+0.004)	+0.0027	0.9334	0.0007	0.483	0.423	0.030	0.410	0.030	0.100
decrease clad ID (-0.004)	-0.0034	0.9273	0.0007	0.483	0.415	0.034	0.410	0.030	0.100
increase clad OD (+0.004)	-0.0041	0.9266	0.0008	0.487	0.419	0.034	0.410	0.030	0.100
decrease clad OD (-0.004)	+0.0023	0.9330	0.0007	0.479	0.419	0.030	0.410	0.030	0.100
increase water rod thickness (+0.015)	-0.0019	0.9288	0.0008	0.483	0.419	0.032	0.410	0.045	0.100
decrease water rod thickness (-0.015)	+0.0001	0.9308	0.0008	0.483	0.419	0.032	0.410	0.015	0.100
remove water rods (i.e., replace the water rod tubes with water)	+0.0021	0.9328	0.0008	0.483	0.419	0.032	0.410	0.000	0.100
remove channel	-0.0039	0.9268	0.0009	0.483	0.419	0.032	0.410	0.030	0.000
increase channel thickness (+0.020)	+0.0005	0.9312	0.0007	0.483	0.419	0.032	0.410	0.030	0.120

Table 6.2.4
 MAXIMUM K_{EFF} VALUES FOR THE 14X14A ASSEMBLY CLASS IN THE MPC-24
 (all dimensions are in inches)

14x14A (4.6% Enrichment, Boral ^{10}B minimum loading of 0.02 g/cm ²)									
179 fuel rods, 17 guide tubes, pitch=0.556, Zr clad									
Fuel Assembly Designation	maximum k_{eff}	calculated k_{eff}	standard deviation	cladding OD	cladding ID	cladding thickness	pellet OD	fuel length	guide tube thickness
14x14A01	0.9378	0.9332	0.0010	0.400	0.3514	0.0243	0.3444	150	0.017
14x14A02	0.9374	0.9328	0.0009	0.400	0.3514	0.0243	0.3444	150	0.019
14x14A03	0.9383	0.9340	0.0008	0.400	0.3514	0.0243	0.3444	150	0.017
Dimensions Listed in Certificate of Compliance				0.400 (min.)	0.3514 (max.)		0.3444 (max.)	150 (max.)	0.017 (min.)
bounding dimensions (14x14A03)	0.9383	0.9340	0.0008	0.400	0.3514	0.0243	0.3444	150	0.017

Table 6.2.5
 MAXIMUM K_{EFF} VALUES FOR THE 14X14B ASSEMBLY CLASS IN THE MPC-24
 (all dimensions are in inches)

14x14B (4.6% Enrichment, Boral ^{10}B minimum loading of 0.02 g/cm ²)									
179 fuel rods, 17 guide tubes, pitch=0.556, Zr clad									
Fuel Assembly Designation	maximum k_{eff}	calculated k_{eff}	standard deviation	cladding OD	cladding ID	cladding thickness	pellet OD	fuel length	guide tube thickness
14x14B01	0.9268	0.9225	0.0008	0.422	0.3734	0.0243	0.3659	150	0.017
14x14B02	0.9243	0.9200	0.0008	0.417	0.3580	0.0295	0.3505	150	0.017
14x14B03	0.9196	0.9152	0.0009	0.424	0.3640	0.0300	0.3565	150	0.017
14x14B04	0.9163	0.9118	0.0009	0.426	0.3640	0.0310	0.3565	150	0.017
Dimensions Listed in Certificate of Compliance				0.417 (min.)	0.3734 (max.)		0.3659 (max.)	150 (max.)	0.017 (min.)
bounding dimensions (B14x14B01)	0.9323	0.9280	0.0008	0.417	0.3734	0.0218	0.3659	150	0.017

Table 6.2.6
 MAXIMUM K_{EFF} VALUES FOR THE 14X14C ASSEMBLY CLASS IN THE MPC-24
 (all dimensions are in inches)

14x14C (4.6% Enrichment, Boral ^{10}B minimum loading of 0.02 g/cm ²)									
176 fuel rods, 5 guide tubes, pitch=0.580, Zr clad									
Fuel Assembly Designation	maximum k_{eff}	calculated k_{eff}	standard deviation	cladding OD	cladding ID	cladding thickness	pellet OD	fuel length	guide tube thickness
14x14C01	0.9361	0.9317	0.0009	0.440	0.3840	0.0280	0.3765	150	0.040
14x14C02	0.9355	0.9312	0.0008	0.440	0.3840	0.0280	0.3770	150	0.040
14x14C03	0.9400	0.9357	0.0008	0.440	0.3880	0.0260	0.3805	150	0.038
Dimensions Listed in Certificate of Compliance				0.440 (min.)	0.3880 (max.)		0.3805 (max.)	150 (max.)	0.038 (min.)
bounding dimensions (14x14C01)	0.9400	0.9357	0.0008	0.440	0.3880	0.0260	0.3805	150	0.038

Table 6.2.7
 MAXIMUM K_{EFF} VALUES FOR THE 14X14D ASSEMBLY CLASS IN THE MPC-24
 (all dimensions are in inches)

14x14D (4.0% Enrichment, Boral ^{10}B minimum loading of 0.02 g/cm ²)									
180 fuel rods, 16 guide tubes, pitch=0.556, SS clad									
Fuel Assembly Designation	maximum k_{eff}	calculated k_{eff}	standard deviation	cladding OD	cladding ID	cladding thickness	pellet OD	fuel length	guide tube thickness
14x14D01	0.8576	0.8536	0.0007	0.422	0.3890	0.0165	0.3835	144	0.0145
Dimensions Listed in Certificate of Compliance				0.422 (min.)	0.3890 (max.)		0.3835 (max.)	144 (max.)	0.0145 (min.)

Table 6.2.8
 MAXIMUM K_{EFF} VALUES FOR THE 15X15A ASSEMBLY CLASS IN THE MPC-24
 (all dimensions are in inches)

15x15A (4.1% Enrichment, Boral ^{10}B minimum loading of 0.02 g/cm ²)									
204 fuel rods, 21 guide tubes, pitch=0.550, Zr clad									
Fuel Assembly Designation	maximum k_{eff}	calculated k_{eff}	standard deviation	cladding OD	cladding ID	cladding thickness	pellet OD	fuel length	guide tube thickness
15x15A01	0.9301	0.9259	0.0008	0.418	0.3660	0.0260	0.3580	150	0.0165
Dimensions Listed in Certificate of Compliance				0.418 (min.)	0.3660 (max.)		0.3580 (max.)	150 (max.)	0.0165 (min.)

Table 6.2.9
 MAXIMUM K_{EFF} VALUES FOR THE 15X15B ASSEMBLY CLASS IN THE MPC-24
 (all dimensions are in inches)

15x15B (4.1% Enrichment, Boral ^{10}B minimum loading of 0.02 g/cm ²)									
204 fuel rods, 21 guide tubes, pitch=0.563, Zr clad									
Fuel Assembly Designation	maximum k_{eff}	calculated k_{eff}	standard deviation	cladding OD	cladding ID	cladding thickness	pellet OD	fuel length	guide tube thickness
15x15B01	0.9427	0.9384	0.0008	0.422	0.3730	0.0245	0.3660	150	0.017
15x15B02	0.9441	0.9396	0.0009	0.422	0.3730	0.0245	0.3660	150	0.017
15x15B03	0.9462	0.9420	0.0008	0.422	0.3734	0.0243	0.3660	150	0.017
15x15B04	0.9452	0.9407	0.0009	0.422	0.3734	0.0243	0.3659	150	0.015
15x15B05	0.9473	0.9431	0.0008	0.422	0.3736	0.0242	0.3659	150	0.015
15x15B06	0.9448	0.9404	0.0008	0.420	0.3720	0.0240	0.3671	150	0.015
Dimensions Listed in Certificate of Compliance				0.420 (min.)	0.3736 (max.)		0.3671 (max.)	150 (max.)	0.015 (min.)
bounding dimensions (B15x15B01)	0.9471 [†]	0.9428	0.0008	0.420	0.3736	0.0232	0.3671	150	0.015

[†] The k_{eff} value listed for the 15x15B05 case is slightly higher than that for the case with the bounding dimensions. However, the difference (0.0002) is well within the statistical uncertainties, and thus, the two values are statistically equivalent (within 1σ). Therefore, the 0.9473 value is listed in Table 6.1.1 as the maximum.

Table 6.2.10
 MAXIMUM K_{EFF} VALUES FOR THE 15X15C ASSEMBLY CLASS IN THE MPC-24
 (all dimensions are in inches)

15x15C (4.1% Enrichment, Boral ^{10}B minimum loading of 0.02 g/cm^2)									
204 fuel rods, 21 guide tubes, pitch=0.563, Zr clad									
Fuel Assembly Designation	maximum k_{eff}	calculated k_{eff}	standard deviation	cladding OD	cladding ID	cladding thickness	pellet OD	fuel length	guide tube thickness
15x15C01	0.9332	0.9290	0.0007	0.424	0.3640	0.0300	0.3570	150	0.0255
15x15C02	0.9373	0.9330	0.0008	0.424	0.3640	0.0300	0.3570	150	0.0165
15x15C03	0.9377	0.9335	0.0007	0.424	0.3640	0.0300	0.3565	150	0.0165
15x15C04	0.9378	0.9338	0.0007	0.417	0.3570	0.0300	0.3565	150	0.0165
Dimensions Listed in Certificate of Compliance				0.417 (min.)	0.3640 (max.)		0.3570 (max.)	150 (max.)	0.0165 (min.)
bounding dimensions (B15x15C01)	0.9444	0.9401	0.0008	0.417	0.3640	0.0265	0.3570	150	0.0165

Table 6.2.11
 MAXIMUM K_{EFF} VALUES FOR THE 15X15D ASSEMBLY CLASS IN THE MPC-24
 (all dimensions are in inches)

15x15D (4.1% Enrichment, Boral ^{10}B minimum loading of 0.02 g/cm ²)									
208 fuel rods, 17 guide tubes, pitch=0.568, Zr clad									
Fuel Assembly Designation	maximum k_{eff}	calculated k_{eff}	standard deviation	cladding OD	cladding ID	cladding thickness	pellet OD	fuel length	guide tube thickness
15x15D01	0.9423	0.9380	0.0008	0.430	0.3770	0.0265	0.3690	150	0.0160
15x15D02	0.9430	0.9386	0.0009	0.430	0.3770	0.0265	0.3686	150	0.0160
15x15D03	0.9419	0.9375	0.0009	0.430	0.3770	0.0265	0.3700	150	0.0155
15x15D04	0.9440	0.9398	0.0007	0.430	0.3800	0.0250	0.3735	150	0.0150
Dimensions Listed in Certificate of Compliance				0.430 (min.)	0.3800 (max.)		0.3735 (max.)	150 (max.)	0.0150 (min.)
bounding dimensions (15x15D04)	0.9440	0.9398	0.0007	0.430	0.3800	0.0250	0.3735	150	0.0150

Table 6.2.12
 MAXIMUM K_{EFF} VALUES FOR THE 15X15E ASSEMBLY CLASS IN THE MPC-24
 (all dimensions are in inches)

15x15E (4.1% Enrichment, Boral ^{10}B minimum loading of 0.02 g/cm ²)									
208 fuel rods, 17 guide tubes, pitch=0.568, Zr clad									
Fuel Assembly Designation	maximum k_{eff}	calculated k_{eff}	standard deviation	cladding OD	cladding ID	cladding thickness	pellet OD	fuel length	guide tube thickness
15x15E01	0.9475	0.9433	0.0007	0.428	0.3790	0.0245	0.3707	150	0.0140
Dimensions Listed in Certificate of Compliance				0.428 (min.)	0.3790 (max.)		0.3707 (max.)	150 (max.)	0.0140 (min.)

Table 6.2.13
 MAXIMUM K_{EFF} VALUES FOR THE 15X15F ASSEMBLY CLASS IN THE MPC-24
 (all dimensions are in inches)

15x15F (4.1% Enrichment, Boral ^{10}B minimum loading of 0.02 g/cm^2)									
208 fuel rods, 17 guide tubes, pitch=0.568, Zr clad									
Fuel Assembly Designation	maximum k_{eff}	calculated k_{eff}	standard deviation	cladding OD	cladding ID	cladding thickness	pellet OD	fuel length	guide tube thickness
15x15F01	0.9478 [†]	0.9436	0.0008	0.428	0.3820	0.0230	0.3742	150	0.0140
Dimensions Listed in Certificate of Compliance				0.428 (min.)	0.3820 (max.)		0.3742 (max.)	150 (max.)	0.0140 (min.)

[†] KENO5a verification calculation resulted in a maximum k_{eff} of 0.9466.

Table 6.2.14
 MAXIMUM K_{EFF} VALUES FOR THE 15X15G ASSEMBLY CLASS IN THE MPC-24
 (all dimensions are in inches)

15x15G (4.0% Enrichment, Boral ^{10}B minimum loading of 0.02 g/cm ²)									
204 fuel rods, 21 guide tubes, pitch=0.563, SS clad									
Fuel Assembly Designation	maximum k_{eff}	calculated k_{eff}	standard deviation	cladding OD	cladding ID	cladding thickness	pellet OD	fuel length	guide tube thickness
15x15G01	0.8986	0.8943	0.0008	0.422	0.3890	0.0165	0.3825	144	0.0145
Dimensions Listed in Certificate of Compliance				0.422 (min.)	0.3890 (max.)		0.3825 (max.)	144 (max.)	0.0145 (min.)

Table 6.2.15
 MAXIMUM K_{EFF} VALUES FOR THE 15X15H ASSEMBLY CLASS IN THE MPC-24
 (all dimensions are in inches)

15x15H (3.8% Enrichment, Boral ^{10}B minimum loading of 0.02 g/cm ²)									
208 fuel rods, 17 guide tubes, pitch=0.568, Zr clad									
Fuel Assembly Designation	maximum k_{eff}	calculated k_{eff}	standard deviation	cladding OD	cladding ID	cladding thickness	pellet OD	fuel length	guide tube thickness
15x15H01	0.9411	0.9368	0.0008	0.414	0.3700	0.0220	0.3622	150	0.0140
Dimensions Listed in Certificate of Compliance				0.414 (min.)	0.3700 (max.)		0.3622 (max.)	150 (max.)	0.0140 (min.)

Table 6.2.16
MAXIMUM K_{EFF} VALUES FOR THE 16X16A ASSEMBLY CLASS IN THE MPC-24
 (all dimensions are in inches)

16x16A (4.6% Enrichment, Boral ^{10}B minimum loading of 0.02 g/cm ²)									
236 fuel rods, 5 guide tubes, pitch=0.506, Zr clad									
Fuel Assembly Designation	maximum k_{eff}	calculated k_{eff}	standard deviation	cladding OD	cladding ID	cladding thickness	pellet OD	fuel length	guide tube thickness
16x16A01	0.9383	0.9339	0.0009	0.382	0.3320	0.0250	0.3255	150	0.0400
16x16A02	0.9371	0.9328	0.0008	0.382	0.3320	0.0250	0.3250	150	0.0400
Dimensions Listed in Certificate of Compliance				0.382 (min.)	0.3320 (max.)		0.3255 (max.)	150 (max.)	0.0400 (min.)
bounding dimensions (16x16A01)	0.9383	0.9339	0.0009	0.382	0.3320	0.0250	0.3255	150	0.0400

Table 6.2.17
 MAXIMUM K_{EFF} VALUES FOR THE 17X17A ASSEMBLY CLASS IN THE MPC-24
 (all dimensions are in inches)

17x17A (4.0% Enrichment, Boral ^{10}B minimum loading of 0.02 g/cm ²)									
264 fuel rods, 25 guide tubes, pitch=0.496, Zr clad									
Fuel Assembly Designation	maximum k_{eff}	calculated k_{eff}	standard deviation	cladding OD	cladding ID	cladding thickness	pellet OD	fuel length	guide tube thickness
17x17A01	0.9449	0.9400	0.0011	0.360	0.3150	0.0225	0.3088	144	0.016
17x17A02	0.9452 [†]	0.9408	0.0008	0.360	0.3150	0.0225	0.3088	150	0.016
17x17A03	0.9406	0.9364	0.0008	0.360	0.3100	0.0250	0.3030	150	0.016
Dimensions Listed in Certificate of Compliance				0.360 (min.)	0.3150 (max.)		0.3088 (max.)	150 (max.)	0.016 (min.)
bounding dimensions (17x17A02)	0.9452	0.9408	0.0008	0.360	0.3150	0.0225	0.3088	150	0.016

[†] KENO5a verification calculation resulted in a maximum k_{eff} of 0.9434.

Table 6.2.18
 MAXIMUM K_{EFF} VALUES FOR THE 17X17B ASSEMBLY CLASS IN THE MPC-24
 (all dimensions are in inches)

17x17B (4.0% Enrichment, Boral ^{10}B minimum loading of 0.02 g/cm ²)									
264 fuel rods, 25 guide tubes, pitch=0.496, Zr clad									
Fuel Assembly Designation	maximum k_{eff}	calculated k_{eff}	standard deviation	cladding OD	cladding ID	cladding thickness	pellet OD	fuel length	guide tube thickness
17x17B01	0.9377	0.9335	0.0008	0.374	0.3290	0.0225	0.3225	150	0.016
17x17B02	0.9379	0.9337	0.0008	0.374	0.3290	0.0225	0.3225	150	0.016
17x17B03	0.9330	0.9288	0.0008	0.376	0.3280	0.0240	0.3215	150	0.016
17x17B04	0.9407	0.9365	0.0007	0.372	0.3310	0.0205	0.3232	150	0.014
17x17B05	0.9349	0.9305	0.0009	0.374	0.3260	0.0240	0.3195	150	0.016
17x17B06	0.9436	0.9393	0.0008	0.372	0.3310	0.0205	0.3232	150	0.014
Dimensions Listed in Certificate of Compliance				0.372 (min.)	0.3310 (max.)		0.3232 (max.)	150 (max.)	0.014 (min.)
bounding dimensions (17x17B06)	0.9436	0.9393	0.0008	0.372	0.3310	0.0205	0.3232	150	0.014

Table 6.2.19
 MAXIMUM K_{EFF} VALUES FOR THE 17X17C ASSEMBLY CLASS IN THE MPC-24
 (all dimensions are in inches)

17x17C (4.0% Enrichment, Boral ^{10}B minimum loading of 0.02 g/cm ²)									
264 fuel rods, 25 guide tubes, pitch=0.502, Zr clad									
Fuel Assembly Designation	maximum k_{eff}	calculated k_{eff}	standard deviation	cladding OD	cladding ID	cladding thickness	pellet OD	fuel length	guide tube thickness
17x17C01	0.9383	0.9339	0.0008	0.379	0.3310	0.0240	0.3232	150	0.020
17x17C02	0.9427	0.9384	0.0008	0.377	0.3330	0.0220	0.3252	150	0.020
Dimensions Listed in Certificate of Compliance				0.377 (min.)	0.3330 (max.)		0.3252 (max.)	150 (max.)	0.020 (min.)
bounding dimensions (17x17C02)	0.9427	0.9384	0.0008	0.377	0.3330	0.0220	0.3252	150	0.020

Table 6.2.20
 MAXIMUM K_{EFF} VALUES FOR THE 7X7B ASSEMBLY CLASS IN THE MPC-68
 (all dimensions are in inches)

7x7B (4.2% Enrichment, Boral ^{10}B minimum loading of 0.0279 g/cm ²)										
49 fuel rods, 0 water rods, pitch=0.738, Zr clad										
Fuel Assembly Designation	maximum k_{eff}	calculated k_{eff}	standard deviation	cladding OD	cladding ID	cladding thickness	pellet OD	fuel length	water rod thickness	channel thickness
7x7B01	0.9372	0.9330	0.0007	0.5630	0.4990	0.0320	0.4870	150	n/a	0.080
7x7B02	0.9301	0.9260	0.0007	0.5630	0.4890	0.0370	0.4770	150	n/a	0.102
7x7B03	0.9313	0.9271	0.0008	0.5630	0.4890	0.0370	0.4770	150	n/a	0.080
7x7B04	0.9311	0.9270	0.0007	0.5700	0.4990	0.0355	0.4880	150	n/a	0.080
7x7B05	0.9350	0.9306	0.0008	0.5630	0.4950	0.0340	0.4775	150	n/a	0.080
7x7B06	0.9298	0.9260	0.0006	0.5700	0.4990	0.0355	0.4910	150	n/a	0.080
Dimensions Listed in Certificate of Compliance				0.5630 (min.)	0.4990 (max.)		0.4910 (max.)	150 (max.)	n/a	0.120 (max.)
bounding dimensions (B7x7B01)	0.9375	0.9332	0.0008	0.5630	0.4990	0.0320	0.4910	150	n/a	0.102
bounding dimensions with 120 mil channel (B7x7B02)	0.9386	0.9344	0.0007	0.5630	0.4990	0.0320	0.4910	150	n/a	0.120

Table 6.2.21
 MAXIMUM K_{EFF} VALUES FOR THE 8X8B ASSEMBLY CLASS IN THE MPC-68
 (all dimensions are in inches)

8x8B (4.2% Enrichment, Boral ^{10}B minimum loading of 0.0279 g/cm ²)												
63 or 64 fuel rods [†] , 1 or 0 water rods [†] , pitch [†] = 0.636-0.642, Zr clad												
Fuel Assembly Designation	maximum k_{eff}	calculated k_{eff}	standard deviation	Fuel rods	pitch	cladding OD	cladding ID	cladding thickness	pellet OD	fuel length	water rod thickness	channel thickness
8x8B01	0.9310	0.9265	0.0009	63	0.641	0.4840	0.4140	0.0350	0.4050	150	0.035	0.100
8x8B02	0.9227	0.9185	0.0007	63	0.636	0.4840	0.4140	0.0350	0.4050	150	0.035	0.100
8x8B03	0.9299	0.9257	0.0008	63	0.640	0.4930	0.4250	0.0340	0.4160	150	0.034	0.100
8x8B04	0.9236	0.9194	0.0008	64	0.642	0.5015	0.4295	0.0360	0.4195	150	n/a	0.100
Dimensions Listed in Certificate of Compliance				63 or 64	0.636-0.642	0.4840 (min.)	0.4295 (max.)		0.4195 (max.)	150 (max.)	0.034	0.120 (max.)
bounding (pitch=0.636) (B8x8B01)	0.9346	0.9301	0.0009	63	0.636	0.4840	0.4295	0.02725	0.4195	150	0.034	0.120
bounding (pitch=0.640) (B8x8B02)	0.9385	0.9343	0.0008	63	0.640	0.4840	0.4295	0.02725	0.4195	150	0.034	0.120
bounding (pitch=0.642) (B8x8B03)	0.9416	0.9375	0.0007	63	0.642	0.4840	0.4295	0.02725	0.4195	150	0.034	0.120

[†] This assembly class was analyzed and qualified for a small variation in the pitch and a variation in the number of fuel and water rods.

Table 6.2.22
 MAXIMUM K_{eff} VALUES FOR THE 8X8C ASSEMBLY CLASS IN THE MPC-68
 (all dimensions are in inches)

8x8C (4.2% Enrichment, Boral ^{10}B minimum loading of 0.0279 g/cm ²)											
62 fuel rods, 2 water rods, pitch [†] = 0.636-0.641, Zr clad											
Fuel Assembly Designation	maximum k_{eff}	calculated k_{eff}	standard deviation	pitch	cladding OD	cladding ID	cladding thickness	pellet OD	fuel length	water rod thickness	channel thickness
8x8C01	0.9315	0.9273	0.0007	0.641	0.4840	0.4140	0.0350	0.4050	150	0.035	0.100
8x8C02	0.9313	0.9268	0.0009	0.640	0.4830	0.4190	0.0320	0.4100	150	0.030	0.000
8x8C03	0.9329	0.9286	0.0008	0.640	0.4830	0.4190	0.0320	0.4100	150	0.030	0.800
8x8C04	0.9348 ^{††}	0.9307	0.0007	0.640	0.4830	0.4190	0.0320	0.4100	150	0.030	0.100
8x8C05	0.9353	0.9312	0.0007	0.640	0.4830	0.4190	0.0320	0.4100	150	0.030	0.120
8x8C06	0.9353	0.9312	0.0007	0.640	0.4830	0.4190	0.0320	0.4110	150	0.030	0.100
8x8C07	0.9314	0.9273	0.0007	0.640	0.4830	0.4150	0.0340	0.4100	150	0.030	0.100
8x8C08	0.9339	0.9298	0.0007	0.640	0.4830	0.4190	0.0320	0.4100	150	0.034	0.100
8x8C09	0.9301	0.9260	0.0007	0.640	0.4930	0.4250	0.0340	0.4160	150	0.034	0.100
8x8C10	0.9317	0.9275	0.0008	0.640	0.4830	0.4150	0.0340	0.4100	150	0.030	0.120
8x8C11	0.9328	0.9287	0.0007	0.640	0.4830	0.4150	0.0340	0.4100	150	0.030	0.120
8x8C12	0.9285	0.9242	0.0008	0.636	0.4830	0.4190	0.0320	0.4110	150	0.030	0.120
Dimensions Listed in Certificate of Compliance				0.636-0.641	0.4830 (min.)	0.4250 (max.)		0.4160 (max.)	150 (max.)	0.000 (min.)	0.120 (max.)
bounding (pitch=0.636) (B8x8C01)	0.9357	0.9313	0.0009	0.636	0.4830	0.4250	0.0290	0.4160	150	0.000	0.120
bounding (pitch=0.640) (B8x8C02)	0.9425	0.9384	0.0007	0.640	0.4830	0.4250	0.0290	0.4160	150	0.000	0.120
Bounding (pitch=0.641) (B8x8C03)	0.9418	0.9375	0.0008	0.641	0.4830	0.4250	0.0290	0.4160	150	0.000	0.120

[†] This assembly class was analyzed and qualified for a small variation in the pitch.

^{††} KENO5a verification calculation resulted in a maximum k_{eff} of 0.9343.

Table 6.2.23
 MAXIMUM K_{EFF} VALUES FOR THE 8X8D ASSEMBLY CLASS IN THE MPC-68
 (all dimensions are in inches)

8x8D (4.2% Enrichment, Boral ^{10}B minimum loading of 0.0279 g/cm ²)										
60-61 fuel rods, 1-4 water rods [†] , pitch=0.640, Zr clad										
Fuel Assembly Designation	maximum k_{eff}	calculated k_{eff}	standard deviation	cladding OD	cladding ID	cladding thickness	pellet OD	fuel length	water rod thickness	channel thickness
8x8D01	0.9342	0.9302	0.0006	0.4830	0.4190	0.0320	0.4110	150	0.03/0.025	0.100
8x8D02	0.9325	0.9284	0.0007	0.4830	0.4190	0.0320	0.4110	150	0.030	0.100
8x8D03	0.9351	0.9309	0.0008	0.4830	0.4190	0.0320	0.4110	150	0.025	0.100
8x8D04	0.9338	0.9296	0.0007	0.4830	0.4190	0.0320	0.4110	150	0.040	0.100
8x8D05	0.9339	0.9294	0.0009	0.4830	0.4190	0.0320	0.4100	150	0.040	0.100
8x8D06	0.9365	0.9324	0.0007	0.4830	0.4190	0.0320	0.4110	150	0.040	0.120
8x8D07	0.9341	0.9297	0.0009	0.4830	0.4190	0.0320	0.4110	150	0.040	0.080
8x8D08	0.9376	0.9332	0.0009	0.4830	0.4230	0.0300	0.4140	150	0.030	0.080
Dimensions Listed in Certificate of Compliance				0.4830 (min.)	0.4230 (max.)		0.4140 (max.)	150 (max.)	0.000 (min.)	0.120 (max.)
bounding dimensions (B8x8D01)	0.9403	0.9363	0.0007	0.4830	0.4230	0.0300	0.4140	150	0.000	0.120

[†] Fuel assemblies 8x8D01 through 8x8D03 have 4 water rods that are similar in size to the fuel rods, while assemblies 8x8D04 through 8x8D07 have 1 large water rod that takes the place of the 4 water rods. Fuel assembly 8x8D08 contains 3 water rods that are similar in size to the fuel rods.

Table 6.2.24
 MAXIMUM K_{EFF} VALUES FOR THE 8X8E ASSEMBLY CLASS IN THE MPC-68
 (all dimensions are in inches)

8x8E (4.2% Enrichment, Boral ^{10}B minimum loading of 0.0279 g/cm ²)										
59 fuel rods, 5 water rods, pitch=0.640, Zr clad										
Fuel Assembly Designation	maximum k_{eff}	calculated k_{eff}	standard deviation	cladding OD	cladding ID	cladding thickness	pellet OD	fuel length	water rod thickness	channel thickness
8x8E01	0.9312	0.9270	0.0008	0.4930	0.4250	0.0340	0.4160	150	0.034	0.100
Dimensions Listed in Certificate of Compliance				0.4930 (min.)	0.4250 (max.)		0.4160 (max.)	150 (max.)	0.034 (min.)	0.100 (max.)

Table 6.2.25
MAXIMUM K_{EFF} VALUES FOR THE 8X8F ASSEMBLY CLASS IN THE MPC-68
 (all dimensions are in inches)

8x8F (3.6% Enrichment, Boral ^{10}B minimum loading of 0.0279 g/cm ²)										
64 fuel rods, 4 rectangular water cross segments dividing the assembly into four quadrants, pitch=0.609, Zr clad										
Fuel Assembly Designation	maximum k_{eff}	calculated k_{eff}	standard deviation	cladding OD	cladding ID	cladding thickness	pellet OD	fuel length	water rod thickness	channel thickness
8x8F01	0.9153	0.9111	0.0007	0.4576	0.3996	0.0290	0.3913	150	0.0315	0.055
Dimensions Listed in Certificate of Compliance				0.4576 (min.)	0.3996 (max.)		0.3913 (max.)	150 (max.)	0.0315 (min.)	0.055 (max.)

Table 6.2.26
 MAXIMUM K_{EFF} VALUES FOR THE 9X9A ASSEMBLY CLASS IN THE MPC-68
 (all dimensions are in inches)

9x9A (4.2% Enrichment, Boral ^{10}B minimum loading of 0.0279 g/cm ²)										
74/66 fuel rods [†] , 2 water rods, pitch=0.566, Zr clad										
Fuel Assembly Designation	maximum k_{eff}	calculated k_{eff}	standard deviation	cladding OD	cladding ID	cladding thickness	pellet OD	fuel length	water rod thickness	channel thickness
9x9A01 (axial segment with all rods)	0.9353	0.9310	0.0008	0.4400	0.3840	0.0280	0.3760	150	0.030	0.100
9x9A02 (axial segment with only the full length rods)	0.9388	0.9345	0.0008	0.4400	0.3840	0.0280	0.3760	150	0.030	0.100
9x9A03 (actual three-dimensional representation of all rods)	0.9351	0.9310	0.0007	0.4400	0.3840	0.0280	0.3760	150/90	0.030	0.100
9x9A04 (axial segment with only the full length rods)	0.9396	0.9355	0.0007	0.4400	0.3840	0.0280	0.3760	150	0.030	0.120
Dimensions Listed in Certificate of Compliance				0.4400 (min.)	0.3840 (max.)		0.3760 (max.)	150 (max.)	0.000 (min.)	0.120 (max.)
bounding dimensions (axial segment with only the full length rods) (B9x9A01)	0.9417	0.9374	0.0008	0.4400	0.3840	0.0280	0.3760	150	0.000	0.120

[†] This assembly class contains 66 full length rods and 8 partial length rods. In order to eliminate a requirement on the length of the partial length rods, separate calculations were performed for the axial segments with and without the partial length rods.

Table 6.2.27
 MAXIMUM K_{EFF} VALUES FOR THE 9X9B ASSEMBLY CLASS IN THE MPC-68
 (all dimensions are in inches)

9x9B (4.2% Enrichment, Boral ^{10}B minimum loading of 0.0279 g/cm ²)											
72 fuel rods, 1 water rod (square, replacing 9 fuel rods), pitch=0.569 to 0.572 [†] , Zr clad											
Fuel Assembly Designation	maximum k_{eff}	calculated k_{eff}	standard deviation	pitch	cladding OD	cladding ID	cladding thickness	pellet OD	fuel length	water rod thickness	channel thickness
9x9B01	0.9368	0.9326	0.0007	0.569	0.4330	0.3807	0.0262	0.3737	150	0.0285	0.100
9x9B02	0.9377	0.9334	0.0008	0.569	0.4330	0.3810	0.0260	0.3737	150	0.0285	0.100
9x9B03	0.9416	0.9373	0.0008	0.572	0.4330	0.3810	0.0260	0.3737	150	0.0285	0.100
Dimensions Listed in Certificate of Compliance				0.572	0.4330 (min.)	0.3810 (max.)		0.3740 (max.)	150 (max.)	0.000 (min.)	0.120 (max.)
bounding dimensions (B9x9B01)	0.9422	0.9380	0.0007	0.572	0.4330	0.3810	0.0260	0.3740 ^{††}	150	0.000	0.120

[†] This assembly class was analyzed and qualified for a small variation in the pitch.

^{††} This value was conservatively defined to be larger than any of the actual pellet diameters.

Table 6.2.28
 MAXIMUM K_{EFF} VALUES FOR THE 9X9C ASSEMBLY CLASS IN THE MPC-68
 (all dimensions are in inches)

9x9C (4.2% Enrichment, Boral ^{10}B minimum loading of 0.0279 g/cm ²)										
80 fuel rods, 1 water rods, pitch=0.572, Zr clad										
Fuel Assembly Designation	maximum k_{eff}	calculated k_{eff}	standard deviation	cladding OD	cladding ID	cladding thickness	pellet OD	fuel length	water rod thickness	channel thickness
9x9C01	0.9395	0.9352	0.0008	0.4230	0.3640	0.0295	0.3565	150	0.020	0.100
Dimensions Listed in Certificate of Compliance				0.4230 (min.)	0.3640 (max.)		0.3565 (max.)	150 (max.)	0.020 (min.)	0.100 (max.)

Table 6.2.29
 MAXIMUM K_{EFF} VALUES FOR THE 9X9D ASSEMBLY CLASS IN THE MPC-68
 (all dimensions are in inches)

9x9D (4.2% Enrichment, Boral ^{10}B minimum loading of 0.0279 g/cm ²)										
79 fuel rods, 2 water rods, pitch=0.572, Zr clad										
Fuel Assembly Designation	maximum k_{eff}	calculated k_{eff}	standard deviation	cladding OD	cladding ID	cladding thickness	pellet OD	fuel length	water rod thickness	channel thickness
9x9D01	0.9394	0.9350	0.0009	0.4240	0.3640	0.0300	0.3565	150	0.0300	0.100
Dimensions Listed in Certificate of Compliance				0.4240 (min.)	0.3640 (max.)		0.3565 (max.)	150 (max.)	0.0300 (min.)	0.100 (max.)

Table 6.2.30
 MAXIMUM K_{EFF} VALUES FOR THE 9X9E ASSEMBLY CLASS IN THE MPC-68
 (all dimensions are in inches)

9x9E (4.1% Enrichment, Boral ^{10}B minimum loading of 0.0279 g/cm ²)										
76 fuel rods, 5 water rods, pitch=0.572, Zr clad										
Fuel Assembly Designation	maximum k_{eff}	calculated k_{eff}	standard deviation	cladding OD	cladding ID	cladding thickness	pellet OD	fuel length	water rod thickness	channel thickness
9x9E01	0.9402	0.9359	0.0008	0.4170	0.3640	0.0265	0.3530	150	0.0120	0.120
9x9E02	0.9424	0.9380	0.0008	0.4170 0.4430	0.3640 0.3860	0.0265 0.0285	0.3530 0.3745	150	0.0120	0.120
Dimensions Listed in Certificate of Compliance [†]				0.4170 (min.)	0.3640 (max.)		0.3530 (max.)	150 (max.)	0.0120 (min.)	0.120 (max.)
bounding dimensions (9x9E02)	0.9424	0.9380	0.0008	0.4170 0.4430	0.3640 0.3860	0.0265 0.0285	0.3530 0.3745	150	0.0120	0.120

[†] This fuel assembly, also known as SPC 9x9-5, contains fuel rods with different cladding and pellet diameters which do not bound each other. To be consistent in the way fuel assemblies are listed in the Certificate of Compliance, two assembly classes (9x9E and 9x9F) are required to specify this assembly. Each class contains the actual geometry (9x9E02 and 9x9F02), as well as a hypothetical geometry with either all small rods (9x9E01) or all large rods (9x9F01). The Certificate of Compliance lists the small rod dimensions for class 9x9E and the large rod dimensions for class 9x9F, and a note that both classes are used to qualify the assembly. The analyses demonstrate that all configurations, including the actual geometry, are acceptable.

Table 6.2.31
 MAXIMUM K_{EFF} VALUES FOR THE 9X9F ASSEMBLY CLASS IN THE MPC-68
 (all dimensions are in inches)

9x9F (4.1% Enrichment, Boral ^{10}B minimum loading of 0.0279 g/cm ²)										
76 fuel rods, 5 water rods, pitch=0.572, Zr clad										
Fuel Assembly Designation	maximum k_{eff}	calculated k_{eff}	standard deviation	cladding OD	cladding ID	cladding thickness	pellet OD	fuel length	water rod thickness	channel thickness
9x9F01	0.9369	0.9326	0.0007	0.4430	0.3860	0.0285	0.3745	150	0.0120	0.120
9x9F02	0.9424	0.9380	0.0008	0.4170 0.4430	0.3640 0.3860	0.0265 0.0285	0.3530 0.3745	150	0.0120	0.120
Dimensions Listed in Certificate of Compliance [†]				0.4430 (min.)	0.3860 (max.)		0.3745 (max.)	150 (max.)	0.0120 (min.)	0.120 (max.)
bounding dimensions (9x9F02)	0.9424	0.9380	0.0008	0.4170 0.4430	0.3640 0.3860	0.0265 0.0285	0.3530 0.3745	150	0.0120	0.120

[†] This fuel assembly, also known as SPC 9x9-5, contains fuel rods with different cladding and pellet diameters which do not bound each other. To be consistent in the way fuel assemblies are listed in the Certificate of Compliance, two assembly classes (9x9E and 9x9F) are required to specify this assembly. Each class contains the actual geometry (9x9E02 and 9x9F02), as well as a hypothetical geometry with either all small rods (9x9E01) or all large rods (9x9F01). The Certificate of Compliance lists the small rod dimensions for class 9x9E and the large rod dimensions for class 9x9F, and a note that both classes are used to qualify the assembly. The analyses demonstrate that all configurations, including the actual geometry, are acceptable.

Table 6.2.32
 MAXIMUM K_{eff} VALUES FOR THE 10X10A ASSEMBLY CLASS IN THE MPC-68
 (all dimensions are in inches)

10x10A (4.2% Enrichment, Boral ^{10}B minimum loading of 0.0279 g/cm ²)										
92/78 fuel rods [†] , 2 water rods, pitch=0.510, Zr clad										
Fuel Assembly Designation	maximum k_{eff}	calculated k_{eff}	standard deviation	cladding OD	cladding ID	cladding thickness	pellet OD	fuel length	water rod thickness	channel thickness
10x10A01 (axial segment with all rods)	0.9377	0.9335	0.0008	0.4040	0.3520	0.0260	0.3450	155	0.030	0.100
10x10A02 (axial segment with only the full length rods)	0.9426	0.9386	0.0007	0.4040	0.3520	0.0260	0.3450	155	0.030	0.100
10x10A03 (actual three-dimensional representation of all rods)	0.9396	0.9356	0.0007	0.4040	0.3520	0.0260	0.3450	155/90	0.030	0.100
Dimensions Listed in Certificate of Compliance				0.4040 (min.)	0.3520 (max.)		0.3455 (max.)	150 ^{††} (max.)	0.030 (min.)	0.120 (max.)
bounding dimensions (axial segment with only the full length rods) (B10x10A01)	0.9457 ^{†††}	0.9414	0.0008	0.4040	0.3520	0.0260	0.3455 [‡]	155	0.030	0.120

[†] This assembly class contains 78 full-length rods and 14 partial-length rods. In order to eliminate the requirement on the length of the partial length rods, separate calculations were performed for axial segments with and without the partial length rods.

^{††} Although the analysis qualifies this assembly for a maximum active fuel length of 155 inches, the Certificate of Compliance limits the active fuel length to 150 inches. This is due to the fact that the Boral panels are 156 inches in length.

^{†††} KENO5a verification calculation resulted in a maximum k_{eff} of 0.9453.

[‡] This value was conservatively defined to be larger than any of the actual pellet diameters.

Table 6.2.33
 MAXIMUM K_{EFF} VALUES FOR THE 10X10B ASSEMBLY CLASS IN THE MPC-68
 (all dimensions are in inches)

10x10B (4.2% Enrichment, Boral ^{10}B minimum loading of 0.0279 g/cm ²)										
91/83 fuel rods [†] , 1 water rods (square, replacing 9 fuel rods), pitch=0.510, Zr clad										
Fuel Assembly Designation	maximum k_{eff}	calculated k_{eff}	standard deviation	cladding OD	cladding ID	cladding thickness	pellet OD	fuel length	water rod thickness	channel thickness
10x10B01 (axial segment with all rods)	0.9384	0.9341	0.0008	0.3957	0.3480	0.0239	0.3413	155	0.0285	0.100
10x10B02 (axial segment with only the full length rods)	0.9416	0.9373	0.0008	0.3957	0.3480	0.0239	0.3413	155	0.0285	0.100
10x10B03 (actual three-dimensional representation of all rods)	0.9375	0.9334	0.0007	0.3957	0.3480	0.0239	0.3413	155/90	0.0285	0.100
Dimensions Listed in Certificate of Compliance				0.3957 (min.)	0.3480 (max.)		0.3420 (max.)	150 ^{††} (max.)	0.000 (min.)	0.120 (max.)
bounding dimensions (axial segment with only the full length rods) (B10x10B01)	0.9436	0.9395	0.0007	0.3957	0.3480	0.0239	0.3420 ^{†††}	155	0.000	0.120

[†] This assembly class contains 83 full length rods and 8 partial length rods. In order to eliminate a requirement on the length of the partial length rods, separate calculations were performed for the axial segments with and without the partial length rods.

^{††} Although the analysis qualifies this assembly for a maximum active fuel length of 155 inches, the Certificate of Compliance limits the active fuel length to 150 inches. This is due to the fact that the Boral panels are 156 inches in length.

^{†††} This value was conservatively defined to be larger than any of the actual pellet diameters.

Table 6.2.34
 MAXIMUM K_{EFF} VALUES FOR THE 10X10C ASSEMBLY CLASS IN THE MPC-68
 (all dimensions are in inches)

10x10C (4.2% Enrichment, Boral ^{10}B minimum loading of 0.0279 g/cm ²)										
96 fuel rods, 5 water rods (1 center diamond and 4 rectangular), pitch=0.488, Zr clad										
Fuel Assembly Designation	maximum k_{eff}	calculated k_{eff}	standard deviation	cladding OD	cladding ID	cladding thickness	pellet OD	fuel length	water rod thickness	channel thickness
10x10C01	0.9021	0.8980	0.0007	0.3780	0.3294	0.0243	0.3224	150	0.031	0.055
Dimensions Listed in Certificate of Compliance				0.3780 (min.)	0.3294 (max.)		0.3224 (max.)	150 (max.)	0.031 (min.)	0.055 (max.)

Table 6.2.35
 MAXIMUM K_{EFF} VALUES FOR THE 10X10D ASSEMBLY CLASS IN THE MPC-68
 (all dimensions are in inches)

10x10D (4.0% Enrichment, Boral ^{10}B minimum loading of 0.0279 g/cm ²)										
100 fuel rods, 0 water rods, pitch=0.565, SS clad										
Fuel Assembly Designation	maximum k_{eff}	calculated k_{eff}	standard deviation	cladding OD	cladding ID	cladding thickness	pellet OD	fuel length	water rod thickness	channel thickness
10x10D01	0.9376	0.9333	0.0008	0.3960	0.3560	0.0200	0.350	83	n/a	0.080
Dimensions Listed in Certificate of Compliance				0.3960 (min.)	0.3560 (max.)		0.350 (max.)	83 (max.)	n/a	0.080 (max.)

Table 6.2.36
MAXIMUM K_{EFF} VALUES FOR THE 10X10E ASSEMBLY CLASS IN THE MPC-68
 (all dimensions are in inches)

10x10E (4.0% Enrichment, Boral ^{10}B minimum loading of 0.0279 g/cm ²)										
96 fuel rods, 4 water rods, pitch=0.557, SS clad										
Fuel Assembly Designation	maximum k_{eff}	calculated k_{eff}	standard deviation	cladding OD	cladding ID	cladding thickness	pellet OD	fuel length	water rod thickness	channel thickness
10x10E01	0.9185	0.9144	0.0007	0.3940	0.3500	0.0220	0.3430	83	0.022	0.080
Dimensions Listed in Certificate of Compliance				0.3940 (min.)	0.3500 (max.)		0.3430 (max.)	83 (max.)	0.022 (min.)	0.080 (max.)

Table 6.2.37
 MAXIMUM K_{EFF} VALUES FOR THE 6X6A ASSEMBLY CLASS IN THE MPC-68F
 (all dimensions are in inches)

6x6A (3.0% Enrichment [†] , Boral ¹⁰ B minimum loading of 0.0067 g/cm ²)												
35 or 36 fuel rods ^{††} , 1 or 0 water rods ^{††} , pitch ^{††} =0.694 to 0.710, Zr clad												
Fuel Assembly Designation	maximum k_{eff}	calculated k_{eff}	standard deviation	pitch	fuel rods	cladding OD	cladding ID	cladding thickness	pellet OD	fuel length	water rod thickness	channel thickness
6x6A01	0.7539	0.7498	0.0007	0.694	36	0.5645	0.4945	0.0350	0.4940	110	n/a	0.060
6x6A02	0.7517	0.7476	0.0007	0.694	36	0.5645	0.4925	0.0360	0.4820	110	n/a	0.060
6x6A03	0.7545	0.7501	0.0008	0.694	36	0.5645	0.4945	0.0350	0.4820	110	n/a	0.060
6x6A04	0.7537	0.7494	0.0008	0.694	36	0.5550	0.4850	0.0350	0.4820	110	n/a	0.060
6x6A05	0.7555	0.7512	0.0008	0.696	36	0.5625	0.4925	0.0350	0.4820	110	n/a	0.060
6x6A06	0.7618	0.7576	0.0008	0.696	35	0.5625	0.4925	0.0350	0.4820	110	0.0	0.060
6x6A07	0.7588	0.7550	0.0007	0.700	36	0.5555	0.4850	0.03525	0.4780	110	n/a	0.060
6x6A08	0.7808	0.7766	0.0007	0.710	36	0.5625	0.5105	0.0260	0.4980	110	n/a	0.060
Dimensions Listed in Certificate of Compliance				0.710 (max.)	35 or 36	0.5550 (min.)	0.5105 (max.)	0.02225	0.4980 (max.)	120 (max.)	0.0	0.060 (max.)
bounding dimensions (B6x6A01)	0.7727	0.7685	0.0007	0.694	35	0.5550	0.5105	0.02225	0.4980	120	0.0	0.060
bounding dimensions (B6x6A02)	0.7782	0.7738	0.0008	0.700	35	0.5550	0.5105	0.02225	0.4980	120	0.0	0.060
bounding dimensions (B6x6A03)	0.7888	0.7846	0.0007	0.710	35	0.5550	0.5105	0.02225	0.4980	120	0.0	0.060

[†] Although the calculations were performed for 3.0%, the enrichment is limited in the Certificate of Compliance to 2.7%.

^{††} This assembly class was analyzed and qualified for a small variation in the pitch and a variation in the number of fuel and water rods.

Table 6.2.38
 MAXIMUM K_{EFF} VALUES FOR THE 6X6B ASSEMBLY CLASS IN THE MPC-68F
 (all dimensions are in inches)

6x6B (3.0% Enrichment [†] , Boral ¹⁰ B minimum loading of 0.0067 g/cm ²)												
35 or 36 fuel rods ^{††} (up to 9 MOX rods), 1 or 0 water rods ^{††} , pitch ^{††} =0.694 to 0.710, Zr clad												
Fuel Assembly Designation	maximum k_{eff}	calculated k_{eff}	standard deviation	pitch	fuel rods	cladding OD	cladding ID	cladding thickness	pellet OD	fuel length	water rod thickness	channel thickness
6x6B01	0.7604	0.7563	0.0007	0.694	36	0.5645	0.4945	0.0350	0.4820	110	n/a	0.060
6x6B02	0.7618	0.7577	0.0007	0.694	36	0.5625	0.4925	0.0350	0.4820	110	n/a	0.060
6x6B03	0.7619	0.7578	0.0007	0.696	36	0.5625	0.4925	0.0350	0.4820	110	n/a	0.060
6x6B04	0.7686	0.7644	0.0008	0.696	35	0.5625	0.4925	0.0350	0.4820	110	0.0	0.060
6x6B05	0.7824	0.7785	0.0006	0.710	35	0.5625	0.4925	0.0350	0.4820	110	0.0	0.060
Dimensions Listed in Certificate of Compliance				0.710 (max.)	35 or 36	0.5625 (min.)	0.4945 (max.)		0.4820 (max.)	120 (max.)	0.0	0.060 (max.)
bounding dimensions (B6x6B01)	0.7822 ^{†††}	0.7783	0.0006	0.710	35	0.5625	0.4945	0.0340	0.4820	120	0.0	0.060

Note:

1. These assemblies contain up to 9 MOX pins. The composition of the MOX fuel pins is given in Table 6.3.4.

[†] The ²³⁵U enrichment of the MOX and UO₂ pins is assumed to be 0.711% and 3.0%, respectively.

^{††} This assembly class was analyzed and qualified for a small variation in the pitch and a variation in the number of fuel and water rods.

^{†††} The k_{eff} value listed for the 6x6B05 case is slightly higher than that for the case with the bounding dimensions. However, the difference (0.0002) is well within the statistical uncertainties, and thus, the two values are statistically equivalent (within 1 σ). Therefore, the 0.7824 value is listed in Tables 6.1.2 and 6.1.3 as the maximum.

Table 6.2.39
 MAXIMUM K_{EFF} VALUES FOR THE 6X6C ASSEMBLY CLASS IN THE MPC-68F
 (all dimensions are in inches)

6x6C (3.0% Enrichment [†] , Boral ¹⁰ B minimum loading of 0.0067 g/cm ²)										
36 fuel rods, 0 water rods, pitch=0.740, Zr clad										
Fuel Assembly Designation	maximum k_{eff}	calculated k_{eff}	standard deviation	cladding OD	cladding ID	cladding thickness	pellet OD	fuel length	water rod thickness	channel thickness
6x6C01	0.8021	0.7980	0.0007	0.5630	0.4990	0.0320	0.4880	77.5	n/a	0.060
Dimensions Listed in Certificate of Compliance				0.5630 (min.)	0.4990 (max.)		0.4880 (max.)	77.5 (max.)	n/a	0.060 (max.)

[†] Although the calculations were performed for 3.0%, the enrichment is limited in the Certificate of Compliance to 2.7%.

Table 6.2.40
 MAXIMUM K_{EFF} VALUES FOR THE 7X7A ASSEMBLY CLASS IN THE MPC-68F
 (all dimensions are in inches)

7x7A (3.0% Enrichment [†] , Boral ¹⁰ B minimum loading of 0.0067 g/cm ²)										
49 fuel rods, 0 water rods, pitch=0.631, Zr clad										
Fuel Assembly Designation	maximum k_{eff}	calculated k_{eff}	standard deviation	cladding OD	cladding ID	cladding thickness	pellet OD	fuel length	water rod thickness	channel thickness
7x7A01	0.7974	0.7932	0.0008	0.4860	0.4204	0.0328	0.4110	80	n/a	0.060
Dimensions Listed in Certificate of Compliance				0.4860 (min.)	0.4204 (max.)		0.4110 (max.)	80 (max.)	n/a	0.060 (max.)

[†] Although the calculations were performed for 3.0%, the enrichment is limited in the Certificate of Compliance to 2.7%.

Table 6.2.41
 MAXIMUM K_{EFF} VALUES FOR THE 8X8A ASSEMBLY CLASS IN THE MPC-68F
 (all dimensions are in inches)

8x8A (3.0% Enrichment [†] , Boral ¹⁰ B minimum loading of 0.0067 g/cm ²)											
63 or 64 fuel rods ^{††} , 0 water rods, pitch=0.523, Zr clad											
Fuel Assembly Designation	maximum k_{eff}	calculated k_{eff}	standard deviation	fuel rods	cladding OD	cladding ID	cladding thickness	pellet OD	fuel length	water rod thickness	channel thickness
8x8A01	0.7685	0.7644	0.0007	64	0.4120	0.3620	0.0250	0.3580	110	n/a	0.100
8x8A02	0.7697	0.7656	0.0007	63	0.4120	0.3620	0.0250	0.3580	120	n/a	0.100
Dimensions Listed in Certificate of Compliance				63	0.4120 (min.)	0.3620 (max.)		0.3580 (max.)	120 (max.)	n/a	0.100 (max.)
bounding dimensions (8x8A02)	0.7697	0.7656	0.0007	63	0.4120	0.3620	0.0250	0.3580	120	n/a	0.100

[†] Although the calculations were performed for 3.0%, the enrichment is limited in the Certificate of Compliance to 2.7%.

^{††} This assembly class was analyzed and qualified for a variation in the number of fuel rods.

Table 6.2.42

SPECIFICATION OF THE THORIA ROD CANISTER AND THE THORIA RODS

Canister ID	4.81"
Canister Wall Thickness	0.11"
Separator Assembly Plates Thickness	0.11"
Cladding OD	0.412"
Cladding ID	0.362"
Pellet OD	0.358"
Active Length	110.5"
Fuel Composition	1.8% UO ₂ and 98.2% ThO ₂
Initial Enrichment	93.5 wt% ²³⁵ U for 1.8% of the fuel
Maximum k _{eff}	0.1813
Calculated k _{eff}	0.1779
Standard Deviation	0.0004

6.3 MODEL SPECIFICATION

6.3.1 Description of Calculational Model

Figures 6.3.1 and 6.3.3 show representative horizontal cross sections of the two types of cells used in the calculations, and Figures 6.3.4 and 6.3.6 illustrate the basket configurations used. Two different MPC fuel basket designs were evaluated as follows:

- a 24 PWR assembly basket
- a 68 BWR assembly basket.

Full three-dimensional calculations were used, assuming the axial configuration shown in Figure 6.3.7, and conservatively neglecting the absorption in the overpack neutron shielding material (Holtite-A). Although the Boral neutron absorber panels are 156 inches in length, which is much longer than the active fuel length (maximum of 150 inches), they are assumed equal to the active fuel length in the calculations. As shown on the Design Drawings in Section 1.5, 12 of the 24 periphery Boral panels on the MPC-24 have reduced width (i.e., 6.25 inches wide as opposed to 7.5 inches). However, as shown in Figure 6.3.4, the calculational models for the MPC-24 conservatively assume all of the periphery Boral panels are 5.0 inches in width.

The off-normal and accident conditions defined in Chapter 2 and considered in Chapter 11 have no adverse effect on the design conditions important to criticality safety, and thus from a criticality standpoint, the normal, off-normal, and accident conditions are identical and do not require individual models.

The calculational model explicitly defines the fuel rods and cladding, the guide tubes (or water rods for BWR assemblies), the water-gaps and Boral absorber panels on the stainless steel walls of the storage cells. Under the conditions of storage, when the MPC is dry, the resultant reactivity with the design basis fuel is very low ($k_{\text{eff}} < 0.4$). For the flooded condition (loading and unloading), water was assumed to be present in the fuel rod pellet-to-clad gaps. Appendix 6.D provides sample input files for each of the two MPC basket designs in the HI-STAR 100 System.

The water thickness above and below the fuel is intentionally maintained less than or equal to the actual water thickness. This assures that any positive reactivity effect of the steel in the MPC is conservatively included.

As indicated in Figures 6.3.1 and 6.3.3 and in Tables 6.3.1 and 6.3.2, calculations were made with dimensions assumed to be at their most conservative value with respect to criticality. CASMO-3 was used to determine the direction of the manufacturing tolerances which produced the most adverse effect on criticality. After the directional effect (positive effect with an increase

in reactivity; or negative effect with a decrease in reactivity) of the manufacturing tolerances was determined, the criticality analyses were performed using the worst case tolerances in the direction which would increase reactivity. These effects are shown in Table 6.3.1 which also identifies the approximate magnitude of the tolerances on reactivity.

The various basket dimensions are inter-dependent, and therefore cannot be individually varied (i.e., reduction in one parameter requires a corresponding reduction or increase in another parameter). Thus, it is not possible to determine the reactivity effect of each individual dimensional tolerance separately. However, it is possible to determine the reactivity effect of the dimensional tolerances by evaluating the various possible dimensional combinations. To this end, an evaluation of the various possible dimensional combinations was performed using MCNP4a. Calculated k_{eff} results (which do not include the bias, uncertainties, or calculational statistics), along with the actual dimensions, for a number of dimensional combinations are shown in Table 6.3.2 for the reference PWR and BWR assemblies. In Table 6.3.2, the box I.D. is the inner box dimension and the minimum, nominal, and maximum values correspond to those values permitted by the tolerances in the Design Drawings in Section 1.5. For each of the MPC designs, the reactivity effects of the tolerances are very small, generally within one standard deviation. The effect of the box wall thickness tolerance is negligible, being either slightly negative or within one standard deviation of the reference.

Based on the MCNP4a and CASMO-3 calculations, the conservative dimensional assumptions listed in Table 6.3.3 were determined. Because the reactivity effect (positive or negative) of the manufacturing tolerances are not assembly dependent, these dimensional assumptions were employed for the criticality analyses.

As demonstrated in this section, design parameters important to criticality safety are: fuel enrichment, the inherent geometry of the fuel basket structure, and the fixed neutron absorbing panels (Boral). As shown in Chapter 11, none of these parameters are affected during any of the design basis off-normal or accident conditions involving handling, packaging, transfer or storage.

6.3.2 Cask Regional Densities

Composition of the various components of the principal designs of the HI-STAR 100 Systems are listed in Table 6.3.4.

The HI-STAR 100 System is designed such that the fixed neutron absorber (Boral) will remain effective for a storage period greater than 20 years, and there are no credible means to lose it. A detailed physical description, historical applications, unique characteristics, service experience, and manufacturing quality assurance of Boral are provided in Section 1.2.1.3.1.

The continued efficacy of the Boral is assured by acceptance testing, documented in Section

9.1.5.3, to validate the ^{10}B (poison) concentration in the Boral. To demonstrate that the neutron flux from the irradiated fuel results in a negligible depletion of the poison material over the storage period, an MCNP4a calculation of the number of neutrons absorbed in the ^{10}B was performed. The calculation conservatively assumed a constant neutron source for 50 years equal to the initial source for the design basis fuel, as determined in Section 5.2, and shows that the fraction of ^{10}B atoms destroyed is only $2.6\text{E}-09$ in 50 years. Thus, the reduction in ^{10}B concentration in the Boral by neutron absorption is negligible. In addition, analysis in Appendix 3.M.1 demonstrates that the sheathing, which affixes the Boral panel, remains in place during all credible accident conditions, and thus, the Boral panel remains permanently fixed. Therefore, in accordance with NUREG-1536, there is no need to provide a surveillance or monitoring program to verify the continued efficacy of the neutron absorber, as required by 10CFR72.124(b).

Table 6.3.1

CASMO-3 CALCULATIONS FOR EFFECT OF TOLERANCES AND TEMPERATURE

Change in Nominal Parameter [†]	Δk for Maximum Tolerance		Action/Modeling Assumption
	MPC-24	MPC-68	
Reduce Boral Width to Minimum ^{††}	+0.0003 min. = 7.4375" nom. = 7.500"	N/A ^{†††} min. = nom. = 4.75"	Assume minimum Boral width
Increase UO ₂ Density to Maximum	+0.0012 max. = 10.522 g/cc nom. = 10.412 g/cc	+0.0014 max. = 10.522 g/cc nom. = 10.412 g/cc	Assume maximum UO ₂ density
Reduce Box Inside Dimension (I.D.) to Minimum	-0.0016 min. = 8.69" nom. = 8.75"	See Table 6.3.2	Assume maximum box I.D. for the MPC-24
Increase Box Inside Dimension (I.D.) to Maximum	+0.0014 max. = 8.81" nom. = 8.75"	-0.0030 max. = 6.113" nom. = 6.053"	Assume minimum box I.D. for the MPC-68
Decrease Water Gap to Minimum	+0.0058 min. = 1.09" nom. = 1.15"	N/A	Assume minimum water gap in the MPC-24

† Reduction (or increase) in a parameter indicates that the parameter is changed to its minimum (or maximum) value.

†† Although the most prevalent Boral width for the MPC-24 is 7.50" +0.125, -0", the analyses conservatively assumed the Boral width to be 7.4375". Further, the analyses conservatively assumed the periphery Boral width to be 5.0".

††† The Boral width for the MPC-68 is 4.75" +0.125", -0" (i.e., the nominal and minimum values are the same).

Table 6.3.1 (continued)

CASMO-3 CALCULATIONS FOR EFFECT OF TOLERANCES AND TEMPERATURE

Change in Nominal Parameter	Δk Maximum Tolerance		Action/Modeling Assumption
	MPC-24	MPC-68	
Increase in Temperature			Assume 20°C
20°C	Ref.	Ref.	
40°C	-0.0031	-0.0039	
70°C	-0.0093	-0.0136	
100°C	-0.0170	-0.0193	
10% Void in Moderator			Assume no void
20°C with no void	Ref.	Ref.	
20°C	-0.0271	-0.0241	
100°C	-0.0439	-0.0432	
Removal of Flow Channel (BWR)	N/A	-0.0073	Assume flow channel present for MPC-68

Table 6.3.2

MCNP4a EVALUATION OF BASKET MANUFACTURING TOLERANCES[†]

Pitch		Box I.D.		Box Wall Thickness		MCNP4a Calculated k_{eff}
MPC-24 ^{††} (17x17A01 @ 4.0% Enrichment)						
nominal	(10.777")	maximum	(8.81")	nominal	(5/16")	0.9400±0.0011 ^{†††}
minimum	(10.717")	nominal	(8.75")	nominal	(5/16")	0.9365±0.0009
nominal	(10.777")	nom. - 0.05"	(8.70")	nom. + 0.05"	(0.3625")	0.9395±0.0008
MPC-68 (8x8C04 @ 4.2% Enrichment)						
minimum	(6.43")	minimum	(5.993")	nominal	(1/4")	0.9307±0.0007
nominal	(6.49")	nominal	(6.053")	nominal	(1/4")	0.9274±0.0007
maximum	(6.55")	maximum	(6.113")	nominal	(1/4")	0.9272±0.0008
nom. + 0.05"	(6.54")	nominal	(6.053")	nom. + 0.05"	(0.30")	0.9267±0.0007

Note: Values in parentheses are the actual value used.

† Tolerance for pitch and box I.D. are ± 0.06".
Tolerance for box wall thickness is +0.05", -0.00".

†† All calculations for the MPC-24 assume minimum water gap thickness (1.09").

††† Numbers are 1σ statistical uncertainties.

Table 6.3.3

BASKET DIMENSIONAL ASSUMPTIONS

Basket Type	Pitch	Box I.D.	Box Wall Thickness	Water-Gap Flux Trap
MPC-24	nominal (10.777")	maximum (8.81")	nominal (5/16")	minimum (1.09")
MPC-68	minimum (6.43")	minimum (5.993")	nominal (1/4")	N/A

Table 6.3.4

COMPOSITION OF THE MAJOR COMPONENTS OF THE HI-STAR 100 SYSTEM

MPC-24		
UO₂ 4.0% ENRICHMENT, DENSITY (g/cc) = 10.522		
Nuclide	Atom-Density	Wgt. Fraction
8016	4.693E-02	1.185E-01
92235	9.505E-04	3.526E-02
92238	2.252E-02	8.462E-01
BORAL (0.02 g ¹⁰B/cm sq), DENSITY (g/cc) = 2.660		
Nuclide	Atom-Density	Wgt. Fraction
5010	8.707E-03	5.443E-02
5011	3.512E-02	2.414E-01
6012	1.095E-02	8.210E-02
13027	3.694E-02	6.222E-01

Table 6.3.4 (continued)

COMPOSITION OF THE MAJOR COMPONENTS OF THE HI-STAR 100 SYSTEM

MPC-68		
UO₂ 4.2% ENRICHMENT, DENSITY (g/cc) = 10.522		
Nuclide	Atom-Density	Wgt. Fraction
8016	4.697E-02	1.185E-01
92235	9.983E-04	3.702E-02
92238	2.248E-02	8.445E-01
UO₂ 3.0% ENRICHMENT, DENSITY (g/cc) = 10.522		
Nuclide	Atom-Density	Wgt. Fraction
8016	4.695E-02	1.185E-01
92235	7.127E-04	2.644E-02
92238	2.276E-02	8.550E-01
MOX FUEL[†], DENSITY (g/cc) = 10.522		
Nuclide	Atom-Density	Wgt. Fraction
8016	4.714E-02	1.190E-01
92235	1.719E-04	6.380E-03
92238	2.285E-02	8.584E-01
94239	3.876E-04	1.461E-02
94240	9.177E-06	3.400E-04
94241	3.247E-05	1.240E-03
94242	2.118E-06	7.000E-05

† The Pu-238, which is an absorber, was conservatively neglected in the MOX description for analysis purposes.

Table 6.3.4 (continued)

COMPOSITION OF THE MAJOR COMPONENTS OF THE HI-STAR 100 SYSTEM

BORAL (0.0279 g ¹⁰B/cm sq), DENSITY (g/cc) = 2.660		
Nuclide	Atom-Density	Wgt. Fraction
5010	8.071E-03	5.089E-02
5011	3.255E-02	2.257E-01
6012	1.015E-02	7.675E-02
13027	3.805E-02	6.467E-01
FUEL IN THORIA RODS, DENSITY (g/cc) = 10.522		
Nuclide	Atom-Density	Wgt. Fraction
8016	4.798E-02	1.212E-01
92235	4.001E-04	1.484E-02
92238	2.742E-05	1.030E-03
90232	2.357E-02	8.630E-01

Table 6.3.4 (continued)

COMPOSITION OF THE MAJOR COMPONENTS OF THE HI-STAR 100 SYSTEM

COMMON MATERIALS		
ZR CLAD, DENSITY (g/cc) = 6.550		
Nuclide	Atom-Density	Wgt. Fraction
40000	4.323E-02	1.000E+00
MODERATOR (H₂O), DENSITY (g/cc) = 1.000		
Nuclide	Atom-Density	Wgt. Fraction
1001	6.688E-02	1.119E-01
8016	3.344E-02	8.881E-01
STAINLESS STEEL, DENSITY (g/cc) = 7.840		
Nuclide	Atom-Density	Wgt. Fraction
24000	1.761E-02	1.894E-01
25055	1.761E-03	2.001E-02
26000	5.977E-02	6.905E-01
28000	8.239E-03	1.000E-01
ALUMINUM, DENSITY (g/cc) = 2.700		
Nuclide	Atom-Density	Wgt. Fraction
13027	6.026E-02	1.000E+00

FIGURE WITHHELD AS SENSITIVE
UNCLASSIFIED INFORMATION

FIGURE 6.3.1; TYPICAL CELL IN THE CALCULATION MODEL (PLANAR CROSS-SECTION)
WITH REPRESENTATIVE FUEL IN THE MPC-24 BASKET

(SEE CHAPTER 1 FOR TRUE BASKET DIMENSIONS)

DELETED

FIGURE 6.3.2

**FIGURE WITHHELD AS
SENSITIVE UNCLASSIFIED
INFORMATION**

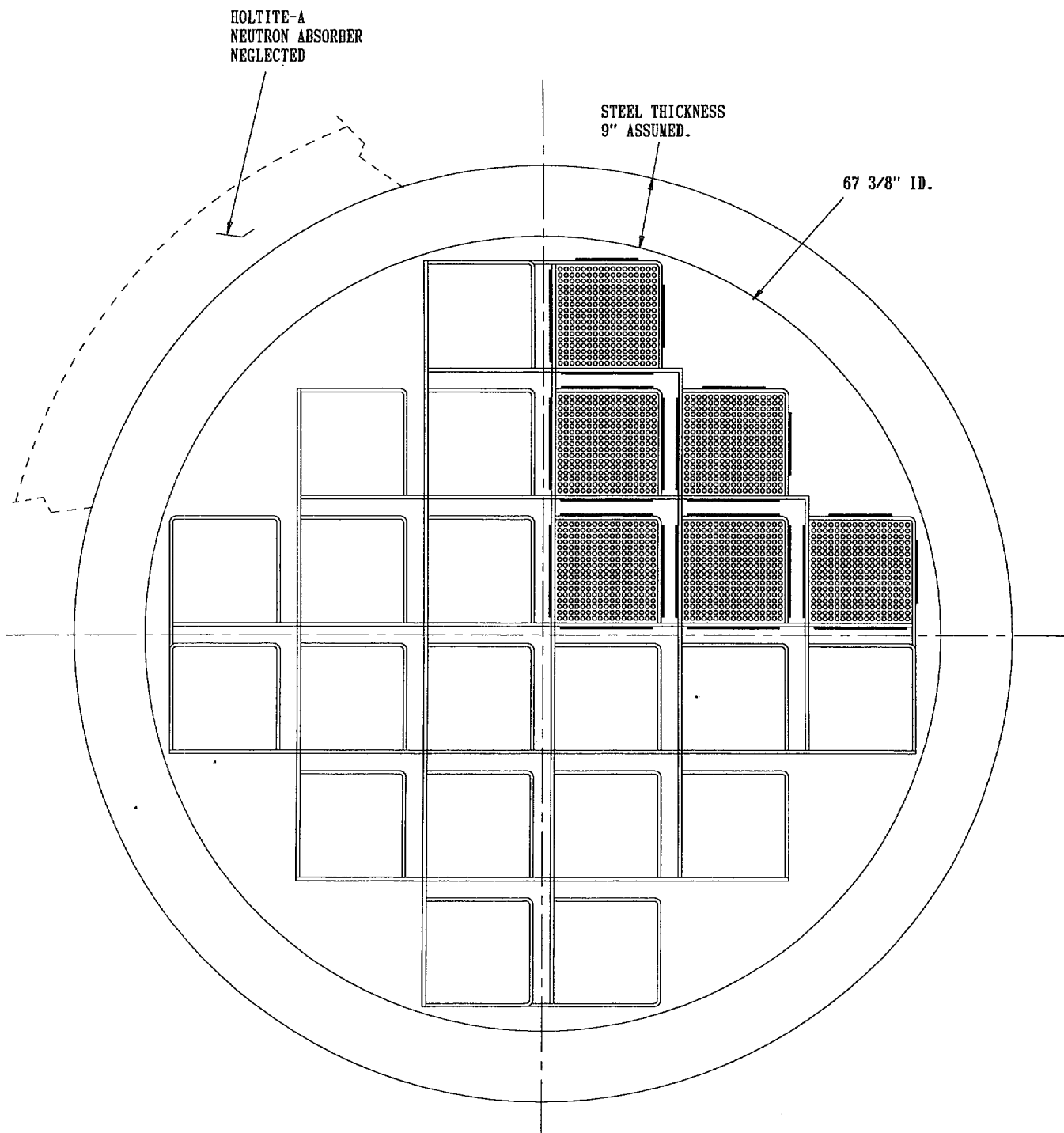


FIGURE 6.3.4; CALCULATION MODEL (PLANAR CROSS-SECTION)
 WITH FUEL ILLUSTRATED IN ONE QUADRANT OF
 THE MPC-24.

(SEE CHAPTER 1 FOR TRUE BASKET DIMENSIONS)

DELETED

FIGURE 6.3.5

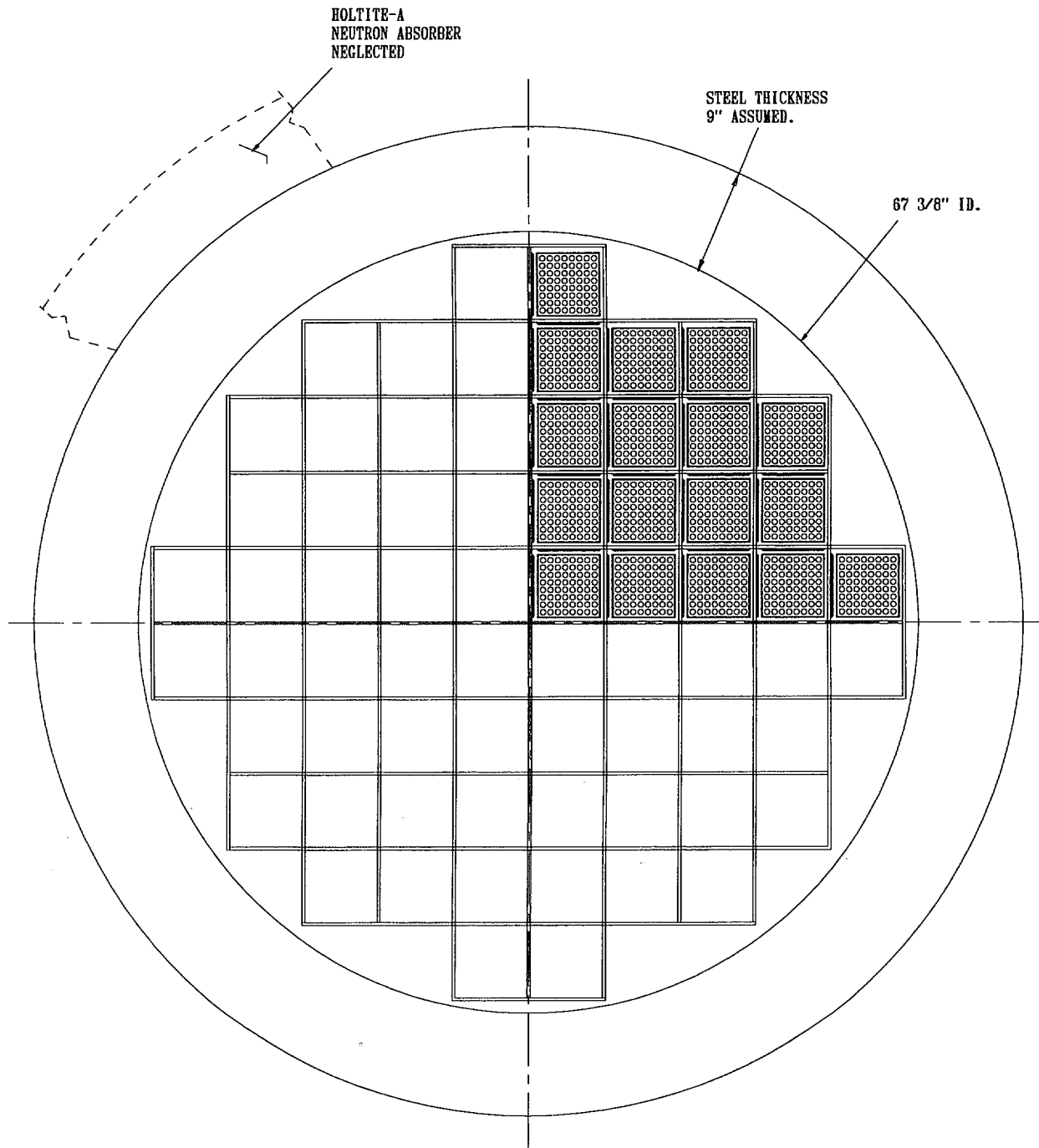


FIGURE 6.3.6; CALCULATION MODEL (PLANAR CROSS-SECTION)
 WITH FUEL ILLUSTRATED IN ONE QUADRANT OF
 THE MPC-68
 (SEE CHAPTER 1 FOR TRUE BASKET DIMENSIONS)

**FIGURE WITHHELD AS SENSITIVE
UNCLASSIFIED INFORMATION**

6.4 CRITICALITY CALCULATIONS

6.4.1 Calculational or Experimental Method

6.4.1.1 Basic Criticality Safety Calculations

The principal method for the criticality analysis is the general three-dimensional continuous energy Monte Carlo N-Particle code MCNP4a [6.1.4] developed at the Los Alamos National Laboratory. MCNP4a was selected because it has been extensively used and verified and has all of the necessary features for this analysis. MCNP4a calculations used continuous energy cross-section data based on ENDF/B-V, as distributed with the code [6.1.4]. Independent verification calculations were performed with NITAWL-KENO5a [6.1.5], which is a three-dimensional multigroup Monte Carlo code developed at the Oak Ridge National Laboratory. The KENO5a calculations used the 238-group cross-section library, which is based on ENDF/B-V data and is distributed as part of the SCALE-4.3 package [6.4.1], compiled with the NITAWL-II program [6.1.6], which adjusts the uranium-238 cross sections to compensate for resonance self-shielding effects. The Dancoff factors required by NITAWL-II were calculated with the CELLDAN code [6.1.13], which includes the SUPERDAN code [6.1.7] as a subroutine.

The convergence of a Monte Carlo criticality problem is sensitive to the following parameters: (1) number of histories per cycle, (2) the number of cycles skipped before averaging, (3) the total number of cycles and (4) the initial source distribution. The MCNP4a criticality output contains a great deal of useful information that may be used to determine the acceptability of the problem convergence. This information was used in parametric studies to develop appropriate values for the aforementioned criticality parameters to be used in the criticality calculations for this submittal. Based on these studies, a minimum of 5,000 histories were simulated per cycle, a minimum of 20 cycles were skipped before averaging, a minimum of 100 cycles were accumulated, and the initial source was specified as uniform over the fueled regions (assemblies). Further, the output was examined to ensure that each calculation achieved acceptable convergence. These parameters represent an acceptable compromise between calculational precision and computational time. Appendix 6.D provides sample input files for each of the MPC baskets in the HI-STAR 100 System.

CASMO-3 [6.1.9] was used for determining the small incremental reactivity effects of manufacturing tolerances. Although CASMO-3 has been extensively benchmarked, these calculations are used only to establish direction of reactivity uncertainties due to manufacturing tolerances (and their magnitude). This allows the MCNP4a calculational model to use the worst combination of manufacturing tolerances. Table 6.3.1 shows results of the CASMO-3 calculations.

6.4.2 Fuel Loading or Other Contents Loading Optimization

The basket designs are intended to safely accommodate fuel with enrichments indicated in Tables 6.1.1 and 6.1.2. These calculations were based on the assumption that the HI-STAR 100 System was fully flooded with clean unborated water. In all cases, the calculations include bias and calculational uncertainties, as well as the reactivity effects of manufacturing tolerances, determined by assuming the worst case geometry.

Nominally, the fuel assemblies would be centrally positioned in each MPC basket cell. However, in accordance with NUREG-1536, the consequence of eccentric positioning was also evaluated and found to be negligible. To simulate eccentric positioning (and possible closer approach to the thick steel shield), calculations were made analytically decreasing the inner radius of the steel until it was 1 cm away[†] from the nearest fuel. Results showed a minor increase in reactivity of 0.0026 Δk maximum (MPC-68) which implies that the effect of eccentric location of fuel is negligible at the actual reflector spacing.

6.4.2.1 Internal and External Moderation

As required by NUREG-1536, calculations in this section demonstrate that the HI-STAR 100 System remains subcritical for all credible conditions of moderation.

With a neutron absorber present (i.e., the Boral sheets or the steel walls of the storage compartments), the phenomenon of a peak in reactivity at a hypothetical low moderator density (sometimes called "optimum" moderation) does not occur to any significant extent. In a definitive study, Cano, et al. [6.4.2] has demonstrated that the phenomenon of a peak in reactivity at low moderator densities does not occur when strong neutron absorbing material is present or in the absence of large water spaces between fuel assemblies in storage. Nevertheless, calculations for a single reflected cask were made to confirm that the phenomenon does not occur with low density water inside or outside the casks.

Calculations for the MPC designs with internal and external moderators of various densities are shown in Table 6.4.1. For comparison purposes, a calculation for a single unreflected cask (Case 1) is also included in Table 6.4.1. At 100% external moderator density, Case 2 corresponds to a single fully-flooded cask, fully reflected by water. Results listed in Table 6.4.1 support the following conclusions:

† PNL critical experiments have shown a small positive reactivity effect of thick steel reflectors, with the maximum effect at 1 cm distance from the fuel. In the cask designs, the fuel is mechanically prohibited from being positioned at a 1 cm spacing from the overpack steel.

- For each type of MPC, the calculated k_{eff} for a fully-flooded cask is independent of the external moderator (the small variations in the listed values are due to statistical uncertainties which are inherent to the calculational method (Monte Carlo)), and
- For each type of MPC, reducing the internal moderation results in a monotonic reduction in reactivity, with no evidence of any optimum moderation. Thus, the fully flooded condition corresponds to the highest reactivity, and the phenomenon of optimum low-density moderation does not occur and is not applicable to the HI-STAR 100 System.

For each of the MPC designs, the maximum k_{eff} values are shown to be less than or statistically equal to that of a single internally flooded unreflected cask and are below the regulatory limit of 0.95.

6.4.2.2 Partial Flooding

As required by NUREG-1536, calculations in this section address partial flooding in the HI-STAR 100 System and demonstrate that the fully flooded condition is the most reactive.

The reactivity changes during the flooding process were evaluated in both the vertical and horizontal positions for all MPC designs. For these calculations, the cask is partially filled (at various levels) with full density (1.0 g/cc) water and the remainder of the cask is filled with steam consisting of ordinary water at partial density (0.002 g/cc), as suggested in NUREG-1536. Results of these calculations are shown in Table 6.4.2. In all cases, the reactivity increases monotonically as the water level rises, confirming that the most reactive condition is fully flooded.

6.4.2.3 Clad Gap Flooding

As required by NUREG-1536, the reactivity effect of flooding the fuel rod pellet-to-clad gap regions, in the fully flooded condition, has been investigated. Table 6.4.3 presents maximum k_{eff} values that demonstrate the positive reactivity effect associated with flooding the pellet-to-clad gap regions. These results confirm that it is conservative to assume that the pellet-to-clad gap regions are flooded. For all cases that involve flooding, the pellet-to-clad gap regions are assumed to be flooded.

6.4.2.4 Preferential Flooding

Preferential or uneven flooding within the HI-STAR 100 System was not evaluated because such a condition is not credible for any of the MPC basket designs loaded in the HI-STAR cask. Preferential flooding of any of the MPC fuel basket designs is not possible because flow holes are present on all four walls of each basket cell and on the two flux trap walls at both the top and bottom of the MPC basket. The flow holes are sized to ensure that they cannot be blocked by crud deposits (see Chapter 11). Because the fuel cladding temperatures remain below their design limits (as demonstrated in Chapter 4) and the inertial loading remains below 63g's (the inertial loadings associated with the design basis drop accidents discussed in Chapter 11 are limited to 60g's), the cladding remains intact (see Section 3.5). For damaged BWR fuel assemblies and BWR fuel debris, the assemblies or debris are pre-loaded into stainless steel Damaged Fuel Containers fitted with 250 micron fine mesh screens which prevent damaged fuel assemblies or fuel debris from blocking the basket flow holes. Therefore, the flow holes cannot be blocked.

Once established, the integrity of the MPC confinement boundary is maintained during all credible off-normal and accident conditions, and thus, the MPC cannot be flooded. Therefore, it is concluded that the MPC fuel baskets cannot be preferentially flooded.

6.4.2.5 Design Basis Accidents

The analyses presented in Chapters 3 and 11 demonstrate that the damage resulting from the design basis accidents is limited to a loss of the neutron shield material as a result of the fire accident. Because the criticality analyses do not take credit for the neutron shield material (Holtite-A), this condition has no effect on the criticality analyses.

As reported in Chapter 3, the minimum factor of safety for the MPC-24 as a result of the hypothetical cask drop or tip-over accident is 1.17 against the Level D allowables for Subsection NG, Section III of the ASME Code. Therefore, because the maximum box wall stresses are well within the ASME Level D allowables, the flux-trap gap change will be insignificant compared to the characteristic dimension of the flux trap.

In summary, the design basis accidents have no adverse effect on the design parameters important to criticality safety, and therefore, there is no increase in reactivity as a result of any of the credible off-normal or accident conditions involving handling, packaging, transfer or storage. Consequently, the HI-STAR 100 System is in full compliance with the requirement of 10CRF72.124, which states that "before a nuclear criticality accident is possible, at least two unlikely, independent, and concurrent or sequential changes have occurred in the conditions essential to nuclear criticality safety."

6.4.3 Criticality Results

Results of the criticality safety calculations for the condition of flooding with clean unborated water are presented in Section 6.2 and summarized in Section 6.1. These data confirm that for each of the candidate fuel types and basket configurations the effective multiplication factor (k_{eff}), including all biases and uncertainties at a 95-percent confidence level, do not exceed 0.95 under all credible normal, off-normal, and accident conditions.

Additional calculations (CASMO-3) at elevated temperatures confirm that the temperature coefficients of reactivity are negative as shown in Table 6.3.1. This confirms that the calculations for the storage baskets are conservative.

In calculating the maximum reactivity, the analysis used the following equation:

$$k_{\text{eff}}^{\text{max}} = k_c + K_c \sigma_c + \text{Bias} + \sigma_B$$

where:

- ⇒ k_c is the calculated k_{eff} under the worst combination of tolerances;
- ⇒ K_c is the K multiplier for a one-sided statistical tolerance limit with 95% probability at the 95% confidence level [6.1.8]. Each final k_{eff} value calculated by MCNP4a (or KENO5a) is the result of averaging 100 (or more) cycle k_{eff} values, and thus, is based on a sample size of 100. The K multiplier corresponding to a sample size of 100 is 1.93. However, for this analysis a value of 2.00 was assumed for the K multiplier, which is larger (more conservative) than the value corresponding to a sample size of 100;
- ⇒ σ_c is the standard deviation of the calculated k_{eff} , as determined by the computer code (MCNP4a or KENO5a);
- ⇒ **Bias** is the systematic error in the calculations (code dependent) determined by comparison with critical experiments in Appendix 6.A; and
- ⇒ σ_B is the standard error of the bias (which includes the K multiplier for 95% probability at the 95% confidence level; see Appendix 6.A).

Appendix 6.A presents the critical experiment benchmarking and the derivation of the bias and standard error of the bias (95% probability at the 95% confidence level).

6.4.4 Damaged Fuel Container

Both damaged BWR fuel assemblies and BWR fuel debris are required to be loaded into Damaged Fuel Containers (DFCs) prior to being loaded into the MPC. Two different DFC types

with slightly different cross sections are analyzed. DFCs containing fuel debris must be stored in the MPC-68F. DFCs containing damaged fuel assemblies may be stored in either the MPC-68 or MPC-68F. Evaluation of the capability of storing damaged fuel and fuel debris (loaded in DFCs) is limited to very low reactivity fuel in the MPC-68F. Because the MPC-68 has a higher specified ^{10}B loading, the evaluation of the MPC-68F conservatively bounds the storage of damaged BWR fuel assemblies in a standard MPC-68. Although the maximum planar-average enrichment of the damaged fuel is limited to 2.7% ^{235}U as specified in Appendix B to the Certificate of Compliance, analyses have been made for three possible scenarios, conservatively assuming fuel^{††} of 3.0% enrichment. The scenarios considered included the following:

1. Lost or missing fuel rods, calculated for various numbers of missing rods in order to determine the maximum reactivity. The configurations assumed for analysis are illustrated in Figures 6.4.2 through 6.4.8.
2. Broken fuel assembly with the upper segments falling into the lower segment creating a close-packed array (described as a 8x8 array). For conservatism, the array analytically retained the same length as the original fuel assemblies in this analysis. This configuration is illustrated in Figure 6.4.9.
3. Fuel pellets lost from the assembly and forming powdered fuel dispersed through a volume equivalent to the height of the original fuel. (Flow channel and clad material assumed to disappear).

Results of the analyses, shown in Table 6.4.5, confirm that, in all cases, the maximum reactivity is well below the regulatory limit. There is no significant difference in reactivity between the two DFC types. Collapsed fuel reactivity (simulating fuel debris) is low because of the reduced moderation. Dispersed powdered fuel results in low reactivity because of the increase in ^{238}U neutron capture (higher effective resonance integral for ^{238}U absorption).

The loss of fuel rods results in a small increase in reactivity (i.e., rods assumed to collapse, leaving a smaller number of rods still intact). The peak reactivity occurs for 8 missing rods, and a smaller (or larger) number of intact rods will have a lower reactivity, as indicated in Table 6.4.5.

The analyses performed and summarized in Table 6.4.5 provides the relative magnitude of the effects on the reactivity. This information coupled with the maximum k_{eff} values listed in Table 6.1.3 and the conservatism in the analyses, demonstrate that the maximum k_{eff} of the damaged fuel in the most adverse post-accident condition will remain well below the regulatory requirement of $k_{\text{eff}} < 0.95$.

Appendix 6.D provides sample input files for the damaged fuel analysis.

†† 6x6A01 and 7x7A01 fuel assemblies were used as representative assemblies.

6.4.5 Fuel Assemblies with Missing Rods

For fuel assemblies that are qualified for damaged fuel storage, missing and/or damaged fuel rods are acceptable. However, for fuel assemblies to meet the limitations of intact fuel assembly storage, missing fuel rods must be replaced with dummy rods that displace a volume of water that is equal to, or larger than, that displaced by the original rods.

6.4.6 Thoria Rod Canister

The Thoria Rod Canister is similar to a DFC with an internal separator assembly containing 18 intact fuel rods. The configuration is illustrated in Figure 6.4.10. The k_{eff} value for an MPC-68F filled with Thoria Rod Canisters is calculated to be 0.1813. This low reactivity is attributed to the relatively low content in ^{235}U (equivalent to UO_2 fuel with an enrichment of approximately 1.7 wt% ^{235}U), the large spacing between the rods (the pitch is approximately 1", the cladding OD is 0.412") and the absorption in the separator assembly. Together with the maximum k_{eff} values listed in Tables 6.1.2 and 6.1.3 this result demonstrates, that the k_{eff} for a Thoria Rod Canister loaded into the MPC68 or the MPC68F together with other approved fuel assemblies or DFCs will remain well below the regulatory requirement of $k_{\text{eff}} < 0.95$.

6.4.7 Sealed Rods replacing BWR Water Rods

Some BWR fuel assemblies contain sealed rods filled with a non-fissile instead of water rods. Compared to the configuration with water rods, the configuration with sealed rods has a reduced amount of moderator, while the amount of fissile material is maintained. Thus, the reactivity of the configuration with sealed rods will be lower compared to the configuration with water rods. Any configuration containing sealed rods instead of water rods is therefore bounded by the analysis for the configuration with water rods and no further analysis is required to demonstrate the acceptability. Therefore, for all BWR fuel assemblies analyzed, it is permissible that water rods are replaced by sealed rods filled with a non-fissile material.

6.4.8 Inserts in PWR Fuel Assemblies

Inserts into PWR fuel assemblies such as Thimble Plugs (TPs) and Burnable Poison Rod Assemblies (BPRAs) and similar devices are permitted for storage with all PWR fuel types. The reactivity of any PWR assembly with inserts is bounded by (i.e. lower than) the reactivity of the same assembly without the insert. This is due to the fact that the insert reduces the amount of moderator in the assembly, while the amount of fissile material remains unchanged. Therefore,

from a criticality safety perspective, inserts into PWR assemblies are acceptable for all allowable PWR types, and increase the safety margin.

6.4.9 Neutron Sources in Fuel Assemblies

Fuel assemblies containing start-up neutron sources are permitted for storage in the HI-STAR 100 System. The reactivity of a fuel assembly is not affected by the presence of a neutron source (other than by the presence of the material of the source, which is discussed later). This is true because in a system with a k_{eff} less than 1.0, any given neutron population at any time, regardless of its origin or size, will decrease over time. Therefore, a neutron source of any strength will not increase reactivity, but only the neutron flux in a system, and no additional criticality analyses are required. Sources are inserted as rods into fuel assemblies, i.e. they replace either a fuel rod or water rod (moderator). Therefore, the insertion of the material of the source into a fuel assembly will not lead to an increase of reactivity either.

Table 6.4.1

MAXIMUM REACTIVITIES WITH REDUCED WATER DENSITIES FOR CASK ARRAYS[†]

Case Number	Water Density		MCNP4a Maximum k_{eff} ^{††}	
	Internal	External	MPC-24 (17x17A01 @ 4.0%)	MPC-68 (8x8C04 @ 4.2%)
1	100%	single cask	0.9449	0.9348
2	100%	100%	0.9434	0.9339
3	100%	70%	0.9465	0.9339
4	100%	50%	0.9444	0.9347
5	100%	20%	0.9439	0.9338
6	100%	10%	0.9424	0.9336
7	100%	5%	0.9446	0.9333
8	100%	0%	0.9457	0.9338
9	70%	0%	0.8497	0.8488
10	50%	0%	0.7632	0.7631
11	20%	0%	0.5787	0.5797
12	10%	0%	0.5012	0.5139
13	5%	0%	0.4629	0.4763
14	10%	100%	0.4839	0.4946

† For an infinite square array of casks with 60cm spacing between cask surfaces

†† Maximum k_{eff} includes the bias, uncertainties, and calculational statistics, evaluated for the worst case combination of manufacturing tolerances.

Table 6.4.2

REACTIVITY EFFECTS OF PARTIAL CASK FLOODING

MPC-24 (17x17A01 @ 4.0% ENRICHMENT)			
Flooded Condition (% Full)	Vertical Orientation	Flooded Condition (% Full)	Horizontal Orientation
25	0.9219	25	0.9119
50	0.9397	50	0.9321
75	0.9443	75	0.9423
100	0.9449	100	0.9449
MPC-68 (8x8C04 @ 4.2% ENRICHMENT)			
Flooded Condition (% Full)	Vertical Orientation	Flooded Condition (% Full)	Horizontal Orientation
25	0.9132	23.5	0.8586
50	0.9307	50	0.9088
75	0.9312	76.5	0.9275
100	0.9348	100	0.9348

Notes:

1. All values are maximum k_{eff} which include bias, uncertainties, and calculational statistics, evaluated for the worst case combination of manufacturing tolerances.

Table 6.4.3

REACTIVITY EFFECT OF FLOODING THE PELLETT-TO-CLAD GAP

Pellet-to-Clad Condition	MPC-24 17x17A01 4.0% Enrichment	MPC-68 8x8C04 4.2% Enrichment
dry	0.9404	0.9279
flooded	0.9449	0.9348

Notes:

1. All values are maximum k_{eff} which includes bias, uncertainties, and calculational statistics, evaluated for the worst case combination of manufacturing tolerances.

Table 6.4.4

DELETED

Table 6.4.5

MAXIMUM k_{eff} VALUES[†] IN THE DAMAGED FUEL CONTAINER

Condition	MCNP4a Maximum ^{††} k_{eff}	
	DFC Dimensions: ID 4.93" THK. 0.12"	DFC Dimensions: ID 4.81" THK. 0.11"
<u>6x6 Fuel Assembly</u>		
6x6 Intact Fuel	0.7086	0.7016
w/32 Rods Standing	0.7183	0.7117
w/28 Rods Standing	0.7315	0.7241
w/24 Rods Standing	0.7086	0.7010
w/18 Rods Standing	0.6524	0.6453
Collapsed to 8x8 array	0.7845	0.7857
Dispersed Powder	0.7628	0.7440
<u>7x7 Fuel Assembly</u>		
7x7 Intact Fuel	0.7463	0.7393
w/41 Rods Standing	0.7529	0.7481
w/36 Rods Standing	0.7487	0.7444
w/25 Rods Standing	0.6718	0.6644

† These calculations were performed with a planar-average enrichment of 3.0% and a ¹⁰B loading of 0.0067 g/cm², which is 75% of a minimum ¹⁰B loading of 0.0089 g/cm². The minimum ¹⁰B loading in the MPC-68F is 0.010 g/cm². Therefore, the listed maximum k_{eff} values are conservative.

†† Maximum k_{eff} includes bias, uncertainties, and calculational statistics, evaluated for the worst case combination of manufacturing tolerances.

DELETED

FIGURE 6.4.1

**FIGURE WITHHELD AS SENSITIVE
UNCLASSIFIED INFORMATION**

**FIGURE WITHHELD AS SENSITIVE
UNCLASSIFIED INFORMATION**

**FIGURE WITHHELD AS
SENSITIVE UNCLASSIFIED
INFORMATION**

**FIGURE WITHHELD AS SENSITIVE
UNCLASSIFIED INFORMATION**

**FIGURE WITHHELD AS SENSITIVE
UNCLASSIFIED INFORMATION**

**FIGURE WITHHELD AS SENSITIVE
UNCLASSIFIED INFORMATION**

**FIGURE WITHHELD AS SENSITIVE
UNCLASSIFIED INFORMATION**

**FIGURE WITHHELD AS SENSITIVE
UNCLASSIFIED INFORMATION**

**FIGURE WITHHELD AS SENSITIVE
UNCLASSIFIED INFORMATION**

Benchmark calculations have been made on selected critical experiments, chosen, insofar as possible, to bound the range of variables in the cask designs. The most important parameters are (1) the enrichment, (2) the water-gap size (MPC-24) or cell spacing (MPC-68), and (3) the ^{10}B loading of the neutron absorber panels. Other parameters, within the normal range of cask and fuel designs, have a smaller effect, but are also included. No significant trends were evident in the benchmark calculations or the derived bias. Detailed benchmark calculations are presented in Appendix 6.A.

The benchmark calculations were performed with the same computer codes and cross-section data, described in Section 6.4, that were used to calculate the k_{eff} values for the cask. Further, all calculations were performed on the same computer hardware, specifically, personal computers using the pentium processor.

This chapter documents the criticality evaluation of the HI-STAR 100 System for the storage of spent nuclear fuel. This evaluation demonstrates that the HI-STAR 100 System is in full compliance with the criticality requirements of 10CFR72 and NUREG-1536.

Structures, systems, and components important to criticality safety are described in sufficient detail in this chapter to enable an evaluation of their effectiveness.

The HI-STAR 100 System is designed to be subcritical under all credible conditions. The criticality design is based on favorable geometry and fixed neutron poisons (Boral). An appraisal of the fixed neutron poisons has shown that they will remain effective for a storage period greater than 20 years, and there is no credible way to lose it, therefore there is no need to provide a positive means to verify their continued efficacy as required by 10CFR72.124(b).

The criticality evaluation has demonstrated that the cask will enable the storage of spent fuel for a minimum of 20 years with an adequate margin of safety. Further, the evaluation has demonstrated that the design basis accidents have no adverse effect on the design parameters important to criticality safety, and therefore, the HI-STAR 100 System is in full compliance with the double contingency requirements of 10CFR72.124. Therefore, it is concluded that the criticality design features for the HI-STAR 100 System are in compliance with 10 CFR Part 72 and that the applicable design and acceptance criteria have been satisfied. The criticality evaluation provides reasonable assurance that the HI-STAR 100 System will allow safe storage of spent fuel.

REFERENCES

- [6.1.1] NUREG-1536, Standard Review Plan for Dry Cask Storage Systems, USNRC, Washington, D.C., January 1997.
- [6.1.2] 10CFR72.124, "Criteria For Nuclear Criticality Safety."
- [6.1.3] USNRC Standard Review Plan, NUREG-0800, Section 9.1.2, Spent Fuel Storage, Rev. 2 - July 1981.
- [6.1.4] J.F. Briesmeister, Ed., "MCNP - A General Monte Carlo N-Particle Transport Code, Version 4A," Los Alamos National Laboratory, LA-12625-M (1993).
- [6.1.5] L.M. Petrie and N.F. Landers, "KENOVa - An Improved Monte Carlo Criticality Program with Supergrouping," Volume 2, Section F11 from "SCALE: A Modular System for Performing Standardized Computer Analysis for Licensing Evaluation," NUREG/CR-0200, Rev. 4, January 1990.
- [6.1.6] N.M. Greene, L.M. Petrie and R.M. Westfall, "NITAWL-II: Scale-System Module For Performing Resonance Shielding and Working Library Production," Volume 1, Section F1 from "SCALE: A Modular System for Performing Standardized Computer Analysis for Licensing Evaluation," NUREG/CR-0200, Rev. 4, January 1990.
- [6.1.7] J.R. Knight, "SUPERDAN: Computer Programs for Calculating the Dancoff Factor of Spheres, Cylinders, and Slabs," Oak Ridge National Laboratory, ORNL/NUREG/CSD/TM-2, March 1978, with correction published in "Proceedings of Seminar on SCALE-4," Saclay, France, 1991.
- [6.1.8] M.G. Natrella, Experimental Statistics, National Bureau of Standards, Handbook 91, August 1963.
- [6.1.9] A. Ahlin, M. Edenius, and H. Haggblom, "CASMO - A Fuel Assembly Burnup Program," AE-RF-76-4158, Studsvik report.

- [6.1.10] A. Ahlin and M. Edenius, "CASMO - A Fast Transport Theory Depletion Code for LWR Analysis," *Trans. Am. Nucl. Soc.*, **26**, 604 (1977).
- [6.1.11] "CASMO-3 A Fuel Assembly Burnup Program, Users Manual," Studsvik/NFA-87/7, Studsvik Energitechnik AB, November 1986.
- [6.1.12] M. Edenius and A. Ahlin, "CASMO-3: New Features, Benchmarking, and Advanced Applications," *Nucl. Sci. Eng.*, **100**, 342-351, (1988).
- [6.1.13] "QA Validation Manual for Computer Code CELLDAN," Holtec International Report HI-90577.
- [6.4.1] "SCALE 4.3: A Modular System for Performing Standardized Computer Analysis for Licensing Evaluations," NUREG-CR-0200, Rev. 5, Oak Ridge National Laboratory (1995).
- [6.4.2] J.M. Cano, R. Caro, and J.M. Martinez-Val, "Supercriticality Through Optimum Moderation in Nuclear Fuel Storage," *Nucl. Technol.*, **48**, 251-260, (1980).

APPENDIX 6.A: BENCHMARK CALCULATIONS

6.A.1 INTRODUCTION AND SUMMARY

Benchmark calculations have been made on selected critical experiments, chosen, in so far as possible, to bound the range of variables in the cask designs. Two independent methods of analysis were used, differing in cross section libraries and in the treatment of the cross sections. MCNP4a [6.A.1] is a continuous energy Monte Carlo code and KENO5a [6.A.2] uses group-dependent cross sections. For the KENO5a analyses reported here, the 238-group library was chosen, processed through the NITAWL-II [6.A.2] program to create a working library and to account for resonance self-shielding in uranium-238 (Nordheim integral treatment). The 238 group library was chosen to avoid or minimize the errors[†] (trends) that have been reported (e.g., [6.A.3 through 6.A.5]) for calculations with collapsed cross section sets.

In cask designs, the three most significant parameters affecting criticality are (1) the fuel enrichment, (2) the ¹⁰B loading in the neutron absorber, and (3) the lattice spacing (or water-gap thickness if a flux-trap design is used). Other parameters, within the normal range of cask and fuel designs, have a smaller effect, but are also included in the analyses.

Table 6.A.1 summarizes results of the benchmark calculations for all cases selected and analyzed, as referenced in the table. The effect of the major variables are discussed in subsequent sections below. It is important to note that there is obviously considerable overlap in parameters since it is not possible to vary a single parameter and maintain criticality; some other parameter or parameters must be concurrently varied to maintain criticality.

One possible way of representing the data is through a spectrum index that incorporates all of the variations in parameters. KENO5a computes and prints the "energy of the average lethargy causing fission". In MCNP4a, by utilizing the tally option with the identical 238-group energy structure as in KENO5a, the number of fissions in each group may be collected and the energy of the average lethargy causing fission determined (post-processing).

Figures 6.A.1 and 6.A.2 show the calculated k_{eff} for the benchmark critical experiments as a function of the "energy of the average lethargy causing fission" for MCNP4a and KENO5a, respectively (UO₂ fuel only). The scatter in the data (even for comparatively minor variation in critical parameters) represents

[†] Small but observable trends (errors) have been reported for calculations with the 27-group and 44-group collapsed libraries. These errors are probably due to the use of a single collapsing spectrum when the spectrum should be different for the various cases analyzed, as evidenced by the spectrum indices.

experimental error[†] in performing the critical experiments within each laboratory, as well as between the various testing laboratories. The B&W critical experiments show a larger experimental error than the PNL criticals. This would be expected since the B&W criticals encompass a greater range of critical parameters than the PNL criticals.

Linear regression analysis of the data in Figures 6.A.1 and 6.A.2 show that there are no trends, as evidenced by very low values of the correlation coefficient (0.13 for MCNP4a and 0.21 for KENO5a). The total bias (systematic error, or mean of the deviation from a k_{eff} of exactly 1.000) for the two methods of analysis are shown in the table below.

Calculational Bias of MCNP4a and KENO5a		
	Total	Truncated
MCNP4a	0.0009±0.0011	0.0021±0.0006
KENO5a	0.0030±0.0012	0.0036±0.0009

The values of bias shown in this table include both the bias derived directly from the calculated k_{eff} values in Table 6.A.1, and a more conservative value derived by arbitrarily truncating to 1.000 any calculated value that exceeds 1.000. The bias and standard error of the bias were calculated by the following equations^{††}, with the standard error multiplied by the one-sided K-factor for 95% probability at the 95% confidence level from NBS Handbook 91 [6.A.18] (for the number of cases analyzed, the K-factor is -2.05 or slightly more than 2).

$$\bar{k} = \frac{1}{n} \sum_i^n k_i \quad (6.A.1)$$

† A classical example of experimental error is the corrected enrichment in the PNL experiments, first as an addendum to the initial report and, secondly, by revised values in subsequent reports for the same fuel rods.

†† These equations may be found in any standard text on statistics, for example, reference [6.A.6] (or the MCNP4a manual) and is the same methodology used in MCNP4a and in KENO5a.

$$\sigma_{\bar{k}}^2 = \frac{\sum_{i=1}^n k_i^2 - (\sum_{i=1}^n k_i)^2 / n}{n(n-1)} \quad (6.A.2)$$

$$Bias = (1 - \bar{k}) \pm K\sigma_{\bar{k}} \quad (6.A.3)$$

where k_i are the calculated reactivities for n critical experiments; $\sigma_{\bar{k}}$ is the unbiased estimator of the standard deviation of the mean (also called the standard error of the mean); and K is the one-sided multiplier for 95% probability at the 95% confidence level (NBS Handbook 91 [6.A.18]).

Formula 6.A.3 is based on the methodology of the National Bureau of Standards (now NIST) and is used to calculate the values presented on page 6.A-2. The first portion of the equation, $(1-\bar{k})$, is the actual bias which is added to the MCNP4a and KENO5a results. The second term, $K\sigma_{\bar{k}}$, which corresponds to σ_B in Section 6.4.3, is the uncertainty or standard error associated with the bias. The K values used were obtained from the National Bureau of Standards Handbook 91 and are for one-sided statistical tolerance limits for 95% probability at the 95% confidence level. The actual K values for the 56 critical experiments evaluated with MCNP4a and the 53 critical experiments evaluated with KENO5a are 2.04 and 2.05, respectively.

The larger of the calculational biases (truncated bias) was used to evaluate the maximum k_{eff} values for the two cask designs.

6.A.2 Effect of Enrichment

The benchmark critical experiments include those with enrichments ranging from 2.46% to 5.74% and therefore span the enrichment range for the MPC designs. Figures 6.A.3 and 6.A.4 show the calculated k_{eff} values (Table 6.A.1) as a function of the fuel enrichment reported for the critical experiments. Linear regression analyses for these data confirms that there are no trends, as indicated by low values of the correlation coefficients (0.03 for MCNP4a and 0.38 for KENO5a). Thus, there are no corrections to the bias for the various enrichments.

As further confirmation of the absence of any trends with enrichment, the MPC-68 configuration was calculated with both MCNP4a and KENO5a for various enrichments. The cross-comparison of calculations with codes of comparable sophistication is suggested in Reg. Guide 3.41. Results of this

comparison, shown in Table 6.A.2 and Figure 6.A.5, confirm no significant difference in the calculated values of k_{eff} for the two independent codes as evidenced by the 45E slope of the curve. Since it is very unlikely that two independent methods of analysis would be subject to the same error, this comparison is considered confirmation of the absence of an enrichment effect (trend) in the bias.

6.A.3 Effect of ^{10}B Loading

Several laboratories have performed critical experiments with a variety of thin absorber panels similar to the Boral panels in the cask designs. Of these critical experiments, those performed by B&W are the most representative of the cask designs. PNL has also made some measurements with absorber plates, but, with one exception (a flux-trap experiment), the reactivity worth of the absorbers in the PNL tests is very low and any significant errors that might exist in the treatment of strong thin absorbers could not be revealed.

Table 6.A.3 lists the subset of experiments using thin neutron absorbers (from Table 6.A.1) and shows the reactivity worth (Δk) of the absorber.[†]

No trends with reactivity worth of the absorber are evident, although based on the calculations shown in Table 6.A.3, some of the B&W critical experiments seem to have unusually large experimental errors. B&W made an effort to report some of their experimental errors. Other laboratories did not evaluate their experimental errors.

To further confirm the absence of a significant trend with ^{10}B concentration in the absorber, a cross-comparison was made with MCNP4a and KENO5a (as suggested in Reg. Guide 3.41). Results are shown in Figure 6.A.6 and Table 6.A.4 for the MPC-68 cask^{††} geometry. These data substantiate the absence of any error (trend) in either of the two codes for the conditions analyzed (data points fall on a 45E line, within an expected 95% probability limit).

[†] The reactivity worth of the absorber panels was determined by repeating the calculation with the absorber analytically removed and calculating the incremental (Δk) change in reactivity due to the absorber.

^{††} The MPC-68 geometry was chosen for this comparison since it contains the greater number of Boral panels and would therefore be expected to be the most sensitive to trends (errors) in calculations.

6.A.4 Miscellaneous and Minor Parameters

6.A.4.1 Reflector Material and Spacings

PNL has performed a number of critical experiments with thick steel and lead reflectors.[†] Analysis of these critical experiments are listed in Table 6.A.5 (subset of data in Table 6.A.1). There appears to be a small tendency toward overprediction of k_{eff} at the lower spacing, although there are an insufficient number of data points in each series to allow a quantitative determination of any trends. The tendency toward overprediction at close spacing means that the cask calculations may be slightly more conservative than otherwise.

6.A.4.2 Fuel Pellet Diameter and Lattice Pitch

The critical experiments selected for analysis cover a range of fuel pellet diameters from 0.311 to 0.444 inches, and lattice spacings from 0.476 to 1.00 inches. In the cask designs, the fuel pellet diameters range from 0.303 to 0.3835 inches O.D. (0.496 to 0.580 inch lattice spacing) for PWR fuel and from 0.3224 to 0.494 inches O.D. (0.488 to 0.740 inch lattice spacing) for BWR fuel. Thus, the critical experiments analyzed provide a reasonable representation of the fuel in the MPC designs. Based on the data in Table 6.A.1, there does not appear to be any observable trend with either fuel pellet diameter or lattice pitch, at least over the range of the critical experiments or the cask designs.

6.A.4.3 Soluble Boron Concentration Effects

Various soluble boron concentrations were used in the B&W series of critical experiments and in one PNL experiment, with boron concentrations ranging up to 2550 ppm. Results of MCNP4a (and one KENO5a) calculations are shown in Table 6.A.6. Analyses of the very high boron concentration experiments (>1300 ppm) show a tendency to slightly overpredict reactivity for the three experiments exceeding 1300 ppm. In turn, this would suggest that the evaluation of the MPC-32 with various soluble boron concentration could be slightly conservative for the high soluble boron concentration.

6.A.5 MOX Fuel

The number of critical experiments with PuO₂ bearing fuel (MOX) is more limited than for UO₂ fuel. However, a number of MOX critical experiments have been analyzed and the results are shown in Table

[†] Parallel experiments with a depleted uranium reflector were also performed but not included in the present analysis since they are not pertinent to the Holtec cask design. A lead reflector is also not directly pertinent, but might be used in future designs.

6.A.7. Results of these analyses are generally above a k_{eff} of 1.00, indicating that when Pu is present, both MCNP4a and KENO5a overpredict the reactivity.

This may indicate that calculation for MOX fuel will be expected to be conservative, especially with MCNP4a. It may be noted that for the larger lattice spacings, the KENO5a calculated reactivities are below 1.00, suggesting that a small trend may exist with KENO5a. It is also possible that the overprediction in k_{eff} for both codes may be due to a small inadequacy in the determination of the Pu-241 decay and Am-241 growth. This possibility is supported by the consistency in calculated k_{eff} over a wide range of the spectral index (energy of the average lethargy causing fission).

6.A.6 References

- [6.A.1] J.F. Briesmeister, Ed., "MCNP - A General Monte Carlo N-Particle Transport Code, Version 4A; Los Alamos National Laboratory, LA-12625-M (1993).
- [6.A.2] SCALE 4.3, "A Modular Code System for Performing Standardized Computer Analyses for Licensing Evaluation", NUREG-0200 (ORNL-NUREG-CSD-2/U2/R5, Revision 5, Oak Ridge National Laboratory, September 1995.
- [6.A.3] M.D. DeHart and S.M. Bowman, "Validation of the SCALE Broad Structure 44-G Group ENDF/B-Y Cross-Section Library for Use in Criticality Safety Analyses", NUREG/CR-6102 (ORNL/TM-12460) Oak Ridge National Laboratory, September 1994.
- [6.A.4] W.C. Jordan et al., "Validation of KENOv.a", CSD/TM-238, Martin Marietta Energy Systems, Inc., Oak Ridge National Laboratory, December 1986.
- [6.A.5] O.W. Hermann et al., "Validation of the Scale System for PWR Spent Fuel Isotopic Composition Analysis", ORNL-TM-12667, Oak Ridge National Laboratory, undated.
- [6.A.6] R.J. Larsen and M.L. Marx, An Introduction to Mathematical Statistics and its Applications, Prentice-Hall, 1986.
- [6.A.7] M.N. Baldwin et al., Critical Experiments Supporting Close Proximity Water Storage of Power Reactor Fuel, BAW-1484-7, Babcock and Wilcox Company, July 1979.

- [6.A.8] G.S. Hoovier et al., Critical Experiments Supporting Underwater Storage of Tightly Packed Configurations of Spent Fuel Pins, BAW-1645-4, Babcock & Wilcox Company, November 1991.
- [6.A.9] L.W. Newman et al., Urania Gadolinia: Nuclear Model Development and Critical Experiment Benchmark, BAW-1810, Babcock and Wilcox Company, April 1984.
- [6.A.10] J.C. Manaranche et al., "Dissolution and Storage Experimental Program with 4.75% Enriched Uranium-Oxide Rods," Trans. Am. Nucl. Soc. 33: 362-364 (1979).
- [6.A.11] S.R. Bierman and E.D. Clayton, Criticality Experiments with Subcritical Clusters of 2.35 wt % and 4.31 wt % ²³⁵U Enriched UO₂ Rods in Water with Steel Reflecting Walls, PNL-3602, Battelle Pacific Northwest Laboratory, April 1981.
- [6.A.12] S.R. Bierman et al., Criticality Experiments with Subcritical Clusters of 2.35 Wt% and 4.31 Wt% ²³⁵U Enriched UO₂ Rods in Water with Uranium or Lead Reflecting Walls, PNL-3926, Battelle Pacific Northwest Laboratory, December, 1981.
- [6.A.13] S.R. Bierman et al., Critical Separation Between Subcritical Clusters of 4.31 Wt % ²³⁵U Enriched UO₂ Rods in Water with Fixed Neutron Poisons, PNL-2615, Battelle Pacific Northwest Laboratory, October 1977.
- [6.A.14] S.R. Bierman, Criticality Experiments with Neutron Flux Traps Containing Voids, PNL-7167, Battelle Pacific Northwest Laboratory, April 1990.
- [6.A.15] B.M. Durst et al., Critical Experiments with 4.31 wt % ²³⁵U Enriched UO₂ Rods in Highly Borated Water Lattices, PNL-4267, Battelle Pacific Northwest Laboratory, August 1982.
- [6.A.16] S.R. Bierman, Criticality Experiments with Fast Test Reactor Fuel Pins in Organic Moderator, PNL-5803, Battelle Pacific Northwest Laboratory, December 1986.

- [6.A.17] E.G. Taylor et al., Saxton Plutonium Program Critical Experiments for the Saxton Partial Plutonium core, WCAP-3385-54, Westinghouse Electric Corp., Atomic Power Division, December 1965.
- [6.A.18] M.G. Natrella, Experimental Statistics, National Bureau of Standards, Handbook 91, August 1963.

Table 6.A.1
Summary of Criticality Benchmark Calculations

	Reference	Identification	Enrich.	Calculated k_{eff}		EALF [†] (eV)	
				MCNP4a	KENO5a	MCNP4a	KENO5a
1	B&W-1484 (6.A.7)	Core I	2.46	0.9964 ± 0.0010	0.9898 ± 0.0006	0.1759	0.1753
2	B&W-1484 (6.A.7)	Core II	2.46	1.0008 ± 0.0011	1.0015 ± 0.0005	0.2553	0.2446
3	B&W-1484 (6.A.7)	Core III	2.46	1.0010 ± 0.0012	1.0005 ± 0.0005	0.1999	0.1939
4	B&W-1484 (6.A.7)	Core IX	2.46	0.9956 ± 0.0012	0.9901 ± 0.0006	0.1422	0.1426
5	B&W-1484 (6.A.7)	Core X	2.46	0.9980 ± 0.0014	0.9922 ± 0.0006	0.1513	0.1499
6	B&W-1484 (6.A.7)	Core XI	2.46	0.9978 ± 0.0012	1.0005 ± 0.0005	0.2031	0.1947
7	B&W-1484 (6.A.7)	Core XII	2.46	0.9988 ± 0.0011	0.9978 ± 0.0006	0.1718	0.1662
8	B&W-1484 (6.A.7)	Core XIII	2.46	1.0020 ± 0.0010	0.9952 ± 0.0006	0.1988	0.1965
9	B&W-1484 (6.A.7)	Core XIV	2.46	0.9953 ± 0.0011	0.9928 ± 0.0006	0.2022	0.1986
10	B&W-1484 (6.A.7)	Core XV ^{††}	2.46	0.9910 ± 0.0011	0.9909 ± 0.0006	0.2092	0.2014
11	B&W-1484 (6.A.7)	Core XVI ^{††}	2.46	0.9935 ± 0.0010	0.9889 ± 0.0006	0.1757	0.1713
12	B&W-1484 (6.A.7)	Core XVII	2.46	0.9962 ± 0.0012	0.9942 ± 0.0005	0.2083	0.2021

Table 6.A.1
Summary of Criticality Benchmark Calculations

Reference	Identification	Enrich.	Calculated k_{eff}		EALF [†] (eV)		
			MCNP4a	KENO5a	MCNP4a	KENO5a	
13	B&W-1484 (6.A.7)	Core XVIII	2.46	1.0036 ± 0.0012	0.9931 ± 0.0006	0.1705	0.1708
14	B&W-1484 (6.A.7)	Core XIX	2.46	0.9961 ± 0.0012	0.9971 ± 0.0005	0.2103	0.2011
15	B&W-1484 (6.A.7)	Core XX	2.46	1.0008 ± 0.0011	0.9932 ± 0.0006	0.1724	0.1701
16	B&W-1484 (6.A.7)	Core XXI	2.46	0.9994 ± 0.0010	0.9918 ± 0.0006	0.1544	0.1536
17	B&W-1645 (6A.8)	S-type Fuel, w/886 ppm B	2.46	0.9970 ± 0.0010	0.9924 ± 0.0006	1.4475	1.4680
18	B&W-1645 (6A.8)	S-type Fuel, w/746 ppm B	2.46	0.9990 ± 0.0010	0.9913 ± 0.0006	1.5463	1.5660
19	B&W-1645 (6A.8)	SO-type Fuel, w/1156 ppm B	2.46	0.9972 ± 0.0009	0.9949 ± 0.0005	0.4241	0.4331
20	B&W-1810 (6A.9)	Case 1 1337 ppm B	2.46	1.0023 ± 0.0010	NC	0.1531	NC
21	B&W-1810 (6A.9)	Case 12 1899 ppm B	2.46/4.02	1.0060 ± 0.0009	NC	0.4493	NC
22	French (6A.10)	Water Moderator 0 gap	4.75	0.9966 ± 0.0013	NC	0.2172	NC
23	French (6A.10)	Water Moderator 2.5 cm gap	4.75	0.9952 ± 0.0012	NC	0.1778	NC
24	French (6A.10)	Water Moderator 5 cm gap	4.75	0.9943 ± 0.0010	NC	0.1677	NC

Table 6.A.1
Summary of Criticality Benchmark Calculations

Reference	Identification	Enrich.	Calculated k_{eff}		EALF [†] (eV)		
			MCNP4a	KENO5a	MCNP4a	KENO5a	
25	French (6A.10)	Water Moderator 10 cm gap	4.75	0.9979 ± 0.0010	NC	0.1736	NC
26	PNL-3602 (6A.11)	Steel Reflector, 0 separation	2.35	NC	1.0004 ± 0.0006	NC	0.1018
27	PNL-3602 (6A.11)	Steel Reflector, 1.321 cm sepn.	2.35	0.9980 ± 0.0009	0.9992 ± 0.0006	0.1000	0.0909
28	PNL-3602 (6A.11)	Steel Reflector, 2.616 cm sepn	2.35	0.9968 ± 0.0009	0.9964 ± 0.0006	0.0981	0.0975
29	PNL-3602 (6A.11)	Steel Reflector, 3.912 cm sepn.	2.35	0.9974 ± 0.0010	0.9980 ± 0.0006	0.0976	0.0970
30	PNL-3602 (6A.11)	Steel Reflector, infinite sepn.	2.35	0.9962 ± 0.0008	0.9939 ± 0.0006	0.0973	0.0968
31	PNL-3602 (6A.11)	Steel Reflector, 0 cm sepn.	4.306	NC	1.0003 ± 0.0007	NC	0.3282
32	PNL-3602 (6A.11)	Steel Reflector, 1.321 cm sepn.	4.306	0.9997 ± 0.0010	1.0012 ± 0.0007	0.3016	0.3039
33	PNL-3602 (6A.11)	Steel Reflector, 2.616 cm sepn.	4.306	0.9994 ± 0.0012	0.9974 ± 0.0007	0.2911	0.2927
34	PNL-3602 (6A.11)	Steel Reflector, 5.405 cm sepn.	4.306	0.9969 ± 0.0011	0.9951 ± 0.0007	0.2828	0.2860
35	PNL-3602 (6A.11)	Steel Reflector, Infinite sepn.	4.306	0.9910 ± 0.0020	0.9947 ± 0.0007	0.2851	0.2864
36	PNL-3602 (6A.11)	Steel Reflector, with Boral Sheets	4.306	0.9941 ± 0.0011	0.9970 ± 0.0007	0.3135	0.3150

Table 6.A.1
Summary of Criticality Benchmark Calculations

Reference	Identification	Enrich.	Calculated k_{eff}		EALF [†] (eV)		
			MCNP4a	KENO5a	MCNP4a	KENO5a	
37	PNL-3926 (6A.12)	Lead Reflector, 0 cm sepn.	4.306	NC	1.0003 ± 0.0007	NC	0.3159
38	PNL-3926 (6A.12)	Lead Reflector, 0.55 cm sepn.	4.306	1.0025 ± 0.0011	0.9997 ± 0.0007	0.3030	0.3044
39	PNL-3926 (6A.12)	Lead Reflector, 1.956 cm sepn.	4.306	1.0000 ± 0.0012	0.9985 ± 0.0007	0.2883	0.2930
40	PNL-3926 (6A.12)	Lead Reflector, 5.405 cm sepn.	4.306	0.9971 ± 0.0012	0.9946 ± 0.0007	0.2831	0.2854
41	PNL-2615 (6A.13)	Experiment 004/032 - no absorber	4.306	0.9925 ± 0.0012	0.9950 ± 0.0007	0.1155	0.1159
42	PNL-2615 (6A.13)	Experiment 030 - Zr plates	4.306	NC	0.9971 ± 0.0007	NC	0.1154
43	PNL-2615 (6A.13)	Experiment 013 - Steel plates	4.306	NC	0.9965 ± 0.0007	NC	0.1164
44	PNL-2615 (6A.13)	Experiment 014 - Steel plates	4.306	NC	0.9972 ± 0.0007	NC	0.1164
45	PNL-2615 (6A.13)	Exp. 009 1.05% Boron-Steel plates	4.306	0.9982 ± 0.0010	0.9981 ± 0.0007	0.1172	0.1162
46	PNL-2615 (6A.13)	Exp. 012 1.62% Boron-Steel plates	4.306	0.9996 ± 0.0012	0.9982 ± 0.0007	0.1161	0.1173
47	PNL-2615 (6A.13)	Exp. 031 - Boral plates	4.306	0.9994 ± 0.0012	0.9969 ± 0.0007	0.1165	0.1171
48	PNL-7167 (6A.14)	Experiment 214R - with flux trap	4.306	0.9991 ± 0.0011	0.9956 ± 0.0007	0.3722	0.3812

Table 6.A.1
Summary of Criticality Benchmark Calculations

Reference	Identification	Enrich.	Calculated k_{eff}		EALF [†] (eV)		
			MCNP4a	KENO5a	MCNP4a	KENO5a	
49	PNL-7167 (6A.14)	Experiment 214V3 - with flux trap	4.306	0.9969 ± 0.0011	0.9963 ± 0.0007	0.3742	0.3826
50	PNL-4267 (6A.15)	Case 173 - 0 ppm B	4.306	0.9974 ± 0.0012	NC	0.2893	NC
51	PNL-4267 (6A.15)	Case 177 - 2550 ppm B	4.306	1.0057 ± 0.0010	NC	0.5509	NC
52	PNL-5803 (6A.16)	MOX Fuel - Type 3.2 Exp. 21	20% Pu	1.0041 ± 0.0011	1.0046 ± 0.0006	0.9171	0.8868
53	PNL-5803 (6A.16)	MOX Fuel - Type 3.2 Exp. 43	20% Pu	1.0058 ± 0.0012	1.0036 ± 0.0006	0.2968	0.2944
54	PNL-5803 (6A.16)	MOX Fuel - Type 3.2 Exp. 13	20% Pu	1.0083 ± 0.0011	0.9989 ± 0.0006	0.1665	0.1706
55	PNL-5803 (6A.16)	MOX Fuel - Type 3.2 Exp. 32	20% Pu	1.0079 ± 0.0011	0.9966 ± 0.0006	0.1139	0.1165
56	WCAP-3385 (6A.17)	Saxton Case 52 PuO ₂ 0.52" pitch	6.6% Pu	0.9996 ± 0.0011	1.0005 ± 0.0006	0.8665	0.8417
57	WCAP-3385 (6A.17)	Saxton Case 52 U 0.52" pitch	5.74	1.0000 ± 0.0010	0.9956 ± 0.0007	0.4476	0.4580
58	WCAP-3385 (6A.17)	Saxton Case 56 PuO ₂ 0.56" pitch	6.6% Pu	1.0036 ± 0.0011	1.0047 ± 0.0006	0.5289	0.5197
59	WCAP-3385 (6A.17)	Saxton Case 56 borated PuO ₂	6.6% Pu	1.0008 ± 0.0010	NC	0.6389	NC
60	WCAP-3385 (6A.17)	Saxton Case 56 U 0.56" pitch	5.74	0.9994 ± 0.0011	0.9967 ± 0.0007	0.2923	0.2954

Table 6.A.1

Summary of Criticality Benchmark Calculations

	Reference	Identification	Enrich.	Calculated k_{eff}		EALF [†] (eV)	
				MCNP4a	KENO5a	MCNP4a	KENO5a
61	WCAP-3385 (6A.17)	Saxton Case 79 PuO ₂ 0.79" pitch	6.6% Pu	1.0063 ± 0.0011	1.0133 ± 0.0006	0.1520	0.1555
62	WCAP-3385 (6A.17)	Saxton Case 79 U 0.79" pitch	5.74	1.0039 ± 0.0011	1.0008 ± 0.0006	0.1036	0.1047

Notes: NC stands for not calculated.

[†] EALF is the energy of the average lethargy causing fission.

^{††} These experimental results appear to be statistical outliers ($> 3\sigma$) suggesting the possibility of unusually large experimental error. Although they could justifiably be excluded, for conservatism, they were retained in determining the calculational basis.

Table 6.A.2

COMPARISON OF MCNP4a AND KENO5a CALCULATED REACTIVITIES[†]
FOR VARIOUS ENRICHMENTS

Enrichment	Calculated $k_{eff} \pm 1\sigma$	
	MCNP4a	KENO5a
3.0	0.8465 \pm 0.0011	0.8478 \pm 0.0004
3.5	0.8820 \pm 0.0011	0.8841 \pm 0.0004
3.75	0.9019 \pm 0.0011	0.8987 \pm 0.0004
4.0	0.9132 \pm 0.0010	0.9140 \pm 0.0004
4.2	0.9276 \pm 0.0011	0.9237 \pm 0.0004
4.5	0.9400 \pm 0.0011	0.9388 \pm 0.0004

[†] Based on the MPC-68 with the GE 8x8R.

Table 6.A.3

MCNP4a CALCULATED REACTIVITIES FOR
CRITICAL EXPERIMENTS WITH NEUTRON ABSORBERS

Ref.	Experiment		Δk Worth of Absorber r	MCNP4a Calculated k_{eff}	EALF [†] (eV)
6.A.13	PNL-2615	Boral Sheet	0.0139	0.9994±0.0012	0.1165
6.A.7	BAW-1484	Core XX	0.0165	1.0008±0.0011	0.1724
6.A.13	PNL-2615	1.62% Boron-steel	0.0165	0.9996±0.0012	0.1161
6.A.7	BAW-1484	Core XIX	0.0202	0.9961±0.0012	0.2103
6.A.7	BAW-1484	Core XXI	0.0243	0.9994±0.0010	0.1544
6.A.7	BAW-1484	Core XVII	0.0519	0.9962±0.0012	0.2083
6.A.11	PNL-3602	Boral Sheet	0.0708	0.9941±0.0011	0.3135
6.A.7	BAW-1484	Core XV	0.0786	0.9910±0.0011	0.2092
6.A.7	BAW-1484	Core XVI	0.0845	0.9935±0.0010	0.1757
6.A.7	BAW-1484	Core XIV	0.1575	0.9953±0.0011	0.2022
6.A.7	BAW-1484	Core XIII	0.1738	1.0020±0.0011	0.1988
6.A.14	PNL-7167	Expt 214R flux trap	0.1931	0.9991±0.0011	0.3722

[†] EALF is the energy of the average lethargy causing fission.

Table 6.A.4

COMPARISON OF MCNP4a AND KENO5a
CALCULATED REACTIVITIES[†] FOR VARIOUS ¹⁰B LOADINGS

¹⁰ B, g/cm ²	Calculated $k_{\text{eff}} \pm 1\sigma$	
	MCNP4a	KENO5a
0.005	1.0381 ± 0.0012	1.0340 ± 0.0004
0.010	0.9960 ± 0.0010	0.9941 ± 0.0004
0.015	0.9727 ± 0.0009	0.9713 ± 0.0004
0.020	0.9541 ± 0.0012	0.9560 ± 0.0004
0.025	0.9433 ± 0.0011	0.9428 ± 0.0004
0.03	0.9325 ± 0.0011	0.9338 ± 0.0004
0.035	0.9234 ± 0.0011	0.9251 ± 0.0004
0.04	0.9173 ± 0.0011	0.9179 ± 0.0004

[†] Based on 4.5% enrichment GE 8x8R in the MPC-68 cask.

Table 6.A.5

CALCULATIONS FOR CRITICAL EXPERIMENTS WITH
THICK LEAD AND STEEL REFLECTORS[†]

Ref.	Case	Enrichment, wt%	Separation, cm	MCNP4a k_{eff}	KENO5a k_{eff}
6.A.11	Steel Reflector	2.35	1.321	0.9980±0.0009	0.9992±0.0006
		2.35	2.616	0.9968±0.0009	0.9964±0.0006
		2.35	3.912	0.9974±0.0010	0.9980±0.0006
		2.35	4	0.9962±0.0008	0.9939±0.0006
6.A.11	Steel Reflector	4.306	1.321	0.9997±0.0010	1.0012±0.0007
		4.306	2.616	0.9994±0.0012	0.9974±0.0007
		4.306	3.405	0.9969±0.0011	0.9951±0.0007
		4.306	4	0.9910±0.0020	0.9947±0.0007
6.A.12	Lead Reflector	4.306	0.55	1.0025±0.0011	0.9997±0.0007
		4.306	1.956	1.0000±0.0012	0.9985±0.0007
		4.306	5.405	0.9971±0.0012	0.9946±0.0007

[†] Arranged in order of increasing reflector-fuel spacing.

Table 6.A.6

CALCULATIONS FOR CRITICAL EXPERIMENTS WITH VARIOUS SOLUBLE
BORON CONCENTRATIONS

Reference	Experiment	Boron Concentration, ppm	Calculated k_{eff}	
			MCNP4a	KENO5a
6.A.15	PNL-4267	0	0.9974 ± 0.0012	-
6.A.8	BAW-1645-4	886	0.9970 ± 0.0010	0.9924 ± 0.0006
6.A.9	BAW-1810	1337	1.0023 ± 0.0010	-
6.A.9	BAW-1810	1899	1.0060 ± 0.0009	-
6.A.15	PNL-4267	2550	1.0057 ± 0.0010	-

Table 6.A.7

CALCULATIONS FOR CRITICAL EXPERIMENTS WITH MOX FUEL

Reference	Case [†]	MCNP4a		KENO5a	
		k _{eff}	EALF (eV) ^{††}	k _{eff}	EALF ^{††} (eV)
PNL-5803 [6.A.16]	MOX Fuel - Exp. No. 21	1.0041±0.0011	0.9171	1.0046±0.0006	0.8868
	MOX Fuel - Exp. No. 43	1.0058±0.0012	0.2968	1.0036±0.0006	0.2944
	MOX Fuel - Exp. No. 13	1.0083±0.0011	0.1665	0.9989±0.0006	0.1706
	MOX Fuel - Exp. No. 32	1.0079±0.0011	0.1139	0.9966±0.0006	0.1165
WCAP-3385-54 [6.A.17]	Saxton @ 0.52" pitch	0.9996±0.0011	0.8665	1.0005±0.0006	0.8417
	Saxton @ 0.56" pitch	1.0036±0.0011	0.5289	1.0047±0.0006	0.5197
	Saxton @ 0.56" pitch borated	1.0008±0.0010	0.6389	NC	NC
	Saxton @ 0.79" pitch	1.0063±0.0011	0.1520	1.0133±0.0006	0.1555

† Arranged in order of increasing lattice spacing.

†† EALF is the energy of the average lethargy causing fission.

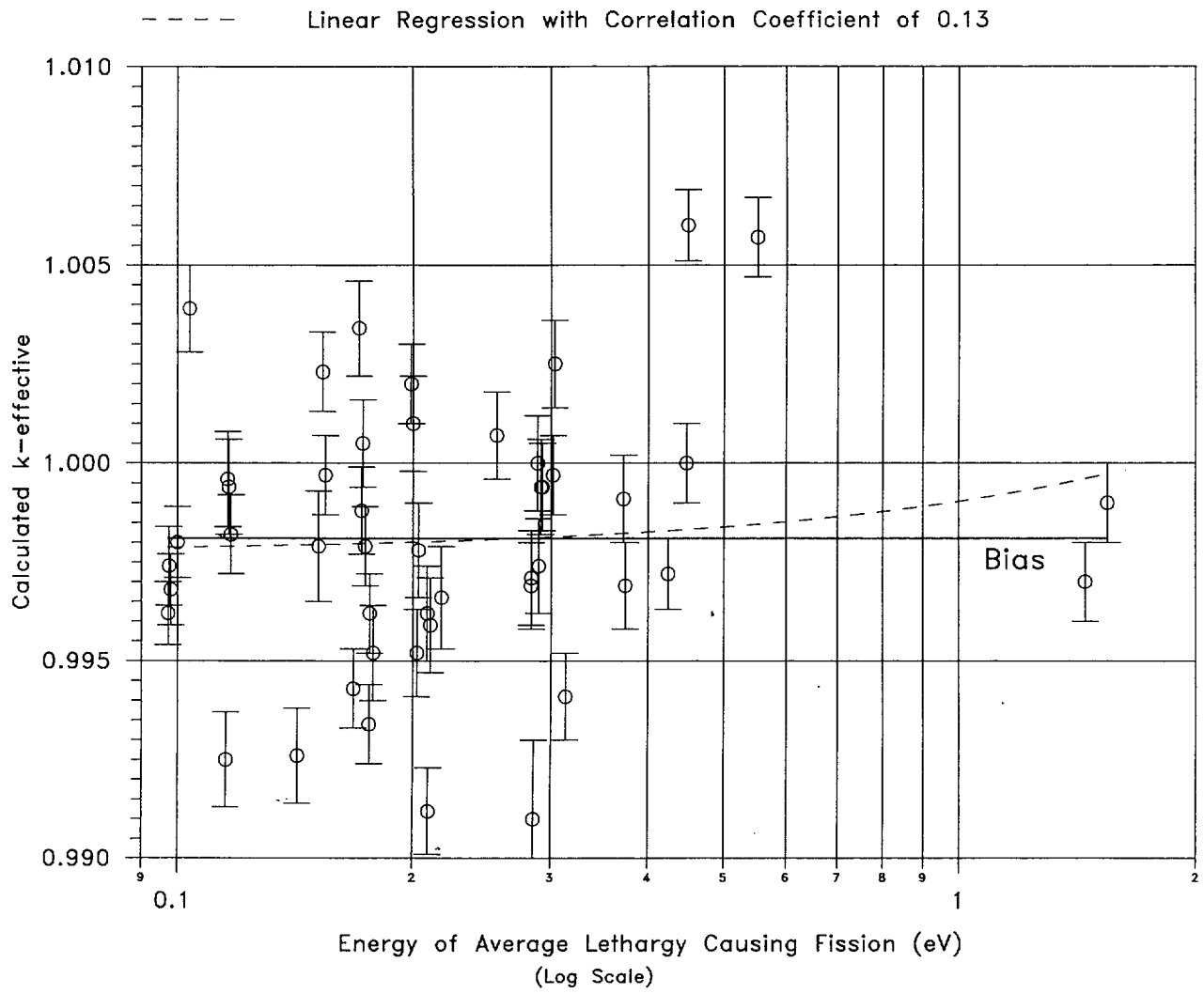


FIGURE 6.A.1 MCNP4a CALCULATED k-eff VALUES FOR VARIOUS VALUES OF THE SPECTRAL INDEX

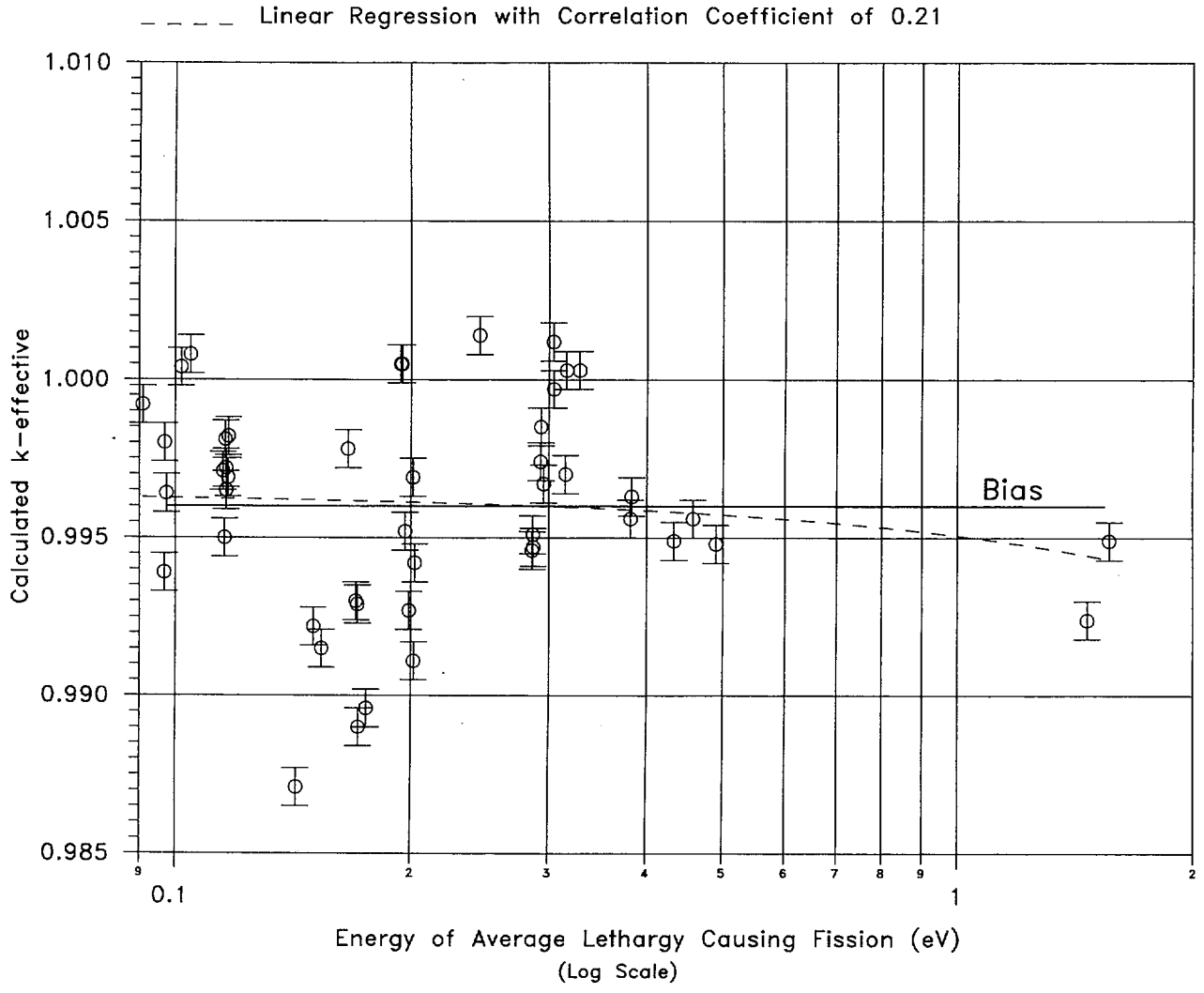


FIGURE 6.A.2 KEN05a CALCULATED k-eff VALUES FOR VARIOUS VALUES OF THE SPECTRAL INDEX

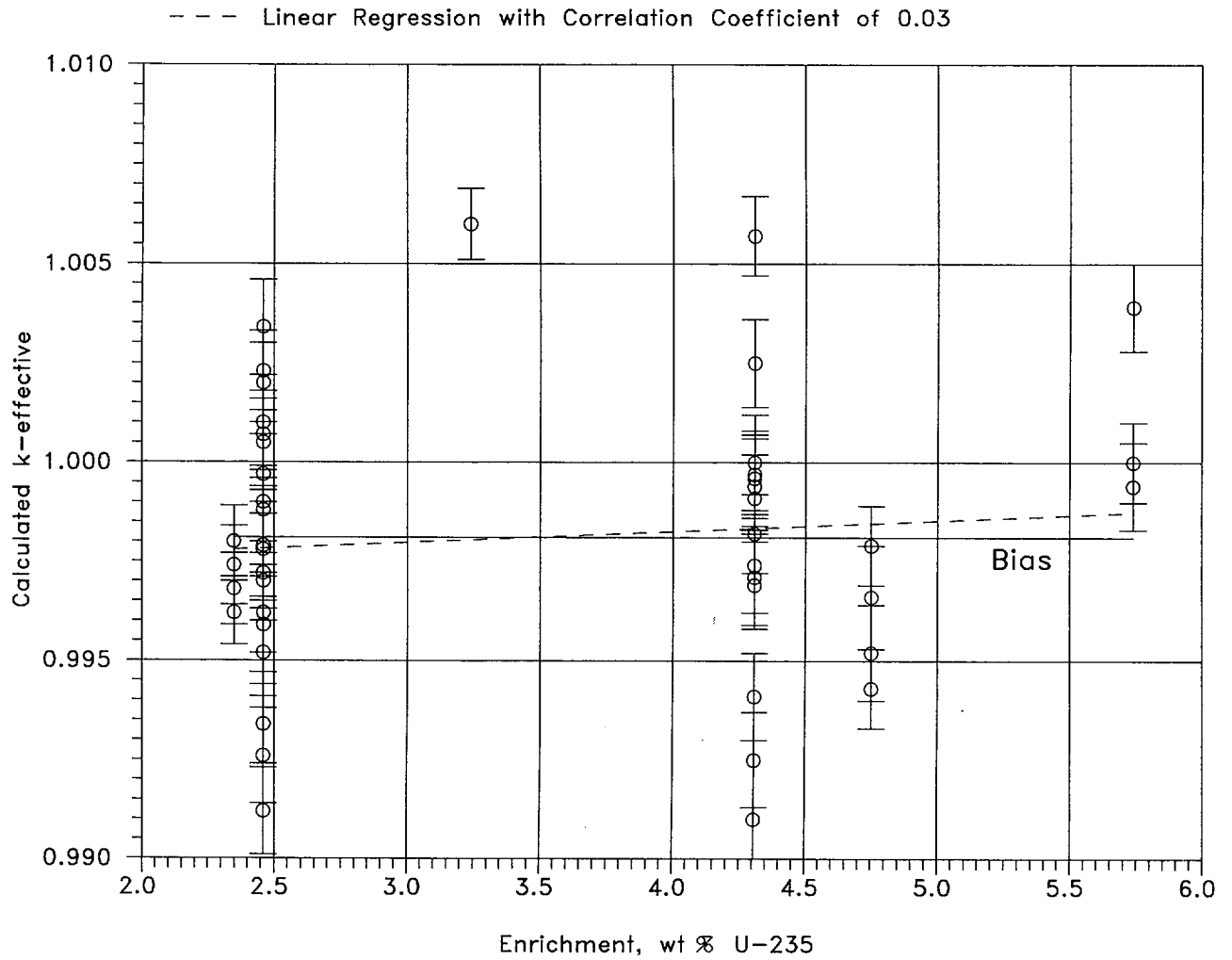


FIGURE 6.A.3 MCNP4a CALCULATED k-eff VALUES AT VARIOUS U-235 ENRICHMENTS

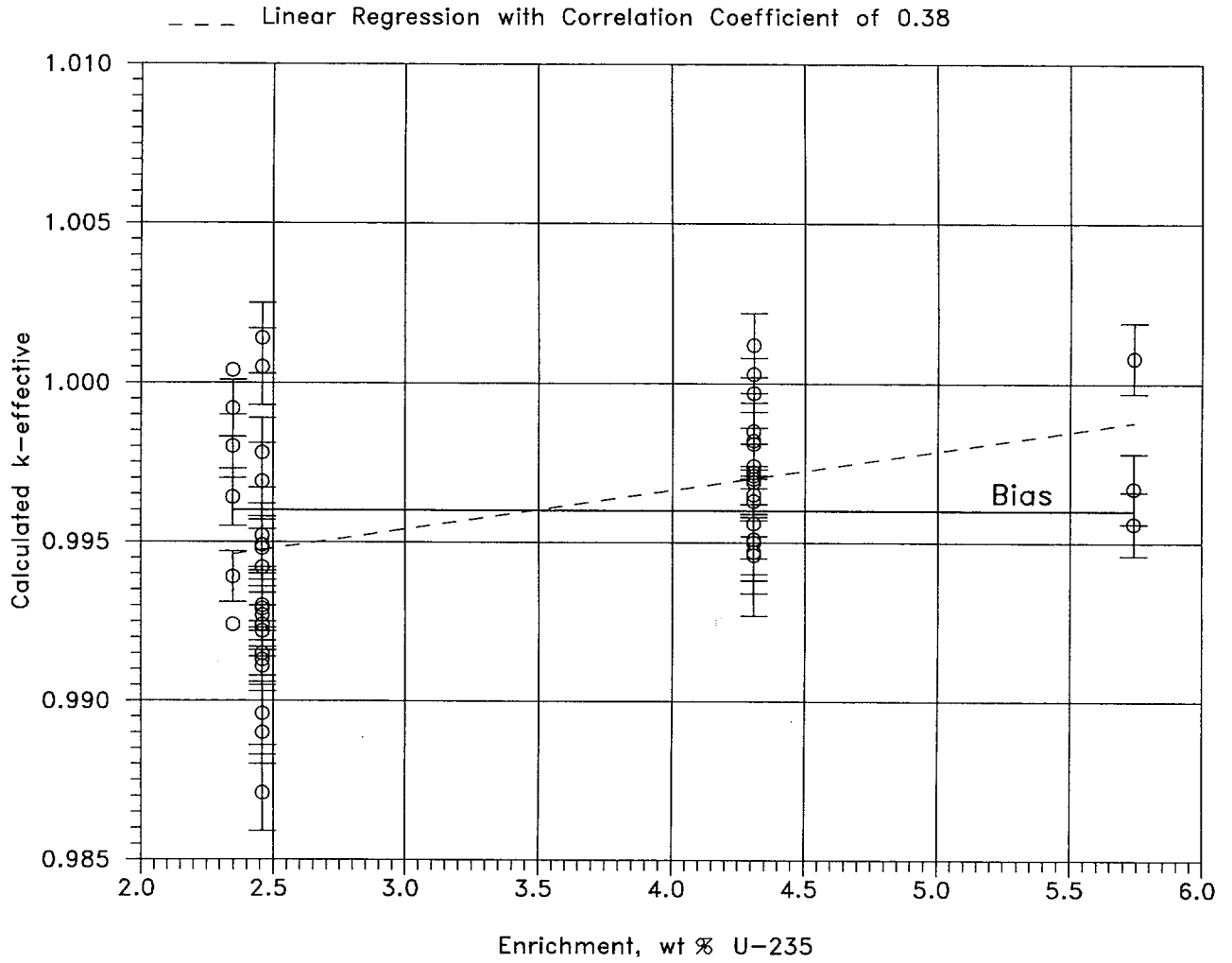


FIGURE 6.A.4 KENO5a CALCULATED k-eff VALUES AT VARIOUS U-235 ENRICHMENTS

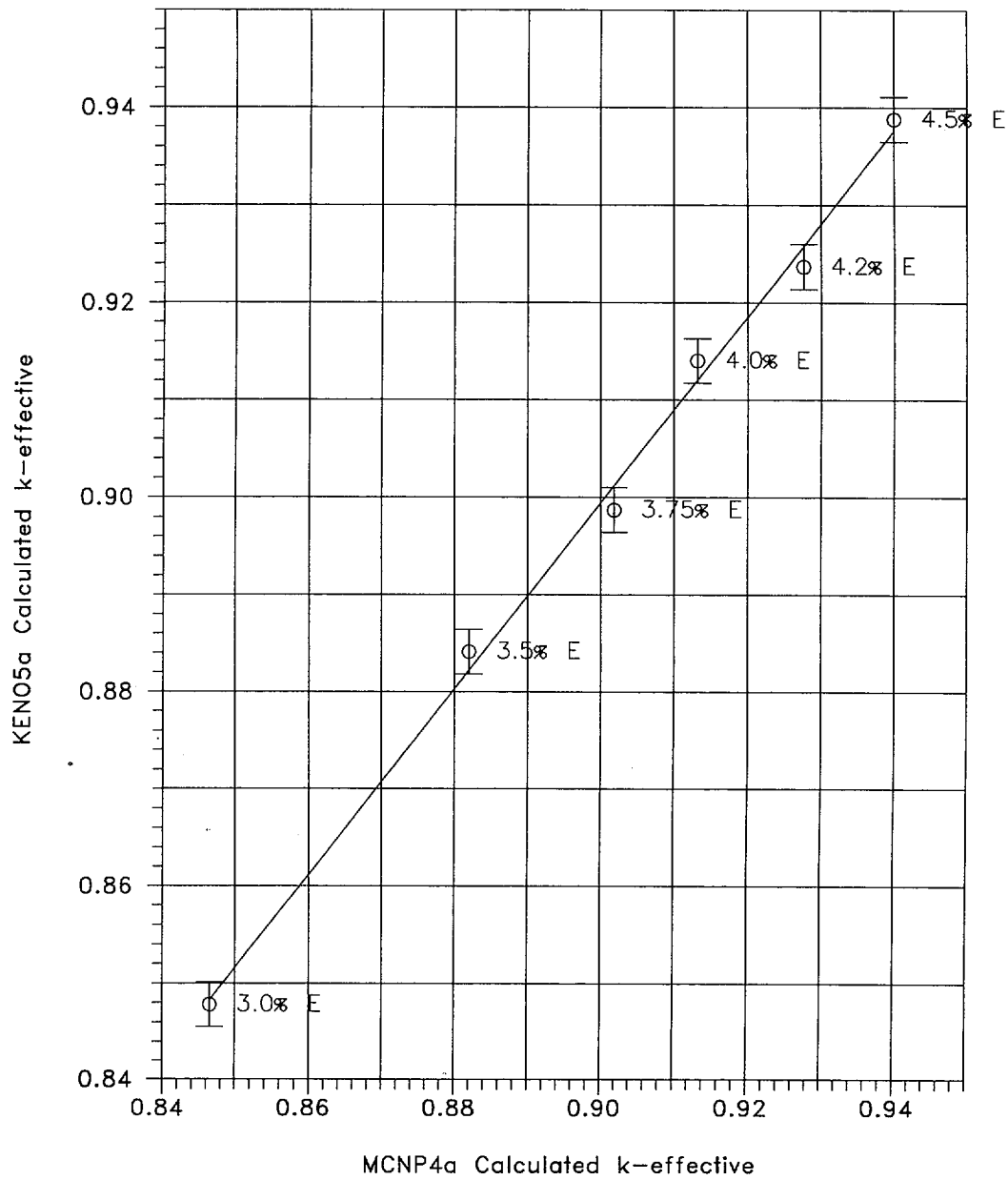


FIGURE 6.A.5 COMPARISON OF MCNP4a AND KENO5a CALCULATIONS FOR VARIOUS FUEL ENRICHMENTS

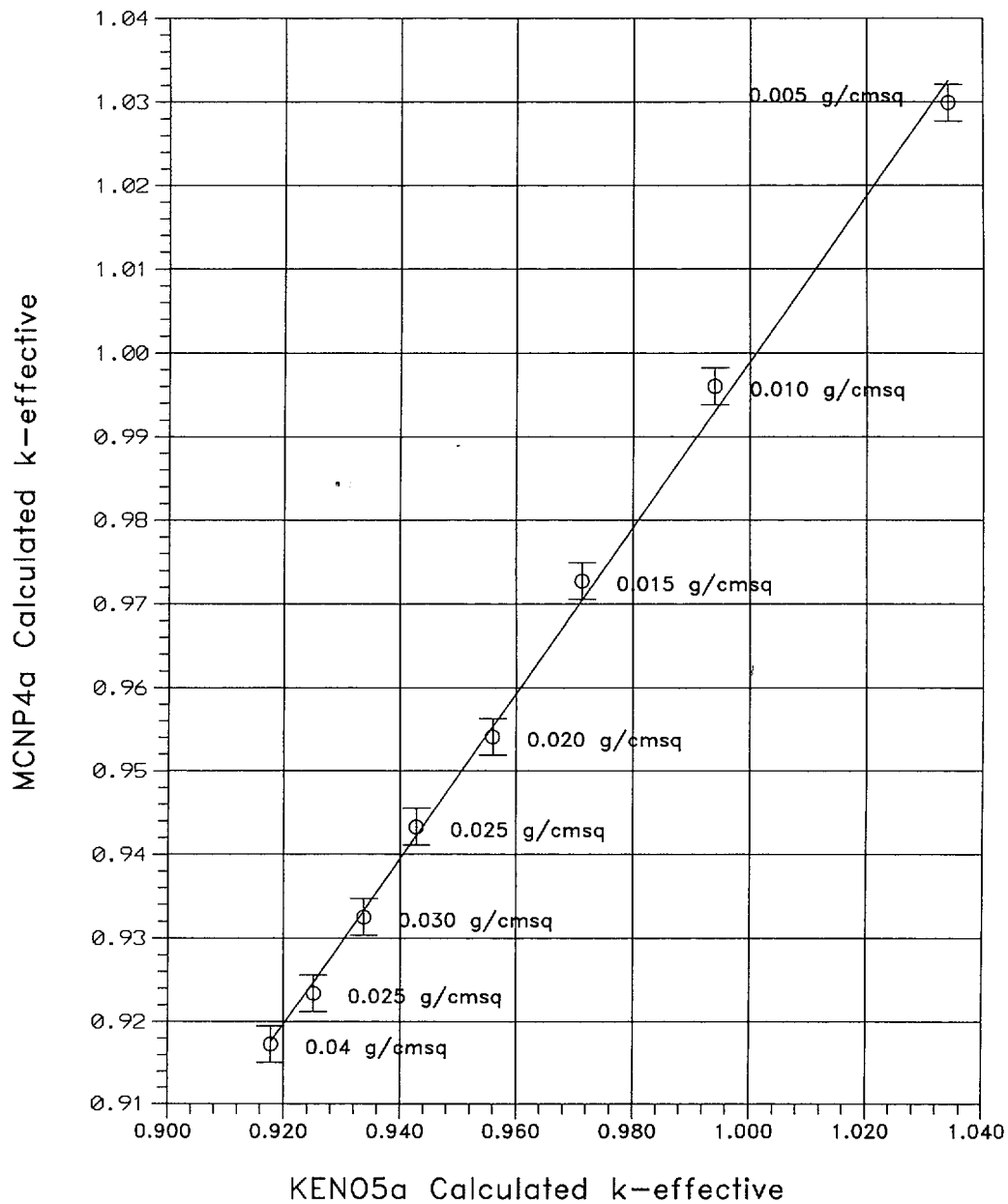


FIGURE 6.A.6 COMPARISON OF MCNP4a AND KEN05a CALCULATIONS FOR VARIOUS BORON-10 AREAL DENSITIES

APPENDIX 6.B: DISTRIBUTED ENRICHMENTS IN BWR FUEL

Fuel assemblies used in BWRs utilize fuel rods of varying enrichments as a means of controlling power peaking during in-core operation. For calculations involving BWR assemblies, the use of a uniform (planar-average) enrichment, as opposed to the distributed enrichments normally used in BWR fuel, produces conservative results. Calculations have been performed to confirm that this statement remains valid in the geometry of the MPC-68. These calculations are based on fuel assembly designs currently in use and two hypothetical distributions, all intended to illustrate that calculations with uniform average enrichments are conservative.

The average enrichment is calculated as the linear average of the various fuel rod enrichments, i.e.,

$$\bar{E} = \frac{1}{n} \sum_{i=1}^n E_i,$$

where E_i is the enrichment in each of the n rods, and E is the assembly average enrichment. This parameter conservatively characterizes the fuel assembly and is readily available for specific fuel assemblies in determining the acceptability of the assembly for placement in the MPC-68 cask.

The criticality calculations for average and distributed enrichment cases are compared in Table 6.B.1 to illustrate and confirm the conservatism inherent in using average enrichments. With two exceptions, the cases analyzed represent realistic designs currently in use and encompass fuel with different ratios of maximum pin enrichment to average assembly enrichment. The two exceptions are hypothetical cases intended to extend the models to higher enrichments and to demonstrate that using the average enrichment remains conservative.

Table 6.B.1 shows that, in all cases, the averaged enrichment yields conservative values of reactivity relative to distributed enrichments for both the actual fuel designs and the hypothetical higher enrichment cases. Thus, it is concluded that uniform average enrichments will always yield higher (more conservative) values for reactivity than the corresponding distributed enrichments[†].

[†] This conclusion implicitly assumes the higher enrichment fuel rods are located internal to the assembly (as in BWR fuel), and the lower enriched rods are on the outside.

Table 6.B.1

**COMPARISON CALCULATIONS FOR BWR FUEL WITH AVERAGE AND
DISTRIBUTED ENRICHMENTS**

Case	Average %E	Peak Rod E%	Calculated k_{eff}	
			Average E	Distributed E
8x8C04	3.01	3.80	0.8549	0.8429
8x8C04	3.934	4.9	0.9128	0.9029
8x8D05	3.42	3.95	0.8790	0.8708
8x8D05	3.78	4.40	0.9030	0.8974
8x8D05	3.90	4.90	0.9062	0.9042
9x9B01	4.34	4.71	0.9347	0.9285
9x9D01	3.35	4.34	0.8793	0.8583
Hypothetical #1 (48 outer rods of 3.967%E, 14 inner rods of 5.0%)	4.20	5.00	0.9289	0.9151
Hypothetical #2 (48 outer rods of 4.354%E, 14 inner rods of 5.0%)	4.50	5.00	0.9422	0.9384

APPENDIX 6.C: CALCULATIONAL SUMMARY

The following table lists the maximum k_{eff} (including bias, uncertainties, and calculational statistics), MCNP calculated k_{eff} , standard deviation, and energy of average lethargy causing fission (EALF) for each of the candidate fuel types and basket configurations.

Table 6.C.1
CALCULATIONAL SUMMARY FOR ALL CANDIDATE FUEL TYPES
AND BASKET CONFIGURATIONS

MPC-24				
Fuel Assembly Designation	Maximum k_{eff}	Calculated k_{eff}	Std. Dev. (1-sigma)	EALF (eV)
14x14A01	0.9378	0.9332	0.0010	0.2147
14x14A02	0.9374	0.9328	0.0009	0.2137
14x14A03	0.9383	0.9340	0.0008	0.2125
14x14B01	0.9268	0.9225	0.0008	0.2788
14x14B02	0.9243	0.9200	0.0008	0.2398
14x14B03	0.9196	0.9152	0.0009	0.2598
14x14B04	0.9163	0.9118	0.0009	0.2631
B14x14B01	0.9323	0.9280	0.0008	0.2730
14x14C01	0.9361	0.9317	0.0009	0.2821
14x14C02	0.9355	0.9312	0.0008	0.2842
14x14C03	0.9400	0.9357	0.0008	0.2900
14x14D01	0.8576	0.8536	0.0007	0.3414
15x15A01	0.9301	0.9259	0.0008	0.2660
15x15B01	0.9427	0.9384	0.0008	0.2704
15C15B02	0.9441	0.9396	0.0009	0.2711
15x15B03	0.9462	0.9420	0.0008	0.2708
15x15B04	0.9452	0.9407	0.0009	0.2692
15x15B05	0.9473	0.9431	0.0008	0.2693
15x15B06	0.9448	0.9404	0.0008	0.2732
B15x15B01	0.9471	0.9428	0.0008	0.2722
15x15C01	0.9332	0.9290	0.0007	0.2563

Table 6.C.1 (continued)
 CALCULATIONAL SUMMARY FOR ALL CANDIDATE FUEL TYPES
 AND BASKET CONFIGURATIONS

MPC-24				
Fuel Assembly Designation	Maximum k_{eff}	Calculated k_{eff}	Std. Dev. (1-sigma)	EALF (eV)
15x15C02	0.9373	0.9330	0.0008	0.2536
15x15C03	0.9377	0.9335	0.0007	0.2525
15x15C04	0.9378	0.9338	0.0007	0.2499
B15x15C01	0.9444	0.9401	0.0008	0.2456
15x15D01	0.9423	0.9380	0.0008	0.2916
15x15D02	0.9430	0.9386	0.0009	0.2900
15x15D03	0.9419	0.9375	0.0009	0.2966
15x15D04	0.9440	0.9398	0.0007	0.3052
15x15E01	0.9475	0.9433	0.0007	0.2916
15x15F01	0.9478	0.9436	0.0008	0.3006
15x15G01	0.8986	0.8943	0.0008	0.3459
15x15H01	0.9411	0.9368	0.0008	0.2425
16x16A01	0.9383	0.9339	0.0009	0.2786
16x16A02	0.9371	0.9328	0.0008	0.2768
17x17A01	0.9449	0.9400	0.0011	0.2198
17x17A02	0.9452	0.9408	0.0008	0.2205
17x17A03	0.9406	0.9364	0.0008	0.2082
17x17B01	0.9377	0.9335	0.0008	0.2697
17x17B02	0.9379	0.9337	0.0008	0.2710
17x17B03	0.9330	0.9288	0.0008	0.2714
17x17B04	0.9407	0.9365	0.0007	0.2666
17x17B05	0.9349	0.9305	0.0009	0.2629

Table 6.C.1 (continued)
 CALCULATIONAL SUMMARY FOR ALL CANDIDATE FUEL TYPES
 AND BASKET CONFIGURATIONS

MPC-24				
Fuel Assembly Designation	Maximum k_{eff}	Calculated k_{eff}	Std. Dev. (1-sigma)	EALF (eV)
17x17B06	0.9436	0.9393	0.0008	0.2657
17x17C01	0.9383	0.9339	0.0008	0.2683
17x17C02	0.9427	0.9384	0.0008	0.2703

MPC-68				
Fuel Assembly Designation	Maximum k_{eff}	Calculated k_{eff}	Std. Dev. (1-sigma)	EALF (eV)
6x6A01	0.7539	0.7498	0.0007	0.2754
6x6A02	0.7517	0.7476	0.0007	0.2510
6x6A03	0.7545	0.7501	0.0008	0.2494
6x6A04	0.7537	0.7494	0.0008	0.2494
6x6A05	0.7555	0.7512	0.0008	0.2470
6x6A06	0.7618	0.7576	0.0008	0.2298
6x6A07	0.7588	0.7550	0.0005	0.2360
6x6A08	0.7808	0.7766	0.0007	0.2527
B6x6A01	0.7888	0.7846	0.0007	0.2310
6x6B01	0.7604	0.7563	0.0007	0.2461
6x6B02	0.7618	0.7577	0.0006	0.2450
6x6B03	0.7619	0.7578	0.0007	0.2439
6x6B04	0.7686	0.7644	0.0008	0.2286
6x6B05	0.7824	0.7785	0.0006	0.2184
B6x6B01	0.7822	0.7783	0.0006	0.2190

Table 6.C.1 (continued)
 CALCULATIONAL SUMMARY FOR ALL CANDIDATE FUEL TYPES
 AND BASKET CONFIGURATIONS

MPC-68				
Fuel Assembly Designation	Maximum k_{eff}	Calculated k_{eff}	Std. Dev. (1-sigma)	EALF (eV)
6x6C01	0.8021	0.7980	0.0007	0.2139
7x7A01	0.7973	0.7930	0.0008	0.2015
7x7B01	0.9372	0.9330	0.0007	0.3658
7x7B02	0.9301	0.9260	0.0007	0.3524
7x7B03	0.9313	0.9271	0.0008	0.3438
7x7B04	0.9311	0.9270	0.0007	0.3816
7x7B05	0.9350	0.9306	0.0008	0.3382
7x7B06	0.9298	0.9260	0.0006	0.3957
B7x7B01	0.9375	0.9332	0.0008	0.3887
B7x7B02	0.9386	0.9344	0.0007	0.3983
8x8A01	0.7685	0.7644	0.0007	0.2227
8x8A02	0.7697	0.7656	0.0007	0.2158
8x8B01	0.9310	0.9265	0.0009	0.2935
8x8B02	0.9227	0.9185	0.0007	0.2993
8x8B03	0.9299	0.9257	0.0008	0.3319
8x8B04	0.9236	0.9194	0.0008	0.3700
B8x8B01	0.9346	0.9301	0.0009	0.3389
B8x8B02	0.9385	0.9343	0.0008	0.3329
B8x8B03	0.9416	0.9375	0.0007	0.3293
8x8C01	0.9315	0.9273	0.0007	0.2822
8x8C02	0.9313	0.9268	0.0009	0.2716
8x8C03	0.9329	0.9286	0.0008	0.2877

Table 6.C.1 (continued)
 CALCULATIONAL SUMMARY FOR ALL CANDIDATE FUEL TYPES
 AND BASKET CONFIGURATIONS

MPC-68				
Fuel Assembly Designation	Maximum k_{eff}	Calculated k_{eff}	Std. Dev. (1-sigma)	EALF (eV)
8x8C04	0.9348	0.9307	0.0007	0.2915
8x8C05	0.9353	0.9312	0.0007	0.2971
8x8C06	0.9353	0.9312	0.0007	0.2944
8x8C07	0.9314	0.9273	0.0007	0.2972
8x8C08	0.9339	0.9298	0.0007	0.2915
8x8C09	0.9301	0.9260	0.0007	0.3183
8x8C10	0.9317	0.9275	0.0008	0.3018
8x8C11	0.9328	0.9287	0.0007	0.3001
8x8C12	0.9285	0.9242	0.0008	0.3062
B8x8C01	0.9357	0.9313	0.0009	0.3141
B8x8C02	0.9425	0.9384	0.0007	0.3081
B8x8C03	0.9418	0.9375	0.0008	0.3056
8x8D01	0.9342	0.9302	0.0006	0.2733
8x8D02	0.9325	0.9284	0.0007	0.2750
8x8D03	0.9351	0.9309	0.0008	0.2731
8x8D04	0.9338	0.9296	0.0007	0.2727
8x8D05	0.9339	0.9294	0.0009	0.2700
8x8D06	0.9365	0.9324	0.0007	0.2777
8x8D07	0.9341	0.9297	0.0009	0.2694
8x8D08	0.9376	0.9332	0.0009	0.2841
B8x8D01	0.9403	0.9363	0.0007	0.2778
8x8E01	0.9312	0.9270	0.0008	0.2831

Table 6.C.1 (continued)
 CALCULATIONAL SUMMARY FOR ALL CANDIDATE FUEL TYPES
 AND BASKET CONFIGURATIONS

MPC-68				
Fuel Assembly Designation	Maximum k_{eff}	Calculated k_{eff}	Std. Dev. (1-sigma)	EALF (eV)
8x8F01	0.9153	0.9111	0.0007	0.2143
9x9A01	0.9353	0.9310	0.0008	0.2875
9x9A02	0.9388	0.9345	0.0008	0.2228
9x9A03	0.9351	0.9310	0.0007	0.2837
9x9A04	0.9396	0.9355	0.0007	0.2262
B9x9A01	0.9417	0.9374	0.0008	0.2236
9x9B01	0.9368	0.9326	0.0007	0.2561
9x9B02	0.9377	0.9334	0.0008	0.2547
9x9B03	0.9416	0.9373	0.0008	0.2517
B9x9B01	0.9422	0.9380	0.0007	0.2501
9x9C01	0.9395	0.9352	0.0008	0.2698
9x9D01	0.9394	0.9350	0.0009	0.2625
9x9E01	0.9402	0.9359	0.0008	0.2249
9x9E02	0.9424	0.9380	0.0008	0.2088
9x9F01	0.9369	0.9326	0.0008	0.2954
9x9F02	0.9424	0.9380	0.0008	0.2088
10x10A01	0.9377	0.9335	0.0008	0.3170
10x10A02	0.9426	0.9386	0.0007	0.2159
10x10A03	0.9396	0.9356	0.0007	0.3169
B10x10A01	0.9457	0.9414	0.0008	0.2212
10x10B01	0.9384	0.9341	0.0008	0.2881
10x10B02	0.9416	0.9373	0.0008	0.2333

Table 6.C.1 (continued)
 CALCULATIONAL SUMMARY FOR ALL CANDIDATE FUEL TYPES
 AND BASKET CONFIGURATIONS

MPC-68				
Fuel Assembly Designation	Maximum k_{eff}	Calculated k_{eff}	Std. Dev. (1-sigma)	EALF (eV)
10x10B03	0.9375	0.9334	0.0007	0.2856
B10x10B01	0.9436	0.9395	0.0007	0.2366
10x10C01	0.9021	0.8980	0.0007	0.2610
10x10D01	0.9376	0.9333	0.0008	0.3355
10x10E01	0.9185	0.9144	0.0007	0.2936

Note: Maximum k_{eff} = Calculated k_{eff} + $K_c \times \sigma_c$ + Bias + σ_B
 where:

- K_c = 2.0
- σ_c = Std. Dev. (1-sigma)
- Bias = 0.0021
- σ_B = 0.0006

See Subsection 6.4.3 for further explanation.

APPENDIX 6.D: SAMPLE INPUT FILES

(Total number of pages in this appendix : 44)

File Description	Starting Page
MCNP4a input file for MPC-24	Appendix 6.D-2
MCNP4a input file for MPC-68	Appendix 6.D-12
MCNP4a input file for MPC-68F	Appendix 6.D-18
MCNP4a input file for MPC-68F with Dresden damaged fuel in the Damaged Fuel Container	Appendix 6.D-24
MCNP4a input file for MPC-68F with Humbolt Bay damaged fuel in the Damaged Fuel Container	Appendix 6.D-30
KENO5a input file for MPC-24	Appendix 6.D-36
KENO5a input file for MPC-68	Appendix 6.D-40

HI-STAR containing MPC24, 17x17 @ 4.0 wt% Enrich.

c 4.00 % uniform enrichment, unreflected cask, 0.0200 g/cmsq B-10 in Boral

c

c

1 1 -10.522 -1 u=2 \$ fuel
2 4 -1.0 1 -2 u=2 \$ gap
3 3 -6.55 2 -3 u=2 \$ Zr Clad
4 4 -1.0 3 u=2 \$ water in fuel region
5 4 -1.0 -4:5 u=3 \$ water in guide tubes
6 3 -6.55 4 -5 u=3 \$ guide tubes
7 4 -1.0 -6 +7 -8 +9 u=1 lat=1

fill= -9:9 -9:9 0:0
1
1 2 2 2 2 2 2 2 2 2 2 2 2 2 2 2 2 2 2 1
1 2 2 2 2 2 2 2 2 2 2 2 2 2 2 2 2 2 2 1
1 2 2 2 2 2 3 2 2 3 2 2 3 2 2 2 2 2 2 1
1 2 2 2 3 2 2 2 2 2 2 2 2 2 2 2 3 2 2 1
1 2 2 2 2 2 2 2 2 2 2 2 2 2 2 2 2 2 2 1
1 2 2 3 2 2 3 2 2 3 2 2 3 2 2 3 2 2 2 1
1 2 2 2 2 2 2 2 2 2 2 2 2 2 2 2 2 2 2 1
1 2 2 2 2 2 2 2 2 2 2 2 2 2 2 2 2 2 2 1
1 2 2 3 2 2 3 2 2 3 2 2 3 2 2 3 2 2 2 1
1 2 2 2 2 2 2 2 2 2 2 2 2 2 2 2 2 2 2 1
1 2 2 2 2 2 2 2 2 2 2 2 2 2 2 2 2 2 2 1
1 2 2 3 2 2 3 2 2 3 2 2 3 2 2 3 2 2 2 1
1 2 2 2 2 2 2 2 2 2 2 2 2 2 2 2 2 2 2 1
1 2 2 2 2 2 2 2 2 2 2 2 2 2 2 2 2 2 2 1
1 2 2 2 2 2 2 2 2 2 2 2 2 2 2 2 2 2 2 1
1 1 1 1 1 1 1 1 1 1 1 1 1 1 1 1 1 1 1 1

c

c

TYPE A CELL

c

c

Right Side

c

c

c

c

c

c

c

c

c

c

c

c

c

c

c

c

c

c

c

c

c

c

c

c

c

c

c

c

c

c

c

c

c

c

c

c

c

c

c

c

c

HI-STAR FSAR

REPORT HI-2012610

Appendix 6.D-2

Rev. 0

29	4	-1.0	41	-25	13	-47	u=4
30	4	-1.0	41	-25	46		u=4
31	5	-7.84	41	-25	47	-48	u=4
32	5	-7.84	41	-25	45	-46	u=4

c

c Top

c

33	5	-7.84	11	-10	12	-26	u=4
34	4	-1.0	51	-52	26	-30	u=4
35	7	-2.7	51	-52	30	-130	u=4
36	6	-2.66	51	-52	130	-134	u=4
37	7	-2.7	51	-52	134	-34	u=4
38	4	-1.0	51	-52	34	-38	u=4
39	5	-7.84	51	-52	38	-42	u=4
40	4	-1.0	11	-24	42		u=4
41	4	-1.0	11	-50	26	-42	u=4
42	4	-1.0	53	-24	26	-42	u=4
43	5	-7.84	50	-51	26	-42	u=4
44	5	-7.84	52	-53	26	-42	u=4

c

c Bottom

c

45	5	-7.84	27			-13	u=4
46	4	-1.0	51	-52	31	-27	u=4
47	7	-2.7	51	-52	131	-31	u=4
48	6	-2.66	51	-52	135	-131	u=4
49	7	-2.7	51	-52	35	-135	u=4
50	4	-1.0	51	-52	39	-35	u=4
51	5	-7.84	51	-52	43	-39	u=4
52	4	-1.0	11			-43	u=4
53	4	-1.0	11	-50	43	-27	u=4
54	4	-1.0	53		43	-27	u=4
55	5	-7.84	50	-51	43	-27	u=4
56	5	-7.84	52	-53	43	-27	u=4
57	5	-7.84	25	-11		-27	u=4
58	4	-1.0		-25		-27	u=4

c

c TYPE B CELL - Short Boral on top and right

c

c Right Side

c

59	0		-10	11	-12	13	u=5 fill=1
60	5	-7.84	10	-24	13	-26	u=5
70	4	-1.0	24	-28	148	-145	u=5
71	7	-2.7	28	-128	148	-145	u=5
72	6	-2.66	128	-132	148	-145	u=5
73	7	-2.7	132	-32	148	-145	u=5
74	4	-1.0	32	-36	148	-145	u=5
75	5	-7.84	36	-40	148	-145	u=5
76	4	-1.0	40		13		u=5
77	4	-1.0	24	-40	13	-147	u=5
78	4	-1.0	24	-40	146		u=5
79	5	-7.84	24	-40	147	-148	u=5
80	5	-7.84	24	-40	145	-146	u=5

c

c Left Side

c

81	5	-7.84	25	-11	13		u=5
82	4	-1.0	29	-25	48	-45	u=5
83	7	-2.7	129	-29	48	-45	u=5

84	6	-2.66	133	-129	48	-45	u=5
85	7	-2.7	33	-133	48	-45	u=5
86	4	-1.0	37	-33	48	-45	u=5
87	5	-7.84	41	-37	48	-45	u=5
88	4	-1.0		-41	13		u=5
89	4	-1.0	41	-25	13	-47	u=5
90	4	-1.0	41	-25	46		u=5
91	5	-7.84	41	-25	47	-48	u=5
92	5	-7.84	41	-25	45	-46	u=5

c

Top

93	5	-7.84	11	-10	12	-26	u=5
94	4	-1.0	151	-152	26	-30	u=5
95	7	-2.7	151	-152	30	-130	u=5
96	6	-2.66	151	-152	130	-134	u=5
97	7	-2.7	151	-152	134	-34	u=5
98	4	-1.0	151	-152	34	-38	u=5
99	5	-7.84	151	-152	38	-42	u=5
100	4	-1.0	11	-24	42		u=5
101	4	-1.0	11	-150	26	-42	u=5
102	4	-1.0	153	-24	26	-42	u=5
103	5	-7.84	150	-151	26	-42	u=5
104	5	-7.84	152	-153	26	-42	u=5

c

Bottom

105	5	-7.84	27			-13	u=5
106	4	-1.0	51	-52	31	-27	u=5
107	7	-2.7	51	-52	131	-31	u=5
108	6	-2.66	51	-52	135	-131	u=5
109	7	-2.7	51	-52	35	-135	u=5
110	4	-1.0	51	-52	39	-35	u=5
111	5	-7.84	51	-52	43	-39	u=5
112	4	-1.0	11			-43	u=5
113	4	-1.0	11	-50	43	-27	u=5
114	4	-1.0	53		43	-27	u=5
115	5	-7.84	50	-51	43	-27	u=5
116	5	-7.84	52	-53	43	-27	u=5
117	5	-7.84	25	-11		-27	u=5
118	4	-1.0		-25		-27	u=5

c

TYPE c CELL - short Boral on bottom and right

c

Right Side

119	0		-10	11	-12	13	u=6 fill=1
120	5	-7.84	10	-24	13	-26	u=6
121	4	-1.0	24	-28	148	-145	u=6
122	7	-2.7	28	-128	148	-145	u=6
123	6	-2.66	128	-132	148	-145	u=6
124	7	-2.7	132	-32	148	-145	u=6
125	4	-1.0	32	-36	148	-145	u=6
126	5	-7.84	36	-40	148	-145	u=6
127	4	-1.0	40		13		u=6
128	4	-1.0	24	-40	13	-147	u=6
129	4	-1.0	24	-40	146		u=6
130	5	-7.84	24	-40	147	-148	u=6
131	5	-7.84	24	-40	145	-146	u=6

c

```

c   Left Side
c
132  5 -7.84    25 -11   13      u=6
133  4 -1.0     29 -25   48 -45   u=6
134  7 -2.7    129 -29   48 -45   u=6
135  6 -2.66   133 -129  48 -45   u=6
136  7 -2.7    33 -133  48 -45   u=6
137  4 -1.0     37 -33   48 -45   u=6
138  5 -7.84    41 -37   48 -45   u=6
139  4 -1.0     -41  13    u=6
140  4 -1.0     41 -25   13 -47   u=6
141  4 -1.0     41 -25   46      u=6
142  5 -7.84    41 -25   47 -48   u=6
143  5 -7.84    41 -25   45 -46   u=6
c
c   Top
c
144  5 -7.84    11 -10   12 -26   u=6
145  4 -1.0     51 -52   26 -30   u=6
146  7 -2.7     51 -52   30 -130  u=6
147  6 -2.66   51 -52   130 -134  u=6
148  7 -2.7     51 -52   134 -34   u=6
149  4 -1.0     51 -52   34 -38   u=6
150  5 -7.84   51 -52   38 -42   u=6
151  4 -1.0     11 -24   42      u=6
152  4 -1.0     11 -50   26 -42   u=6
153  4 -1.0     53 -24   26 -42   u=6
154  5 -7.84   50 -51   26 -42   u=6
155  5 -7.84   52 -53   26 -42   u=6
c
c   Bottom
c
156  5 -7.84    27      -13   u=6
157  4 -1.0    151 -152   31 -27   u=6
158  7 -2.7    151 -152  131 -31   u=6
159  6 -2.66   151 -152  135 -131  u=6
160  7 -2.7    151 -152   35 -135  u=6
161  4 -1.0    151 -152   39 -35   u=6
162  5 -7.84   151 -152   43 -39   u=6
163  4 -1.0     11      -43   u=6
164  4 -1.0     11 -150   43 -27   u=6
165  4 -1.0    153      43 -27   u=6
166  5 -7.84   150 -151   43 -27   u=6
167  5 -7.84   152 -153   43 -27   u=6
168  5 -7.84    25 -11    -27   u=6
169  4 -1.0     -25    -27   u=6
c
c   TYPE D CELL - Short Boral on left and bottom
c
c   Right Side
c
170  0      -10  11 -12  13      u=7 fill=1
171  5 -7.84   10 -24  13 -26   u=7
172  4 -1.0    24 -28  48 -45   u=7
173  7 -2.7    28 -128  48 -45   u=7
174  6 -2.66  128 -132  48 -45   u=7
175  7 -2.7    132 -32  48 -45   u=7
176  4 -1.0    32 -36  48 -45   u=7
177  5 -7.84   36 -40  48 -45   u=7
178  4 -1.0    40      13      u=7

```

179	4	-1.0	24	-40	13	-47	u=7
180	4	-1.0	24	-40	46		u=7
181	5	-7.84	24	-40	47	-48	u=7
182	5	-7.84	24	-40	45	-46	u=7

c

c Left Side

c

183	5	-7.84	25	-11	13		u=7
184	4	-1.0	29	-25	148	-145	u=7
185	7	-2.7	129	-29	148	-145	u=7
186	6	-2.66	133	-129	148	-145	u=7
187	7	-2.7	33	-133	148	-145	u=7
188	4	-1.0	37	-33	148	-145	u=7
189	5	-7.84	41	-37	148	-145	u=7
190	4	-1.0		-41	13		u=7
191	4	-1.0	41	-25	13	-147	u=7
192	4	-1.0	41	-25	146		u=7
193	5	-7.84	41	-25	147	-148	u=7
194	5	-7.84	41	-25	145	-146	u=7

c

c Top

c

195	5	-7.84	11	-10	12	-26	u=7
196	4	-1.0	51	-52	26	-30	u=7
197	7	-2.7	51	-52	30	-130	u=7
198	6	-2.66	51	-52	130	-134	u=7
199	7	-2.7	51	-52	134	-34	u=7
200	4	-1.0	51	-52	34	-38	u=7
201	5	-7.84	51	-52	38	-42	u=7
202	4	-1.0	11	-24	42		u=7
203	4	-1.0	11	-50	26	-42	u=7
204	4	-1.0	53	-24	26	-42	u=7
205	5	-7.84	50	-51	26	-42	u=7
206	5	-7.84	52	-53	26	-42	u=7

c

c Bottom

c

207	5	-7.84	27			-13	u=7
208	4	-1.0	151	-152	31	-27	u=7
209	7	-2.7	151	-152	131	-31	u=7
210	6	-2.66	151	-152	135	-131	u=7
211	7	-2.7	151	-152	35	-135	u=7
212	4	-1.0	151	-152	39	-35	u=7
213	5	-7.84	151	-152	43	-39	u=7
214	4	-1.0	11			-43	u=7
215	4	-1.0	11	-150	43	-27	u=7
216	4	-1.0	153		43	-27	u=7
217	5	-7.84	150	-151	43	-27	u=7
218	5	-7.84	152	-153	43	-27	u=7
219	5	-7.84	25	-11		-27	u=7
220	4	-1.0		-25		-27	u=7

c

c TYPE E CELL - short Boral on top and left

c

c Right Side

c

221	0		-10	11	-12	13	u=8 fill=1
222	5	-7.84	10	-24	13	-26	u=8
223	4	-1.0	24	-28	48	-45	u=8
224	7	-2.7	28	-128	48	-45	u=8

225	6	-2.66	128	-132	48	-45	u=8
226	7	-2.7	132	-32	48	-45	u=8
227	4	-1.0	32	-36	48	-45	u=8
228	5	-7.84	36	-40	48	-45	u=8
229	4	-1.0	40		13		u=8
230	4	-1.0	24	-40	13	-47	u=8
231	4	-1.0	24	-40	46		u=8
232	5	-7.84	24	-40	47	-48	u=8
233	5	-7.84	24	-40	45	-46	u=8
c							
c	Left Side						
c							
234	5	-7.84	25	-11	13		u=8
235	4	-1.0	29	-25	148	-145	u=8
236	7	-2.7	129	-29	148	-145	u=8
237	6	-2.66	133	-129	148	-145	u=8
238	7	-2.7	33	-133	148	-145	u=8
239	4	-1.0	37	-33	148	-145	u=8
240	5	-7.84	41	-37	148	-145	u=8
241	4	-1.0		-41	13		u=8
242	4	-1.0	41	-25	13	-147	u=8
243	4	-1.0	41	-25	146		u=8
244	5	-7.84	41	-25	147	-148	u=8
245	5	-7.84	41	-25	145	-146	u=8
c							
c	Top						
c							
246	5	-7.84	11	-10	12	-26	u=8
247	4	-1.0	151	-152	26	-30	u=8
248	7	-2.7	151	-152	30	-130	u=8
249	6	-2.66	151	-152	130	-134	u=8
250	7	-2.7	151	-152	134	-34	u=8
251	4	-1.0	151	-152	34	-38	u=8
252	5	-7.84	151	-152	38	-42	u=8
253	4	-1.0	11	-24	42		u=8
254	4	-1.0	11	-150	26	-42	u=8
255	4	-1.0	153	-24	26	-42	u=8
256	5	-7.84	150	-151	26	-42	u=8
257	5	-7.84	152	-153	26	-42	u=8
c							
c	Bottom						
c							
258	5	-7.84	27			-13	u=8
259	4	-1.0	51	-52	31	-27	u=8
260	7	-2.7	51	-52	131	-31	u=8
261	6	-2.66	51	-52	135	-131	u=8
262	7	-2.7	51	-52	35	-135	u=8
263	4	-1.0	51	-52	39	-35	u=8
264	5	-7.84	51	-52	43	-39	u=8
265	4	-1.0	11			-43	u=8
266	4	-1.0	11	-50	43	-27	u=8
267	4	-1.0	53		43	-27	u=8
268	5	-7.84	50	-51	43	-27	u=8
269	5	-7.84	52	-53	43	-27	u=8
270	5	-7.84	25	-11		-27	u=8
271	4	-1.0		-25		-27	u=8
C							
C							
272	4	-1.0	-16	17	-18	19	u=9 lat=1 fill=-4:3 -4:3 0:0
			9	9	9	9	9

```

          9 9 9 7 6 9 9 9
          9 9 7 4 4 6 9 9
          9 7 4 4 4 4 6 9
          9 8 4 4 4 4 5 9
          9 9 8 4 4 5 9 9
          9 9 9 8 5 9 9 9
          9 9 9 9 9 9 9 9
273    0          -22
274    4  -1.0    -22          60  -20
275    4  -1.0    -22          21  -61
276    5  -7.84   -23          62  -60
277    5  -7.84   -23          61  -63
278    5  -7.84    22  -23  60  -61
279    0          23  :-62:  63
          20 -21  fill=9 (13.7909  13.7909  0)
          $ Water below Fuel
          $ Water above Fuel
          $ Steel below Fuel
          $ Steel above Fuel
          $ Radial Steel
          $ outside world

```

```

1     cz          0.3922
2     cz          0.4001
3     cz          0.4572
4     cz          0.5613
5     cz          0.6020
6     px          0.6299
7     px         -0.6299
8     py          0.6299
9     py         -0.6299
10    px          11.1864
11    px         -11.1864
12    py          11.1864
13    py         -11.1864
16    px          13.6446
17    px         -13.7239
18    py          13.6446
19    py         -13.7239
20    pz          0.
21    pz          381.0      $ 150 inch active fuel length
22    cz          85.57
23    cz          108.43
24    px          11.9009
25    px         -11.9802
26    py          11.9009
27    py         -11.9802
28    px          11.9098
29    px         -11.9891
30    py          11.9098
31    py         -11.9891
32    px          12.1003
33    px         -12.1796
34    py          12.1003
35    py         -12.1796
36    px          12.1092
37    px         -12.1885
38    py          12.1092
39    py         -12.1885
40    px          12.2616
41    px         -12.3409
42    py          12.2616
43    py         -12.3409
45    py          9.4456
46    py          9.6361
47    py         -9.6361
48    py         -9.4456

```

```

50 px -9.6361
51 px -9.4456
52 px 9.4456
53 px 9.6361
60 pz -10.16
61 pz 396.24 $ 6.0 inches of water above fuel
62 pz -31.75
63 pz 435.61 $ 15.5 inches of steel above water
128 px 11.9352
129 px -12.0145
130 py 11.9352
131 py -12.0145
132 px 12.0749
133 px -12.1542
134 py 12.0749
135 py -12.1542
145 py 6.2706
146 py 6.4611
147 py -6.4611
148 py -6.2706
150 px -6.4611
151 px -6.2706
152 px 6.2706
153 px 6.4611

```

```

imp:n 1 268r 0
print
kcode 10000 .94 20 120
sdef par=1 erg=d1 axs=0 0 1 x=d4 y=fx d5 z=d3
c
sp1 -2 1.2895
si3 h 0 381.0
sp3 0 1
c
si4 s 13 14
12 13 14 15
↓ 11 12 13 14 15 16
11 12 13 14 15 16
12 13 14 15
13 14
sp4 1 23r
c
ds5 s 26 26
25 25 25 25
24 24 24 24 24 24
23 23 23 23 23 23
22 22 22 22
21 21
c
si11 -79.25435 -57.61355
si12 -51.88077 -30.23997
si13 -24.50719 -2.86639
si14 2.86639 24.50719
si15 30.23997 51.88077
si16 57.61355 79.25435
c
si21 -79.25435 -57.61355
si22 -51.88077 -30.23997
si23 -24.50719 -2.86639
si24 2.86639 24.50719

```

```

si25 30.23997 51.88077
si26 57.61355 79.25435
c
sp11 0 1
sp12 0 1
sp13 0 1
sp14 0 1
sp15 0 1
sp16 0 1
sp21 0 1
sp22 0 1
sp23 0 1
sp24 0 1
sp25 0 1
sp26 0 1
c
m1          92235.50c -0.03526      $ Fuel
           92238.50c -0.84624
           8016.50c  -0.1185
m2          8016.50c   1.          $ Void
m3          40000.56c  1.          $ Zr Clad
m4          1001.50c  0.6667      $ Water
           8016.50c   0.3333
m5          24000.50c  0.01761      $ Steel
           25055.50c  0.001761
           26000.55c  0.05977
           28000.50c  0.008239
m6          5010.50c -0.054427      $ Boral Central Section @ 0.02 g/cmsq
           5011.50c -0.241373
           13027.50c -0.6222
           6000.50c -0.0821
m7          13027.50c  1.0
mt4         lwtr.01t
prcjmp      j  -120   j  2
fm4         1000   1  -6
f4:n        1
sd4         1000
e4          1.000E-11  1.000E-10  5.000E-10  7.500E-10  1.000E-09  1.200E-09
           1.500E-09  2.000E-09  2.500E-09  3.000E-09
           4.700E-09  5.000E-09  7.500E-09  1.000E-08  2.530E-08
           3.000E-08  4.000E-08  5.000E-08  6.000E-08  7.000E-08
           8.000E-08  9.000E-08  1.000E-07  1.250E-07  1.500E-07
           1.750E-07  2.000E-07  2.250E-07  2.500E-07  2.750E-07
           3.000E-07  3.250E-07  3.500E-07  3.750E-07  4.000E-07
           4.500E-07  5.000E-07  5.500E-07  6.000E-07  6.250E-07
           6.500E-07  7.000E-07  7.500E-07  8.000E-07  8.500E-07
           9.000E-07  9.250E-07  9.500E-07  9.750E-07  1.000E-06
           1.010E-06  1.020E-06  1.030E-06  1.040E-06  1.050E-06
           1.060E-06  1.070E-06  1.080E-06  1.090E-06  1.100E-06
           1.110E-06  1.120E-06  1.130E-06  1.140E-06  1.150E-06
           1.175E-06  1.200E-06  1.225E-06  1.250E-06  1.300E-06
           1.350E-06  1.400E-06  1.450E-06  1.500E-06  1.590E-06
           1.680E-06  1.770E-06  1.860E-06  1.940E-06  2.000E-06
           2.120E-06  2.210E-06  2.300E-06  2.380E-06  2.470E-06
           2.570E-06  2.670E-06  2.770E-06  2.870E-06  2.970E-06
           3.000E-06  3.050E-06  3.150E-06  3.500E-06  3.730E-06
           4.000E-06  4.750E-06  5.000E-06  5.400E-06  6.000E-06
           6.250E-06  6.500E-06  6.750E-06  7.000E-06  7.150E-06
           8.100E-06  9.100E-06  1.000E-05  1.150E-05  1.190E-05
           1.290E-05  1.375E-05  1.440E-05  1.510E-05  1.600E-05

```

1.700E-05	1.850E-05	1.900E-05	2.000E-05	2.100E-05
2.250E-05	2.500E-05	2.750E-05	3.000E-05	3.125E-05
3.175E-05	3.325E-05	3.375E-05	3.460E-05	3.550E-05
3.700E-05	3.800E-05	3.910E-05	3.960E-05	4.100E-05
4.240E-05	4.400E-05	4.520E-05	4.700E-05	4.830E-05
4.920E-05	5.060E-05	5.200E-05	5.340E-05	5.900E-05
6.100E-05	6.500E-05	6.750E-05	7.200E-05	7.600E-05
8.000E-05	8.200E-05	9.000E-05	1.000E-04	1.080E-04
1.150E-04	1.190E-04	1.220E-04	1.860E-04	1.925E-04
2.075E-04	2.100E-04	2.400E-04	2.850E-04	3.050E-04
5.500E-04	6.700E-04	6.830E-04	9.500E-04	1.150E-03
1.500E-03	1.550E-03	1.800E-03	2.200E-03	2.290E-03
2.580E-03	3.000E-03	3.740E-03	3.900E-03	6.000E-03
8.030E-03	9.500E-03	1.300E-02	1.700E-02	2.500E-02
3.000E-02	4.500E-02	5.000E-02	5.200E-02	6.000E-02
7.300E-02	7.500E-02	8.200E-02	8.500E-02	1.000E-01
1.283E-01	1.500E-01	2.000E-01	2.700E-01	3.300E-01
4.000E-01	4.200E-01	4.400E-01	4.700E-01	4.995E-01
5.500E-01	5.730E-01	6.000E-01	6.700E-01	6.790E-01
7.500E-01	8.200E-01	8.611E-01	8.750E-01	9.000E-01
9.200E-01	1.010E+00	1.100E+00	1.200E+00	1.250E+00
1.317E+00	1.356E+00	1.400E+00	1.500E+00	1.850E+00
2.354E+00	2.479E+00	3.000E+00	4.304E+00	4.800E+00
6.434E+00	8.187E+00	1.000E+01	1.284E+01	1.384E+01
1.455E+01	1.568E+01	1.733E+01	2.000E+01	

HI-STAR containing MPC68, 08x08 @ 4.2 wt% Enrich.

c 4.20 % uniform enrichment, unreflected cask, 0.0279 g/cmsq B-10 in Boral

c
c

1	1	-10.522		-1	u=2		\$ fuel
2	4	-1.0	1	-2	u=2		\$ gap
3	3	-6.55	2	-3	u=2		\$ Zr Clad
4	4	-1.0		3	u=2		\$ water in fuel region
5	4	-1.0	-4:5		u=3		\$ water in guide tubes
6	3	-6.55	4	-5	u=3		\$ guide tubes
7	4	-1.0	-6	+7	-8	+9	u=1 lat=1

fill= -5:4 -5:4 0:0

1	1	1	1	1	1	1	1	1	1
1	2	2	2	2	2	2	2	2	1
1	2	2	2	2	2	2	2	2	1
1	2	2	2	2	2	2	2	2	1
1	2	2	2	3	2	2	2	2	1
1	2	2	2	2	3	2	2	2	1
1	2	2	2	2	2	2	2	2	1
1	2	2	2	2	2	2	2	2	1
1	2	2	2	2	2	2	2	2	1
1	2	2	2	2	2	2	2	2	1
1	1	1	1	1	1	1	1	1	1

c

BOX TYPE R

c

8	0	-10	11	-12	13		u=4 fill=1 (0.8128 0.8128 0)
9	3	-6.55	60	-61	62	-63 #8	u=4 \$ Zr flow channel
10	4	-1.	64	-65	66	-67 #8 #9	u=4 \$ water
11	5	-7.84	20	-23	67	-14	u=4 \$ 0.075" STEEL
12	4	-1.	20	-23	14	-15	u=4 \$ WATER POCKET
13	7	-2.7	20	-23	15	-16	u=4 \$ Al CLAD
14	6	-2.66	20	-23	16	-17	u=4 \$ BORAL Absorber
15	7	-2.7	20	-23	17	-18	u=4 \$ Al Clad
16	4	-1.	20	-23	18	-118	u=4 \$ Water
17	5	-7.84	118:-129:65:-66				u=4 \$ Steel
18	4	-1.	64	-21	67	-118	u=4 \$ Water
19	4	-1.	24	-65	67	-118	u=4 \$ water
20	5	-7.84	21	-20	67	-118	u=4 \$ Steel
21	5	-7.84	23	-24	67	-118	u=4 \$ Steel
22	4	-1.	129	-64	33	-118	u=4 \$ Water
c							
23	5	-7.84	25	-64	30	-31	u=4 \$ Steel
24	4	-1.	26	-25	30	-31	u=4 \$ Water
25	7	-2.7	27	-26	30	-31	u=4 \$ Al clad
26	6	-2.66	28	-27	30	-31	u=4 \$ Boral
27	7	-2.7	29	-28	30	-31	u=4 \$ Al clad
28	4	-1.	129	-29	30	-31	u=4 \$ water
29	5	-7.84	129	-64	32	-30	u=4 \$ Steel ends
30	5	-7.84	129	-64	31	-33	u=4 \$ Steel ends
31	4	-1.	129	-64	66	-32	u=4 \$ Water

c

Type A box - Boral only on left side

c

32	0	-10	11	-12	13		u=6 fill=1 (0.8128 0.8128 0)
33	3	-6.55	60	-61	62	-63 #8	u=6 \$ Zr flow channel
34	4	-1.	64	-65	66	-118 #8 #9	u=6 \$ water
35	5	-7.84	118:-129:65:-66				u=6 \$ Steel
36	4	-1.	129	-64	67	-118	u=6 \$ Water
c							
37	5	-7.84	25	-64	30	-31	u=6 \$ Steel

38	4	-1.	26	-25	30	-31	u=6	\$ Water
39	7	-2.7	27	-26	30	-31	u=6	\$ Al clad
40	6	-2.66	28	-27	30	-31	u=6	\$ Boral
41	7	-2.7	29	-28	30	-31	u=6	\$ Al clad
42	4	-1.	129	-29	30	-31	u=6	\$ water
43	4	-1.	129	-64	33	-67	u=6	\$ Water
44	5	-7.84	129	-64	32	-30	u=6	\$ Steel ends
45	5	-7.84	129	-64	31	-33	u=6	\$ Steel ends
46	4	-1.	129	-64	66	-32	u=6	\$ Water
c								
c	Type B box - Boral on Top only							
c								
47	0	-10	11	-12	13		u=7 fill=1 (0.8128	0.8128 0)
48	3	-6.55	60	-61	62	-63	#8	u=7 \$ Zr flow channel
49	4	-1.	64	-65	66	-67	#8 #9	u=7 \$ water
50	5	-7.84	20	-23	67	-14		u=7 \$ 0.075" STEEL
51	4	-1.	20	-23	14	-15		u=7 \$ WATER POCKET
52	7	-2.7	20	-23	15	-16		u=7 \$ Al CLAD
53	6	-2.66	20	-23	16	-17		u=7 \$ BORAL Absorber
54	7	-2.7	20	-23	17	-18		u=7 \$ water
55	4	-1.	20	-23	18	-118		u=7 \$ Water
56	5	-7.84	118:-129:65:-66					u=7 \$ Steel
57	4	-1.	64	-21	67	-118		u=7 \$ Water
58	4	-1.	24	-65	67	-118		u=7 \$ water
59	5	-7.84	21	-20	67	-118		u=7 \$ Steel
60	5	-7.84	23	-24	67	-118		u=7 \$ Steel
61	4	-1.	129	-64	66	-118		u=7 \$ Water
c								
c	Type E box - No Boral Panels							
c								
62	0	-10	11	-12	13		u=8 fill=1 (0.8128	0.8128 0)
63	3	-6.55	60	-61	62	-63	#8	u=8 \$ Zr flow channel
64	4	-1.	129	-65	66	-118	#8 #9	u=8 \$ water
65	5	-7.84	118:-129:65:-66					u=8 \$ Steel
c								
c	Type F box - No Boral Panels or fuel							
c								
66	4	-1.	129	-65	66	-118		u=9 \$ water
67	5	-7.84	118:-129:65:-66					u=9 \$ Steel
c								
68	4	-1.0	-34	35	-36	37	u=5 lat=1 fill=-7:6	-7:6 0:0
			5 5 5 5 5 5 5 5 5 5 5 5					
			5 9 9 9 9 9 9 9 9 9 9 9 5					
			5 9 9 9 9 9 7 4 9 9 9 9 5					
			5 9 9 9 7 4 4 4 4 4 9 9 5					
			5 9 9 7 4 4 4 4 4 4 4 9 5					
			5 9 9 7 4 4 4 4 4 4 4 9 5					
			5 9 7 4 4 4 4 4 4 4 4 9 5					
			5 9 8 4 4 4 4 4 4 4 4 6 9 5					
			5 9 9 7 4 4 4 4 4 4 4 9 9 5					
			5 9 9 8 4 4 4 4 4 4 4 6 9 9 5					
			5 9 9 9 8 4 4 4 6 6 9 9 9 5					
			5 9 9 9 9 9 8 6 9 9 9 9 9 5					
			5 9 9 9 9 9 9 9 9 9 9 9 9 5					
			5 5 5 5 5 5 5 5 5 5 5 5 5					
69	0		-41			50	-49	fill=5 (8.1661 8.1661 0)
70	4	-1.0	-41		43	-50		\$ Water below Fuel
71	4	-1.0	-41		49	-44		\$ Water above Fuel
72	5	-7.84	-42		68	-43		\$ Steel below Fuel
73	5	-7.84	-42		44	-69		\$ Steel above Fuel

74	5	-7.84	41	-42	43	-44		\$ Radial Steel
75	0		42	:-68:	69			\$ outside world
1	cz	0.5207						\$ Fuel OD
2	cz	0.5321						\$ Clad ID
3	cz	0.6134						\$ Clad OD
4	cz	0.6744						\$ Thimble ID
5	cz	0.7506						\$ Thimble OD
6	px	0.8128						\$ Pin Pitch
7	px	-0.8128						
8	py	0.8128						
9	py	-0.8128						
10	px	6.7031						\$ Channel ID
11	px	-6.7031						
12	py	6.7031						
13	py	-6.7031						
14	py	7.8016						
15	py	7.8155						
16	py	7.8410						
17	py	8.0467						
18	py	8.0721						
118	py	8.0861						
20	px	-6.0325						
21	px	-6.2230						
23	px	6.0325						
24	px	6.2230						
25	px	-7.8016						
26	px	-7.8155						
27	px	-7.8410						
28	px	-8.0467						
29	px	-8.0721						
129	px	-8.0861						
30	py	-6.0325						
31	py	6.0325						
32	py	-6.2230						
33	py	6.2230						
34	px	7.6111						
35	px	-8.7211						
36	py	8.7211						
37	py	-7.6111						
41	cz	85.57						
42	cz	108.43						
43	pz	-18.54						
44	pz	402.5						
49	pz	381.						\$ Top of Active Fuel
50	pz	0						\$ Start of Active Fuel
60	px	-6.9571						\$ Channel OD
61	px	6.9571						
62	py	-6.9571						
63	py	6.9571						
64	px	-7.6111						\$ Cell Box ID
65	px	7.6111						
66	py	-7.6111						
67	py	7.6111						
68	pz	-40.13						
69	pz	441.9						

imp:n 1 73r 0
kcode 10000 0.94 20 120
c

sdef par=1 erg=d1 axs=0 0 1 x=d4 y=fx d5 z=d3

c

sp1 -2 1.2895

c

c

si3 h 0 365.76

sp3 0 1

c

c

si4 s 15 16
 13 14 15 16 17 18
 12 13 14 15 16 17 18 19
 12 13 14 15 16 17 18 19
 11 12 13 14 15 16 17 18 19 20
 11 12 13 14 15 16 17 18 19 20
 12 13 14 15 16 17 18 19
 12 13 14 15 16 17 18 19
 13 14 15 16 17 18
 15 16

sp4 1 67r

c

ds5 s 30 30
 29 29 29 29 29 29
 28 28 28 28 28 28 28 28
 27 27 27 27 27 27 27 27
 26 26 26 26 26 26 26 26 26 26
 25 25 25 25 25 25 25 25 25 25
 24 24 24 24 24 24 24 24
 23 23 23 23 23 23 23 23
 22 22 22 22 22 22
 21 21

c

si11 -80.6831 -67.6783

si12 -64.1985 -51.1937

si13 -47.7139 -34.7091

si14 -31.2293 -18.2245

si15 -14.7447 -1.7399

si16 1.7399 14.7447

si17 18.2245 31.2293

si18 34.7091 47.7139

si19 51.1937 64.1985

si20 67.6783 80.6831

c

si21 -80.6831 -67.6783

si22 -64.1985 -51.1937

si23 -47.7139 -34.7091

si24 -31.2293 -18.2245

si25 -14.7447 -1.7399

si26 1.7399 14.7447

si27 18.2245 31.2293

si28 34.7091 47.7139

si29 51.1937 64.1985

si30 67.6783 80.6831

sp11 0 1

sp12 0 1

sp13 0 1

sp14 0 1

sp15 0 1

sp16 0 1

sp17 0 1

sp18 0 1
 sp19 0 1
 sp20 0 1
 sp21 0 1
 sp22 0 1
 sp23 0 1
 sp24 0 1
 sp25 0 1
 sp26 0 1
 sp27 0 1
 sp28 0 1
 sp29 0 1
 sp30 0 1

c
 m1 92235.50c 9.98343E-04 \$ 4.20% E Fuel
 92238.50c 0.022484
 8016.50c 0.046965
 m2 8016.50c 1. \$ Void
 m3 40000.56c 1. \$ Zr Clad
 m4 1001.50c 0.6667 \$ Water
 8016.50c 0.3333
 m5 24000.50c 0.01761 \$ Steel
 25055.50c 0.001761
 26000.55c 0.05977
 28000.50c 0.008239
 m6 5010.50c 8.0707E-03 \$ Boral
 5011.50c 3.2553E-02
 6000.50c 1.0146E-02
 13027.50c 3.8054E-02
 m7 13027.50c 1. \$ Al Clad

mt4 lwtr.01t
 prdmp j -30 1 2
 fm4 1000 1 -6
 f4:n 1
 sd4 1000

e4	1.000E-11	1.000E-10	5.000E-10	7.500E-10	1.000E-09	1.200E-09
	1.500E-09	2.000E-09	2.500E-09	3.000E-09		
	4.700E-09	5.000E-09	7.500E-09	1.000E-08	2.530E-08	
	3.000E-08	4.000E-08	5.000E-08	6.000E-08	7.000E-08	
	8.000E-08	9.000E-08	1.000E-07	1.250E-07	1.500E-07	
	1.750E-07	2.000E-07	2.250E-07	2.500E-07	2.750E-07	
	3.000E-07	3.250E-07	3.500E-07	3.750E-07	4.000E-07	
	4.500E-07	5.000E-07	5.500E-07	6.000E-07	6.250E-07	
	6.500E-07	7.000E-07	7.500E-07	8.000E-07	8.500E-07	
	9.000E-07	9.250E-07	9.500E-07	9.750E-07	1.000E-06	
	1.010E-06	1.020E-06	1.030E-06	1.040E-06	1.050E-06	
	1.060E-06	1.070E-06	1.080E-06	1.090E-06	1.100E-06	
	1.110E-06	1.120E-06	1.130E-06	1.140E-06	1.150E-06	
	1.175E-06	1.200E-06	1.225E-06	1.250E-06	1.300E-06	
	1.350E-06	1.400E-06	1.450E-06	1.500E-06	1.590E-06	
	1.680E-06	1.770E-06	1.860E-06	1.940E-06	2.000E-06	
	2.120E-06	2.210E-06	2.300E-06	2.380E-06	2.470E-06	
	2.570E-06	2.670E-06	2.770E-06	2.870E-06	2.970E-06	
	3.000E-06	3.050E-06	3.150E-06	3.500E-06	3.730E-06	
	4.000E-06	4.750E-06	5.000E-06	5.400E-06	6.000E-06	
	6.250E-06	6.500E-06	6.750E-06	7.000E-06	7.150E-06	
	8.100E-06	9.100E-06	1.000E-05	1.150E-05	1.190E-05	
	1.290E-05	1.375E-05	1.440E-05	1.510E-05	1.600E-05	
	1.700E-05	1.850E-05	1.900E-05	2.000E-05	2.100E-05	
	2.250E-05	2.500E-05	2.750E-05	3.000E-05	3.125E-05	

3.175E-05	3.325E-05	3.375E-05	3.460E-05	3.550E-05
3.700E-05	3.800E-05	3.910E-05	3.960E-05	4.100E-05
4.240E-05	4.400E-05	4.520E-05	4.700E-05	4.830E-05
4.920E-05	5.060E-05	5.200E-05	5.340E-05	5.900E-05
6.100E-05	6.500E-05	6.750E-05	7.200E-05	7.600E-05
8.000E-05	8.200E-05	9.000E-05	1.000E-04	1.080E-04
1.150E-04	1.190E-04	1.220E-04	1.860E-04	1.925E-04
2.075E-04	2.100E-04	2.400E-04	2.850E-04	3.050E-04
5.500E-04	6.700E-04	6.830E-04	9.500E-04	1.150E-03
1.500E-03	1.550E-03	1.800E-03	2.200E-03	2.290E-03
2.580E-03	3.000E-03	3.740E-03	3.900E-03	6.000E-03
8.030E-03	9.500E-03	1.300E-02	1.700E-02	2.500E-02
3.000E-02	4.500E-02	5.000E-02	5.200E-02	6.000E-02
7.300E-02	7.500E-02	8.200E-02	8.500E-02	1.000E-01
1.283E-01	1.500E-01	2.000E-01	2.700E-01	3.300E-01
4.000E-01	4.200E-01	4.400E-01	4.700E-01	4.995E-01
5.500E-01	5.730E-01	6.000E-01	6.700E-01	6.790E-01
7.500E-01	8.200E-01	8.611E-01	8.750E-01	9.000E-01
9.200E-01	1.010E+00	1.100E+00	1.200E+00	1.250E+00
1.317E+00	1.356E+00	1.400E+00	1.500E+00	1.850E+00
2.354E+00	2.479E+00	3.000E+00	4.304E+00	4.800E+00
6.434E+00	8.187E+00	1.000E+01	1.284E+01	1.384E+01
1.455E+01	1.568E+01	1.733E+01	2.000E+01	

HI-STAR containing MPC68F, 06x06 @ 3.0 wt% Enrich.

c 3.00 % uniform enrichment, unreflected cask, 0.0067 g/cmsq B-10 in Boral
 c Dresden-1 6x6

c
 c
 c
 1 1 -10.522 -1 u=2 \$ fuel
 2 4 -1.0 1 -2 u=2 \$ gap
 3 3 -6.55 2 -3 u=2 \$ Zr Clad
 4 4 -1.0 3 u=2 \$ water in fuel region
 5 4 -1.0 -4:5 u=3 \$ water in guide tubes
 6 3 -6.55 4 -5 u=3 \$ guide tubes
 7 4 -1.0 -6 +7 -8 +9 u=1 lat=1
 fill= -4:3 -4:3 0:0
 1 1 1 1 1 1 1
 1 2 2 2 2 2 2 1
 1 2 2 2 2 2 2 1
 1 2 2 2 2 2 2 1
 1 2 2 2 2 2 2 1
 1 2 2 2 2 2 2 1
 1 2 2 2 2 2 2 1
 1 2 2 2 2 2 2 1
 1 1 1 1 1 1 1 1

c
 C BOX TYPE R

c
 8 0 -10 11 -12 13 u=4 fill=1 (0.8814 0.8814 0)
 9 3 -6.55 60 -61 62 -63 #8 u=4 \$ Zr flow channel
 10 4 -1. 64 -65 66 -67 #8 #9 u=4 \$ water
 11 5 -7.84 20 -23 67 -14 u=4 \$ 0.075" STEEL
 12 4 -1. 20 -23 14 -15 u=4 \$ WATER POCKET
 13 7 -2.7 20 -23 15 -16 u=4 \$ Al CLAD
 14 6 -2.66 20 -23 16 -17 u=4 \$ BORAL Absorber
 15 7 -2.7 20 -23 17 -18 u=4 \$ Al Clad
 16 4 -1. 20 -23 18 -118 u=4 \$ Water
 17 5 -7.84 118:-129:65:-66 u=4 \$ Steel
 18 4 -1. 64 -21 67 -118 u=4 \$ Water
 19 4 -1. 24 -65 67 -118 u=4 \$ water
 20 5 -7.84 21 -20 67 -118 u=4 \$ Steel
 21 5 -7.84 23 -24 67 -118 u=4 \$ Steel
 22 4 -1. 129 -64 33 -118 u=4 \$ Water
 c
 23 5 -7.84 25 -64 30 -31 u=4 \$ Steel
 24 4 -1. 26 -25 30 -31 u=4 \$ Water
 25 7 -2.7 27 -26 30 -31 u=4 \$ Al clad
 26 6 -2.66 28 -27 30 -31 u=4 \$ Boral
 27 7 -2.7 29 -28 30 -31 u=4 \$ Al clad
 28 4 -1. 129 -29 30 -31 u=4 \$ water
 29 5 -7.84 129 -64 32 -30 u=4 \$ Steel ends
 30 5 -7.84 129 -64 31 -33 u=4 \$ Steel ends
 31 4 -1. 129 -64 66 -32 u=4 \$ Water

c
 c Type A box - Boral only on left side

c
 32 0 -10 11 -12 13 u=6 fill=1 (0.8814 0.8814 0)
 33 3 -6.55 60 -61 62 -63 #8 u=6 \$ Zr flow channel
 34 4 -1. 64 -65 66 -118 #8 #9 u=6 \$ water
 35 5 -7.84 118:-129:65:-66 u=6 \$ Steel
 36 4 -1. 129 -64 67 -118 u=6 \$ Water
 c
 37 5 -7.84 25 -64 30 -31 u=6 \$ Steel
 38 4 -1. 26 -25 30 -31 u=6 \$ Water

```

39 7 -2.7 27 -26 30 -31 u=6 $ Al clad
40 6 -2.66 28 -27 30 -31 u=6 $ Boral
41 7 -2.7 29 -28 30 -31 u=6 $ Al clad
42 4 -1. 129 -29 30 -31 u=6 $ water
43 4 -1. 129 -64 33 -67 u=6 $ Water
44 5 -7.84 129 -64 32 -30 u=6 $ Steel ends
45 5 -7.84 129 -64 31 -33 u=6 $ Steel ends
46 4 -1. 129 -64 66 -32 u=6 $ Water
c
c Type B box - Boral on Top only
c
47 0 -10 11 -12 13 u=7 fill=1 (0.8814 0.8814 0)
48 3 -6.55 60 -61 62 -63 #8 u=7 $ Zr flow channel
49 4 -1. 64 -65 66 -67 #8 #9 u=7 $ water
50 5 -7.84 20 -23 67 -14 u=7 $ 0.075" STEEL
51 4 -1. 20 -23 14 -15 u=7 $ WATER POCKET
52 7 -2.7 20 -23 15 -16 u=7 $ Al CLAD
53 6 -2.66 20 -23 16 -17 u=7 $ BORAL Absorber
54 7 -2.7 20 -23 17 -18 u=7 $ water
55 4 -1. 20 -23 18 -118 u=7 $ Water
56 5 -7.84 118:-129:65:-66 u=7 $ Steel
57 4 -1. 64 -21 67 -118 u=7 $ Water
58 4 -1. 24 -65 67 -118 u=7 $ water
59 5 -7.84 21 -20 67 -118 u=7 $ Steel
60 5 -7.84 23 -24 67 -118 u=7 $ Steel
61 4 -1. 129 -64 66 -118 u=7 $ Water
c
c Type E box - No Boral Panels
c
62 0 -10 11 -12 13 u=8 fill=1 (0.8814 0.8814 0)
63 3 -6.55 60 -61 62 -63 #8 u=8 $ Zr flow channel
64 4 -1. 129 -65 66 -118 #8 #9 u=8 $ water
65 5 -7.84 118:-129:65:-66 u=8 $ Steel
c
c Type F box - No Boral Panels or fuel
c
66 4 -1. 129 -65 66 -118 u=9 $ water
67 5 -7.84 118:-129:65:-66 u=9 $ Steel
c
68 4 -1.0 -34 35 -36 37 u=5 lat=1 fill=-7:6 -7:6 0:0
5 5 5 5 5 5 5 5 5 5 5 5 5 5
5 9 9 9 9 9 9 9 9 9 9 9 9 9 5
5 9 9 9 9 9 7 4 9 9 9 9 9 9 5
5 9 9 9 7 4 4 4 4 4 4 9 9 9 5
5 9 9 7 4 4 4 4 4 4 4 4 9 9 5
5 9 9 7 4 4 4 4 4 4 4 4 9 9 5
5 9 7 4 4 4 4 4 4 4 4 4 4 9 5
5 9 8 4 4 4 4 4 4 4 4 4 6 9 5
5 9 9 7 4 4 4 4 4 4 4 4 4 9 9 5
5 9 9 8 4 4 4 4 4 4 4 4 6 9 9 5
5 9 9 9 8 4 4 4 6 6 9 9 9 5
5 9 9 9 9 9 8 6 9 9 9 9 9 5
5 9 9 9 9 9 9 9 9 9 9 9 9 5
5 5 5 5 5 5 5 5 5 5 5 5 5 5
69 0 -41 50 -49 fill=5 (8.1661 8.1661 0)
70 4 -1.0 -41 43 -50 $ Water below Fuel
71 4 -1.0 -41 49 -44 $ Water above Fuel
72 5 -7.84 -42 68 -43 $ Steel below Fuel
73 5 -7.84 -42 44 -69 $ Steel above Fuel
74 5 -7.84 41 -42 43 -44 $ Radial Steel

```

75 0 42 :-68: 69 \$ outside world

1	cz	0.6274	\$ Fuel OD
2	cz	0.6280	\$ Clad ID
3	cz	0.7169	\$ Clad OD
4	cz	0.6280	\$ Thimble ID
5	cz	0.7169	\$ Thimble OD
6	px	0.8814	\$ Pin Pitch
7	px	-0.8814	
8	py	0.8814	
9	py	-0.8814	
10	px	5.4483	\$ Channel ID
11	px	-5.4483	
12	py	5.4483	
13	py	-5.4483	
14	py	7.8016	
15	py	7.8155	
16	py	7.8410	
17	py	8.0467	
18	py	8.0721	
118	py	8.0861	
20	px	-6.0325	
21	px	-6.2230	
23	px	6.0325	
24	px	6.2230	
25	px	-7.8016	
26	px	-7.8155	
27	px	-7.8410	
28	px	-8.0467	
29	px	-8.0721	
129	px	-8.0861	
30	py	-6.0325	
31	py	6.0325	
32	py	-6.2230	
33	py	6.2230	
34	px	7.6111	
35	px	-8.7211	
36	py	8.7211	
37	py	-7.6111	
41	cz	85.57	
42	cz	108.43	
43	pz	11.46	
44	pz	331.0	
49	pz	309.4	\$ Top of Active F
50	pz	30.	\$ Start of Active
60	px	-5.6007	\$ Channel OD
61	px	5.6007	
62	py	-5.6007	
63	py	5.6007	
64	px	-7.6111	\$ Cell Box ID
65	px	7.6111	
66	py	-7.6111	
67	py	7.6111	
68	pz	-10.13	
69	pz	370.36	

imp:n 1 73r 0
kcode 10000 0.94 20 120
c
sdef par=1 erg=d1 axs=0 0 1 x=d4 y=fx d5 z=d3

```

c
sp1 -2 1.2895
c
si3 h 30. 309.
sp3 0 1
c
c
si4 s
      15 16
      13 14 15 16 17 18
      12 13 14 15 16 17 18 19
      12 13 14 15 16 17 18 19
      11 12 13 14 15 16 17 18 19 20
      11 12 13 14 15 16 17 18 19 20
      12 13 14 15 16 17 18 19
      12 13 14 15 16 17 18 19
      13 14 15 16 17 18
      15 16

sp4 1 67r
c
ds5 s
      30 30
      29 29 29 29 29 29
      28 28 28 28 28 28 28 28
      27 27 27 27 27 27 27 27
      26 26 26 26 26 26 26 26 26
      25 25 25 25 25 25 25 25 25
      24 24 24 24 24 24 24 24
      23 23 23 23 23 23 23 23
      22 22 22 22 22 22
      21 21

c
si11 -80.6831 -67.6783
si12 -64.1985 -51.1937
si13 -47.7139 -34.7091
si14 -31.2293 -18.2245
si15 -14.7447 -1.7399
si16  1.7399  14.7447
si17  18.2245  31.2293
si18  34.7091  47.7139
si19  51.1937  64.1985
si20  67.6783  80.6831
c
si21 -80.6831 -67.6783
si22 -64.1985 -51.1937
si23 -47.7139 -34.7091
si24 -31.2293 -18.2245
si25 -14.7447 -1.7399
si26  1.7399  14.7447
si27  18.2245  31.2293
si28  34.7091  47.7139
si29  51.1937  64.1985
si30  67.6783  80.6831
sp11 0 1
sp12 0 1
sp13 0 1
sp14 0 1
sp15 0 1
sp16 0 1
sp17 0 1
sp18 0 1
sp19 0 1

```

sp20 0 1
 sp21 0 1
 sp22 0 1
 sp23 0 1
 sp24 0 1
 sp25 0 1
 sp26 0 1
 sp27 0 1
 sp28 0 1
 sp29 0 1
 sp30 0 1

c

m1	92235.50c	-0.02644		\$ 3.00% E Fuel		
	92238.50c	-0.85504				
	8016.50c	-0.11852				
m3	40000.56c	1.		\$ Zr Clad		
m4	1001.50c	0.6667		\$ Water		
	8016.50c	0.3333				
m5	24000.50c	0.01761		\$ Steel		
	25055.50c	0.001761				
	26000.55c	0.05977				
	28000.50c	0.008239				
m6	5010.50c	1.9592E-03		\$ Boral 0.0067 gm/cm2		
	5011.50c	8.1175E-03				
	6000.50c	2.5176E-03				
	13027.50c	5.4933E-02				
m7	13027.50c	1.		\$ Al Clad		
mt4	lwtr.01t					
prdmp	j	-120	j	2		
fm4	1000	1	-6			
f4:n	1					
sd4	1000					
e4	1.000E-11	1.000E-10	5.000E-10	7.500E-10	1.000E-09	1.200E-09
	1.500E-09	2.000E-09	2.500E-09	3.000E-09		
	4.700E-09	5.000E-09	5.000E-09	6.000E-08	2.530E-08	7.000E-08
	3.000E-08	4.000E-08	5.000E-08	6.000E-08		
	8.000E-08	9.000E-08	1.000E-07	1.250E-07	1.500E-07	
	1.750E-07	2.000E-07	2.250E-07	2.500E-07	2.750E-07	
	3.000E-07	3.250E-07	3.500E-07	3.750E-07	4.000E-07	
	4.500E-07	5.000E-07	5.500E-07	6.000E-07	6.250E-07	
	6.500E-07	7.000E-07	7.500E-07	8.000E-07	8.500E-07	
	9.000E-07	9.250E-07	9.500E-07	9.750E-07	1.000E-06	
	1.010E-06	1.020E-06	1.030E-06	1.040E-06	1.050E-06	
	1.060E-06	1.070E-06	1.080E-06	1.090E-06	1.100E-06	
	1.110E-06	1.120E-06	1.130E-06	1.140E-06	1.150E-06	
	1.175E-06	1.200E-06	1.225E-06	1.250E-06	1.300E-06	
	1.350E-06	1.400E-06	1.450E-06	1.500E-06	1.590E-06	
	1.680E-06	1.770E-06	1.860E-06	1.940E-06	2.000E-06	
	2.120E-06	2.210E-06	2.300E-06	2.380E-06	2.470E-06	
	2.570E-06	2.670E-06	2.770E-06	2.870E-06	2.970E-06	
	3.000E-06	3.050E-06	3.150E-06	3.500E-06	3.730E-06	
	4.000E-06	4.750E-06	5.000E-06	5.400E-06	6.000E-06	
	6.250E-06	6.500E-06	6.750E-06	7.000E-06	7.150E-06	
	8.100E-06	9.100E-06	1.000E-05	1.150E-05	1.190E-05	
	1.290E-05	1.375E-05	1.440E-05	1.510E-05	1.600E-05	
	1.700E-05	1.850E-05	1.900E-05	2.000E-05	2.100E-05	
	2.250E-05	2.500E-05	2.750E-05	3.000E-05	3.125E-05	
	3.175E-05	3.325E-05	3.375E-05	3.460E-05	3.550E-05	
	3.700E-05	3.800E-05	3.910E-05	3.960E-05	4.100E-05	
	4.240E-05	4.400E-05	4.520E-05	4.700E-05	4.830E-05	

4.920E-05	5.060E-05	5.200E-05	5.340E-05	5.900E-05
6.100E-05	6.500E-05	6.750E-05	7.200E-05	7.600E-05
8.000E-05	8.200E-05	9.000E-05	1.000E-04	1.080E-04
1.150E-04	1.190E-04	1.220E-04	1.860E-04	1.925E-04
2.075E-04	2.100E-04	2.400E-04	2.850E-04	3.050E-04
5.500E-04	6.700E-04	6.830E-04	9.500E-04	1.150E-03
1.500E-03	1.550E-03	1.800E-03	2.200E-03	2.290E-03
2.580E-03	3.000E-03	3.740E-03	3.900E-03	6.000E-03
8.030E-03	9.500E-03	1.300E-02	1.700E-02	2.500E-02
3.000E-02	4.500E-02	5.000E-02	5.200E-02	6.000E-02
7.300E-02	7.500E-02	8.200E-02	8.500E-02	1.000E-01
1.283E-01	1.500E-01	2.000E-01	2.700E-01	3.300E-01
4.000E-01	4.200E-01	4.400E-01	4.700E-01	4.995E-01
5.500E-01	5.730E-01	6.000E-01	6.700E-01	6.790E-01
7.500E-01	8.200E-01	8.611E-01	8.750E-01	9.000E-01
9.200E-01	1.010E+00	1.100E+00	1.200E+00	1.250E+00
1.317E+00	1.356E+00	1.400E+00	1.500E+00	1.850E+00
2.354E+00	2.479E+00	3.000E+00	4.304E+00	4.800E+00
6.434E+00	8.187E+00	1.000E+01	1.284E+01	1.384E+01
1.455E+01	1.568E+01	1.733E+01	2.000E+01	

HI-STAR containing MPC68F, 06x06 in DFC with 08 missing rods
 c 3.00 % uniform enrichment, unreflected cask, 0.0067 g/cmsq B-10 in Boral

c
 c
 1 1 -10.522 -1 u=2 \$ fuel
 2 4 -1.0 1 -2 u=2 \$ gap
 3 3 -6.55 2 -3 u=2 \$ Zr Clad
 4 4 -1.0 3 u=2 \$ water in fuel region
 5 4 -1.0 -4:5 u=3 \$ water in guide tubes
 6 3 -6.55 4 -5 u=3 \$ guide tubes
 7 4 -1.0 -6 +7 -8 +9 u=1 lat=1
 fill=-4:3 -4:3 0:0
 1 1 1 1 1 1 1 1
 1 2 2 2 2 2 2 1
 1 2 1 2 1 2 2 1
 1 2 2 1 2 1 2 1
 1 2 1 2 1 2 2 1
 1 2 2 1 2 1 2 1
 1 2 2 2 2 2 2 1
 1 1 1 1 1 1 1 1

c
 C BOX TYPE R
 c
 8 0 -10 11 -12 13 u=4 fill=1 (0.8814 0.8814 0)
 9 3 -6.55 60 -61 62 -63 #8 u=4 \$ Zr flow channel
 100 5 -7.84 74 -75 76 -77 (-70:71:-72:73) u=4 \$ DFC
 10 4 -1. 64 -65 66 -67 #8 #9 #100 u=4 \$ water
 11 5 -7.84 20 -23 67 -14 u=4 \$ 0.075" STEEL
 12 4 -1. 20 -23 14 -15 u=4 \$ WATER POCKET
 13 7 -2.7 20 -23 15 -16 u=4 \$ Al CLAD
 14 6 -2.66 20 -23 16 -17 u=4 \$ BORAL Absorber
 15 7 -2.7 20 -23 17 -18 u=4 \$ Al Clad
 16 4 -1. 20 -23 18 -118 u=4 \$ Water
 17 5 -7.84 118:-129:65:-66 u=4 \$ Steel
 18 4 -1. 64 -21 67 -118 u=4 \$ Water
 19 4 -1. 24 -65 67 -118 u=4 \$ water
 20 5 -7.84 21 -20 67 -118 u=4 \$ Steel
 21 5 -7.84 23 -24 67 -118 u=4 \$ Steel
 22 4 -1. 129 -64 33 -118 u=4 \$ Water
 c
 23 5 -7.84 25 -64 30 -31 u=4 \$ Steel
 24 4 -1. 26 -25 30 -31 u=4 \$ Water
 25 7 -2.7 27 -26 30 -31 u=4 \$ Al clad
 26 6 -2.66 28 -27 30 -31 u=4 \$ Boral
 27 7 -2.7 29 -28 30 -31 u=4 \$ Al clad
 28 4 -1. 129 -29 30 -31 u=4 \$ water
 29 5 -7.84 129 -64 32 -30 u=4 \$ Steel ends
 30 5 -7.84 129 -64 31 -33 u=4 \$ Steel ends
 31 4 -1. 129 -64 66 -32 u=4 \$ Water

c
 c Type A box - Boral only on left side
 c
 32 0 -10 11 -12 13 u=6 fill=1 (0.8814 0.8814 0)
 33 3 -6.55 60 -61 62 -63 #8 u=6 \$ Zr flow channel
 101 5 -7.84 74 -75 76 -77 (-70:71:-72:73) u=6 \$ DFC
 34 4 -1. 64 -65 66 -118 #8 #9 #101 u=6 \$ water
 35 5 -7.84 118:-129:65:-66 u=6 \$ Steel
 36 4 -1. 129 -64 67 -118 u=6 \$ Water
 c
 37 5 -7.84 25 -64 30 -31 u=6 \$ Steel

38	4	-1.	26	-25	30	-31		u=6	\$ Water	
39	7	-2.7	27	-26	30	-31		u=6	\$ Al clad	
40	6	-2.66	28	-27	30	-31		u=6	\$ Boral	
41	7	-2.7	29	-28	30	-31		u=6	\$ Al clad	
42	4	-1.	129	-29	30	-31		u=6	\$ water	
43	4	-1.	129	-64	33	-67		u=6	\$ Water	
44	5	-7.84	129	-64	32	-30		u=6	\$ Steel ends	
45	5	-7.84	129	-64	31	-33		u=6	\$ Steel ends	
46	4	-1.	129	-64	66	-32		u=6	\$ Water	
c										
c	Type B box - Boral on Top only									
c										
47	0	-10	11	-12	13			u=7 fill=1 (0.8814	0.8814 0)	
48	3	-6.55	60	-61	62	-63	#8	u=7	\$ Zr flow channel	
102	5	-7.84	74	-75	76	-77	(-70:71:-72:73)	u=7	\$ DFC	
49	4	-1.	64	-65	66	-67	#8 #9 #102	u=7	\$ water	
50	5	-7.84	20	-23	67	-14		u=7	\$ 0.075" STEEL	
51	4	-1.	20	-23	14	-15		u=7	\$ WATER POCKET	
52	7	-2.7	20	-23	15	-16		u=7	\$ Al CLAD	
53	6	-2.66	20	-23	16	-17		u=7	\$ BORAL Absorber	
54	7	-2.7	20	-23	17	-18		u=7	\$ water	
55	4	-1.	20	-23	18	-118		u=7	\$ Water	
56	5	-7.84	118:-129:65:-66					u=7	\$ Steel	
57	4	-1.	64	-21	67	-118		u=7	\$ Water	
58	4	-1.	24	-65	67	-118		u=7	\$ water	
59	5	-7.84	21	-20	67	-118		u=7	\$ Steel	
60	5	-7.84	23	-24	67	-118		u=7	\$ Steel	
61	4	-1.	129	-64	66	-118		u=7	\$ Water	
c										
c	Type E box - No Boral Panels									
c										
62	0	-10	11	-12	13			u=8 fill=1 (0.8814	0.8814 0)	
63	3	-6.55	60	-61	62	-63	#8	u=8	\$ Zr flow channel	
103	5	-7.84	74	-75	76	-77	(-70:71:-72:73)	u=8	\$ DFC	
64	4	-1.	129	-65	66	-118	#8 #9 #103	u=8	\$ water	
65	5	-7.84	118:-129:65:-66					u=8	\$ Steel	
c										
c	Type F box - No Boral Panels or fuel									
c										
66	4	-1.	129	-65	66	-118		u=9	\$ water	
67	5	-7.84	118:-129:65:-66					u=9	\$ Steel	
c										
68	4	-1.0	-34	35	-36	37		u=5 lat=1 fill=-7:6	-7:6 0:0	
			5	5	5	5	5	5	5	
			5	9	9	9	9	9	9	
			5	9	9	9	7	4	9	
			5	9	9	7	4	4	4	
			5	9	9	7	4	4	4	
			5	9	9	7	4	4	4	
			5	9	7	4	4	4	4	
			5	9	8	4	4	4	4	
			5	9	9	7	4	4	4	
			5	9	9	8	4	4	4	
			5	9	9	9	8	6	9	
			5	9	9	9	9	9	9	
			5	5	5	5	5	5	5	
69	0		-41					50	-49 fill=5 (8.1661	8.1661 0)
70	4	-1.0	-41		43	-50			\$ Water below Fuel	
71	4	-1.0	-41		49	-44			\$ Water above Fuel	

72	5	-7.84	-42	68	-43	\$ Steel below Fuel	
73	5	-7.84	-42	44	-69	\$ Steel above Fuel	
74	5	-7.84	41	-42	43	-44	\$ Radial Steel
75	0		42	:-68:	69	\$ outside world	

1	cz	0.6274				\$ Fuel OD
2	cz	0.6280				\$ Clad ID
3	cz	0.7169				\$ Clad OD
4	cz	0.6280				\$ Thimble ID
5	cz	0.7169				\$ Thimble OD
6	px	0.8814				\$ Pin Pitch
7	px	-0.8814				
8	py	0.8814				
9	py	-0.8814				
10	px	5.4483				\$ Channel ID
11	px	-5.4483				
12	py	5.4483				
13	py	-5.4483				
14	py	7.8016				
15	py	7.8155				
16	py	7.8410				
17	py	8.0467				
18	py	8.0721				
118	py	8.0861				
20	px	-6.0325				
21	px	-6.2230				
23	px	6.0325				
24	px	6.2230				
25	px	-7.8016				
26	px	-7.8155				
27	px	-7.8410				
28	px	-8.0467				
29	px	-8.0721				
129	px	-8.0861				
30	py	-6.0325				
31	py	6.0325				
32	py	-6.2230				
33	py	6.2230				
34	px	7.6111				
35	px	-8.7211				
36	py	8.7211				
37	py	-7.6111				
41	cz	85.57				
42	cz	108.43				
43	pz	11.46				
44	pz	331.0				
49	pz	309.4				\$ Top of Active F
50	pz	30.				\$ Start of Active
60	px	-5.6007				\$ Channel OD
61	px	5.6007				
62	py	-5.6007				
63	py	5.6007				
64	px	-7.6111				\$ Cell Box ID
65	px	7.6111				
66	py	-7.6111				
67	py	7.6111				
68	pz	-10.13				
69	pz	370.36				
70	px	-6.2611				\$ DFC ID
71	px	6.2611				

```

72  py      -6.2611
73  py      6.2611
74  px      -6.5659      $ DFC OD
75  px      6.5659
76  py      -6.5659
77  py      6.5659

```

```

imp:n      1 77r 0
kcode     10000 0.94 20 120
c
sdef par=1 erg=d1 axs=0 0 1 x=d4 y=fx d5 z=d3
c

```

```

sp1 -2 1.2895
c

```

```

si3 h 30. 309.
sp3 0 1
c

```

```

c
si4 s
      15 16
      13 14 15 16 17 18
      12 13 14 15 16 17 18 19
      12 13 14 15 16 17 18 19
      11 12 13 14 15 16 17 18 19 20
      11 12 13 14 15 16 17 18 19 20
      12 13 14 15 16 17 18 19
      12 13 14 15 16 17 18 19
      13 14 15 16 17 18
      15 16

```

```

sp4 1 67r
c

```

```

ds5 s
      30 30
      29 29 29 29 29 29
      28 28 28 28 28 28 28 28
      27 27 27 27 27 27 27 27
      26 26 26 26 26 26 26 26 26
      25 25 25 25 25 25 25 25 25
      24 24 24 24 24 24 24 24
      23 23 23 23 23 23 23 23
      22 22 22 22 22 22
      21 21

```

```

c
si11 -80.6831 -67.6783
si12 -64.1985 -51.1937
si13 -47.7139 -34.7091
si14 -31.2293 -18.2245
si15 -14.7447 -1.7399
si16  1.7399  14.7447
si17  18.2245  31.2293
si18  34.7091  47.7139
si19  51.1937  64.1985
si20  67.6783  80.6831

```

```

c
si21 -80.6831 -67.6783
si22 -64.1985 -51.1937
si23 -47.7139 -34.7091
si24 -31.2293 -18.2245
si25 -14.7447 -1.7399
si26  1.7399  14.7447
si27  18.2245  31.2293
si28  34.7091  47.7139

```

si29 51.1937 64.1985
 si30 67.6783 80.6831
 sp11 0 1
 sp12 0 1
 sp13 0 1
 sp14 0 1
 sp15 0 1
 sp16 0 1
 sp17 0 1
 sp18 0 1
 sp19 0 1
 sp20 0 1
 sp21 0 1
 sp22 0 1
 sp23 0 1
 sp24 0 1
 sp25 0 1
 sp26 0 1
 sp27 0 1
 sp28 0 1
 sp29 0 1
 sp30 0 1
 c

m1	92235.50c	-0.02644		\$ 3.00% E Fuel		
	92238.50c	-0.85504				
	8016.50c	-0.11852				
m3	40000.56c	1.		\$ Zr Clad		
m4	1001.50c	0.6667		\$ Water		
	8016.50c	0.3333				
m5	24000.50c	0.01761		\$ Steel		
	25055.50c	0.001761				
	26000.55c	0.05977				
	28000.50c	0.008239				
m6	5010.50c	1.9592E-03		\$ Boral 0.0067 gm/cm2		
	5011.50c	8.1175E-03				
	6000.50c	2.5176E-03				
	13027.50c	5.4933E-02				
m7	13027.50c	1.		\$ Al Clad		
mt4	lwtr.01t					
prdmp	j -120	j 2				
fm4	1000 1	-6				
f4:n	1					
sd4	1000					
e4	1.000E-11	1.000E-10	5.000E-10	7.500E-10	1.000E-09	1.200E-09
	1.500E-09	2.000E-09	2.500E-09	3.000E-09		
	4.700E-09	5.000E-09	7.500E-09	1.000E-08	2.530E-08	
	3.000E-08	4.000E-08	5.000E-08	6.000E-08	7.000E-08	
	8.000E-08	9.000E-08	1.000E-07	1.250E-07	1.500E-07	
	1.750E-07	2.000E-07	2.250E-07	2.500E-07	2.750E-07	
	3.000E-07	3.250E-07	3.500E-07	3.750E-07	4.000E-07	
	4.500E-07	5.000E-07	5.500E-07	6.000E-07	6.250E-07	
	6.500E-07	7.000E-07	7.500E-07	8.000E-07	8.500E-07	
	9.000E-07	9.250E-07	9.500E-07	9.750E-07	1.000E-06	
	1.010E-06	1.020E-06	1.030E-06	1.040E-06	1.050E-06	
	1.060E-06	1.070E-06	1.080E-06	1.090E-06	1.100E-06	
	1.110E-06	1.120E-06	1.130E-06	1.140E-06	1.150E-06	
	1.175E-06	1.200E-06	1.225E-06	1.250E-06	1.300E-06	
	1.350E-06	1.400E-06	1.450E-06	1.500E-06	1.590E-06	
	1.680E-06	1.770E-06	1.860E-06	1.940E-06	2.000E-06	
	2.120E-06	2.210E-06	2.300E-06	2.380E-06	2.470E-06	

2.570E-06	2.670E-06	2.770E-06	2.870E-06	2.970E-06
3.000E-06	3.050E-06	3.150E-06	3.500E-06	3.730E-06
4.000E-06	4.750E-06	5.000E-06	5.400E-06	6.000E-06
6.250E-06	6.500E-06	6.750E-06	7.000E-06	7.150E-06
8.100E-06	9.100E-06	1.000E-05	1.150E-05	1.190E-05
1.290E-05	1.375E-05	1.440E-05	1.510E-05	1.600E-05
1.700E-05	1.850E-05	1.900E-05	2.000E-05	2.100E-05
2.250E-05	2.500E-05	2.750E-05	3.000E-05	3.125E-05
3.175E-05	3.325E-05	3.375E-05	3.460E-05	3.550E-05
3.700E-05	3.800E-05	3.910E-05	3.960E-05	4.100E-05
4.240E-05	4.400E-05	4.520E-05	4.700E-05	4.830E-05
4.920E-05	5.060E-05	5.200E-05	5.340E-05	5.900E-05
6.100E-05	6.500E-05	6.750E-05	7.200E-05	7.600E-05
8.000E-05	8.200E-05	9.000E-05	1.000E-04	1.080E-04
1.150E-04	1.190E-04	1.220E-04	1.860E-04	1.925E-04
2.075E-04	2.100E-04	2.400E-04	2.850E-04	3.050E-04
5.500E-04	6.700E-04	6.830E-04	9.500E-04	1.150E-03
1.500E-03	1.550E-03	1.800E-03	2.200E-03	2.290E-03
2.580E-03	3.000E-03	3.740E-03	3.900E-03	6.000E-03
8.030E-03	9.500E-03	1.300E-02	1.700E-02	2.500E-02
3.000E-02	4.500E-02	5.000E-02	5.200E-02	6.000E-02
7.300E-02	7.500E-02	8.200E-02	8.500E-02	1.000E-01
1.283E-01	1.500E-01	2.000E-01	2.700E-01	3.300E-01
4.000E-01	4.200E-01	4.400E-01	4.700E-01	4.995E-01
5.500E-01	5.730E-01	6.000E-01	6.700E-01	6.790E-01
7.500E-01	8.200E-01	8.611E-01	8.750E-01	9.000E-01
9.200E-01	1.010E+00	1.100E+00	1.200E+00	1.250E+00
1.317E+00	1.356E+00	1.400E+00	1.500E+00	1.850E+00
2.354E+00	2.479E+00	3.000E+00	4.304E+00	4.800E+00
6.434E+00	8.187E+00	1.000E+01	1.284E+01	1.384E+01
1.455E+01	1.568E+01	1.733E+01	2.000E+01	

HI-STAR containing MPC68F, 07x07 in DFC with 13 missing rods
 c 3.00 % uniform enrichment, unreflected cask, 0.0067 g/cmsq B-10 in Boral

c
 c
 1 1 -10.522 -1 u=2 \$ fuel
 2 4 -1.0 1 -2 u=2 \$ gap
 3 3 -6.55 2 -3 u=2 \$ Zr Clad
 4 4 -1.0 3 u=2 \$ water in fuel region
 5 4 -1.0 -4:5 u=3 \$ water in guide tubes
 6 3 -6.55 4 -5 u=3 \$ guide tubes
 7 4 -1.0 -6 +7 -8 +9 u=1 lat=1

fill= -4:4 -4:4 0:0
 1 1 1 1 1 1 1 1
 1 2 2 2 2 2 2 1
 1 2 1 2 1 2 1 1
 1 2 2 1 2 1 2 1
 1 2 1 2 1 2 1 1
 1 2 2 1 2 1 2 1
 1 2 1 2 1 2 1 1
 1 2 2 2 2 2 2 1
 1 1 1 1 1 1 1 1

c
 C BOX TYPE R

c
 8 0 -10 11 -12 13 u=4 fill=1
 9 3 -6.55 60 -61 62 -63 #8 u=4 \$ Zr flow channel
 100 5 -7.84 74 -75 76 -77 (-70:71:-72:73) u=4 \$ DFC
 10 4 -1. 64 -65 66 -67 #8 #9 #100 u=4 \$ water
 11 5 -7.84 20 -23 67 -14 u=4 \$ 0.075" STEEL
 12 4 -1. 20 -23 14 -15 u=4 \$ WATER POCKET
 13 7 -2.7 20 -23 15 -16 u=4 \$ Al CLAD
 14 6 -2.66 20 -23 16 -17 u=4 \$ BORAL Absorber
 15 7 -2.7 20 -23 17 -18 u=4 \$ Al Clad
 16 4 -1. 20 -23 18 -118 u=4 \$ Water
 17 5 -7.84 118:-129:65:-66 u=4 \$ Steel
 18 4 -1. 64 -21 67 -118 u=4 \$ Water
 19 4 -1. 24 -65 67 -118 u=4 \$ water
 20 5 -7.84 21 -20 67 -118 u=4 \$ Steel
 21 5 -7.84 23 -24 67 -118 u=4 \$ Steel
 22 4 -1. 129 -64 33 -118 u=4 \$ Water
 c
 23 5 -7.84 25 -64 30 -31 u=4 \$ Steel
 24 4 -1. 26 -25 30 -31 u=4 \$ Water
 25 7 -2.7 27 -26 30 -31 u=4 \$ Al clad
 26 6 -2.66 28 -27 30 -31 u=4 \$ Boral
 27 7 -2.7 29 -28 30 -31 u=4 \$ Al clad
 28 4 -1. 129 -29 30 -31 u=4 \$ water
 29 5 -7.84 129 -64 32 -30 u=4 \$ Steel ends
 30 5 -7.84 129 -64 31 -33 u=4 \$ Steel ends
 31 4 -1. 129 -64 66 -32 u=4 \$ Water

c Type A box - Boral only on left side

c
 32 0 -10 11 -12 13 u=6 fill=1
 33 3 -6.55 60 -61 62 -63 #8 u=6 \$ Zr flow channel
 101 5 -7.84 74 -75 76 -77 (-70:71:-72:73) u=6 \$ DFC
 34 4 -1. 64 -65 66 -118 #8 #9 #101 u=6 \$ water
 35 5 -7.84 118:-129:65:-66 u=6 \$ Steel
 36 4 -1. 129 -64 67 -118 u=6 \$ Water
 c

71	4	-1.0	-41	49	-44	\$ Water above Fuel
72	5	-7.84	-42	68	-43	\$ Steel below Fuel
73	5	-7.84	-42	44	-69	\$ Steel above Fuel
74	5	-7.84	41	-42	43	\$ Radial Steel
75	0		42 :-68:	69		\$ outside world

1	cz	0.5220		\$ Fuel OD
2	cz	0.5334		\$ Clad ID
3	cz	0.6172		\$ Clad OD
4	cz	0.5398		\$ Thimble ID
5	cz	0.6261		\$ Thimble OD
6	px	0.8014		\$ Pin Pitch
7	px	-0.8014		
8	py	0.8014		
9	py	-0.8014		
10	px	5.7684		\$ Channel ID
11	px	-5.7684		
12	py	5.7684		
13	py	-5.7684		
14	py	7.8016		
15	py	7.8155		
16	py	7.8410		
17	py	8.0467		
18	py	8.0721		
118	py	8.0861		
20	px	-6.0325		
21	px	-6.2230		
23	px	6.0325		
24	px	6.2230		
25	px	-7.8016		
26	px	-7.8155		
27	px	-7.8410		
28	px	-8.0467		
29	px	-8.0721		
129	px	-8.0861		
30	py	-6.0325		
31	py	6.0325		
32	py	-6.2230		
33	py	6.2230		
34	px	7.6111		
35	px	-8.7211		
36	py	8.7211		
37	py	-7.6111		
41	cz	85.57		
42	cz	108.43		
43	pz	11.46		
44	pz	252.15		
49	pz	230.66		\$ Top of Active Fuel
50	pz	30.		\$ Start of Active Fuel
60	px	-5.9207		\$ Channel OD
61	px	5.9207		
62	py	-5.9207		
63	py	5.9207		
64	px	-7.6111		\$ Cell Box ID
65	px	7.6111		
66	py	-7.6111		
67	py	7.6111		
68	pz	-10.13		
69	pz	291.52		
70	px	-6.2611		\$ DFC ID

```

71 px 6.2611
72 py -6.2611
73 py 6.2611
74 px -6.5659 $ DFC OD
75 px 6.5659
76 py -6.5659
77 py 6.5659

```

```

imp:n 1 77r 0
kcode 10000 0.94 20 120
c
sdef par=1 erg=d1 axs=0 0 1 x=d4 y=fx d5 z=d3
c

```

```

sp1 -2 1.2895
c

```

```

si3 h 30. 230.66

```

```

sp3 0 1
c

```

```

c

```

```

si4 s 15 16
      13 14 15 16 17 18
      12 13 14 15 16 17 18 19
      12 13 14 15 16 17 18 19
11 12 13 14 15 16 17 18 19 20
11 12 13 14 15 16 17 18 19 20
      12 13 14 15 16 17 18 19
      12 13 14 15 16 17 18 19
      13 14 15 16 17 18
      15 16

```

```

sp4 1 67r
c

```

```

ds5 s 30 30
      29 29 29 29 29 29
      28 28 28 28 28 28 28 28
      27 27 27 27 27 27 27 27
26 26 26 26 26 26 26 26 26 26
25 25 25 25 25 25 25 25 25 25
      24 24 24 24 24 24 24 24
      23 23 23 23 23 23 23 23
      22 22 22 22 22 22
      21 21

```

```

c

```

```

si11 -80.6831 -67.6783
si12 -64.1985 -51.1937
si13 -47.7139 -34.7091
si14 -31.2293 -18.2245
si15 -14.7447 -1.7399
si16 1.7399 14.7447
si17 18.2245 31.2293
si18 34.7091 47.7139
si19 51.1937 64.1985
si20 67.6783 80.6831

```

```

c

```

```

si21 -80.6831 -67.6783
si22 -64.1985 -51.1937
si23 -47.7139 -34.7091
si24 -31.2293 -18.2245
si25 -14.7447 -1.7399
si26 1.7399 14.7447
si27 18.2245 31.2293

```

si28 34.7091 47.7139
 si29 51.1937 64.1985
 si30 67.6783 80.6831
 sp11 0 1
 sp12 0 1
 sp13 0 1
 sp14 0 1
 sp15 0 1
 sp16 0 1
 sp17 0 1
 sp18 0 1
 sp19 0 1
 sp20 0 1
 sp21 0 1
 sp22 0 1
 sp23 0 1
 sp24 0 1
 sp25 0 1
 sp26 0 1
 sp27 0 1
 sp28 0 1
 sp29 0 1
 sp30 0 1

c

m1	92235.50c	-0.02644	\$ 3.00% E Fuel			
	92238.50c	-0.85504				
	8016.50c	-0.11852				
m3	40000.56c	1.	\$ Zr Clad			
m4	1001.50c	0.6667	\$ Water			
	8016.50c	0.3333				
m5	24000.50c	0.01761	\$ Steel			
	25055.50c	0.001761				
	26000.55c	0.05977				
	28000.50c	0.008239				
m6	5010.50c	1.9592E-03	\$ Boral 0.0067 gm/cm2			
	5011.50c	8.1175E-03				
	6000.50c	2.5176E-03				
	13027.50c	5.4933E-02				
m7	13027.50c	1.	\$ Al Clad			
mt4	lwtr.01t					
prdmp	j	-120	j	2		
fm4	1000	1	-6			
f4:n	1					
sd4	1000					
e4	1.000E-11	1.000E-10	5.000E-10	7.500E-10	1.000E-09	1.200E-09
	1.500E-09	2.000E-09	2.500E-09	3.000E-09		
	4.700E-09	5.000E-09	7.500E-09	1.000E-08	2.530E-08	
	3.000E-08	4.000E-08	5.000E-08	6.000E-08	7.000E-08	
	8.000E-08	9.000E-08	1.000E-07	1.250E-07	1.500E-07	
	1.750E-07	2.000E-07	2.250E-07	2.500E-07	2.750E-07	
	3.000E-07	3.250E-07	3.500E-07	3.750E-07	4.000E-07	
	4.500E-07	5.000E-07	5.500E-07	6.000E-07	6.250E-07	
	6.500E-07	7.000E-07	7.500E-07	8.000E-07	8.500E-07	
	9.000E-07	9.250E-07	9.500E-07	9.750E-07	1.000E-06	
	1.010E-06	1.020E-06	1.030E-06	1.040E-06	1.050E-06	
	1.060E-06	1.070E-06	1.080E-06	1.090E-06	1.100E-06	
	1.110E-06	1.120E-06	1.130E-06	1.140E-06	1.150E-06	
	1.175E-06	1.200E-06	1.225E-06	1.250E-06	1.300E-06	
	1.350E-06	1.400E-06	1.450E-06	1.500E-06	1.590E-06	
	1.680E-06	1.770E-06	1.860E-06	1.940E-06	2.000E-06	

2.120E-06	2.210E-06	2.300E-06	2.380E-06	2.470E-06
2.570E-06	2.670E-06	2.770E-06	2.870E-06	2.970E-06
3.000E-06	3.050E-06	3.150E-06	3.500E-06	3.730E-06
4.000E-06	4.750E-06	5.000E-06	5.400E-06	6.000E-06
6.250E-06	6.500E-06	6.750E-06	7.000E-06	7.150E-06
8.100E-06	9.100E-06	1.000E-05	1.150E-05	1.190E-05
1.290E-05	1.375E-05	1.440E-05	1.510E-05	1.600E-05
1.700E-05	1.850E-05	1.900E-05	2.000E-05	2.100E-05
2.250E-05	2.500E-05	2.750E-05	3.000E-05	3.125E-05
3.175E-05	3.325E-05	3.375E-05	3.460E-05	3.550E-05
3.700E-05	3.800E-05	3.910E-05	3.960E-05	4.100E-05
4.240E-05	4.400E-05	4.520E-05	4.700E-05	4.830E-05
4.920E-05	5.060E-05	5.200E-05	5.340E-05	5.900E-05
6.100E-05	6.500E-05	6.750E-05	7.200E-05	7.600E-05
8.000E-05	8.200E-05	9.000E-05	1.000E-04	1.080E-04
1.150E-04	1.190E-04	1.220E-04	1.860E-04	1.925E-04
2.075E-04	2.100E-04	2.400E-04	2.850E-04	3.050E-04
5.500E-04	6.700E-04	6.830E-04	9.500E-04	1.150E-03
1.500E-03	1.550E-03	1.800E-03	2.200E-03	2.290E-03
2.580E-03	3.000E-03	3.740E-03	3.900E-03	6.000E-03
8.030E-03	9.500E-03	1.300E-02	1.700E-02	2.500E-02
3.000E-02	4.500E-02	5.000E-02	5.200E-02	6.000E-02
7.300E-02	7.500E-02	8.200E-02	8.500E-02	1.000E-01
1.283E-01	1.500E-01	2.000E-01	2.700E-01	3.300E-01
4.000E-01	4.200E-01	4.400E-01	4.700E-01	4.995E-01
5.500E-01	5.730E-01	6.000E-01	6.700E-01	6.790E-01
7.500E-01	8.200E-01	8.611E-01	8.750E-01	9.000E-01
9.200E-01	1.010E+00	1.100E+00	1.200E+00	1.250E+00
1.317E+00	1.356E+00	1.400E+00	1.500E+00	1.850E+00
2.354E+00	2.479E+00	3.000E+00	4.304E+00	4.800E+00
6.434E+00	8.187E+00	1.000E+01	1.284E+01	1.384E+01
1.455E+01	1.568E+01	1.733E+01	2.000E+01	

```

=NITAWL
' HI-STAR containing MPC24, 17x17 @ 4.0% E
0$$ 84 E
1$$ 0 13 0 4R0 1 E T
2$$ 92235 92238
    40000 1001 8016 5010 5011 6012
    13027 24000 25055 26000 28000
3** 92238 294.6 2 .3922 .1980 0. 0.02252 1
    16.0 7.8165 1 235.04 0.4431 1 1.0 T

```

```

END
=KENO5A
HI-STAR containing MPC24, 17x17 @ 4.0% E
READ PARAM TME=10000 GEN=1100 NPG=5000 NSK=100 LIB=4 TBA=5
END PARAM

```

```

READ MIXT SCT=2 EPS=1.0
MIX=1 92235 9.505E-04
      92238 0.02252
      8016 0.04693
MIX=2 40000 0.04323
MIX=3 1001 0.06688
      8016 0.03344
MIX=4 24000 0.01761
      25055 0.001761
      26000 0.05977
      28000 0.008239
MIX=5 5010 8.7066E-03
      5011 3.5116E-02
      6012 1.0948E-02
      13027 3.6936E-02
MIX=6 1001 0.06688
      8016 0.03344
MIX=7 13027 0.06026

```

```

END MIXT
READ GEOM
UNIT 1
COM= "FUEL ROD"
CYLINDER 1 1 0.3922 381.0 0.
CYLINDER 3 1 0.4001 381.0 0.
CYLINDER 2 1 0.4572 381.0 0.
CUBOID 3 1 0.6299 -0.6299 0.6299 -0.6299 381.0 0.
UNIT 2
COM= "GUIDE TUBE CELL"
CYLINDER 3 1 0.5613 381.0 0.
CYLINDER 2 1 0.6020 381.0 0.
CUBOID 3 1 0.6299 -0.6299 0.6299 -0.6299 381.0 0.
UNIT 4
COM= "LONG HORIZONTAL BORAL PANEL - NORTH"
CUBOID 5 1 9.4456 -9.4456 0.06985 -0.06985 381.0 0.
CUBOID 7 1 9.4456 -9.4456 0.09525 -0.09525 381.0 0.
CUBOID 3 1 9.525 -9.525 0.10414 -0.10414 381.0 0.
CUBOID 4 1 9.677 -9.677 0.25654 -0.10414 381.0 0.
UNIT 5
COM= "LONG VERTICAL BORAL PANEL - EAST"
CUBOID 5 1 0.06985 -0.06985 9.4456 -9.4456 381.0 0.
CUBOID 7 1 0.09525 -0.09525 9.4456 -9.4456 381.0 0.
CUBOID 3 1 0.10414 -0.10414 9.525 -9.525 381.0 0.
CUBOID 4 1 0.25654 -0.10414 9.677 -9.677 381.0 0.
UNIT 6
COM= "LONG HORIZONTAL BORAL PANEL - SOUTH"
CUBOID 5 1 9.4456 -9.4456 0.06985 -0.06985 381.0 0.

```

CUBOID	7	1	9.4456	-9.4456	0.09525	-0.09525	381.0	0.
CUBOID	3	1	9.525	-9.525	0.10414	-0.10414	381.0	0.
CUBOID	4	1	9.677	-9.677	0.10414	-0.25654	381.0	0.
UNIT	7							
COM=			"LONG VERTICAL BORAL PANEL - WEST"					
CUBOID	5	1	0.06985	-0.06985	9.4456	-9.4456	381.0	0.
CUBOID	7	1	0.09525	-0.09525	9.4456	-9.4456	381.0	0.
CUBOID	3	1	0.10414	-0.10414	9.525	-9.525	381.0	0.
CUBOID	4	1	0.10414	-0.25654	9.677	-9.677	381.0	0.
UNIT	8		ARRAY 1	-10.7083	-10.7083	0.		
COM=			"CENTRAL FUEL ASSEMBLIES - 4 BORAL PANELS"					
CUBOID	3	1	11.1864	-11.1864	11.1864	-11.1864	381.0	0.
CUBOID	4	1	11.9008	-11.9802	11.9008	-11.9802	381.0	0.
CUBOID	3	1	13.6	-13.6	13.6	-13.6	381.0	0.
HOLE	4		0.	12.005	0.			
HOLE	5		12.005	0.	0.			
HOLE	6		0.	-12.0845	0.			
HOLE	7		-12.0845	0.	0.			
HOLE	17		-11.9802	11.9805	0.			
HOLE	17		-11.9802	-13.59	0.			
HOLE	18		-13.59	-11.90	0.			
UNIT	9							
COM=			"SHORT HORIZONTAL BORAL PANEL - NORTH"					
CUBOID	5	1	6.2706	-6.2706	0.06985	-0.06985	381.0	0.
CUBOID	7	1	6.2706	-6.2706	0.09525	-0.09525	381.0	0.
CUBOID	3	1	6.35	-6.35	0.10414	-0.10414	381.0	0.
CUBOID	4	1	6.5405	-6.5405	0.25654	-0.10414	381.0	0.
UNIT	10							
COM=			"SHORT VERTICAL BORAL PANEL - EAST"					
CUBOID	5	1	0.06985	-0.06985	6.2706	-6.2706	381.0	0.
CUBOID	7	1	0.09525	-0.09525	6.2706	-6.2706	381.0	0.
CUBOID	3	1	0.10414	-0.10414	6.35	-6.35	381.0	0.
CUBOID	4	1	0.25654	-0.10414	6.5405	-6.5405	381.0	0.
UNIT	11							
COM=			"SHORT HORIZONTAL BORAL PANEL - SOUTH"					
CUBOID	5	1	6.2706	-6.2706	0.06985	-0.06985	381.0	0.
CUBOID	7	1	6.2706	-6.2706	0.09525	-0.09525	381.0	0.
CUBOID	3	1	6.35	-6.35	0.10414	-0.10414	381.0	0.
CUBOID	4	1	6.5405	-6.5405	0.10414	-0.25654	381.0	0.
UNIT	12							
COM=			"SHORT VERTICAL BORAL PANEL - WEST"					
CUBOID	5	1	0.06985	-0.06985	6.2706	-6.2706	381.0	0.
CUBOID	7	1	0.09525	-0.09525	6.2706	-6.2706	381.0	0.
CUBOID	3	1	0.10414	-0.10414	6.35	-6.35	381.0	0.
CUBOID	4	1	0.10414	-0.25654	6.5405	-6.5405	381.0	0.
UNIT	13		ARRAY 1	-10.7083	-10.7083	0.		
COM=			"Array B short Boral N & E "					
CUBOID	3	1	11.1864	-11.1864	11.1864	-11.1864	381.0	0.
CUBOID	4	1	11.9008	-11.9802	11.9008	-11.9802	381.0	0.
CUBOID	3	1	13.6	-13.6	13.6	-13.6	381.0	0.
HOLE	9		0.	12.005	0.			
HOLE	10		12.005	0.	0.			
HOLE	6		0.	-12.0845	0.			
HOLE	7		-12.0845	0.	0.			
HOLE	17		-11.9802	11.9805	0.			
HOLE	17		-11.9802	-13.59	0.			
HOLE	18		-13.59	-11.90	0.			
UNIT	14		ARRAY 1	-10.7083	-10.7083	0.		
COM=			"Array C short Boral E & S "					
CUBOID	3	1	11.1864	-11.1864	11.1864	-11.1864	381.0	0.

CUBOID	4	1	11.9008	-11.9802	11.9008	-11.9802	381.0	0.
CUBOID	3	1	13.6	-13.6	13.6	-13.6	381.0	0.
HOLE	4		0.	12.005	0.			
HOLE	10		12.005	0.	0.			
HOLE	11		0.	-12.0845	0.			
HOLE	7		-12.0845	0.	0.			
HOLE	17		-11.9802	11.9805	0.			
HOLE	17		-11.9802	-13.59	0.			
HOLE	18		-13.59	-11.90	0.			
UNIT	15	ARRAY 1	-10.7083	-10.7083	0.			
COM=		"Array D short Boral S & W "						
CUBOID	3	1	11.1864	-11.1864	11.1864	-11.1864	381.0	0.
CUBOID	4	1	11.9008	-11.9802	11.9008	-11.9802	381.0	0.
CUBOID	3	1	13.6	-13.6	13.6	-13.6	381.0	0.
HOLE	4		0.	12.005	0.			
HOLE	5		12.005	0.	0.			
HOLE	11		0.	-12.0845	0.			
HOLE	12		-12.0845	0.	0.			
HOLE	17		-11.9802	11.9805	0.			
HOLE	17		-11.9802	-13.59	0.			
HOLE	18		-13.59	-11.90	0.			
UNIT	16	ARRAY 1	-10.7083	-10.7083	0.			
COM=		"Array E short Boral N & W "						
CUBOID	3	1	11.1864	-11.1864	11.1864	-11.1864	381.0	0.
CUBOID	4	1	11.9008	-11.9802	11.9008	-11.9802	381.0	0.
CUBOID	3	1	13.6	-13.6	13.6	-13.6	381.0	0.
HOLE	9		0.	12.005	0.			
HOLE	5		12.005	0.	0.			
HOLE	6		0.	-12.0845	0.			
HOLE	12		-12.0845	0.	0.			
HOLE	17		-11.9802	11.9805	0.			
HOLE	17		-11.9802	-13.59	0.			
HOLE	18		-13.59	-11.90	0.			
UNIT	17							
CUBOID	4	1	0.7938	-0.	1.60	-0.	381.0	0.
UNIT	18							
CUBOID	4	1	1.60	-0.	0.7938	-0.	381.0	0.
GLOBAL								
UNIT	19							
COM=		"ASSEMBLY ARRAY + X DIRECTION"						
CYLINDER	3	1	86.57				396.24	-10.16
HOLE	8		13.6855	13.6855	0.			
HOLE	8		13.6855	-13.6855	0.			
HOLE	8		13.6855	41.0565	0.			
HOLE	8		13.6855	-41.0565	0.			
HOLE	13		13.6855	68.4275	0.			
HOLE	14		13.6855	-68.4275	0.			
HOLE	8		41.0565	13.6855	0.			
HOLE	8		41.0565	-13.6855	0.			
HOLE	13		41.0565	41.0565	0.			
HOLE	14		41.0565	-41.0565	0.			
HOLE	13		68.4275	13.6855	0.			
HOLE	14		68.4275	-13.6855	0.			
HOLE	8		-13.6855	13.6855	0.			
HOLE	8		-13.6855	-13.6855	0.			
HOLE	8		-13.6855	41.0565	0.			
HOLE	8		-13.6855	-41.0565	0.			
HOLE	16		-13.6855	68.4275	0.			
HOLE	15		-13.6855	-68.4275	0.			
HOLE	8		-41.0565	13.6855	0.			

```

HOLE          8  -41.0565  -13.6855  0.
HOLE         16  -41.0565   41.0565  0.
HOLE         15  -41.0565  -41.0565  0.
HOLE         16  -68.4275   13.6855  0.
HOLE         15  -68.4275  -13.6855  0.
CYLINDER      4   1  108.43
CUBOID        3   1  109  -109  109  -109  435.61  -31.75
END GEOM
READ ARRAY
ARA=1  NUX=17  NUY=17  NUZ=1
COM=   "17 X 17 FUEL ASSEMBLY"
FILL
1 1 1 1 1 1 1 1 1 1 1 1 1 1 1 1 1
1 1 1 1 1 1 1 1 1 1 1 1 1 1 1 1 1
1 1 1 1 1 2 1 1 2 1 1 2 1 1 1 1 1
1 1 1 2 1 1 1 1 1 1 1 1 1 2 1 1 1
1 1 1 1 1 1 1 1 1 1 1 1 1 1 1 1 1
1 1 2 1 1 2 1 1 2 1 1 2 1 1 2 1 1
1 1 1 1 1 1 1 1 1 1 1 1 1 1 1 1 1
1 1 1 1 1 1 1 1 1 1 1 1 1 1 1 1 1
1 1 2 1 1 2 1 1 2 1 1 2 1 1 2 1 1
1 1 1 1 1 1 1 1 1 1 1 1 1 1 1 1 1
1 1 1 1 1 1 1 1 1 1 1 1 1 1 1 1 1
1 1 2 1 1 2 1 1 2 1 1 2 1 1 2 1 1
1 1 1 1 1 1 1 1 1 1 1 1 1 1 1 1 1
1 1 1 2 1 1 1 1 1 1 1 1 1 2 1 1 1
1 1 1 1 1 2 1 1 2 1 1 2 1 1 1 1 1
1 1 1 1 1 1 1 1 1 1 1 1 1 1 1 1 1
1 1 1 1 1 1 1 1 1 1 1 1 1 1 1 1 1
END FILL
END ARRAY
END DATA
END

```

```

=NITAWL
' HI-STAR containing MPC68, 08x08 @ 4.2% E
0$$ 84 E
1$$ 0 13 0 4R0 1 E T
2$$ 92235 92238
    40000 1001 8016 5010 5011 6012
    13027 24000 25055 26000 28000
3** 92238 294.6 2 .5207 .1623 0. 0.02248 1
    16.0 7.8330 1 235.04 0.5662 1 1.0 T
END

```

```

=KENO5A
HI-STAR containing MPC68, 08x08 @ 4.2% E
' GE 8X8R FUEL 2 WATER HOLES
READ PARAM TME=10000 GEN=1100 NPG=5000 NSK=100
    LIB=4 TBA=5 LNG=400000 NB8=900
END PARAM

```

```

READ MIXT SCT=2 EPS=1.
MIX=1 92235 9.983E-04
      92238 0.02248
      8016 0.04697
MIX=2 40000 0.04323
MIX=3 1001 0.06688
      8016 0.03344
MIX=4 24000 0.01761
      25055 0.001761
      26000 0.05977
      28000 0.008239
MIX=5 5010 8.071E-03
      5011 3.255E-02
      6012 1.015E-02
      13027 3.805E-02
MIX=6 13027 0.06026

```

```

END MIXT
READ GEOM

```

```

UNIT 1
COM= "FUEL ROD"
CYLINDER 1 1 0.5207 381.0 0.
CYLINDER 3 1 0.5321 381.0 0.
CYLINDER 2 1 0.6134 381.0 0.
CUBOID 3 1 0.8128 -0.8128 0.8128 -0.8128 381.0 0.
UNIT 2
COM= "GUIDE TUBE CELL"
CYLINDER 3 1 0.6744 381.0 0.
CYLINDER 2 1 0.7506 381.0 0.
CUBOID 3 1 0.8128 -0.8128 0.8128 -0.8128 381.0 0.
UNIT 4
COM= "HORIZONTAL BORAL PANEL"
CUBOID 5 1 6.0325 -6.0325 0.1027 -0.1027 381.0 0.
CUBOID 6 1 6.0325 -6.0325 0.1283 -0.1283 381.0 0.
CUBOID 3 1 6.0325 -6.0325 0.1422 -0.1422 381.0 0.
CUBOID 4 1 6.4611 -6.4611 0.1422 -0.3327 381.0 0.
UNIT 5
COM= "VERTICAL BORAL PANEL"
CUBOID 5 1 0.1027 -0.1027 6.0325 -6.0325 381.0 0.
CUBOID 6 1 0.1283 -0.1283 6.0325 -6.0325 381.0 0.
CUBOID 3 1 0.1422 -0.1422 6.0325 -6.0325 381.0 0.
CUBOID 4 1 0.3327 -0.1422 6.4611 -6.4611 381.0 0.
UNIT 8 ARRAY 1 -6.5024 -6.5024 0.
COM= "FUEL ASSEMBLIES - 2 BORAL PANELS"
CUBOID 3 1 6.7031 -6.7031 6.7031 -6.7031 381.0 0.

```

CUBOID	2	1	6.9571	-6.9571	6.9571	-6.9571	381.0	0.
CUBOID	3	1	7.6111	-8.0861	8.0861	-7.6111	381.0	0.
HOLE	4		0.	7.9438	0.			
HOLE	5		-7.9438	0.	0.			
CUBOID	4	1	7.6111	-8.7211	8.7211	-7.6111	381.0	0.
UNIT	9		ARRAY 1	-6.5024	-6.5024	0.		
COM=			"FUEL ASSEMBLIES - Type A"					
CUBOID	3	1	6.7031	-6.7031	6.7031	-6.7031	381.0	0.
CUBOID	2	1	6.9571	-6.9571	6.9571	-6.9571	381.0	0.
CUBOID	3	1	7.6111	-8.0861	8.0861	-7.6111	381.0	0.
HOLE	5		-7.9438	0.	0.			
CUBOID	4	1	8.2461	-8.7211	8.7211	-7.6111	381.0	0.
UNIT	10		ARRAY 1	-6.5024	-6.5024	0.		
COM=			"FUEL ASSEMBLIES - Type B"					
CUBOID	3	1	6.7031	-6.7031	6.7031	-6.7031	381.0	0.
CUBOID	2	1	6.9571	-6.9571	6.9571	-6.9571	381.0	0.
CUBOID	3	1	7.6111	-8.0861	8.0861	-7.6111	381.0	0.
HOLE	5		-7.9438	0.	0.			
CUBOID	4	1	7.6111	-8.7211	8.7211	-7.6111	381.0	0.
UNIT	11		ARRAY 1	-6.5024	-6.5024	0.		
COM=			"FUEL ASSEMBLIES - Type C"					
CUBOID	3	1	6.7031	-6.7031	6.7031	-6.7031	381.0	0.
CUBOID	2	1	6.9571	-6.9571	6.9571	-6.9571	381.0	0.
CUBOID	3	1	7.6111	-8.0861	8.0861	-7.6111	381.0	0.
HOLE	4		0.	7.9438	0.			
HOLE	5		-7.9438	0.	0.			
CUBOID	4	1	8.2461	-8.7211	8.7211	-7.6111	381.0	0.
UNIT	12		ARRAY 1	-6.5024	-6.5024	0.		
COM=			"FUEL ASSEMBLIES - Type D"					
CUBOID	3	1	6.7031	-6.7031	6.7031	-6.7031	381.0	0.
CUBOID	2	1	6.9571	-6.9571	6.9571	-6.9571	381.0	0.
CUBOID	3	1	7.6111	-8.0861	8.0861	-7.6111	381.0	0.
HOLE	4		0.	7.9438	0.			
HOLE	5		-7.9438	0.	0.			
CUBOID	4	1	8.2461	-8.7211	8.7211	-8.2461	381.0	0.
UNIT	13		ARRAY 1	-6.5024	-6.5024	0.		
COM=			"FUEL ASSEMBLIES - Type E"					
CUBOID	3	1	6.7031	-6.7031	6.7031	-6.7031	381.0	0.
CUBOID	2	1	6.9571	-6.9571	6.9571	-6.9571	381.0	0.
CUBOID	3	1	7.6111	-8.0861	8.0861	-7.6111	381.0	0.
HOLE	4		0.	7.9438	0.			
HOLE	5		-7.9438	0.	0.			
CUBOID	4	1	7.6111	-8.7211	8.7211	-8.2461	381.0	0.
UNIT	14		ARRAY 1	-6.5024	-6.5024	0.		
COM=			"FUEL ASSEMBLIES - Type F"					
CUBOID	3	1	6.7031	-6.7031	6.7031	-6.7031	381.0	0.
CUBOID	2	1	6.9571	-6.9571	6.9571	-6.9571	381.0	0.
CUBOID	3	1	7.6111	-8.0861	8.0861	-7.6111	381.0	0.
HOLE	4		0.	7.9438	0.			
CUBOID	4	1	7.6111	-8.7211	8.7211	-8.2461	381.0	0.
UNIT	15		ARRAY 1	-6.5024	-6.5024	0.		
COM=			"FUEL ASSEMBLIES - TYPE G"					
CUBOID	3	1	6.7031	-6.7031	6.7031	-6.7031	381.0	0.
CUBOID	2	1	6.9571	-6.9571	6.9571	-6.9571	381.0	0.
CUBOID	3	1	7.6111	-8.0861	8.0861	-7.6111	381.0	0.
HOLE	4		0.	7.9438	0.			
CUBOID	4	1	7.6111	-8.7211	8.7211	-7.6111	381.0	0.
UNIT	16		ARRAY 1	-6.5024	-6.5024	0.		
COM=			"FUEL ASSEMBLIES - TYPE H"					
CUBOID	3	1	6.7031	-6.7031	6.7031	-6.7031	381.0	0.

```

CUBOID      2  1  6.9571  -6.9571  6.9571  -6.9571      381.0  0.
CUBOID      3  1  7.6111  -8.0861  8.0861  -7.6111      381.0  0.
CUBOID      4  1  7.6111  -8.7211  8.7211  -7.6111      381.0  0.
UNIT        17  ARRAY 2    -48.9966  -48.9966      0
UNIT        18  ARRAY 3    -16.3322  -7.6111      0.
UNIT        19  ARRAY 4    -48.9966  -7.6111      0.
UNIT        20  ARRAY 5    -8.7211  -16.3322     0.
UNIT        21  ARRAY 6    -8.7211  -50.1068     0.
UNIT        22  ARRAY 7    -8.7211  -16.3322     0.
UNIT        23  ARRAY 8    -8.7211  -16.3322     0.
UNIT        24  ARRAY 9    -8.7211  -16.3322     0.
UNIT        25  ARRAY 10   -8.7211  -16.3322     0.
UNIT        26  ARRAY 11   -16.3322  -8.7213     0.
UNIT        27  ARRAY 12   -16.3322  -7.6111     0.
UNIT        28  ARRAY 13   -16.3322  -8.7213     0.
UNIT        29  ARRAY 14   -16.3322  -8.7213     0.
GLOBAL
UNIT        30
CYLINDER    3  1  85.57      402.5  -18.54.
HOLE        17  0.0      0.0      0.
HOLE        18  0.0      73.4949  0.
HOLE        19  0.0      57.1627  0.
HOLE        20  -73.4949  0.0      0.
HOLE        21  -56.6077  0.0      0.
HOLE        22  57.7177  32.6644  0.
HOLE        23  57.7177  0.0      0.
HOLE        24  74.052   0.0      0.
HOLE        25  57.7177  -32.6644 0.
HOLE        26  32.6644  -57.7177 0.
HOLE        27  0.0      -57.7177 0.
HOLE        28  -32.6644  -57.7177 0.
HOLE        29  0.0      -74.052   0.
CYLINDER    4  1  108.43      441.85  -40.13
CUBOID      3  1  109.      -109.    109.      -109.    442      -40.2
END GEOM
READ ARRAY
ARA=1  NUX=8  NUY=8  NUZ=1
COM=   "8 X 8 FUEL ASSEMBLY"
FILL
  1 1 1 1 1 1 1 1
  1 1 1 1 1 1 1 1
  1 1 1 1 1 1 1 1
  1 1 1 2 1 1 1 1
  1 1 1 1 2 1 1 1
  1 1 1 1 1 1 1 1
  1 1 1 1 1 1 1 1
  1 1 1 1 1 1 1 1
  1 1 1 1 1 1 1 1
END FILL
ARA=2  NUX=6  NUY=6  NUZ=1
COM=   "6 X 6 CENTRAL ARRAY OF FUEL ASSEMBLIES"
FILL
  8 8 8 8 8 8
  8 8 8 8 8 8
  8 8 8 8 8 8
  8 8 8 8 8 8
  8 8 8 8 8 8
  8 8 8 8 8 8
END FILL
ARA=3  NUX=2  NUY=1  NUZ=1
COM=   "2 X 1 ARRAY OF FUEL ASSEMBLIES - TOP ROW"

```

```

FILL
 16 9
END FILL
ARA=4 NUX=6 NUY=1 NUZ=1
COM= "6 X 1 ARRAY OF FUEL ASSEMBLIES - 2ND ROW"
FILL
 16 10 8 8 10 9
END FILL
ARA=5 NUX=1 NUY=2 NUZ=1
COM= "2 X 1 ARRAY OF FUEL ASSEMBLIES - OUTER LEFT"
FILL
 14
 16
END FILL
ARA=6 NUX=1 NUY=6 NUZ=1
COM= "1 X 6 ARRAY OF FUEL ASSEMBLIES - 2ND ROW LEFT"
FILL
 14 15 8 8 15 16
END FILL
ARA=7 NUX=1 NUY=2 NUZ=1
COM= "1 X 2 ARRAY OF FUEL ASSEMBLIES - UPPER RIGHT"
FILL
 11
 9
END FILL
ARA=8 NUX=1 NUY=2 NUZ=1
COM= "1 X 2 ARRAY OF FUEL ASSEMBLIES - MIDDLE RIGHT"
FILL
 8
 8
END FILL
ARA=9 NUX=1 NUY=2 NUZ=1
COM= "1 X 2 ARRAY OF FUEL ASSEMBLIES - MIDDLE RIGHT"
FILL
 11
 9
END FILL
ARA=10 NUX=1 NUY=2 NUZ=1
COM= "1 X 2 ARRAY OF FUEL ASSEMBLIES - LOWER RIGHT"
FILL
 11
 11
END FILL
ARA=11 NUX=2 NUY=1 NUZ=1
COM= "2 X 1 ARRAY OF FUEL ASSEMBLIES - 2ND BOTTOM ROW"
FILL
 13 13
END FILL
ARA=12 NUX=2 NUY=1 NUZ=1
COM= "2 X 1 ARRAY OF FUEL ASSEMBLIES - BOTTOM ROW"
FILL
 8 8
END FILL
ARA=13 NUX=2 NUY=1 NUZ=1
COM= "2 X 1 ARRAY OF FUEL ASSEMBLIES - BOTTOM ROW"
FILL
 14 13
END FILL
ARA=14 NUX=2 NUY=1 NUZ=1
COM= "2 X 1 ARRAY OF FUEL ASSEMBLIES - BOTTOM ROW"

```

FILL
14 13
END FILL
END ARRAY
END DATA
END